**CRANFIELD UNIVERSITY**

**Hernan Andres Amaya Gonzalez**

# Power Consumption Analysis of Rotorcraft Environmental Control Systems

School of Engineering

MSc by research

MSc by Research Thesis

Academic Year: 2013-2014

Supervisor: Dr. C.P Lawson

June 2014

**CRANFIELD UNIVERSITY**

School of Engineering

MSc by research

MSc by Research Thesis

Academic Year: 2013-2014

**Hernan Andres Amaya Gonzalez**

# Power Consumption Analysis of Aircraft Environmental Control Systems

Supervisor: Dr. C.P Lawson

June 2014

This thesis is submitted in fulfilment of the requirements for the degree of

Master of Sciences by Research

# Acknowledgements

I want to thank everyone involved in this long process. I want first to thank God for gave me this fantastic opportunity and for allowing me to be right now enjoying of this new success.

I especially want to thanks to my parents, Jane Gonzalez and Hernan Amaya. Thanks a lot for always being there for me, supporting me and guiding me with valuable advices. Thanks for being my unconditional support and love, an unconditional love that makes me feel like being home despite the distance. To my sister Johana Amaya, without those bad jokes my days would be very boring, thank you for always being looking after me, for taking care of my mom, and for making me smile each time we spoke. My nada Paola, thank you for supporting me every day in this long work, for helping me and joining me in this whole adventure, for the great advices you gave me and cheer me up in those days of so much stress and hard workload. I want to dedicate this thesis to my grandmother Ana Gonzalez, who is always protecting me from above, thank you for giving me these strengths, and thanks for all the time you dedicated to your family, to me, dedication reflected in this study, thank you so much mom Anita. Likewise, I want to thank my whole family that in some way or another were part of this process, thank you very much for your support.

I also want to thank my fellow students, Henry, Leito, Santiago, Rodrigo, Angela, Francis, Charles, Mark, Juano, Alejo. Thanks for make this work much more enjoyable. Thanks for all the tomatas days and for helping me to move forward with this work. I want to thank to my supervisors Craig Lawson and Adrian Clarke, for supporting me and guide me in this process of study.

Thanks to all the people who have accompanied me on this adventure.

# Abstract

Helicopters have now become an essential part for civil and military activities, for the next few years a significant increase in the use of this mean of transportation is expected. Unlike many fixed-wing aircraft, helicopters have no need to be pressurized due to their operating at low altitudes. The Environmental Control Systems (ECS) commonly used in fixed-wing aircraft are air cycle systems, which use the engine compressor's bleed flow to function. These systems are integrated in the aircraft from inception. The ECS in helicopters is commonly added subsequently to an already designed airframe and power plant or as an additional development for modern aircraft. Helicopter engines are not designed to bleed air while producing their rated power, due to this a high penalty in fuel consumption is paid by such refitted systems. A detailed study of the different configurations of ECS for rotorcraft could reduce this penalty by determining the required power resulting from each of the system configurations, and therefore recommend the most appropriate one to be implemented for a particular flight path and aircraft.

This study presents the conducted analysis and subsequent simulation of the environmental control system in a selected representative rotorcraft: the Bell206L-4. This investigation seeks to optimize the rotorcraft's power consumption and energy waste; by taking into consideration the cabin heat load. It consequently aims to minimize these penalties, achieving passenger comfort, an optimally moist air for equipment and a reduction in the environmental impact.

For the purpose of this analysis a civil aircraft was chosen for a rotary-wing type. This helicopter was analysed with different air-conditioning packs complying with the current airworthiness requirements. These systems were optimized with the inclusion of different environmental control models, and the cabin heat load model, which provided the best air-conditioning for many conditions and mission scopes, thus reducing the high fuel consumption in engines and hence the emission of gases into the environment. Each of the models was computed in the Matlab-simulink® software.

Different case studies were carried out by changing aircraft, the system's configurations and flight parameters. Comparisons between the different systems and sub-systems were performed. The results of these simulations permitted the ECS configuration selection for

optimal fuel consumption. Once validated the results obtained through this model were included in Rotorcraft Mission Energy Management Model (RMEM), a tool designed to predict the power requirements of helicopter systems.

The computed ECS model shows that favourable reductions in fuel burn may be achievable if an appropriated configuration of ECS is chosen for a light rotorcraft. The results show that the VCM mixed with engine bleed air is the best configuration for the chosen missions. However, this configuration can vary according to the mission and environment.

**Keywords:**
Environmental Controls System, Bell 206L-4, Compartment loads, Air Cycle Machine, Vapour Cycle Machine, Combustion Heater, Exhaust Gases Heater, Bleed air, Dynamic simulation.

# TABLE OF CONTENTS

# List of Tables

# List of Figures

# List of Equations

# Notations

## List of Symbols

The following dimensions for each symbol are represented in SI system of units.

| Symbol | | Unit |
|---|---|---|
| $A$ | Surface area | $m^2$ |
| $A_1$ | Transparency area | $m^2$ |
| $A_2$ | Un-insulated wall area | $m^2$ |
| $A_3$ | Insulated wall area | $m^2$ |
| $A_4$ | Floor wall area | $m^2$ |
| $A_5$ | Ceiling area | $m^2$ |
| $A_6$ | Bulkhead area | $m^2$ |
| $ab$ | Beam air mass exponent | Dimensionless |
| $A_B$ | Beam bottom area | $m^2$ |
| $A_{bb}$ | Area between the beams | $m^2$ |
| $A_c$ | Beam cross sectional area | $m^2$ |
| $ad$ | Diffuse air mass exponent | Dimensionless |
| $A_f$ | Heat exchanger frontal area | $m^2$ |
| $A_{fcell}$ | Frontal area per unit cell | $m^2$ |
| $A_o$ | Heat exchanger free flow area | $m^2$ |
| $A_{ocell}$ | Free flow area per unit cell | $m^2$ |
| $A_p$ | Heat exchanger primary surface area | $m^2$ |
| $A_{pcell}$ | Primary surface area per unit cell | $m^2$ |
| $A_S$ | Beam sides area | $m^2$ |
| $A_s$ | Heat exchanger secondary surface area | $m^2$ |
| $A_{scell}$ | Secondary surface area per unit cell | $m^2$ |
| $AST$ | Apparent solar time | Dimensionless |
| $A_T$ | Beam top area | $m^2$ |
| $A_t$ | Heat exchanger total surface area | $m^2$ |
| $A_{tcell}$ | Total heat surface area per unit cell | $m^2$ |
| $A_w$ | Heat exchanger total wall area for heat conduction | $m^2$ |
| $A_{wcell}$ | Wall conduction area per unit cell | $m^2$ |
| $b$ | Air-side plate spacing | m |

| | | |
|---|---|---|
| $C$ | Area conversion factor | Dimensionless |
| $C^*$ | Heat capacity rate ratio | Dimensionless |
| $C_b$ | Beam perimeter | m |
| $C_c$ | Cold side fluid capacity rate | W/K |
| $c_c$ | Cold side wetted perimeter | m |
| $C_h$ | Hot side fluid capacity rate | W/K |
| $c_h$ | Hot side wetted perimeter | m |
| $C_{max}$ | Maximum value between $C_c$ and $C_h$ | W/K |
| $C_{min}$ | Minimum value between $C_c$ and $C_h$ | W/K |
| $COP_{ACM}$ | Air Cycle Machine Coefficient of Performance | Dimensionless |
| $COP_{ACM}$ | Vapour Cycle Machine Coefficient of Performance | Dimensionless |
| $C_p$ | Specific heat capacity of air at constant pressure | J/kg |
| $C_{pc}$ | Cold fluid specific heat capacity | J/kg |
| $C_{ph}$ | Hot fluid specific heat capacity | J/kg |
| $D_h$ | Hydraulic diameter of the fin geometry | m |
| $E_b$ | Beam normal irradiance | $W/m^2$ |
| $E_d$ | Diffuse horizontal irradiance | $W/m^2$ |
| $E_o$ | Extraterrestrial radian flux | $W/m^2$ |
| $ET$ | Equation of time | min |
| $F$ | Constant given for a condenser and evaporator | Dimensionless |
| $F_a$ | Emissivity factor | Dimensionless |
| $f_c$ | Heat exchanger cold side friction factor | Dimensionless |
| $f_c'$ | Cold side friction factor for constant fluid properties | Dimensionless |
| $F_e$ | Configuration factor | Dimensionless |
| $F_g$ | Angle factor | Dimensionless |
| $f_h$ | Heat exchanger hot side friction factor | Dimensionless |
| $f_h'$ | Hot side friction factor for constant fluid properties | Dimensionless |
| g | Gravity of earth | $m/s^2$ |
| $G_c$ | Cold side mass flux | $kg/m^2$ |
| $G_h$ | Hot side mass flux | $kg/m^2$ |
| $h$ | Convective heat transfer coefficient | $W/m^2$ |
| $H$ | Hour angle | deg |
| $h'_a$ | Assumed air space heat transfer coefficient | $W/m^2$ |
| $h'_r$ | Assumed air space radiation heat transfer coefficient | $W/m^2$ |
| $h_{1d}$ | Inlet refrigerant enthalpy of the evaporator | J/kg |

| | | |
|---|---|---|
| $h_{2d}$ | outlet refrigerant enthalpy of the evaporator | J/kg |
| $h_{3d}$ | outlet refrigerant enthalpy of the evaporator | J/kg |
| $h_a$ | Air space heat transfer coefficient | $W/m^2$ |
| $h_c$ | Heat exchanger cold side heat transfer coefficient | $W/m^2$ |
| $h_e$ | External surface heat transfer coefficient | $W/m^2$ |
| $h_h$ | Heat exchanger hot side heat transfer coefficient | $W/m^2$ |
| $h_i$ | Internal surface heat transfer coefficient | $W/m^2$ |
| $h_{ki}$ | Insulation heat transfer coefficient | $W/m^2$ |
| $h_{kt}$ | Transparency heat transfer coefficient | $W/m^2$ |
| $h_{kw}$ | Wall heat transfer coefficient | $W/m^2$ |
| $h_r$ | Air space radiation heat transfer coefficient | $W/m^2$ |
| $h_S$ | Beam sides heat transfer coefficient | $W/m^2$ |
| $H_t$ | Tube height | m |
| $I$ | Total solar radiation in flight | $W/m^2$ |
| $I_d$ | Diffuse solar irradiation | $W/m^2$ |
| $I_D$ | Direct solar irradiation | $W/m^2$ |
| $I_g$ | Total solar radiation on ground | $W/m^2$ |
| $I_o$ | Solar constant | $W/m^2$ |
| $I_r$ | Reflected solar irradiation | $W/m^2$ |
| $k$ | Thermal conductivity of the material | $W/m^2$ |
| $k_a$ | Air thermal conductivity | W/m |
| $k_b$ | Beam material thermal conductivity | W/m |
| $k_c$ | Tube material thermal conductivity | W/m |
| $k_{co}$ | Contraction pressure loss coefficient | Dimensionless |
| $k_e$ | Exit pressure loss coefficient | Dimensionless |
| $k_h$ | Fin material thermal conductivity | W/m |
| $k_{hxw}$ | Heat exchanger wall material thermal conductivity | W/m |
| $k_i$ | Insulation material thermal conductivity | W/m |
| $k_w$ | Wall material thermal conductivity | W/m |
| $L$ | Air space height | m |
| $L_2$ | Heat exchanger depth | m |
| $LAT$ | Aircraft latitude | deg |
| $L_b$ | Beam length | m |
| $L_f$ | Fin flow length | m |
| $L_{fc}$ | Cold side fin length | m |

| | | |
|---|---|---|
| $L_{fh}$ | Hot side fin length | m |
| $L_{lc}$ | Louver cut length | m |
| $L_{lf}$ | Louver fin length | m |
| $LON$ | Aircraft longitude | deg |
| $LSM$ | Longitude of local standard time | deg |
| $LST$ | Local standard time | hr |
| $M$ | Airplane Mach number | Dimensionless |
| $m$ | Relative air mass | Dimensionless |
| $\dot{M}'_{tc}$ | Assumed cooling unit mass flow rate | kg/s |
| $\dot{M}'_{th}$ | Assumed heating unit mass flow rate | kg/s |
| $\dot{m}_1$ | Cockpit required mass flow rate | kg/s |
| $M_1$ | Crew metabolic rate | W |
| $\dot{M}_1$ | PHX inlet mass flow rate | kg/s |
| $\dot{M}_{1a}$ | Ram air mass flow rate | kg/s |
| $\dot{M}_{1d}$ | VCM evaporator inlet mass flow rate (refrigerant) | kg/s |
| $\dot{M}_{1e}$ | EGH inlet mass flow rate (exhaust gas) | kg/s |
| $\dot{M}_2$ | ACM compressor inlet mass flow rate | kg/s |
| $\dot{m}_2$ | Cabin required mass flow rate | kg/s |
| $M_2$ | Occupants metabolic rate | W |
| $\dot{M}_{2a}$ | PHX ram air inlet mass flow rate (ACM) | kg/s |
| $\dot{M}_{2d}$ | VCM compressor inlet mass flow rate (refrigerant) | kg/s |
| $\dot{M}_{2e}$ | EGH outlet mass flow rate (exhaust gas) | kg/s |
| $\dot{m}_3$ | Cockpit required mass flow rate (if $\Delta T_3 > \Delta T_2$) | kg/s |
| $\dot{M}_3$ | SHX inlet mass flow rate | kg/s |
| $\dot{M}_{3a}$ | PHX ram air outlet mass flow rate (ACM) | kg/s |
| $\dot{M}_{3d}$ | VCM condenser inlet mass flow rate (refrigerant) | kg/s |
| $\dot{M}_4$ | ACM reheater (high pressure) inlet mass flow rate | kg/s |
| $\dot{m}_4$ | Cabin required mass flow rate (if $\Delta T_4 > \Delta T_2$) | kg/s |
| $\dot{M}_{4a}$ | Evaporator ram air outlet mass flow rate (VCM) | kg/s |
| $\dot{M}_{4d}$ | VCM expansion valve inlet mass flow rate (refrigerant) | kg/s |
| $\dot{M}_5$ | ACM condenser (high pressure) inlet mass flow rate | kg/s |
| $\dot{M}_{5a}$ | EGH ram air outlet mass flow rate | kg/s |
| $\dot{M}_6$ | ACM reheater (low pressure) inlet mass flow rate | kg/s |
| $\dot{M}_7$ | ACM turbine inlet mass flow rate | kg/s |
| $\dot{M}_8$ | ACM condenser (low pressure) inlet mass flow rate | kg/s |

| | | |
|---|---|---|
| $\dot{M}_9$ | ACM total mass flow rate | kg/s |
| $m_b$ | Beam exposed area | m |
| $\dot{m}_{ba}$ | Bleed air mass flow rate | kg/s |
| $\dot{m}_c$ | Cold fluid mass flow rate | kg/s |
| $m_c$ | Cold side exposed edge area | m |
| $\dot{M}_{c1}$ | Cabin outlet mass flow rate | Kg/s |
| $\dot{M}_{c2}$ | VCM evaporator outlet mass flow rate (cabin air) | Kg/s |
| $\dot{M}_{c3}$ | CH outlet mass flow rate (cabin air) | Kg/s |
| $\dot{m}_{ci}$ | ACM compressor inlet mass flow rate, see $\dot{M}_2$ | kg/s |
| $\dot{m}_{co}$ | ACM compressor outlet mass flow rate, see $\dot{M}_3$ | kg/s |
| $\dot{m}_h$ | PHX outlet mass flow rate, see $\dot{M}_2$ | kg/s |
| $\dot{m}_h$ | Hot fluid mass flow rate | kg/s |
| $m_h$ | Hot side exposed edge area | m |
| $\dot{m}_r$ | Required mass flow rate per passenger | kg/s |
| $\dot{m}_t$ | Total required mass flow rate | kg/s |
| $\dot{M}_{tc}$ | Cooling unit (ACM or VCM) mass flow rate | kg/s |
| $\dot{M}_{th}$ | Heating unit (CH, EGH, bleed air) mass flow rate | kg/s |
| $\dot{m}_{ti}$ | ACM turbine inlet mass flow rate, see $\dot{M}_7$ | kg/s |
| $N$ | Day of year | Dimensionless |
| $n$ | Nusselt ratio method correlation | Dimensionless |
| $N_1$ | Number of crew members into the cockpit | Dimensionless |
| $N_2$ | Number of occupants into the cabin | Dimensionless |
| $N_b$ | Floor number of beams | Dimensionless |
| $N_f$ | Total Number of fins | Dimensionless |
| $N_{fp}$ | Number of fin passages | Dimensionless |
| $N_g$ | Grashof number | Dimensionless |
| $N_{nu}$ | Heat load analysis Nusselt number | Dimensionless |
| $N_p$ | Prandtl number | Dimensionless |
| $NTU$ | Number of Transfer Units | Dimensionless |
| $N_{uc}$ | Exchanger Nusselt number of the cold fluid | Dimensionless |
| $N_{uc}'$ | Cold side Nusselt number for constant fluid properties | Dimensionless |
| $N_{uh}$ | Exchanger Nusselt number of the hot fluid | Dimensionless |
| $N_{uh}'$ | Hot side Nusselt number for constant fluid properties | Dimensionless |
| $o$ | friction factor ratio method correlation | Dimensionless |
| $P_1$ | Engine bleed air pressure, PHX inlet pressure | Pa |

| | | |
|---|---|---|
| $P_{1a}$ | SHX ram air inlet pressure | Pa |
| $P_{1d}$ | VCM evaporator inlet pressure (Refrigerant) | Pa |
| $P_{1e}$ | EGH inlet pressure (exhaust gas) | Pa |
| $P_2$ | PHX outlet pressure | Pa |
| $P_{2a}$ | PHX ram air inlet pressure | Pa |
| $P_{2d}$ | VCM compressor inlet pressure (Refrigerant) | Pa |
| $P_{2e}$ | EGH outlet pressure (exhaust gas) | Pa |
| $P_3$ | ACM compressor outlet pressure | Pa |
| $P_{3a}$ | PHX ram air outlet pressure | Pa |
| $P_{3d}$ | VCM condenser inlet pressure (Refrigerant) | Pa |
| $P_4$ | ACM reheater (high pressure) inlet pressure | Pa |
| $P_{4a}$ | Evaporator ram air pressure (VCM) | Pa |
| $P_{4d}$ | VCM expansion valve inlet pressure (Refrigerant) | Pa |
| $P_5$ | ACM condenser (high pressure) inlet pressure | Pa |
| $P_{5a}$ | EGH ram air outlet pressure | Pa |
| $P_6$ | ACM reheater (low pressure) inlet pressure | Pa |
| $P_7$ | ACM turbine inlet pressure | Pa |
| $P_8$ | ACM turbine outlet pressure | Pa |
| $P_9$ | ACM total pressure | Pa |
| $P_{ba}$ | Bleed air pressure | Pa |
| $P_{c1}$ | Atmospheric pressure | Pa |
| $P_{c1}$ | Cabin outlet pressure | Pa |
| $P_{c2}$ | VCM evaporator outlet pressure (cabin air) | Pa |
| $P_{c3}$ | CH outlet pressure (cabin air) | Pa |
| $P_e$ | Electrical power | kVA |
| $P_{ef}$ | Power factor | Dimensionless |
| $P_f$ | Fin pitch | m |
| $P_l$ | Louver pitch | m |
| $P_r$ | Heat exchanger Prandtl number of the fluid | Dimensionless |
| $P_{rc}$ | Compressor pressure ratio | Dimensionless |
| $P_t$ | Tube pitch | m |
| $P_{tc}$ | Cooling unit pressure | Pa |
| $P_{th}$ | Heating unit pressure | Pa |
| $Q$ | Total heat load | W |
| $q_1$ | Transparency heat transfer | W |

| | | |
|---|---|---|
| $q_2$ | Wall (un-insulated) heat transfer | W |
| $q_3$ | Wall (insulated) heat transfer | W |
| $q_4$ | Floor heat transfer | W |
| $q_{4a}$ | Floor wall heat transfer | W |
| $q_{4b}$ | Beam heat transfer | W |
| $q_5$ | Ceiling heat transfer | W |
| $q_6$ | Bulkhead heat transfer | W |
| $q_7$ | Cockpit total metabolic heat gain | W |
| $q_8$ | Cabin total metabolic heat gain | W |
| $q_{as}$ | Floor air space heat transfer | W |
| $q_b$ | Beam heat transfer | W |
| $Q_c$ | Convection heat load | W |
| $Q_e$ | Electrical heat load | W |
| $Q_{hx}$ | Heat transfer rate | W |
| $Q_i$ | Infiltration heat load | W |
| $Q_k$ | Conduction heat load | W |
| $Q_o$ | Occupant heat load | W |
| $Q_{oe}$ | Heat gain | W |
| $Q_r$ | Radiation heat load | W |
| $Q_s$ | Solar heat load | W |
| $Q_{tc}$ | Cooling unit heat load | W |
| $Q_{th}$ | Heating unit heat load | W |
| $r$ | Recovery coefficient | Dimensionless |
| $R_1$ | Hot side fouling resistance | W |
| $R_2$ | Cold side fouling resistance | W |
| $R_c$ | Cold side film convection resistance | W |
| $R_{ec}$ | Reynolds number from cold side | Dimensionless |
| $R_{eh}$ | Reynolds number from hot side | Dimensionless |
| $R_{fc}$ | Cold side fouling resistance | $m^2K/W$ |
| $R_{fh}$ | Hot side fouling resistance | $m^2K/W$ |
| $R_h$ | Hot side film convection resistance | W |
| $r_h$ | Hydraulic radius | m |
| $R_w$ | Wall thermal resistance | W |
| $T$ | Static temperature | K |
| t | Total increase of thermal transmittance | Dimensionless |

| | | |
|---|---|---|
| $T'_{as}$ | Assumed beam sides temperature | K |
| $T'_{hi}$ | Assumed inlet temperature from the exchanger hot side | K |
| $T'_{ho}$ | Assumed outlet temperature from the exchanger hot side | K |
| $T_1$ | PHX inlet temperature | K |
| $T_{1a}$ | SHX ram air inlet temperature | K |
| $T_{1d}$ | VCM evaporator inlet temperature (Refrigerant) | K |
| $T_{1e}$ | EGH inlet temperature (exhaust gas) | K |
| $T_{1i}$ | Temperature of the insulation material | K |
| $T_2$ | ACM compressor inlet temperature | K |
| $T_{2a}$ | PHX ram air inlet temperature | K |
| $T_{2e}$ | EGH outlet temperature (exhaust gas) | K |
| $T_{2w}$ | Internal surface wall temperature | K |
| $T_3$ | ACM compressor outlet temperature | K |
| $T_{3a}$ | PHX ram air outlet temperature | K |
| $T_{3d}$ | VCM condenser inlet temperature (Refrigerant) | K |
| $T_4$ | ACM reheater (high pressure) inlet temperature | K |
| $t_4$ | Floor total increase of thermal transmittance | Dimensionless |
| $T_{4a}$ | Evaporator ram air temperature (VCM) | K |
| $T_{4d}$ | VCM expansion valve inlet temperature (Refrigerant) | K |
| $T_{4d}$ | VCM expansion valve inlet temperature (Refrigerant) | K |
| $T_5$ | ACM condenser (high pressure) inlet temperature | K |
| $t_5$ | Ceiling total increase of thermal transmittance | Dimensionless |
| $T_{5a}$ | EGH ram air outlet temperature | K |
| $T_6$ | ACM reheater (low pressure) inlet temperature | K |
| $t_6$ | Bulkhead total increase of thermal transmittance | Dimensionless |
| $T_7$ | ACM turbine inlet temperature | K |
| $T_8$ | ACM turbine outlet temperature | K |
| $T_9$ | ACM condenser (low pressure) outlet temperature | K |
| $t_\infty$ | Outlet temperature | K |
| $T_{as}$ | Beam sides temperature | K |
| $T_{ba}$ | Bleed air temperature | K |
| $T_c$ | Cabin desired temperature | K |
| $T_{c1}$ | Cabin outlet temperature | K |
| $T_{c2}$ | VCM evaporator outlet temperature (cabin air) | K |
| $T_{c3}$ | CH outlet temperature (cabin air) | K |

| | | |
|---|---|---|
| $T_{cc}$ | CH chamber temperature | K |
| $T_{ci}$ | Inlet temperature from the exchanger cold side | K |
| $T_{co}$ | Outlet temperature from the exchanger cold side | K |
| $T_{ec}$ | External ceiling temperature | K |
| $T_H$ | VCM refrigerant (R11) saturation temperature | K |
| $T_{hi}$ | Inlet temperature from the exchanger hot side | K |
| $T_{ho}$ | Outlet temperature from the exchanger hot side | K |
| $t_i$ | Increase of thermal transmittance | Dimensionless |
| $T_{ic}$ | Cabin inlet temperature | K |
| $T_M$ | Maximum ducts surface temperature | K |
| $T_{mc}$ | Absolute mean temperature from the cold side | K |
| $T_{mc}'$ | Mean temperature on the cold side | K |
| $T_{mh}$ | Absolute mean temperature from the hot side | K |
| $T_{mh}'$ | Mean temperature on the hot side | K |
| $T_r$ | Recovery temperature | K |
| $t_s$ | Inlet temperature | K |
| $t_{s1}$ | Inlet temperature | K |
| $t_{s2}$ | Outlet temperature | K |
| $T_s^4$ | Absolute surface temperature | K |
| $T_{tc}$ | Cooling unit temperature | K |
| $T_{th}$ | Heating unit temperature | K |
| $T_w$ | Skin temperature | K |
| $T_{wa}$ | Weighted average temperature | K |
| $T_{wc}$ | Absolute wall temperature from the cold side | K |
| $T_{wg}$ | Skin temperature on ground | K |
| $T_{wh}$ | Absolute wall temperature from the hot side | K |
| $TZ$ | Time zone | Dimensionless |
| $u$ | Wall surface and beam unit heat load | $W/m^2$ |
| $U_1$ | Overall heat transfer coefficient of transparency area | $W/m^2$ |
| $U_2$ | Overall heat transfer coefficient of un-insulated wall area | $W/m^2$ |
| $U_3$ | Overall heat transfer coefficient of insulated wall area | $W/m^2$ |
| $U_4$ | Overall heat transfer coefficient of floor area | $W/m^2$ |
| $U_5$ | Overall heat transfer coefficient of ceiling area | $W/m^2$ |
| $U_6$ | Overall heat transfer coefficient of bulkhead area | $W/m^2$ |
| $UA_{hx}$ | Overall differential thermal resistance | W |

| | | |
|---|---|---|
| $U_B$ | Overall heat transfer from external surface to bottom beam | $W/m^2$ |
| $U_f$ | Overall heat transfer coefficient of the floor film | $W/m^2$ |
| $U_{hx}$ | Heat exchanger overall heat transfer coefficient | $W/m^2$ |
| $U_{k1}$ | Overall heat transfer from external surface to air space | $W/m^2$ |
| $U_{k2}$ | Overall heat transfer from internal surface to air space | $W/m^2$ |
| $U_T$ | Overall heat transfer from internal surface to top beam | $W/m^2$ |
| $V_b$ | Air velocity through floor beams | m/s |
| $V_e$ | External wind velocity | m/s |
| $V_i$ | Internal air velocity | m/s |
| $w$ | Infiltration rate | kg/s |
| $W_c$ | Core width | m |
| $W_t$ | Tube width | m |
| $x$ | Surface thickness | m |
| $X_a$ | Air space width | m |
| $X_f$ | Fin thickness | m |
| $x_i$ | Insulation material thickness | m |
| $x_w$ | Wall material thickness | m |
| $Y$ | Vertical surface calculation | Dimensionless |
| $\Delta p$ | Heat exchanger Total pressure drop | Pa |
| $\Delta p_{1\text{-}2}$ | Heat exchanger pressure drop at the core entrance | Pa |
| $\Delta p_{2\text{-}3}$ | Heat exchanger pressure drop within the core | Pa |
| $\Delta p_{3\text{-}4}$ | Heat exchanger pressure rise at the core exit | Pa |
| $\Delta p_c$ | Heat exchanger pressure drop in the cold side | Pa |
| $\Delta p_h$ | Heat exchanger pressure drop in the hot side | Pa |
| $\Delta T$ | Temperature difference | K |
| $\Delta T_2$ | Rotorcraft maximum allowable temperature difference | K |
| $\Delta T_3$ | Cockpit maximum allowable temperature difference | K |
| $\Delta T_4$ | Cabin maximum allowable temperature difference | K |
| $\Delta T_a$ | Air space temperature difference | K |
| $\Delta T_{lm}$ | Log-mean temperature difference | K |
| $\Delta T_{t1}$ | Terminal temperature difference | K |
| $\Delta T_{t2}$ | Terminal temperature difference | K |

| | | |
|---|---|---|
| $\alpha$ | Fraction of solar radiation absorbed | Dimensionless |
| $\beta$ | Solar altitude | deg |
| $\Gamma$ | Equation of time variable | Dimensionless |
| $\gamma$ | Ratio of specific heat | Dimensionless |
| $\gamma_s$ | Surface-solar azimuth | deg |
| $\delta$ | Solar declination | deg |
| $\delta_w$ | Heat exchanger fin thickness | m |
| $\varepsilon$ | Surface emissivity | Dimensionless |
| $\varepsilon'_{hx}$ | Assumed Heat exchanger effectiveness | Dimensionless |
| $\varepsilon_{hx}$ | Heat exchanger effectiveness | Dimensionless |
| $\varepsilon_{vc}$ | Condenser and vaporizer effectiveness | Dimensionless |
| $\eta_b$ | Beam effectiveness | Dimensionless |
| $\eta_c$ | Compressor efficiency | Dimensionless |
| $\eta_{fc}$ | Cold side fin efficiency | Dimensionless |
| $\eta_{fh}$ | Hot side fin efficiency | Dimensionless |
| $\eta_{oc}$ | Overall surface effectiveness for the cold side | Dimensionless |
| $\eta_{oh}$ | Overall surface effectiveness for the hot side | Dimensionless |
| $\theta$ | Incident angle | deg |
| $\theta_l$ | Louver angle | deg |
| $\mu$ | Dynamic viscosity of air | Pa·s |
| $\mu_c$ | Cold fluid dynamic viscosity | Pa·s |
| $\mu_h$ | Hot fluid dynamic viscosity | Pa·s |
| $\rho$ | Air density | $kg/m^3$ |
| $\rho_{ci}$ | Inlet fluid density from the cold side | $kg/m^3$ |
| $\rho_{co}$ | Outlet fluid density from the cold side | $kg/m^3$ |
| $\rho_g$ | Ground reflectance | Dimensionless |
| $\rho_{hi}$ | Inlet fluid density from the hot side | $kg/m^3$ |
| $\rho_{ho}$ | Outlet fluid density from the hot side | $kg/m^3$ |
| $\sigma$ | Stefan-Boltzmann constant | $W/m^2$ |
| $\Sigma$ | Tilt angle | deg |
| $\tau_b$ | Beam optical depth | Dimensionless |
| $\tau_d$ | Diffuse optical depth | Dimensionless |
| $\phi$ | Angular difference | deg |
| $\psi$ | Aircraft surface azimuth | deg |

## List of Abbreviations

| | |
|---|---|
| ACARE | Advisory Council for Aeronautics Research in Europe |
| ACM | Air Cycle Machine |
| AST | Apparent solar time |
| ATTMO | Transient Thermal Modelling and Optimization |
| BACM | Bleed Air Cycle Machine |
| C | Convection |
| CAU | Cold Air Unit |
| CFD | Computational Fluid Dynamics |
| CH | Combustion Heater |
| COP | Coefficient of Performance |
| DME | Distance Measuring Equipment |
| EASA | European Aviation Safety Agency |
| ECS | Environmental Control System |
| EEH | Electric Element Heater |
| EGH | Exhaust Gases Heater |
| EPACM | Electrically Powered Air Cycle Machine |
| ISA | International Standard Atmosphere |
| ITD | Integrated Technology Demonstrator |
| K | Conduction |
| LAT | Aircraft latitude |
| LON | Aircraft longitude |
| LSM | Longitude of local standard time |
| LST | Local standard time |
| MCR | Matlab Compiler Runtime |
| NLR | National Aerospace Laboratory |
| PCM | Power Consumption Model |
| PHX | Primary Heat Exchanger |
| PID | Proportional Integral Derivative |
| R | Radiation |
| RMEM | Rotorcraft Mission Energy Management |
| SHX | Secondary Heat Exchanger |
| TACAN | Tactical Air Navigation system |
| TE | Technology Evaluator |

| | |
|---|---|
| VCM | Vapour Cycle Machine |
| VOR | VHF Omnidirectional Radio Range |
| VORTAC | VOR Tactical air navigation system |
| VRP | Visual Reference Point |

# 1. Chapter | Introduction

## 1.1. Background of the project

Helicopters are playing an increasingly important role in different activities such as search and rescue or law enforcement among others. Additionally, a rapid increase in use of helicopters for air transport has been shown between cities and locations which are difficult to access, without the need for a large infrastructure. This increase in rotary aircraft use is contributing to aviation's detrimental environmental impact by emitting polluting gases into the environment, largely generated by burning fuel. The fast acquisition and need for helicopters in the aeronautical industry, has generated great interest within the air transport and aircraft community to optimize the emissions of their rotorcraft, in order to reduce fuel consumption and therefore reduce toxic emissions and operating costs [5].

A medium-term solution would be to optimize the power consumption of onboard systems. Currently, an aircraft includes an environmental control system within its systems; the ECS allows the control of the environment within the cabin and flight deck for pilot and passenger comfort, and to protect them from weather conditions; as high and low temperatures can cause loss of consciousness in the pilot as was shown by Lind and Leithead (1964), and Rivolier (1988). These circumstances could result in fatal accidents that put at risk the integrity of the people inside the airplane or helicopter. The environmental control system commonly utilizes engine compressor bleed air for its operation, by reducing the bleed air temperature and controlling it for human comfort and the avionics equipment. This optimal air is then distributed over the entire aircraft.

Current ECS have three main types of cooling sub-systems: the Bleed Air Cycle Machine (BACM), Electrically Powered Air Cycle Machine (EPACM), and Vapour Cycle Machine (VCM); and three types of sub-systems for heating purposes: the Combustion Heater (CH), Electric Element Heater (EEH), and Exhaust Gases Heater (EGH); alternatively a direct hot Bleed Air configuration can be used [7].

In fixed-wing aircraft the air cycle refrigeration system is currently the most widely used because of its effectiveness in temperature and pressurisation control, integration functionality with new systems, and low penalty weight on the aircraft during all phases of

flight. On the other hand, it is not required in rotary-wing aircraft to have a pressurised environment thereby the Combustion Heater or the direct Bleed Air are most commonly used for heating purposes; and the Vapour Cycle Machine for cooling purpose. However, most helicopters are equipped with an afterthought air-conditioning system design; in other words, the ECS used is not analysed in detail with other existing sub-systems. For this reason, the aircraft may suffer from additional weights and required power, which leads to an increase in fuel consumption, and waste of energy, hence, in order to avoid those penalties it is necessary to conduct an analysis including different air-conditioning packs. This involves the use of different ECS sub-system models to compare and choose the most efficient for a given aircraft. Furthermore, thermal comfort levels will be studied thus avoiding heat stress for people on board, and controlling the temperature of the avionics equipment.

To this end, the efficiency of the Environmental Control Systems and the aircraft thermal comfort were both studied on a civil rotatory-wing aircraft, the Bell 206L-4. Likewise, a survey of the ECS installed on different operating aircraft was conducted and two air-conditioning packs were chosen for a deeper analysis, the air cycle machine and the Vapour Cycle Machine. Similarly in this study heat loads within the cabin, and the various stages of flight have been taken into account.

At the same time, simulations have been generated to help in the optimization process of the environmental control system. Matlab-Simulink® framework was used to model the air-conditioning system.

This research is funded by Cleansky, a project of the European Commission for funding research in Europe.

## 1.2. Aim and objectives

The main objective of this project is to obtain the ECS power consumption for a given mission and aircraft specification. To this end, the efficiency of the different Environmental Control Systems for cooling and heating purposes, and the aircraft thermal comfort were studied in a civil rotatory-wing aircraft, the Bell 206L-4. Likewise, a survey of the ECS installed on different operating aircraft was conducted; additionally, this study takes into

account heat loads within the cabin in the various stages of flight.

Furthermore, multiple simulations were generated to help in the optimization process of the environmental control system. Matlab-Simulink® was used to model the air-conditioning system and subsystems. This research project intends to develop a computed model which can then be used to compare the effectiveness (power consumption) of multiple Environmental Control System configurations for a given mission and aircraft. Therefore, the following research question is to be addressed:

- Could a generic simulation model be created to numerically predict the power requirements of different cooling and heating ECSs found on different modern aircraft?

To achieve the aim mentioned above, the following specific objectives of the project have been identified:

- Environmental Control Systems baseline modelling.
  - Air Cycle Machine System baseline modelling.
  - Vapour Cycle Machine System baseline modelling.
  - Combustion Heater System baseline modelling.
  - Exhaust Gases Heater System baseline modelling.
- Definition of aircraft sizes and components.
  - Definition of Bell 206L-4 areas.
  - Definition of exchanger areas.
  - Definition of cooling unit configurations.
  - Definition of heating unit configurations.
- Calculations and modelling of cockpit and cabin heat loads.
  - Calculations and modelling of external areas.
  - Calculations and modelling of internal areas.
  - Calculations and modelling of transparent areas.
- Calculations and modelling of Cooling and Heating sub-systems.
- ECS Models integration and calculation of required power.

## 1.3. Structure of the thesis

This report is divided into six chapters: Chapter one presents a brief explanation of the project content, its background, objectives and methodology. The specifications of the aircraft and major requirements for the analysis of the ECS are given in chapter two. This chapter also includes different research methods used by other authors for ECS modelling. Additionally, this chapter gives a detailed explanation of the sub-systems, components, and operational conditions taken into consideration for this project.

Chapter three provides a general description of the equations and methods used to develop the computational model and all its contents. A chart description of the input and output data needed during the modelling process is also included in this section. Chapter four contains the development of the model in further detail, including the mathematical analysis, and specifications of the ECS. Section four describes the chosen rotorcraft and the selected mission, while also defining the parameters needed for the calculation of the systems, subsystems and components.

The results of the separate systems models and the integrated model are given in Chapter five. The produced results include the analysis of the cabin heat model, the cooling units' model, the heating units' model and the outputs of the integrated model (pneumatic power requirements and Coefficient of Performance). Chapter 6 consists of a general conclusions, findings, recommendations, and future work for the present research document.

## 1.4. Method

A literature review has been conducted in order to have a clearer view of the current state of the environmental control system and sub-systems in aircraft. Furthermore, this information allowed different equations, methods and models to be obtained as well as the dimensions of the aircraft and materials to be determined; the data acquired thereby was instrumental to the completion of this research. The methodological framework employed is illustrated in the following figure.

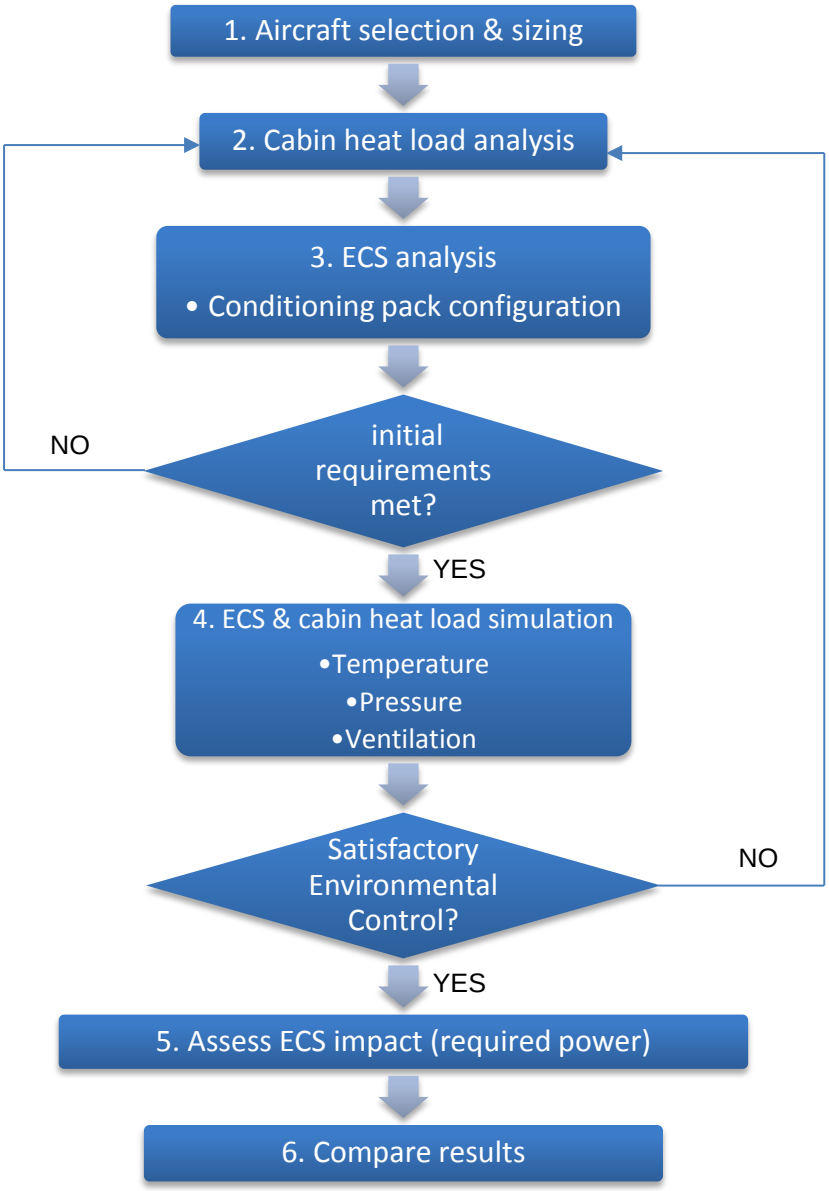


**Figure 1-1 Methodological framework**

The developed model allows setting the aircraft type by entering in the model the area of the studied components (e.g. windows and walls); therefore the first step is to set these parameters, for this study the Bell 206L-4 areas were established. After setting the aircraft configuration, a mathematical model was generated and heat loads inside the aircraft simulated. This analysis takes into account the temperature of different heat sources. Among these sources are those generated by the human body, the avionics, and the structure of the aircraft. These were calculated using thermodynamic equations of heat transfer. This model

also provides the required temperature in the aircraft for an optimal environment and gives the initial data for the study of the environmental control systems.

The next step was the modelling and integration of different existing air-conditioning packs for aircraft. Firstly, various configurations of sub-systems to be analysed were established, as well as their components, available measurements, and locations within the ECS. To this end a modelling program (Matlab-Simulink) was used. Following this, the required temperatures and pressures were obtained at each stage of the ECS. And finally, an on-board aircraft heat balance was performed taking into account the mass flow, heat loads, and temperatures of each of the sub-systems previously modelled.

Finally the integrated model of the different air-conditioning packs for the Environmental Control System was verified against the certification specifications for small rotorcraft CS27 [10]. Furthermore, the results were compared with results obtained in different papers, thesis and books such as SAE Aerospace [23]. Moreover, the validity of this model will be supported by a dynamic analysis.

# 2. Chapter | Literature Review

## 2.1. Clean Sky Project

Clean Sky is an aeronautical research program implemented in Europe. Its mission is to create new technologies that improve the environmental performance of aircraft and air transport, reducing noise emissions and increasing fuel consumption efficiency; therefore achieving greener designs for environmental protection. The Clean Sky initiative began in 2008 and represents a public-private joint initiative between the European Commission and industry. The developed technologies have been integrated into Clean Sky 6 Demonstrators or ITD (Integrated Technology Demonstrators) and the Technology Evaluator, as shown in Figure 2-1. Each ITD is led and funded by two industry leaders among others: Airbus and Rolls- Royce. Cranfield University is one of the active members of the Systems for Green Operation (SGO) and the Technology Evaluator (TE), the latter being responsible for developing, implementing and evaluating different simulations of the technologies developed by Clean Sky.


**Figure 2-1 Clean Sky project framework [27]**

### 2.1.1. Technology Evaluator (TE)

The Technology Evaluator is responsible for assessing the environmental impact and overall benefits of the innovations developed by Clean Sky. Their impact will be estimated based on emissions, noise and fuel consumption as quality indicators of the on-board energy management. For this purpose, two scenarios with and without the use of the technology developed by Clean Sky will be compared to the ACARE (Advisory Council for Aeronautics Research in Europe) environmental objectives [28]. Comparisons are made over a single flight mission, starting between Local airports; and then applied to global air transport.

The Technology Evaluator established in Cranfield University has developed a simulation platform called PHOENIX in order to achieve greener technologies for rotorcraft platforms; this tool includes different models (Engine Performance, Energy Management, Emission, etc.). PHOENIX is used for mission-level analysis, providing the necessary outputs for the estimation of rotorcraft performance.

The research presented in this report will be paramount for the optimization of the current PHOENIX tool, specifically in relation to the Environmental Control System. This model is part of the Rotorcraft Mission Energy Management (RMEM) model which is responsible for predicting the power requirements of the rotorcraft systems.

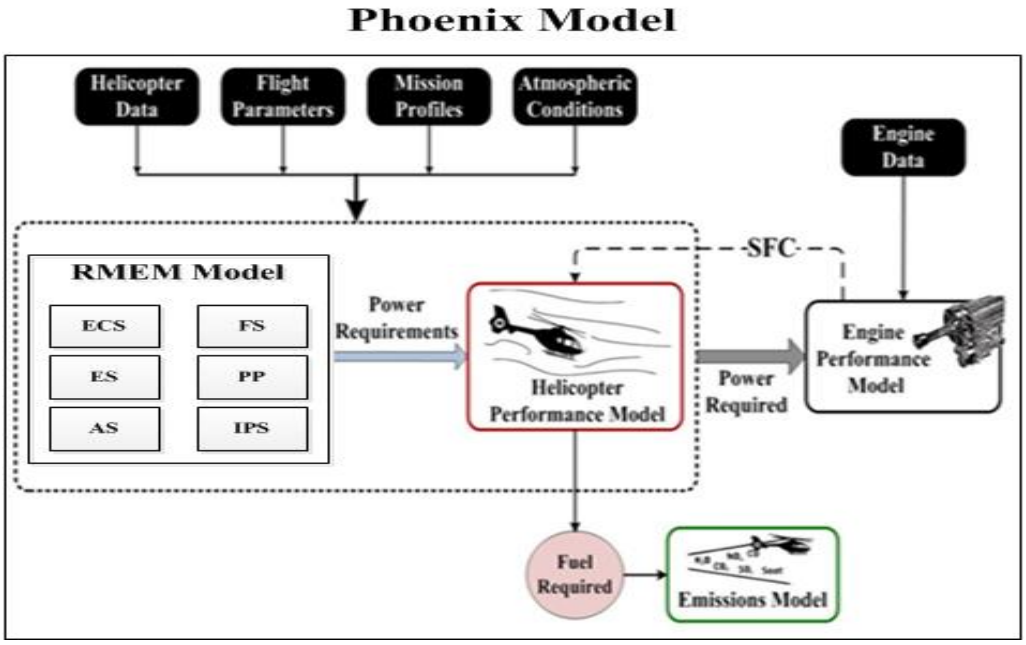


**Figure 2-2 PHOENIX platform model [29]**

## 2.2. Bell 206L-4 specifications

Nowadays, the needs of global aviation are rapidly increasing and with them the economic concern, and environmental awareness that they infer. Air transport is 96% dependent on petroleum fuels, but in the recent years its cost and therefore also operating costs have been increasing. Furthermore, the use of this fuel is damaging to the environment as it increases the global greenhouse gas emission. CleanSky, a European Commission for funding research in Europe, was created in response to these arising problems. Its purpose is to improve the cost-effective energy efficiency on all types of aircraft [5]. To this end, the Bell 206L-4 was identified by CleanSky as a potential aircraft to be improved because of its characteristics as a light-rotorcraft, commonly used in air transport, and also due to the large amount of information available regarding this aircraft necessary to this research. The aircraft's general specifications are given below.

**Table 2-1 Bell 206L-4 general specifications**

| Specification | | Unit |
|---|---|---|
| Standard Configuration Weight | 1057 | kg |
| Normal Gross Weight | 2018 | kg |
| Useful Load | 962 | kg |
| Fuel Capacity | 335 | kg |
| Maximum Cruise Speed | 57.5 | m/s |
| Maximum Endurance | 14760 | s |
| Range | 600000 | m |
| Cabin Volume | 2.3 | $m^3$ |
| Baggage Compartment Volume | 0.45 | $m^3$ |
| Powerplant | 541000 (Rolls-Royce 250-C30P) | W |
| Side walls area | 4.14 | $m^2$ |
| Bottom floor area | 2.6 | $m^2$ |
| Top roof area | 2.4 | $m^2$ |
| Windscreen area | 3.6 | $m^2$ |
| Rear bulkhead | 1.3 | $m^2$ |
| Seating capacity | 7 | ----- |

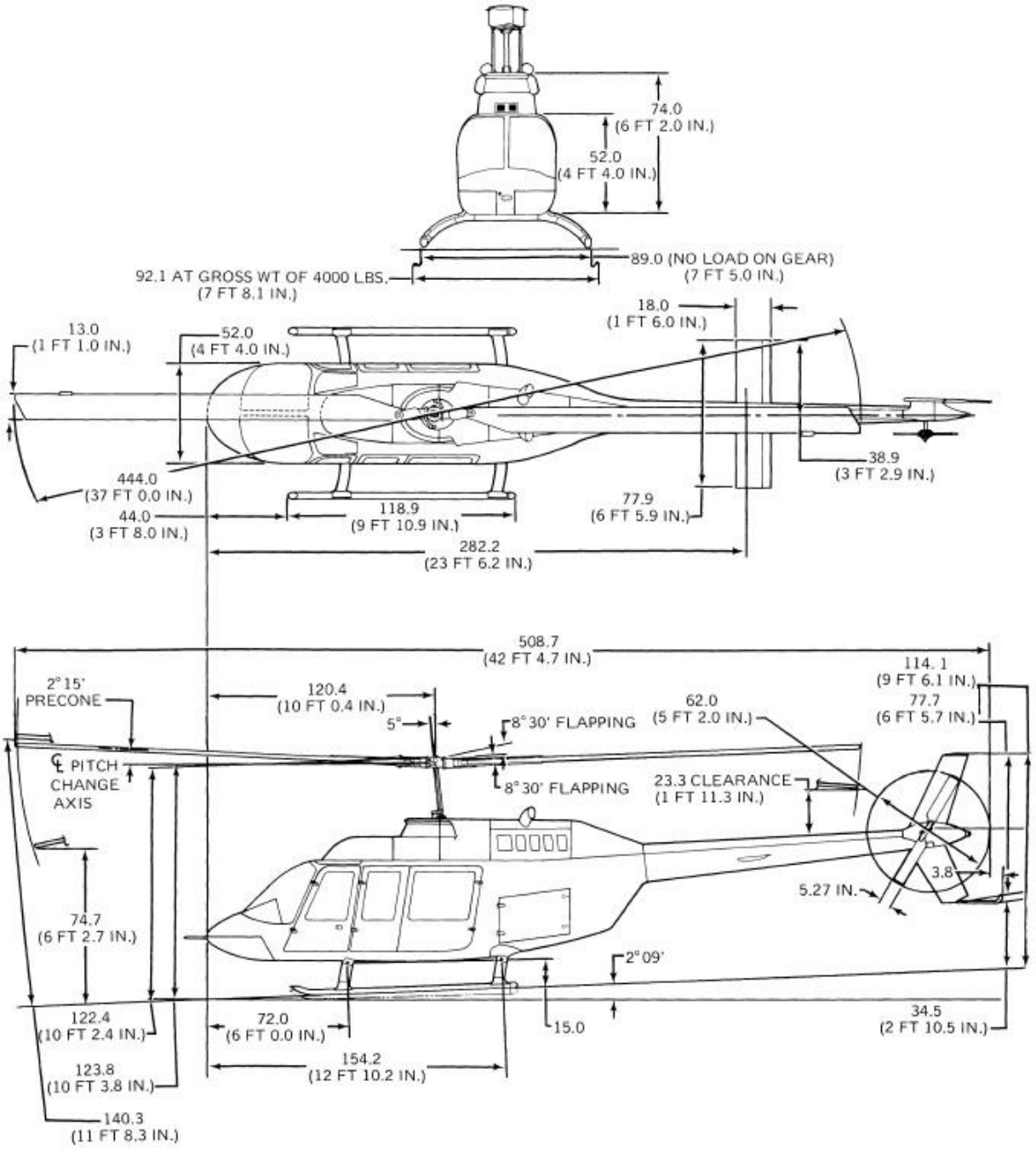


**Figure 2-3 Bell 206L-4 dimensions [4]**

## 2.3. Environmental Control System

The environmental control system is responsible for maintaining the temperature and humidity in an aircraft at a required level; see Sections 2.4 and 2.5. These conditions are determined by the task performed in each area of the vehicle, whether electrical, mechanical or human. Currently, global aviation tends to operate at higher altitudes or in extreme weather conditions, hence causing changes in temperature inside the aircraft. The ECS maintains comfort levels thus avoiding heat stress to people on board, and optimizing the temperature of the avionics equipment.

For many years, the concept of ECS in helicopters has been of little concern at the time of its design, leading engineers to retro-fit the ECS into an already designed infrastructure. For this reason and for its extensive use in other fixed-wing aircraft, the air cycle machine subsystem is commonly used in helicopters. However, helicopter engines have not been designed to bleed air while in use of its full power; this would cause high fuel consumption and power reduction in the engine of the helicopter.

Nowadays, many designers incorporate a vapor cycle machine subsystem in their rotary-wing aircraft designs. Unlike the ACM, VCM is used only for cooling purposes and not for heating. Table 2-2 shows the advantages and disadvantages of the Air Cycle Machine and the Vapour Cycle Machine. A separate subsystem is required to provide aircraft heating; internal combustion heaters, exhaust gas heaters, bleed air, or electric element heaters can be used for this purpose.

**Table 2-2 Characteristics of the Environmental Control subsystems**

| | ACM | VCM |
|---|---|---|
| Advantages | Lighter system weight | High coefficient of performance |
| | High fresh air-to-recirculation air ratios | Low fresh air-to-recirculation air ratios |
| | Direct supply of compressed air for ventilation and air conditioning | High ground cooling capacity |
| | Provides conditioned air for cooling and heating purposes | |
| Disadvantages | Low coefficient of performance | Heavier system weight |
| | Low ground cooling capacity | Only provides conditioned air for cooling purposes |
| | High impact on specific fuel consumption | Separated subsystems must be provided for heating |
| | | Used of toxic refrigerant |

**Table 2-3 Helicopter ECS registered in the United Kingdom [1, 15]**

| United Kingdom Helicopter registration | | | | | |
|---|---|---|---|---|---|
| Helicopter Type | Light single-Turbine | Light Twin-Turbine | Quantity | Market | ECS |
| Augusta A 109 | | x | 35 | Civil | Bleed air heater (optional) |
| Bell 206 JetRanger | x | | 129 | | Bleed air heater (optional) |
| Bell 206L LongRanger | x | | 18 | | Bleed air heater (optional) |
| Bell 407 | x | | 1 | | Vapour cycle machine (optional) |
| Enstrom 480 | x | | 17 | | Vapour cycle machine (optional) |
| Eurocopter EC 120B Colibri | x | | 18 | | Vapour cycle machine (optional) |
| Eurocopter (MBB) BO 105 | | x | 17 | | Bleed air and electrical heater (optional) |
| Eurocopter AS 350 Ecureuil | x | | 35 | | Vapour cycle machine (optional) |
| Eurocopter AS 350 Ecureuil II | | x | 63 | | Vapour cycle machine (optional) |
| Eurocopter EC 135 | | x | 31 | | Vapour cycle machine (optional) |
| Hiller UH-12ET | x | | 1 | | Bleed air heater (optional) |
| Hughes MD 500 (369) | x | | 22 | | Vapour cycle machine (optional) |
| MD 500E (369) | x | | 17 | | Vapour cycle machine (optional) |
| MD 520N | x | | 1 | | Vapour cycle machine (optional) |
| MD 600N | x | | 3 | | Bleed air heater (optional) |
| MD Explorer | | x | 12 | | Vapour cycle machine (optional) |
| Augusta A 109 Power | | x | 3 | Military | Bleed air heater (optional) |
| Augusta A 109A | | x | 4 | | Bleed air heater (optional) |
| Eurocopter AS 350BA Ecureuil | x | | 37 | | Vapour cycle machine (optional) |
| Eurocopter AS 355F1 Ecureuil II | | x | 4 | | Vapour cycle machine (optional) |

Table 2-3 lists a number of helicopters categorized as small rotorcraft registered in the UK. According to data compiled by Jane's Helicopter Markets and Systems (2006), the ECS is optional for helicopters. Similarly, Table 2-3 shows that the vapor cycle machine is the system being most commonly used on helicopters inside the United Kingdom.

## 2.4. Small rotorcraft regulations

One of the requirements for any aircraft is its airworthiness certification. For helicopters, integrated systems such as the Environmental Control should satisfy specific requirements to meet airworthiness certification standards. To this end, the European Aviation Safety Agency (EASA) is responsible for regulating the design of commercial helicopters for operation in Europe, under the CS-27 for small rotorcraft regulation [24]. The following table shows the applicable requirements for the ECS.

**Table 2-4 CS-27 Small rotorcraft applicable requirements**

| Certification Part | |
|---|---|
| 27.831 | Ventilation |
| 27.833 | Heaters |
| 27.859 | Heating systems |
| 27.863 | Flammable fluid fire protection |
| 27.1309 | Equipment, systems, and installations |
| 27.1461 | Equipment containing high energy rotors |

In addition to the above requirements, the following considerations from certification standards and cabin design requirements are included for the ECS analysis.

a. A comfortable level for cabin relative humidity is between 40%-60% [8], and should not exceed 65% [31].
b. For cooling environments the average temperature during flight should be of 297 K (24 ºC), and 299 K (27 ºC) for ground operations [31].
c. For heating environments required to maintain an average temperature of 297 K (24 ºC) on flight, and 294 K (21 ºC) during ground operations [31].
d. Ventilating system must provide no less than 0.005 kg/s of fresh air for each passenger and crew member [10].
e. Air movement in occupied compartments should be between 0.1 to 0.2 m/s for optimal occupant comfort [23].

## 2.5. Operational conditions

### 2.4.1. Environmental conditions

Delivering sufficient avionics cooling as well as the comfort and safety of passengers in an aircraft is essential; this involves controlling the temperature, humidity and ventilation. Temperature in an aircraft may be affected by atmospheric conditions of the mission. In cold conditions it is necessary to increase or heat the atmosphere within the cabin, while in hot climates cooling is required. In each of these scenarios, Figure 2-4, the ECS should be capable of maintaining temperature conditions inside the aircraft. For cooling environments the average temperature during flight should be of 297 K (24 ºC), and 299 K (27 ºC) for ground operations. On the other hand, heating environments required to maintain an average temperature of 297 K (24 ºC) on flight, and 294 K (21 ºC) during ground operations [31].

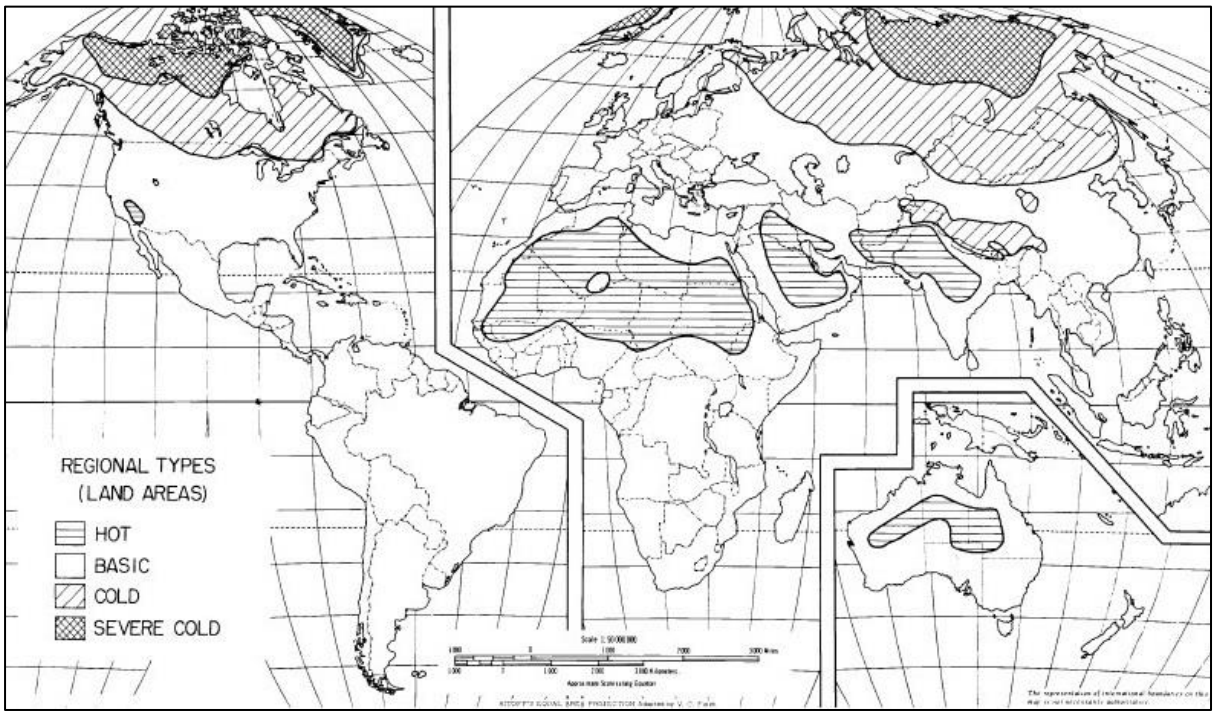


**Figure 2-4 Climatic region types in the world [59]**

The humidity or absolute humidity is the amount of water vapour contained in the air. In an aircraft this moisture is provided by perspiration and respiration of the passengers on board. The level of saturation of the air with water vapour is measured by the relative humidity, where 100% of relative humidity denotes a moisture saturated atmosphere. A comfortable

level for cabin relative humidity is considered to be between 40% and 60% [8], and should not exceed 65% [31].

The ventilation system is responsible for providing fresh air in the helicopter cabin through ambient air or conditioned air from an ECS. Its function is to prevent the presence of gases or vapours in high proportions, such as carbon monoxide and exhaust fumes. According to the European Aviation Safety Agency (EASA), the ventilating system must provide not less than 0.005 kg/s of fresh air for each passenger and crew member [10]. Additionally, the amount of carbon monoxide must be less than one part in 20,000 parts of air.

There are different sources and heat sinks to be considered when performing an analysis on the ECS. The control of air flow for heat dissipation in the system should be appropriate to the conditions that each of these sources provided within the aircraft. This study provided a significant increase in crew and passengers comfort in both, heating and cooling cases. The following are the main sources and heat sinks considered for this analysis:

- Ambient temperature
- Metabolic heat transfer
- Mechanical and electrical heat transfer
- Solar radiation
- Ventilation rate

Aircraft have many sources of air pollution such as the engines, fuel, and hydraulic fluid among others. This contaminated air has to be controlled by means of an effective ventilation to prevent unacceptable concentration levels for humans. Figure 2-5 shows the minimum airflow required per person to avoid this risks of contamination inside a helicopter as a function of the cabin's volume.

Helicopter operations for civilian use are limited to flights at heights that do not require the use of oxygen. Consequently, this project does not consider the required oxygen analysis into the aircraft.

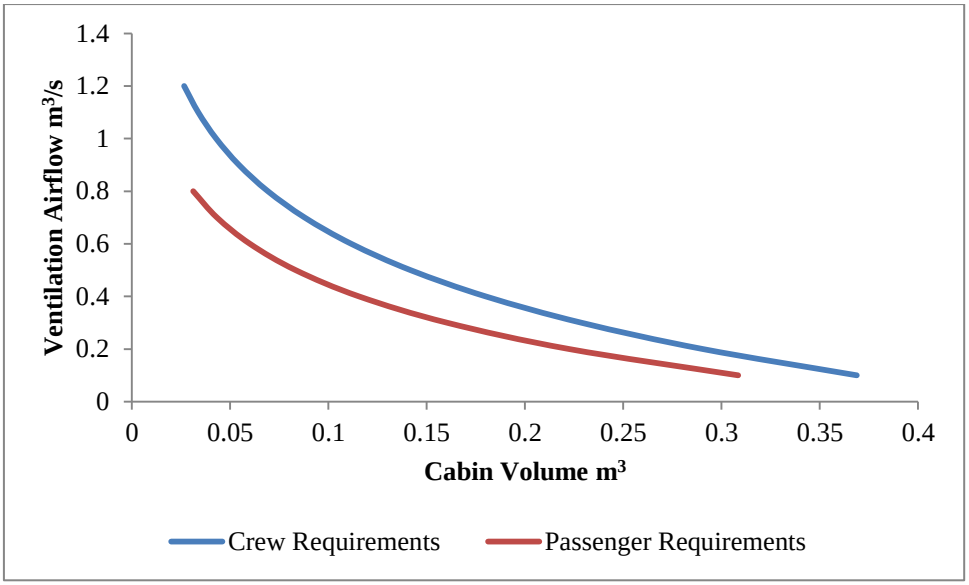


**Figure 2-5 Ventilation flow rate as a function of cabin volume [58]**

### 2.4.2. Thermal stress

The human body is constantly interacting with its surrounding environment; this interaction can lead to death if its reaction is inappropriate and above the accepted levels. The thermal environment determines whether the person is in a state of thermal stress, very hot or very cold, or is in thermal comfort.

There are six basic parameters that can affect the human body's response to the thermal environment, air temperature, radiant temperature, air movement and humidity which together define the external environment. The heat production within the body defines the internal environment of the body between the metabolic heat produced by human activities and the clothing worn by a person. The air temperature is the temperature of the air surrounding the human body, its value was taken as the average temperature inside the cabin described in Section 2.4.1.

A special consideration in the use of radiant temperature is its quality or spectral content, and directional properties. Figure 2-6 shows different wave types and its respective wavelength where the latest together with the level of radiation, changes the radiation intensity. In aircraft, the solar radiation is responsible for thermal environment effects. The level of solar radiation measured by a satellite gives a value of 1373 W/m$^2$; however, many conditions can minimize this value, such as clouds, aerosols and pollution. For instance, Figure 2-7 shows

the solar radiation in three different days with open sky conditions at Rothamsted Research, United Kingdom; at noon there was an increase in solar radiation, while in the morning and evening decreases due to the accumulation of dust in the atmosphere.

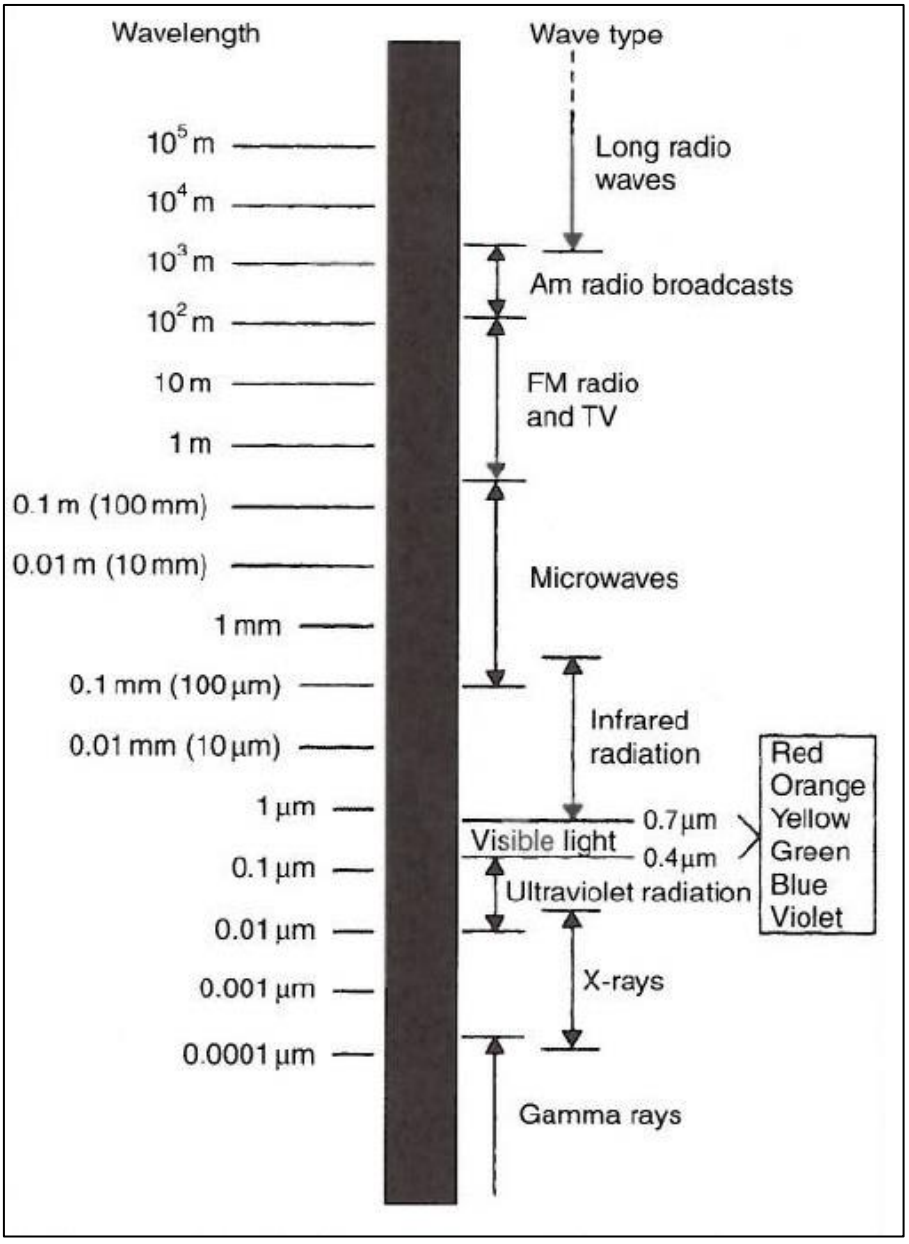


**Figure 2-6 Electromagnetic spectrum [20]**

According to Santee and Gonzalez (1998) there are three terms of solar radiation, direct, diffuse and reflected as shown in Figure 2-8 [20]. In the case of helicopters, solar radiation is transmitted to human body by transparency areas (windows and windscreen) by means of these three terms. A description of how to measure solar radiation is provided in Chapter 4.

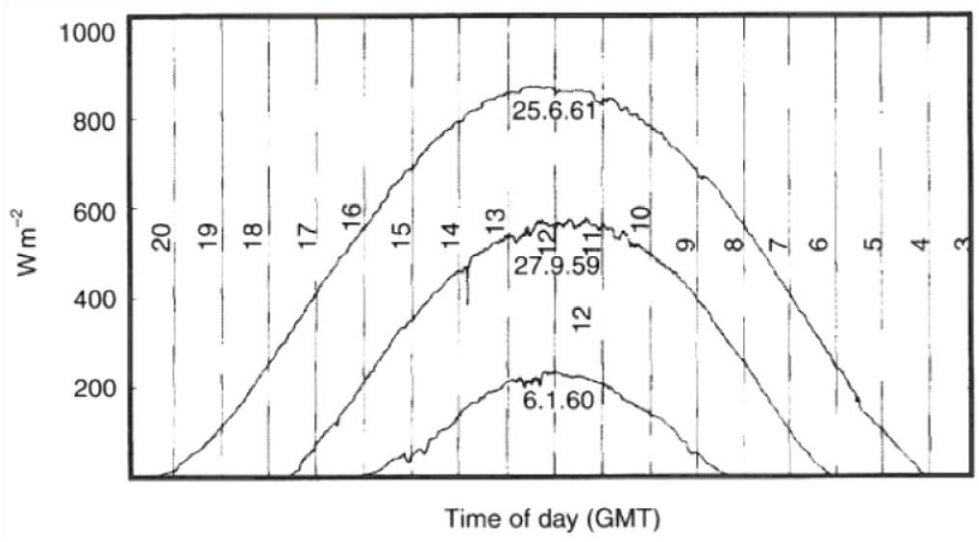


**Figure 2-7 Solar radiation [20]**

The body temperature is directly affected by the heat or vapour taken from the body, which are extracted by means of air movement in conjunction with the air temperature. According to SAE Aerospace ARP 292, for helicopters air movement in occupied compartments should not be greater than 0.3 m/s or less than 0.05 m/s, and should remain between 0.1 to 0.2 m/s for optimal occupant comfort SAE [31].

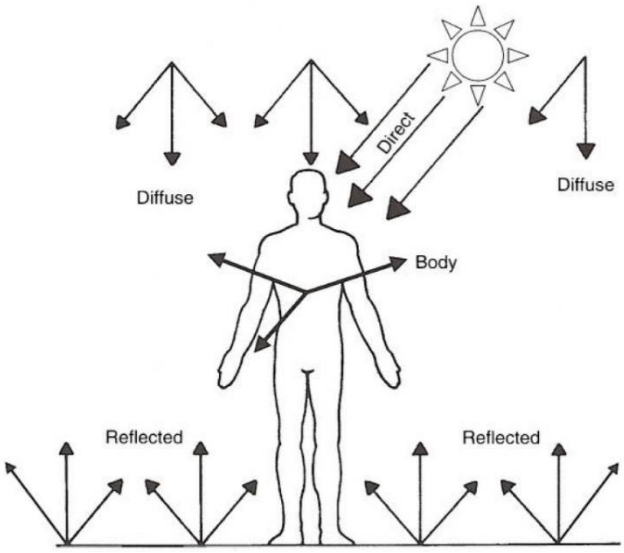


**Figure 2-8 Direct, diffuse and reflected solar radiation [20]**

One more condition that can affect the human body temperature is the humidity. Basically, heat from human body transforms sweat into vapor (humidity) and then transfers it to the atmosphere, resulting in a cooled body. This condition and its value for helicopters are described in Section 2.4.1.

## 2.5. Helicopter compartment loads

As described in the previous sections there are several factors that affect the safety and comfort of the passengers and crew on an aircraft. The geometry of the aircraft is one of these elements, and thereby different heat loads apply for given operational conditions. Heat transfer or heat loads on the aircraft occur by convection, radiation, and conduction and may be given at different points. These places are determined by the configuration and type of aircraft.

The analysis of these surfaces allows determining the requirements of the ECS for an effective extraction of heat loads, which result in a thermal equilibrium within the aircraft. A typical helicopter geometry configuration is shown in Figure 2-9, which illustrates the heat loads that affect a helicopter.

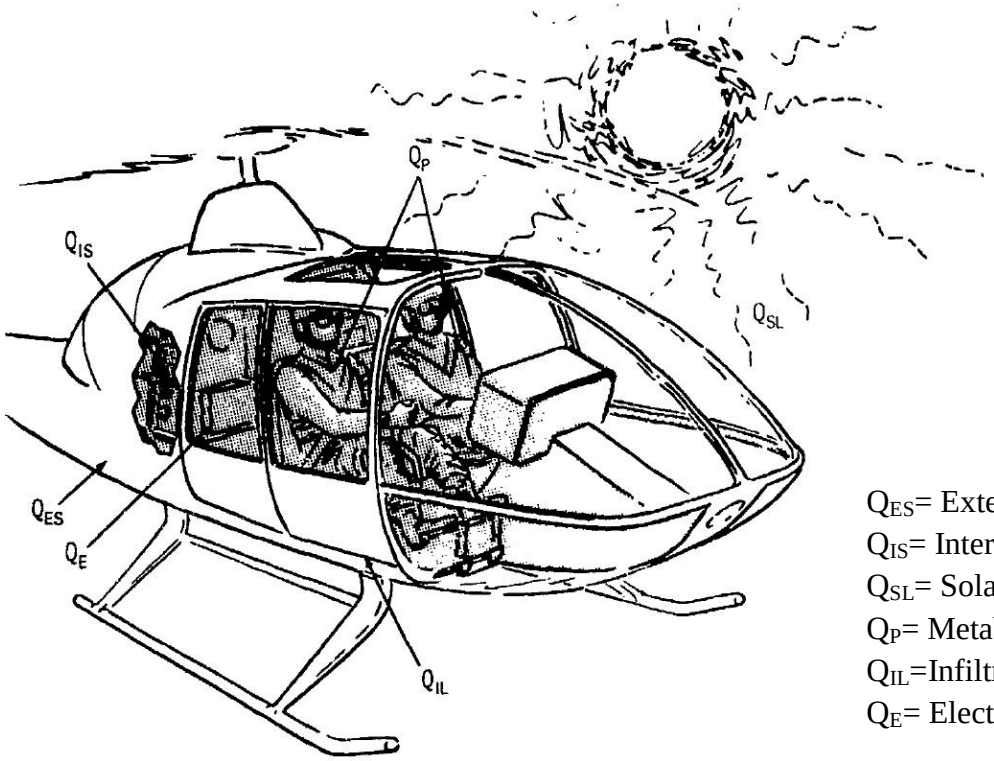


$Q_{ES}$= External Surfaces
$Q_{IS}$= Internal Surfaces
$Q_{SL}$= Solar Radiation
$Q_P$= Metabolic
$Q_{IL}$=Infiltration
$Q_E$= Electrical

**Figure 2-9 Helicopter heat loads [33]**

The geometry of the aircraft is divided into two parts, external and internal. External loads consist of two elements, the heat flow through the wall and the structure, and the internal convection; as shown in Figure 2-10. On the other hand, internal loads contain the floor and bulkheads. The Bell 206L-4 geometric areas are shown in Table 2-1.

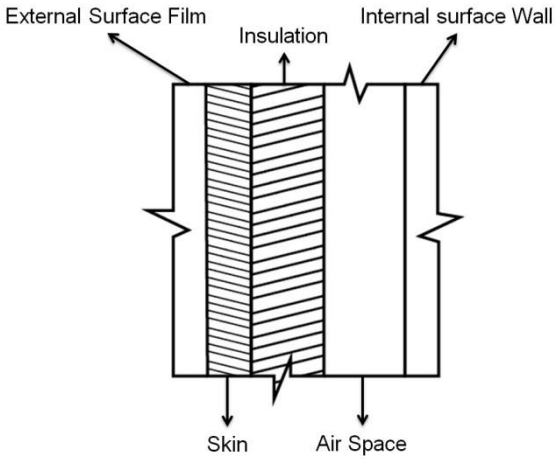


**Figure 2-10 Sections of a simple wall with insulation**

The Bell 206L-4 heat loads are therefore comprised of six main heat sources, internal and external elements, mechanical and electrical components (avionics), transparent surfaces (windows and windshield), Infiltration of outside air into the cabin, and metabolic heat loads caused by its 5 passengers and 2 crew members.

## 2.6. ECS subsystems

The altitudes and operating conditions may vary depending on aircraft type and mission. These differences determine if the air temperature is very cold or very hot, dry or wet. The temperature, humidity and ventilation are three essential parameters that must be controlled to maintain a level of comfort on all aircraft. For helicopters, five types of air-conditioning packs are in use today in order to control these parameters [18].

### 2.6.1. Air Cycle system

The Air Cycle Machine (ACM) is a leading air-conditioning pack in fixed-wing aircraft due to its low weight, good performance and to its simplicity and reliability [31]. This package takes air from the engines (Bleed Air) and outdoor air (Ram Air) which passes through two basic processes. First, this air passes through the heat exchanger which is responsible for reducing the heat air produced by the compression process. Afterwards, the air is expanded and cooled in the turbine, before being sent to the cabin. Figure 2-11 illustrates this process.

One disadvantage of this system is that it requires high pressures in order to maintain the cooling inside the cabin.

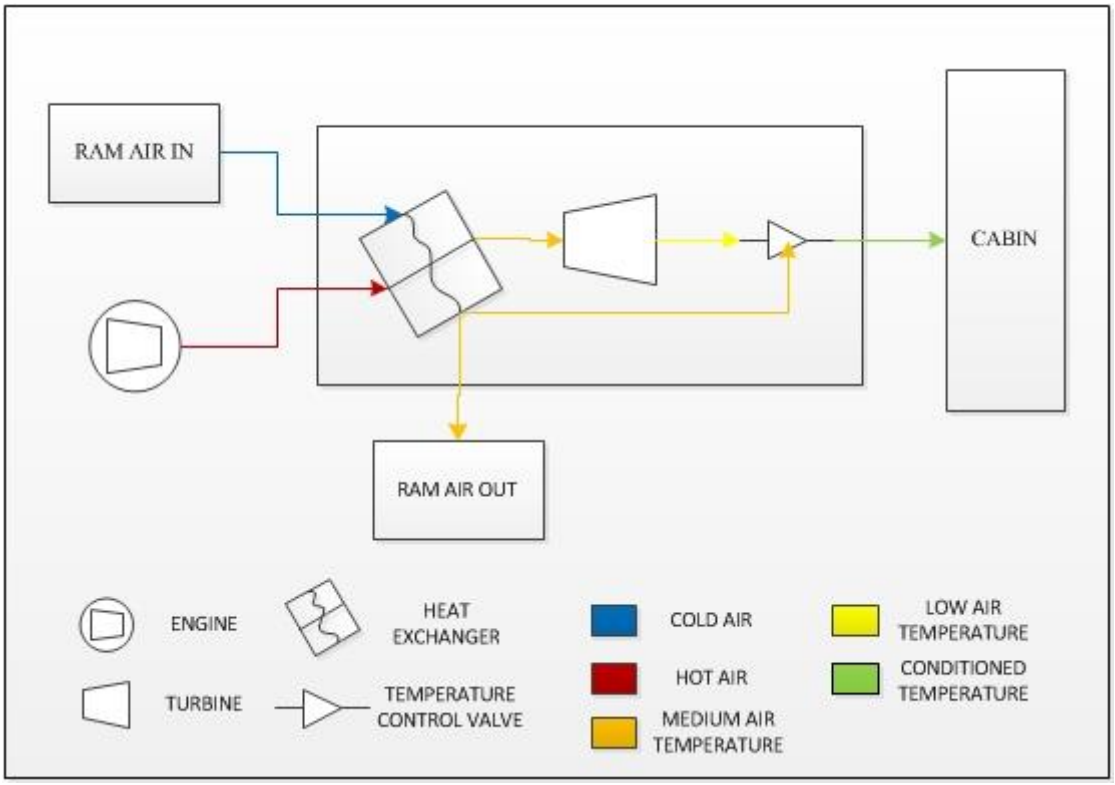


**Figure 2-11 Bleed Air Cycle Machine**

One of the variations in the air-conditioning system is the Bootstrap [31]. Unlike the basic system, this system can be used in aircraft with low pressure levels because of the improvements generated by adding the compressor to the turbine. As shown in Figure 2-12 the Bootstrap has two Heat Exchangers. The first is located before the compressor and its function is to precool the Bleed Air from the engine. The air is then compressed in a compressor to increase its pressure. The second heat exchanger is placed after the compressor, and its role is to reduce the air temperature. Finally, this air is expanded through the turbine to achieve the required pressure in the cabin. Both the first and the second heat exchangers are cooled by ram air. The Bootstrap Air Cycle Machine will be the system used for this study based on its improved capabilities at low altitudes and low pressures.

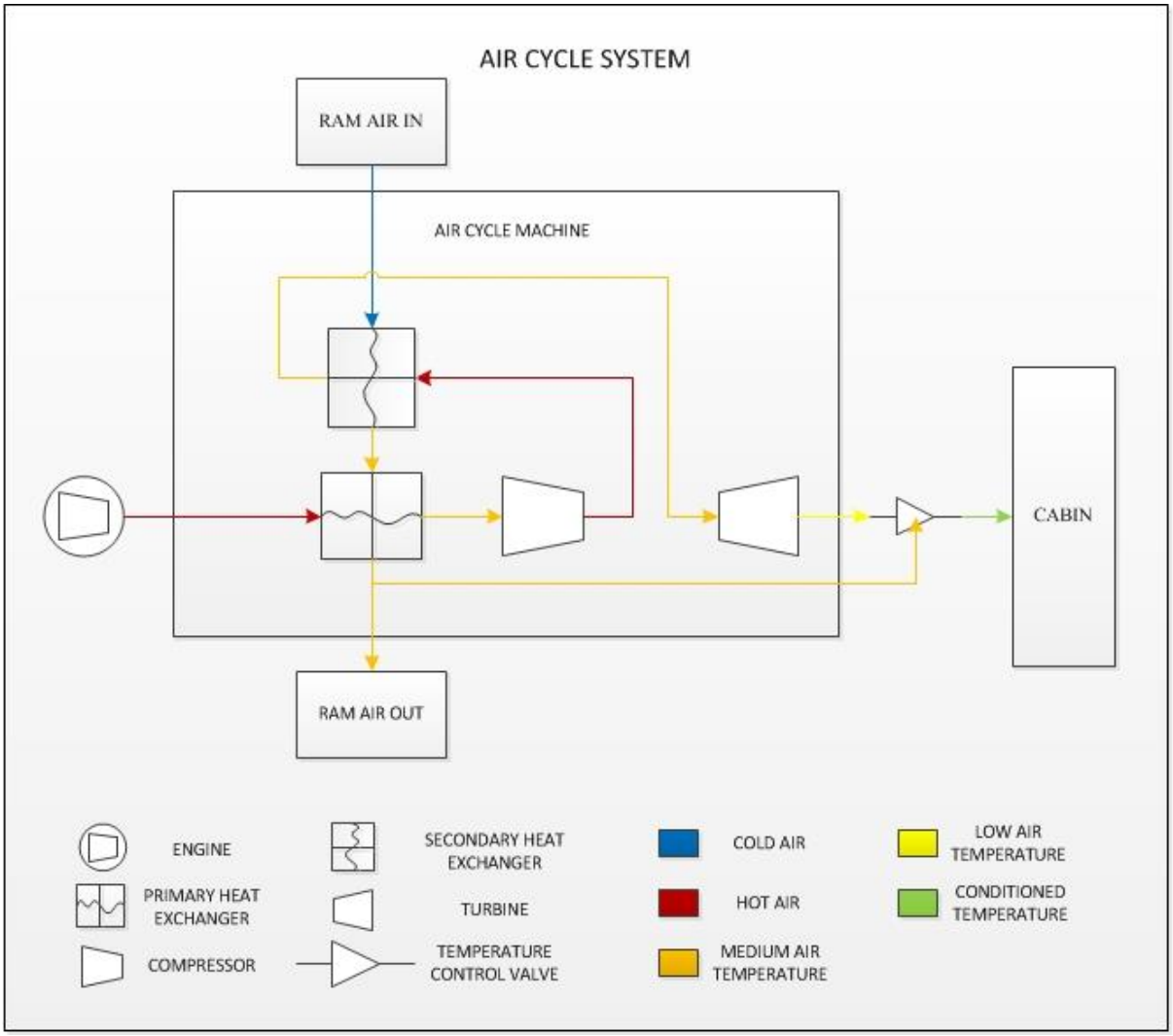


**Figure 2-12 Bootstrap Air Cycle System**

### 2.6.2. Vapour Cycle system

The Vapour Cycle Machine (VCM) is a leading air-conditioning pack in rotor-wing aircraft thanks to its low noise output, energy efficiency and small components and ducts [31]. This system makes use of a liquid refrigerant which is responsible for absorbing the heat of the equipment and heat transferred by passengers aboard. The refrigerant is compressed once it is in a vapour state due to high temperature absorbed, and then is cooled in a condenser. After being condensed, the liquid refrigerant continues the cycle [24]. Generally the liquid refrigerant used is the R-134; nevertheless due to their toxic properties and weight this system has limited applications. Figure 2-13 shows the Vapour Cycle System schematic operation.

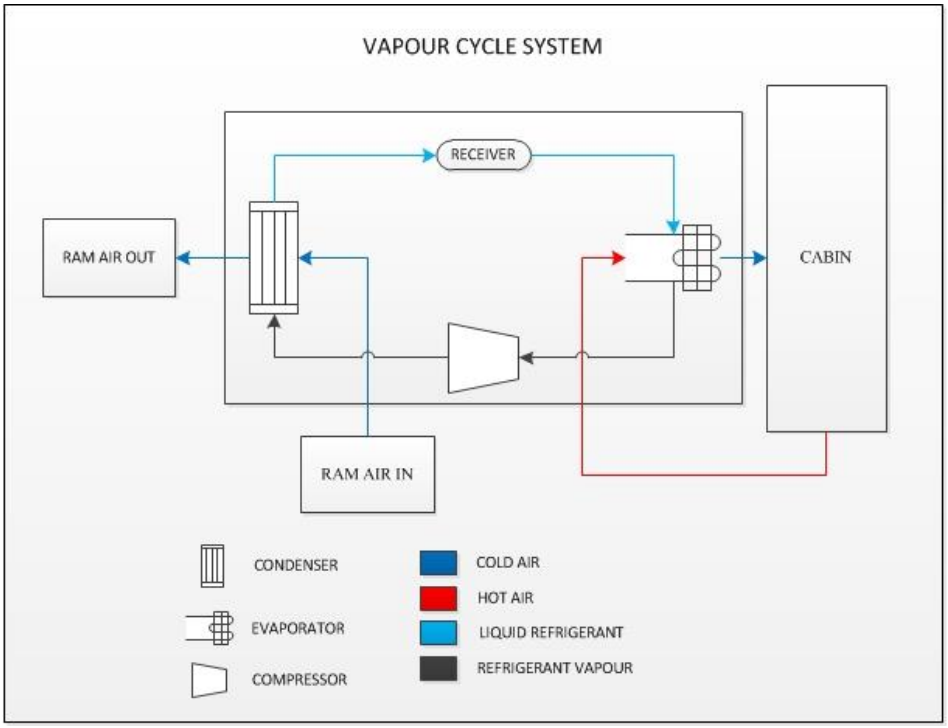


**Figure 2-13 Vapour Cycle system**

### 2.6.3. Combustion Heater system

Unlike previous systems, Combustion Heater System only provides heating in aircraft. This system heats the recirculated cabin air by heat transfer across the wall of the combustion chamber [6].

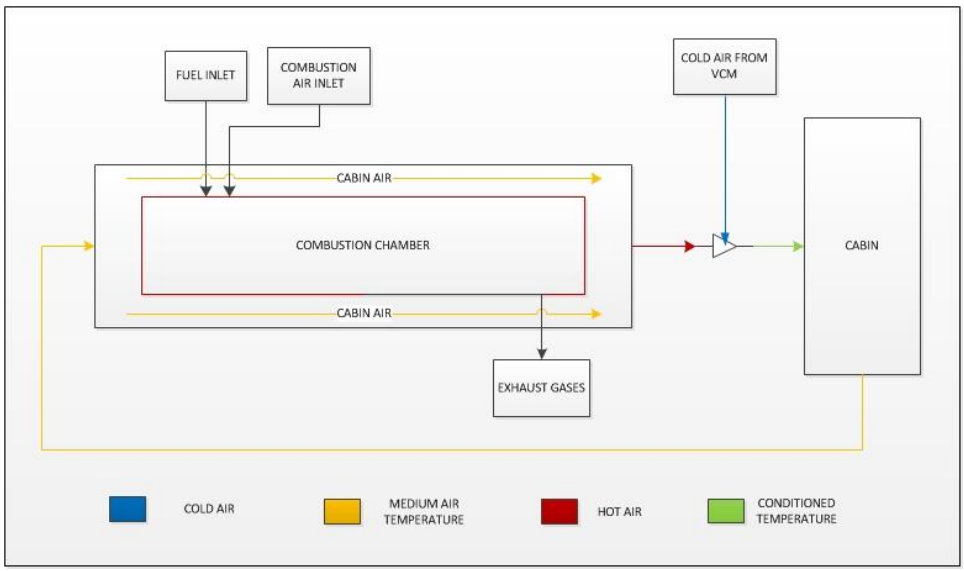


**Figure 2-14 Combustion Heater**

### 2.6.4. Exhaust Gases Heater system

Similar to the Combustion Heater System, the Exhaust Gases Heater System only provides heating in aircraft. This air-conditioning pack heats ram air through an exchanger which transfers heat from the produced Exhaust Gases [57].

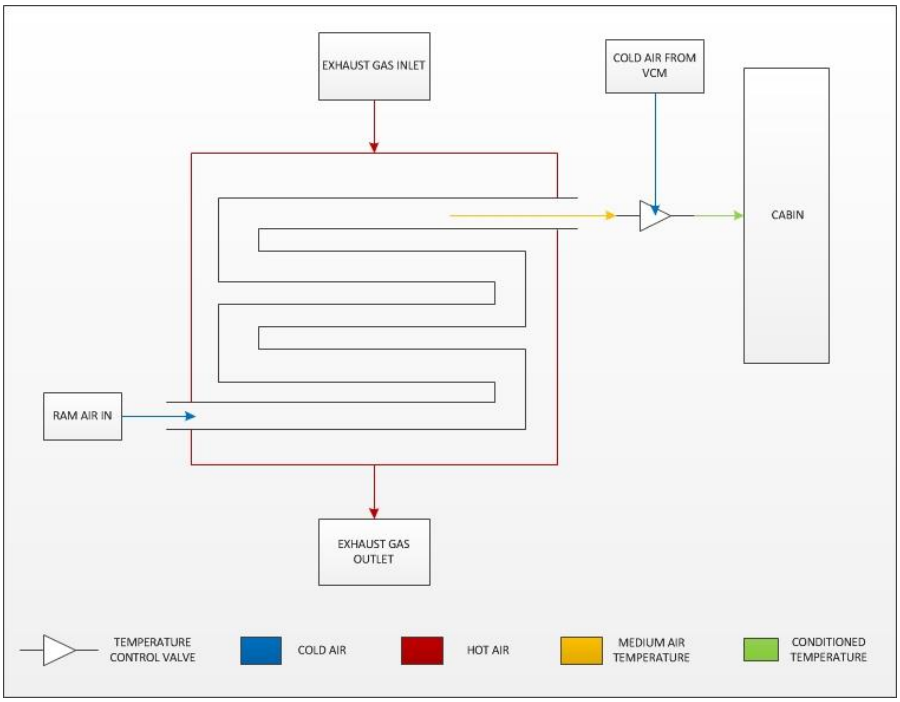


**Figure 2-15 Exhaust Gases Heater**

### 2.6.5. Electric Element Heater system

The Electrical Heater only provides heating; this system uses electrical current to release heat through electrical resistance [12]. However due to the electric power waste caused by such systems, they will not be considered for modelling in this study.

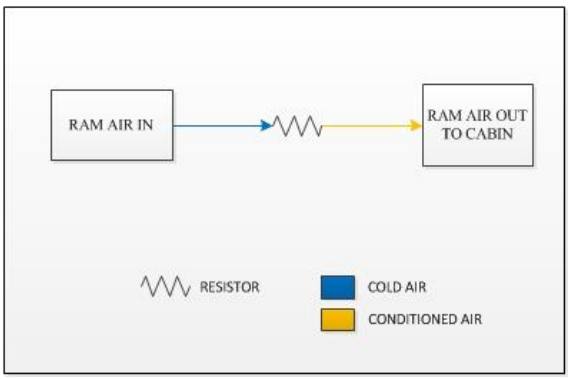


**Figure 2-16 Electric Element Heater system**

## 2.7. Cycle Machine equipment

The Environmental Control Systems in aircraft have different sub-systems and components. Among these components are heat exchangers (regenerator, evaporator, condenser, reheated), Cold Air Units (CAU) and control valves. The main components will be explained in more detail in the following section [26].

### 2.8.1. Heat exchangers

The heat exchanger component is used to transfer thermal energy (enthalpy) between two or more fluids, a solid surface and a fluid, or between solid particles and a fluid, at different temperatures and in thermal contact. Some applications involve heating or cooling of a flow stream (recuperators) and its evaporation or condensation. Heat transfer occurs between the fluids through walls which are responsible for separating the fluid within the heat exchanger. Heat transfer in a recuperator generally takes place by conduction.

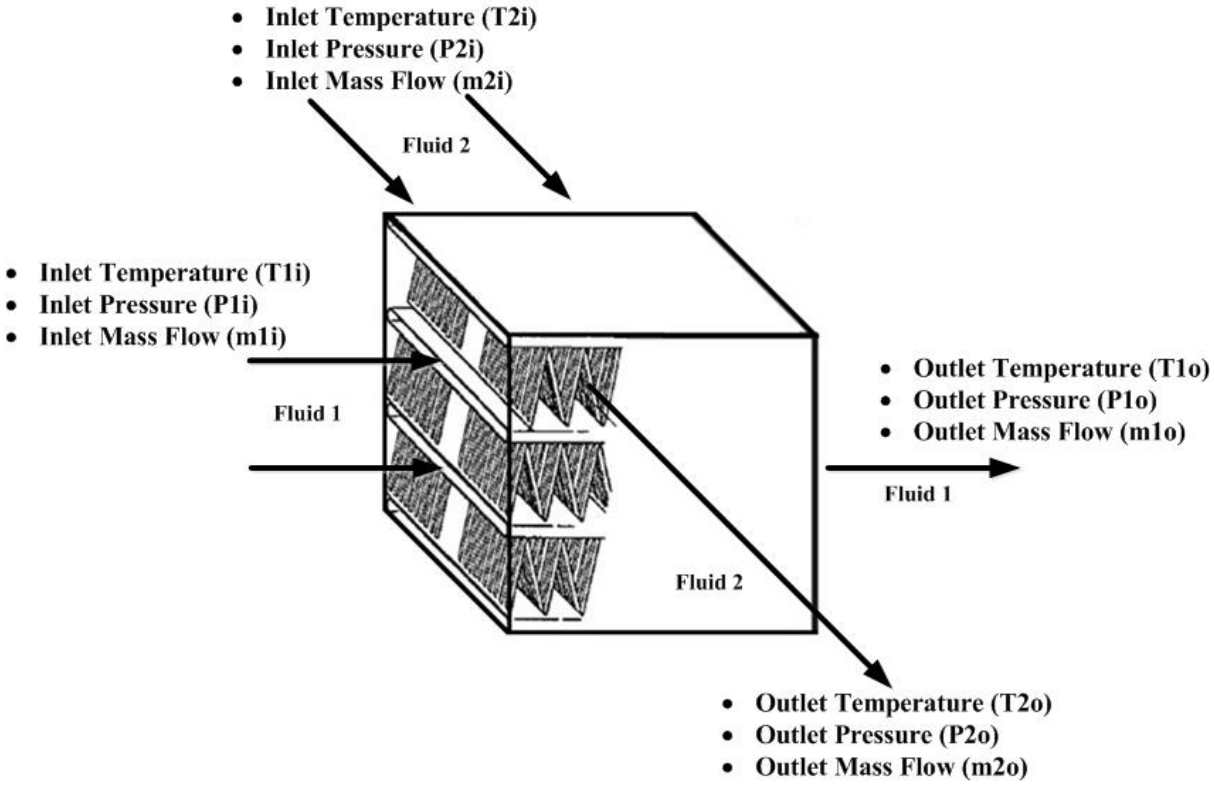


**Figure 2-17 Heat exchanger operation**

The heat of the fluid is transferred by conduction through the heat transfer surface; this surface is part of the exchanger core. The surface in direct contact with both fluids, hot and cold, is called the primary surface. A second surface (secondary surface) is added to the first surface in order to increase its area, and hence increase heat transfer. Connected to the second surface are elements (fins) which are responsible for further extending the surface. Thus, heat is conducted through the fin and connected from the fin, through the surface area, to the surrounding fluid.

The exchangers are classified according to the designer needs as shown in Figure 2-18, Shah and Mueller (1998) [49]. The required specifications of the heat exchanger for the ECS are the following:

• Underweight and short dimensions,
• To work as a recuperator, condenser or evaporator,
• To have a high heat transfer coefficient,
• To work with both liquid refrigerants and gases.

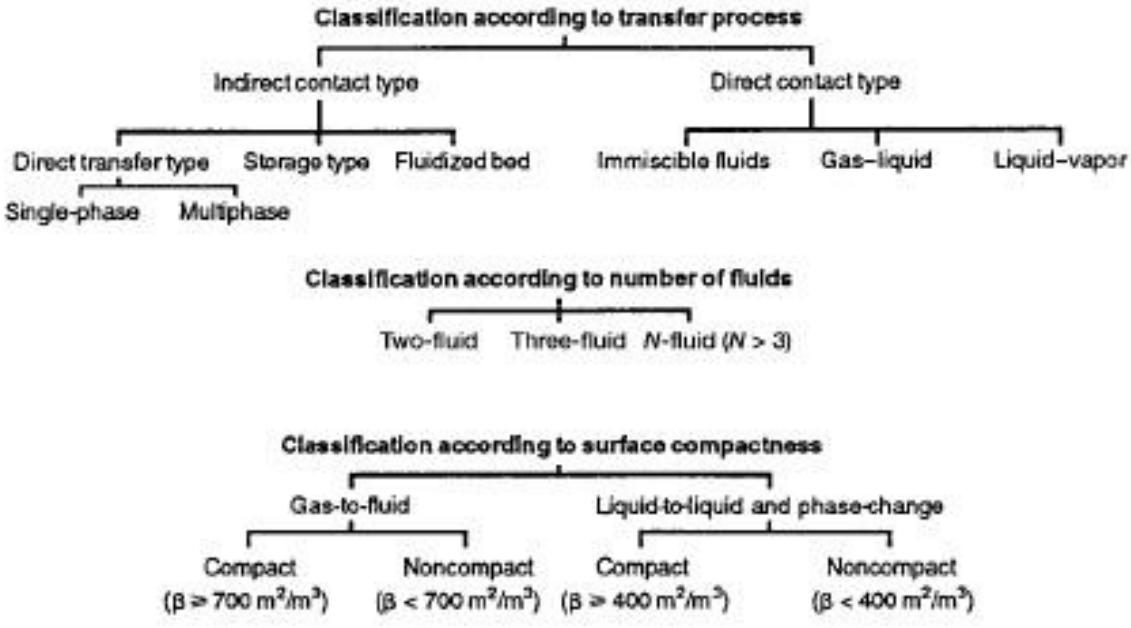


**Figure 2-18 Heat exchanger classification [49]**

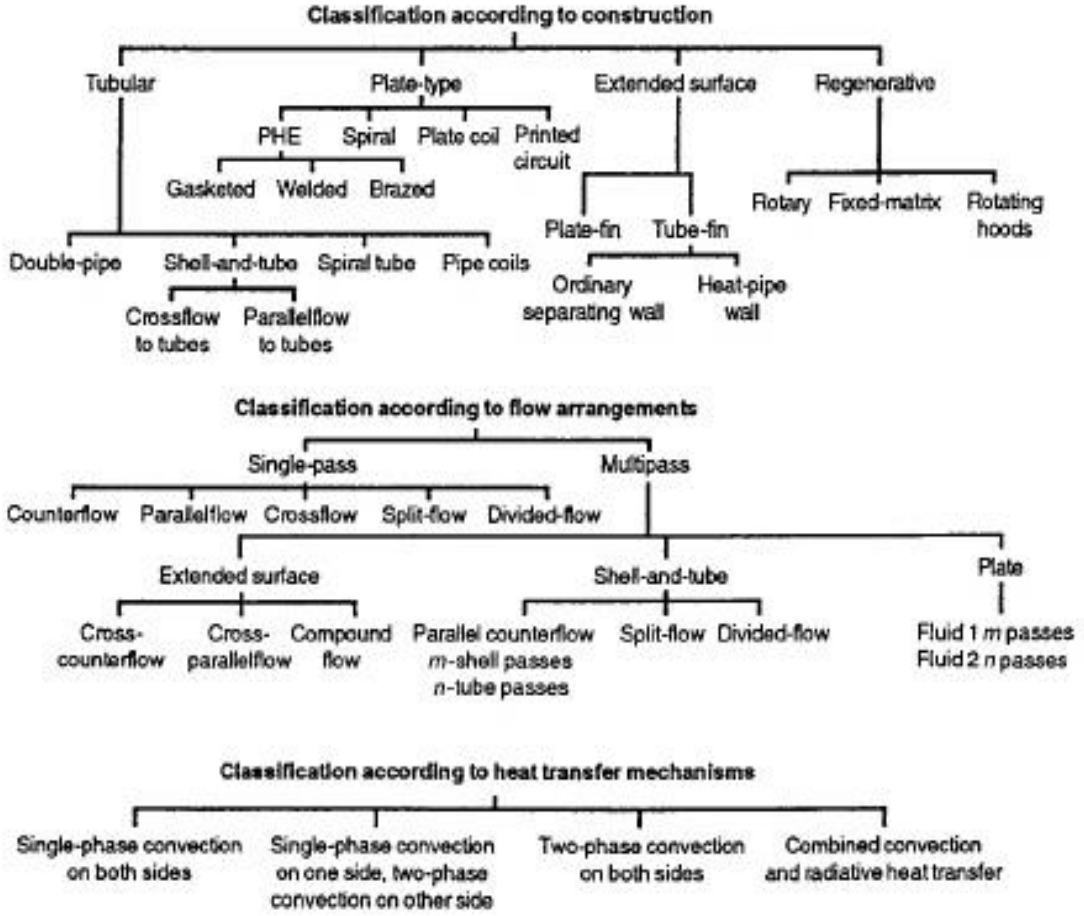


**Figure 2-18 (Continued) [49]**

To reach the heat exchanger selection, a series of stages were followed to discard other configurations and constructions. The first step consists in the selection of the appropriate measures (size) for the heat exchanger in a selected aircraft and for the simulation model in Matlab-Simulink. Taking into consideration the selected aircraft and its internal configuration, the initial heat exchanger size is established in 0.3 X 0.3 X 0.3 m. Another feature that should have the chosen heat exchanger is its functionality for both gas-to-gas and gas-to-fluid. According to these considerations the only configuration that can meet these two requirements is the compact exchanger surface.

The second step is to define the type of construction; in this case, for compact Surface exchanger there are only two configurations: plate-fin and tube-fin. Currently each of the mentioned configurations contemplates different types of geometries (see Figure 2-20), but the only geometry that can be configured as a gas-to-gas and gas-to-liquid exchanger is the

louvered. Additionally, as shown in Table 2-6, the louver has a high heat transfer, an ideal factor for the high demands of the ECS.

The final step is to choose the flow arrangement, which in the case of the compact exchanger surface can be only single-pass. According to the fundamentals of heat exchanger design (2003), the single-pass crossflow configuration is the most commonly used in the aerospace industry due to its high heat transfer into the heat exchanger, and its simple and compact construction, which reduce production costs. Finally, a single-pass crossflow configuration is chosen and simulated [49].

After this analysis of the different types of exchangers available for the aerospace industry and according to the considered environmental conditions and the required features of the ECS heat exchangers mentioned above; a two fluids compact surface exchanger was chosen, its internal body includes an extended fin surface (plate-fin) with a louver fin (gas-to-gas) and a louver tube fin (gas-to-liquid) geometry, and its flow arrangement is a single-pass crossflow.

***Compact heat exchanger*.** The compact heat exchanger is commonly used in aircraft cooling systems due to its large surface area that can reach high heat transfers. Similarly, its compact form helps in decreasing space and weight, as well as reducing energy requirements and its production cost compared to conventional designs such as the shell-and-tube exchangers is relatively low. The configurations most frequently used for gas-to-gas or gas-to-fluid exchangers are plate-fin and tube-fin. Table 2-5 lists some of the advantages and limitations of this type of exchanger compared with other configurations.

**Table 2-5 Heat exchanger types advantage and limitations**

| Compact (plate-fin and tube-fin) heat exchangers | |
|---|---|
| Advantage | Disadvantages |
| Low initial purchase cost (plate type) | Narrower range of allowable pressures and temperatures |
| Many different configurations are available (gasket, semi-welded, welded, spiral) | Subject to plugging/fouling due to very narrow flow path |

| Advantage | Disadvantages |
|---|---|
| High heat transfer coefficients (3 or more times greater than for shell & tube heat exchangers, due to much higher wall shear stress) | Gasket units require specialized opening and closing procedures |
| Tend to exhibit lower fouling characteristics due to the high turbulence within the exchanger | Material of construction selection is critical since wall thickness very thin (typically less than 10 mm) |
| True counter current designs allow significant temperature crosses to be achieved | |
| Require small footprint for installation and have small volume hold-up | |

Shell and tube heat exchangers

| Advantage | Disadvantages |
|---|---|
| Widely known and understood since it is the most common type | Less thermally efficient than other types of heat transfer equipment |
| Most versatile in terms of types of service | Subject to flow induced vibration which Can lead to equipment failure |
| Widest range of allowable design pressures and temperatures | Not well suited for temperature cross conditions (multiple units in series must be used) |
| Rugged mechanical construction can withstand more abuse (physical and process) | Contains stagnant zones (dead zones) on the shell side which can lead to corrosion problems |
| | Subject to flow mal-distribution especially with two phase inlet streams |

***Plate-fin exchanger.*** The Plate-fin exchanger is characterized by the use of corrugated fins, generally with triangular or rectangular shape. Unlike the tube-fin exchanger, the Plate-fin has a much greater compactness due to its block form, constructed from flat plates and corrugated fins. The basic elements of Plate-fin are shown in Figure 2-19. The corrugated fins commonly used in this type of exchanger are offset strip, louver, and perforated, some of the geometries are shown in Figure 2-20. The fins can be used on both sides for gas-to-gas

applications. For gas-to-liquid applications the fins are generally used only in the gas side, while the liquid side is carried by flat tubes attached to fins such as the multiport tubes found in louver fin configurations.

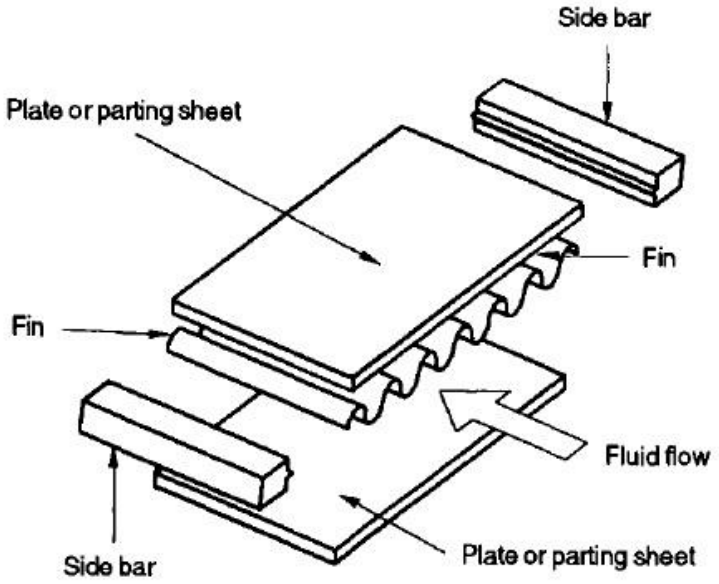


**Figure 2-19 Plate-fin heat exchanger basic elements [34]**

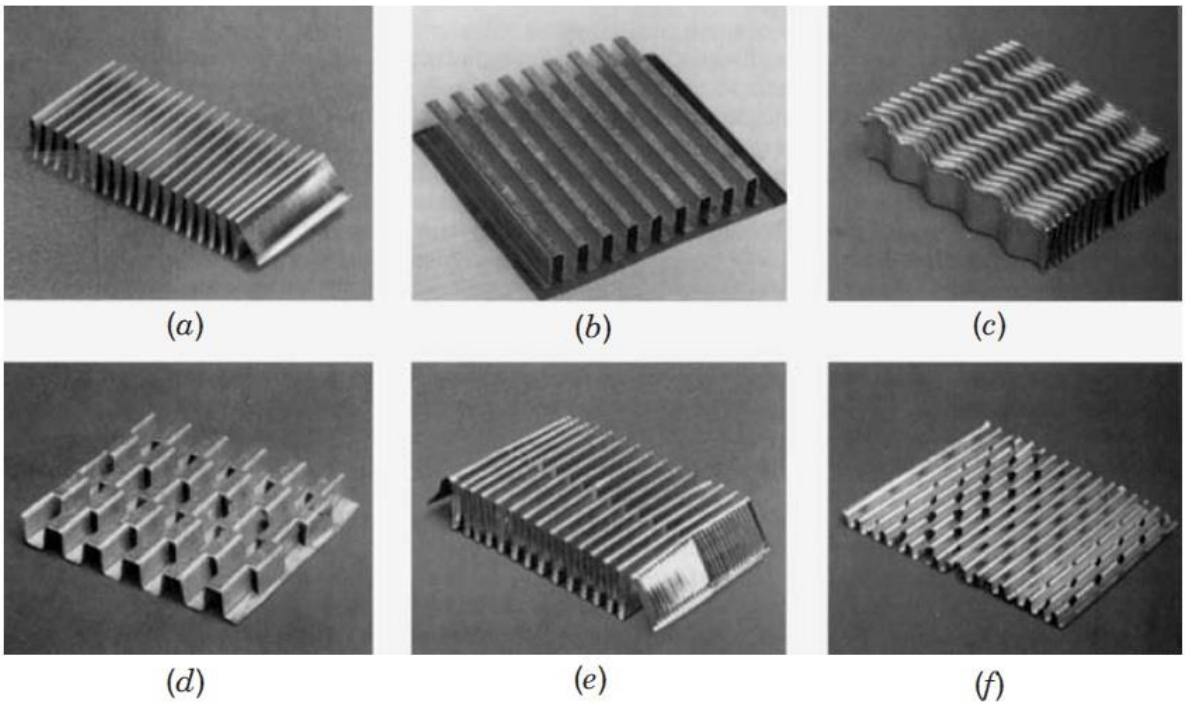


**Figure 2-20 Fin geometries for plate-fin heat exchanger: (a) plain triangular fin; (b) plain rectangular fin; (c) wavy fin; (d) offset strip fin; (e) multilouver fin; (f) perforated fin [34].**

***Louver fin exchanger.*** This type of configuration is widely used in the aerospace industry for its compactness, light weight, and low pumping power for a given heat transfer. The louver fin is recognized for its effective heat transfer surface to deal with cooling. This surface is commonly used for heat exchangers in air conditioners, evaporators and condensers. As described in Table 2-6, the louvered fin or multilouvered fin is obtained by performing different cuts (of different intervals and of different geometries) on the sheet metal that constitutes the fin, and then lifting the cut metal strip out of the plane of the fin.

**Table 2-6 Plate-fin geometries and applications [49]**

| Corrugation | Description | Application | Features | |
|---|---|---|---|---|
| | | | Relative Heat Transfer | Relative Pressure Drop |
| Plain | Straight fins (rectangular or triangular) | Low Reynolds number applications and in applications where the pressure drop is very critical, e.g., condensation | Lowest | Lowest |
| Perforated | Straight fin with small holes | For general use | Low | Low |
| Herribone or wavy fin | Smooth but wavy, about 10 mm pitch | In the Re range of 6000-8000, the wall corrugation increase the heat transfer by about three times compared with the smooth wall channel due to Goertler vortices.<br>Less likely to catch particulates and foul than are OSFs | High | High |
| Louvered fin | The louvers are formed by cutting the sheet metal of the fin at intervals and by rotating the strips of metal thus formed out of the plane of the fin | Radiators, air conditioning heat exchangers (evaporators and condensers), and aircraft oil and air coolers | Highest | Highest |
| OSF | Straight but offset by half a pitch (usually about every 3-4 mm) | Air separation plants and low Reynolds number applications calling for accurate performance predictions, e.g., aerospace applications | Highest | Highest |

***Crossflow exchanger.*** There are three possible fluid flow arrangements in the heat exchanger: parallel flow, counterflow, and crossflow.

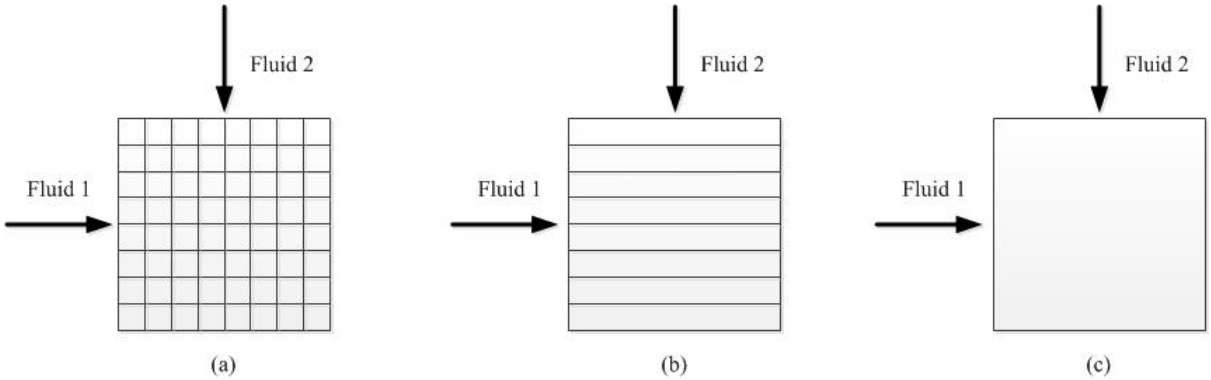


**Figure 2-21 Crossflow exchanger combinations: (a) both fluids unmixed; (b) fluid 1 unmixed, fluid 2 mixed; (c) both fluids mixed.**

Unlike the parallel flow and the counterflow, the crossflow has a high effectiveness in the heat exchanger, and its design and production are easy and its production is fast. This configuration allows for various combinations within the exchanger: both fluids unmixed, one fluid unmixed and the other fluid mixed, and both fluids mixed. For this study both fluids will be considered unmixed, as the chosen exchanger contemplates an individual flow passage (louver multiport tube configuration).

### 2.8.2. Water separators

The water separator is the unit responsible of removing moisture in the air from the ECS before it can be delivered to the cabin. There are two basic types of this unit, low pressure and high pressure. The first is a low pressure water separator that removes moisture from the air at low pressure downstream of the cooling turbine. The second is a high pressure water separator that removes moisture from air at high pressure upstream of the cooling turbine [31].

***Low pressure water separators.*** The low pressure water separator consists of a coalesce section that agglomerates water particles, a section that generates rotation in the airflow, and a collector to collect and drain water droplets which have been centrifuged from the airflow.

The major advantage of this configuration is its light weigh. Among its disadvantages is its low efficiency to remove water, which leads to lower moisture retention. It also requires regular maintenance and cleaning, thus being an undesirable configuration for helicopters operating in areas with sand and dust.

***High pressure water separators.*** The high pressure water separator consists of a heat exchanger (condenser) which is responsible for condensing moisture from the air, and a collector that collects and drains water droplets from condensed moisture. Its main disadvantage is the additional weight required. Its advantages include a high efficiency to remove water and the fact that it requires no maintenance.

The high pressure water separator system was selected for this research. Because of the conditions in which helicopters work (deserts, jungle areas, etc.), is essential to have reliable systems that does not require constant maintenance. As mentioned above, the low pressure water separator system is made of many components that for example in desert environments, are constantly damaged by the presence of sand, leaving the aircraft out of service and unsuitable for operational use. Therefore the high pressure water separator system is the best configuration for the selected aircraft, even if this system leads to greater weight and therefore to fuel consumption increased (unfavourable for the green concept).

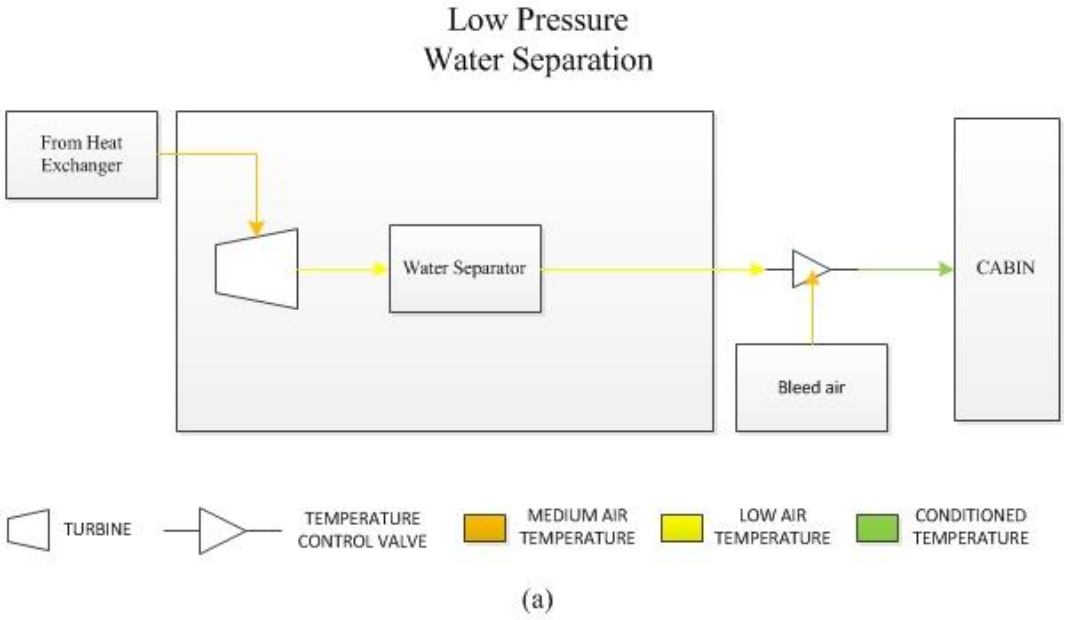


**Figure 2-22 Water separator configurations: (a) low pressure water separation.**

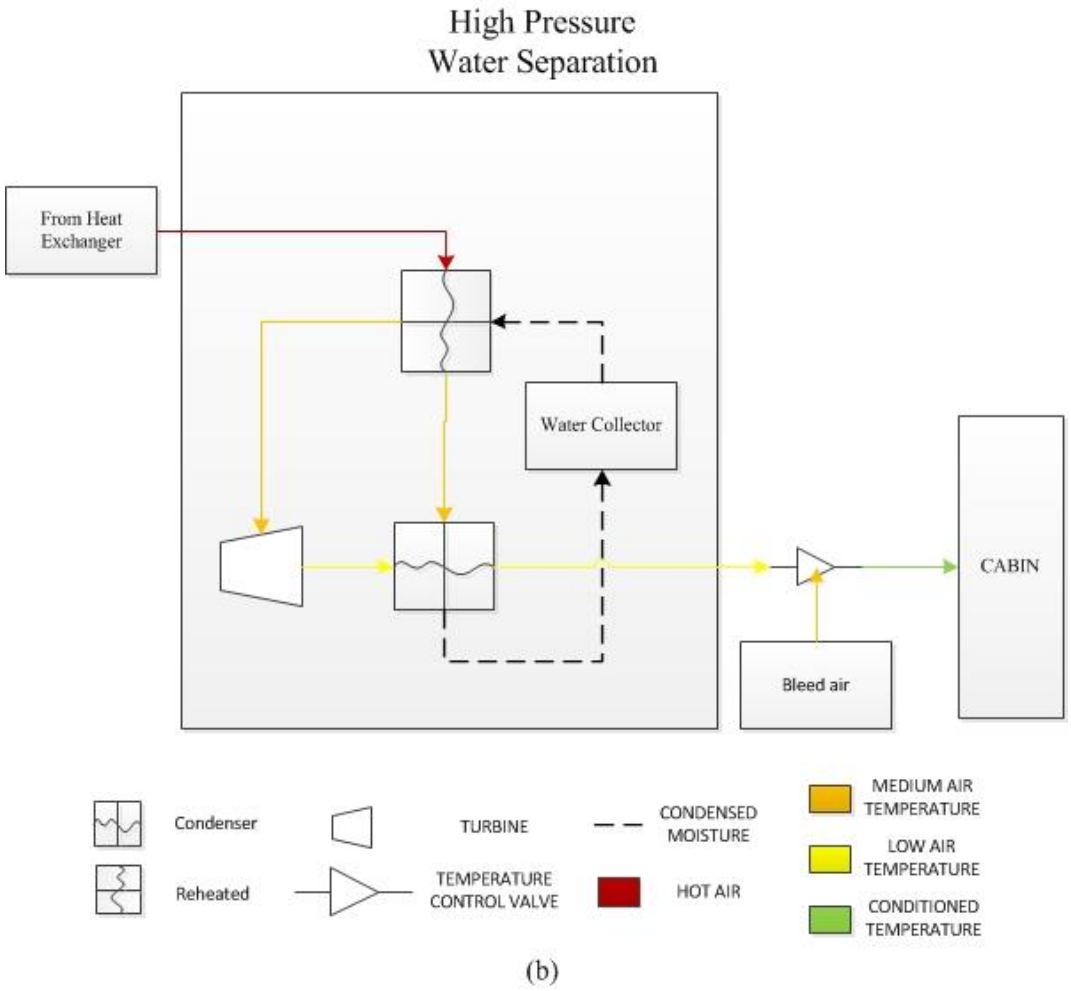


**Figure 2-23 (Continued) Water separator configurations: (b) high pressure water separation.**

### 2.8.3. Cold Air Units

CAU Systems includes a turbomachine (compressor and turbine), and a heat exchanger. These components are responsible for maintaining the required pressure in the cabin at high altitudes, and reducing the temperature in extreme conditions at low altitude [35].

The turbomachine is the combination of a turbine and a compressor on a single shaft. This component is responsible for converting the energy of a fluid (air pressure) into work in the CAU. There are two types of turbomachines: axial and radial. Its function within the Cold Air Unit is to generate the necessary work to extract heat from the air which is then delivered to the cabin.

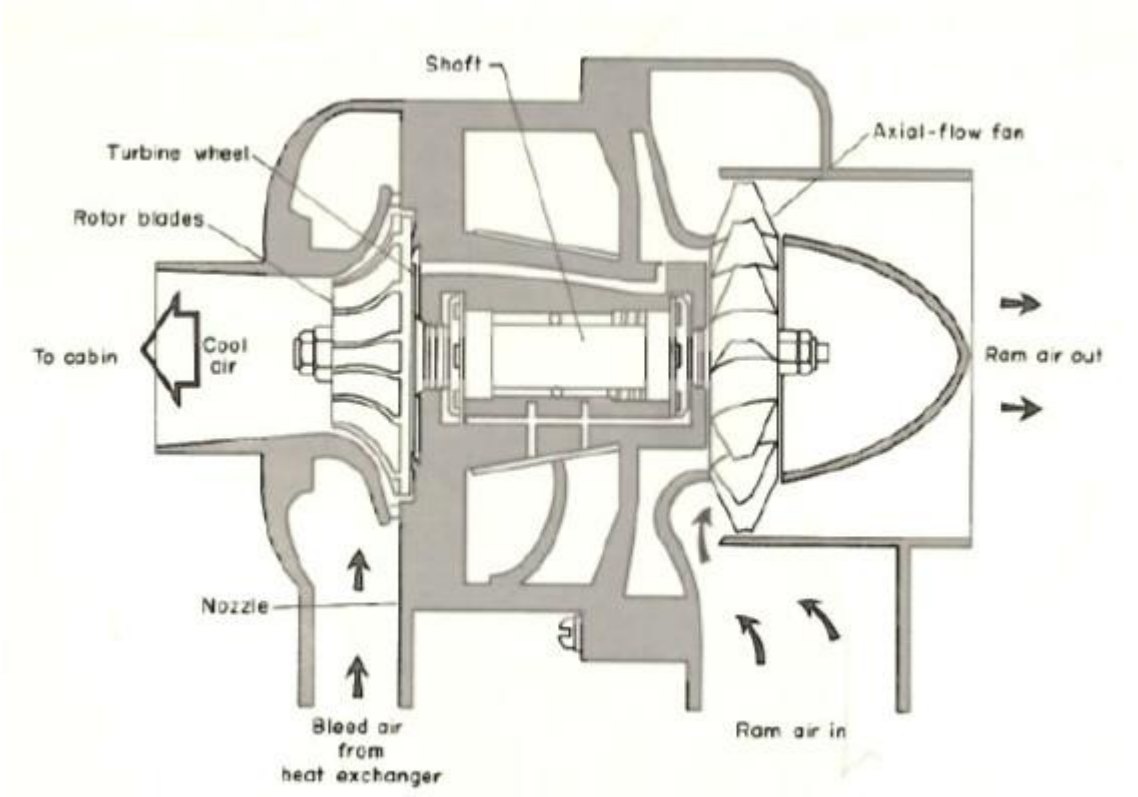


**Figure 2-24 Cold Air Unit [35]**

### 2.8.4. Control valves

As mentioned previously in this section, ventilation, humidity and pressure must be controlled to acquire an effective temperature within the aircraft. In the ECS, these conditions are controlled by valves that control the system automatically. There are 5 typical applications for these control valves: shut-off, flow control, pressure control, flow check valves, and pressure ratio control [35]. The use of control valves will not be considered in this study for the sake of the simplicity of the model, the results will thereby not be affected as the loss generated through the valves is negligible.

A shut-off valve is electrically - and in some cases manually - controlled. The function of this valve is to shut off the flow of air to protect the system in case of high pressures and temperatures.

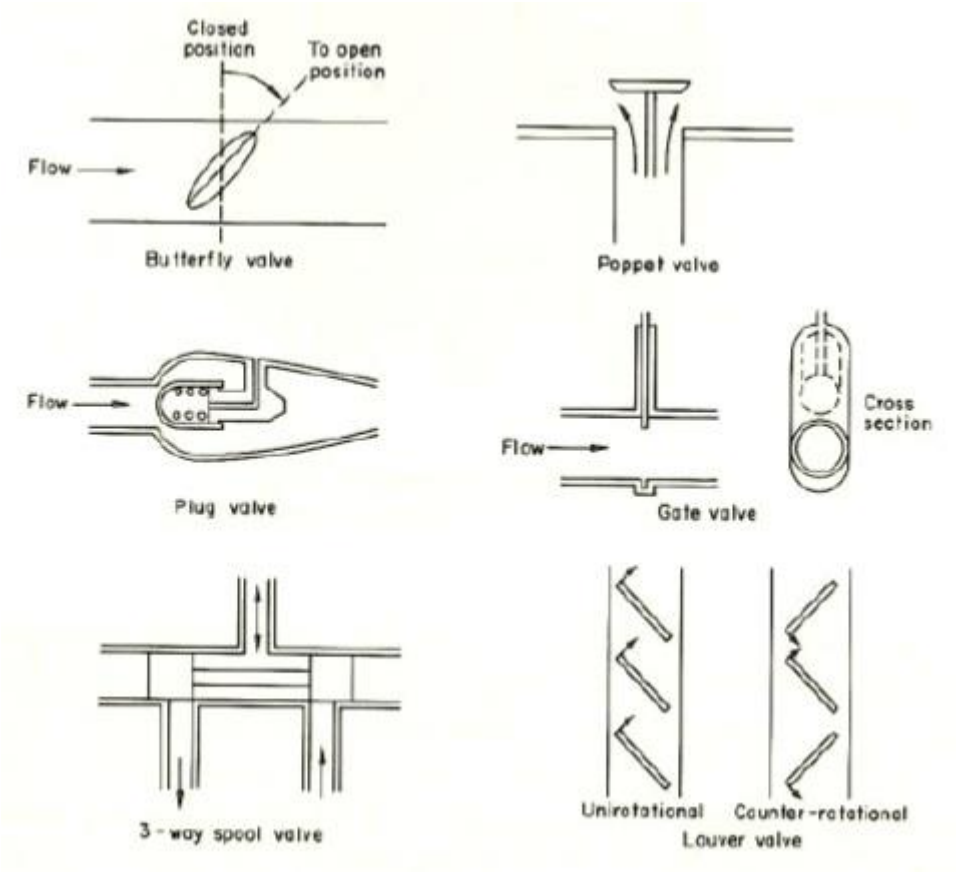


**Figure 2-25 Basic valve types [35]**

The flow control valve is normally responsible for controlling the amount of air flow within the system. This valve is controlled electronically; however in case of a power failure it can also be controlled manually.

The pressure control valve is designed to reduce high inlet pressure to the system. The pressure released from this system is commonly redirected to other pressurised sections, such as avionics and fuel tanks.

The flow check valve avoids the leaking of the downstream air or reversal of the air flow in the pressurizing systems. This valve is responsible for shutting down the system if the air pressure is lower than the pressure generated by the downstream air.

Lastly, the ratio pressure control valve is responsible for maintaining the pressure ratio between CAU and cabin pressure by controlling the turbine speeds.

## 2.9. ECS modelling

Nowadays engineering design makes use of multiple tools in order to verify the effectiveness and capabilities of its designs. There are currently two predominant methods to do so: experimental measurements or numerical simulations. Experimental methods are generally seen as the most effective and safe techniques to obtain results but at a high cost and time consumption. Catching up with the experimental methods, computational tools are today a viable method for engineering design. These numerical simulations are becoming very effective for the evaluation of designs at certain operating points. However, it is still not possible to achieve a complete numerical exploration of the phenomena involved in a design. Despite this, these computational tools are very reliable and useful in making and validating a design without compromising time and requiring high costs [36]. This section illustrates different models and methods used as means of simulating numerically the design and analysis of environmental control systems.

### 2.9.1. Aircraft cabin comfort models

Similar research has made use of computer models for the design of the ECS for an aircraft cabin. A study by the Applied Laboratory of Mathematics and Systems (MAS) and the Centre of Mathematics and its Applications (CMLA), shows the results obtained through simulations of Environmental Control System [37]. The objective of this research was to optimize the ECS of future aircraft, providing a comfortable cabin with minimal power consumption. The proposed solution was to create a simple Computational Fluid Dynamics (CFD) model integrated with Navier-Stokes equations and thermal diffusion. This model simulates three factors: Human thermal control air movement and heat transfer by convection and radiation inside the cabin. Figure 2-25 shows the configuration of the cabin and its conditions in the simulation. This model considers an inlet temperature, outlet temperature, and the heat transferred by the wall.

For this simulation a minimum temperature of 294.5 K and maximum of 301.15 K were kept inside the cabin, for the comfort of passengers.

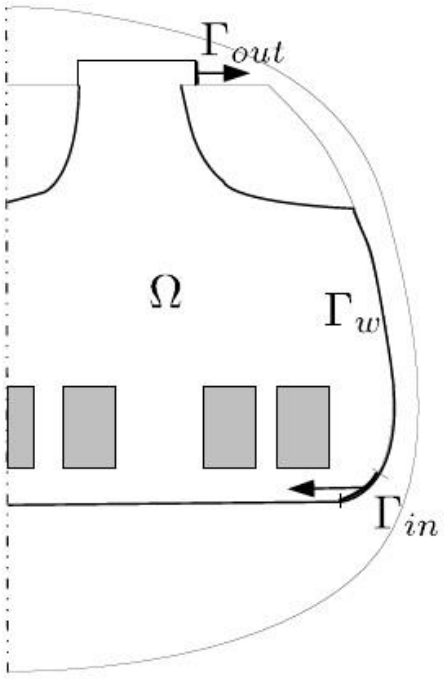


**Figure 2-26 Cabin boundary conditions [37]**

A different study developed by the National Aerospace Laboratory (NLR), shows the development of a computer-simulated inside of a cockpit environment [38]. This simulation seeks to analyse the thermal comfort of passengers in an aircraft. The simulation environment includes convection and radiation heat transfer, temperature and heat transferred by different elements found inside an aircraft (e.g. lights, avionic, etc.). Figure 2-27 shows the configuration of this model. The first block simulates different thermal transfers that affect the human body. The second block simulates the airflow inside the cabin. Finally the third block simulates heat transfer emitted by the infrared radiation within the cabin. This block shows the generals effects and heat loads inside an aircraft cabin.

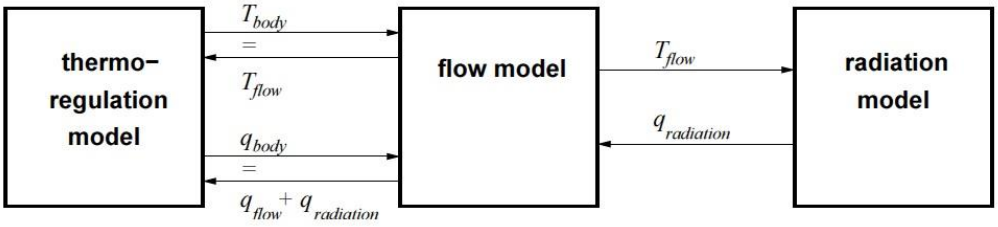


**Figure 2-27 Cabin model integration [38]**

In this case relative humidity of the air of 30% was assumed for the thermoregulatory model. This study considers a starboard-side semi-section of the aircraft cabin, containing 3 seats and

a single passenger seated in the centre to the aisle for the integrated model. The inlet temperature was assumed to be 293.15 K with a cabin ambient temperature of 296.15 K. The air behaviour and the temperature changes within the cabin are illustrated in Figure 2-28. In this case, the Environmental Control System blows the air almost directly onto the passenger, generating an uncomfortable situation for the passenger. As a result, the top of the passenger's head give the impression to be cold as its right arm.

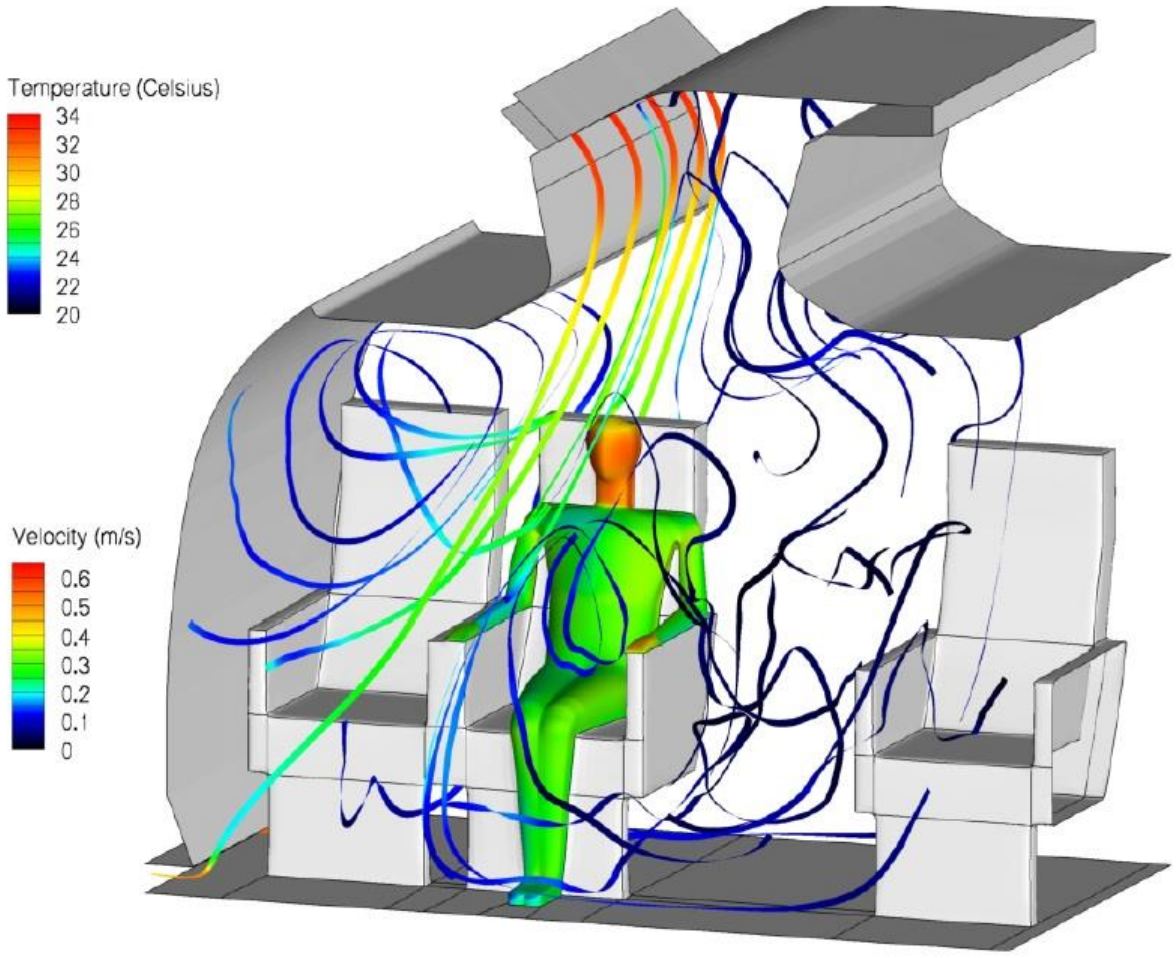


**Figure 2-28 Cabin air and temperature distribution [38]**

The above simulations were performed in a commercial fixed wing aircraft, so their results are limited only to those geometries and flight operations.

### 2.9.2. Cycle Machine models

Different models and methods can now be found in Cycle Machine Systems. The Beijing University of Aeronautics and Astronautics has developed a dynamic model of a Bootstrap three-wheel Environmental Control System with a high pressure water separation unit [39]. This model was created based on the Flowmaster software platform. This simulation provides a dynamic model of an Air Cycle Machine System, and also covers a dynamic analysis of the cabin control temperature which was developed using Expert PID and Fuzzy theory. The ACM model contains: a primary heat exchanger, secondary heat exchanger, a CAU with high pressure water separation unit, and a fan. The schematic of the configuration of the three-wheel ACM is illustrated in Figure 2-29.

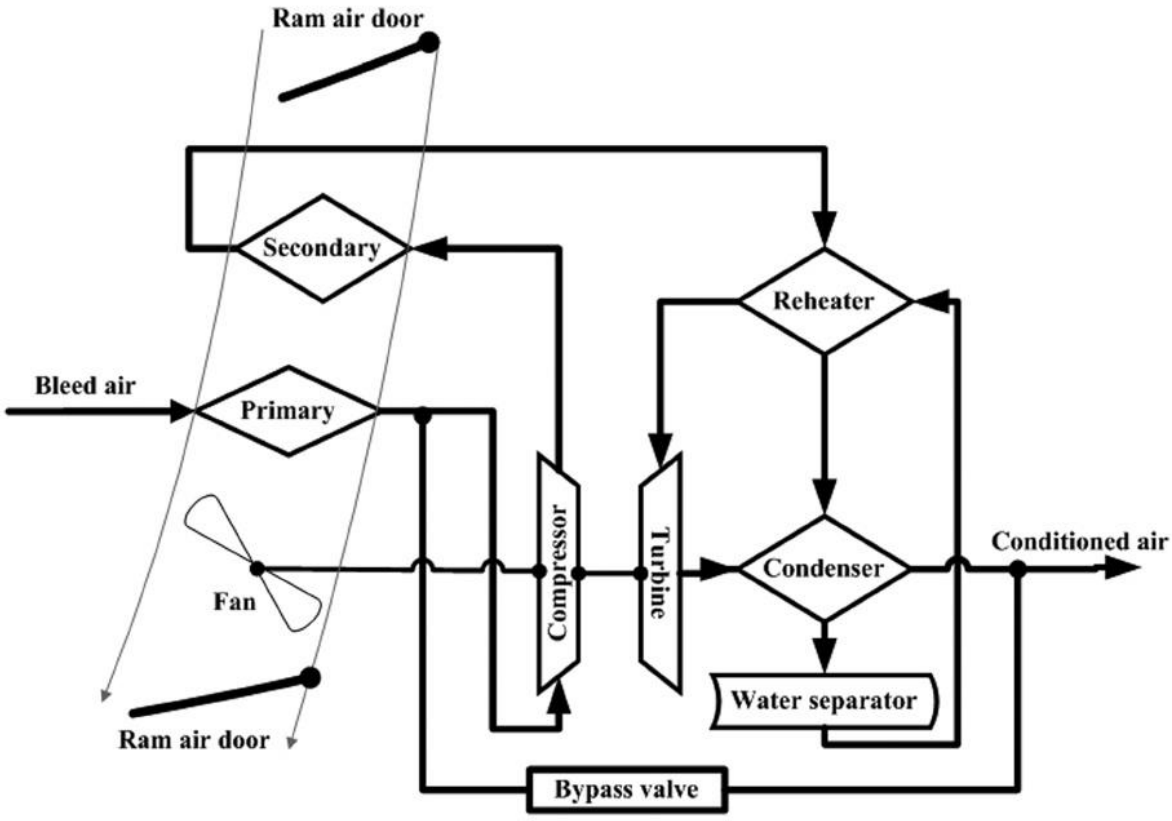


**Figure 2-29 Three-wheel ACM configuration [39]**

The dynamic analysis was carried out in hot weather conditions with an outside ambient temperature of 311.15 K; the temperature inside the cabin was set to 298.15 K. The results of the simulations in cooling condition are shown in Figure 2-30. The variation of temperature

with time under heating conditions of the several systems that compose the ECS is shown in Figure 2-31.

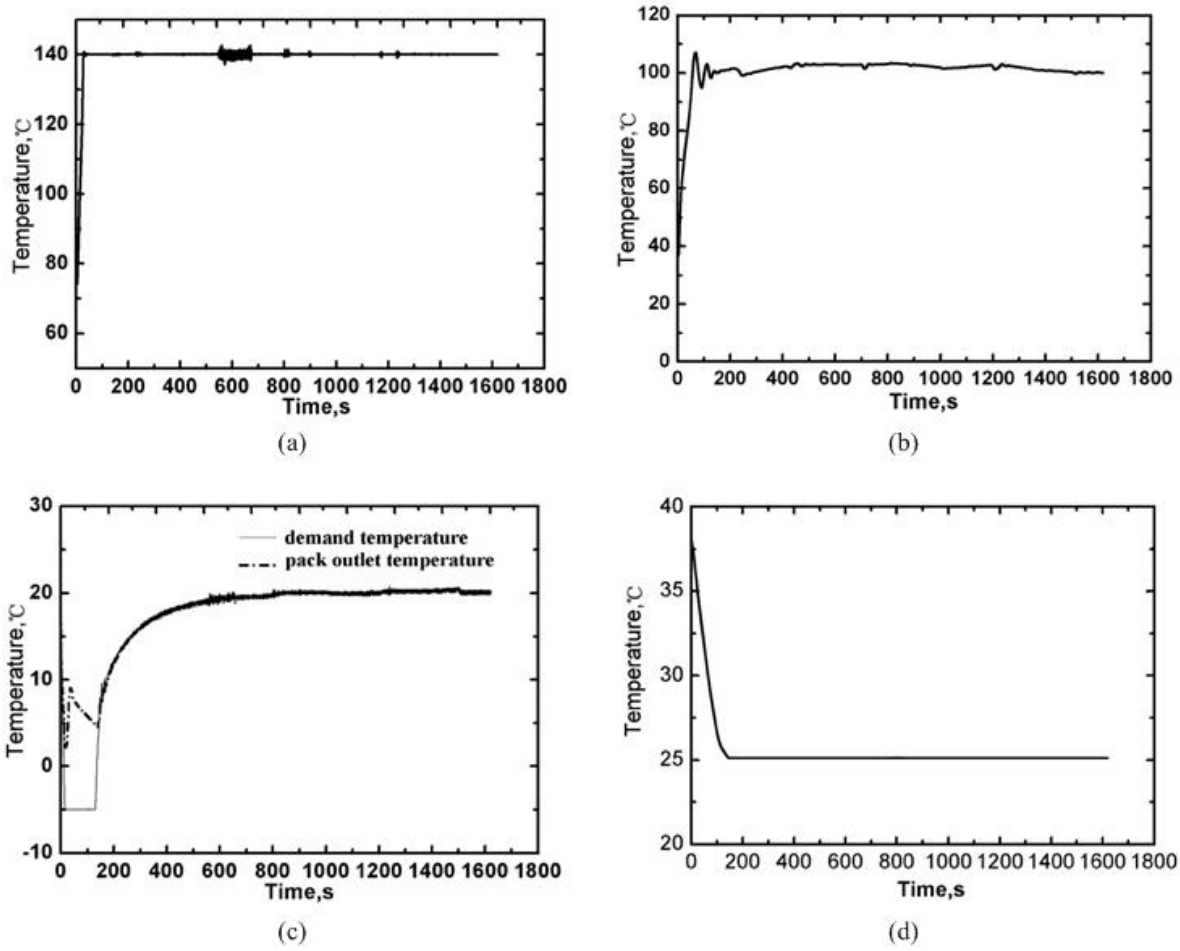


**Figure 2-30 Three-wheel ACM cooling condition: (a) compressor outlet temperature; (b) primary heat exchanger outlet temperature; (c) CAU outlet temperature; (d) cabin average temperature [39].**

Furthermore, a dynamic model of the Vapour Cycle Machine was developed between the University of Illinois, PC Krause and Associates Inc., and the U.S. Air Force Research Laboratory. This tool, also known as Transient Thermal Modelling and Optimization (ATTMO), was created within the Matlab-simulink ® framework. This model is divided into four parts: system actuation devices (valve, compressor), heat exchangers (evaporator, condenser), flow passageways (pipe geometries), and support functions (inlet and outlet flow). Figure 2-32 illustrates the scheme used to simulate the operation of the VCM. Two variables were considered in this model: the mass flow and compressor speed. The mass flow established for the refrigerant decrease from 0.007 to 0.004 kg/s in 500 seconds and with a

setback of 1000 seconds on the other hand. The compressor speed requested to vary from 1800 to 1500 RPM in 750 seconds and with a setback of 1250 seconds. Figure 2-33 shows the results of this simulation.

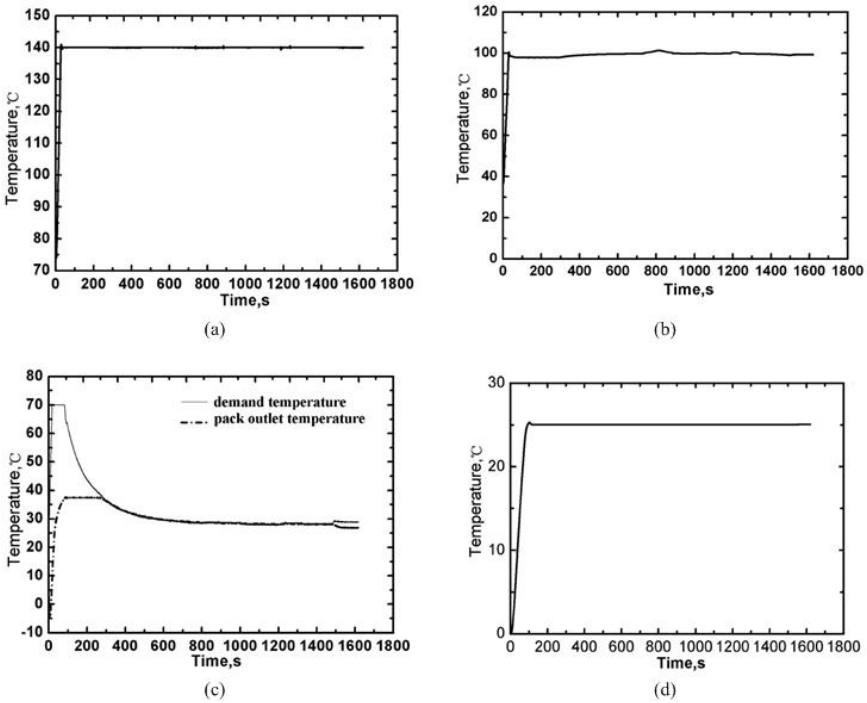


**Figure 2-31 Three-wheel ACM heating condition: (a) compressor outlet temperature; (b) primary heat exchanger outlet temperature; (c) CAU outlet temperature; (d) cabin average temperature [40].**

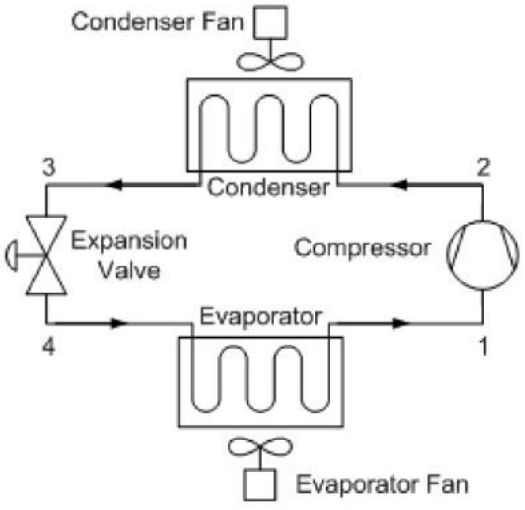


**Figure 2-32 Schematic of the VCM [40]**

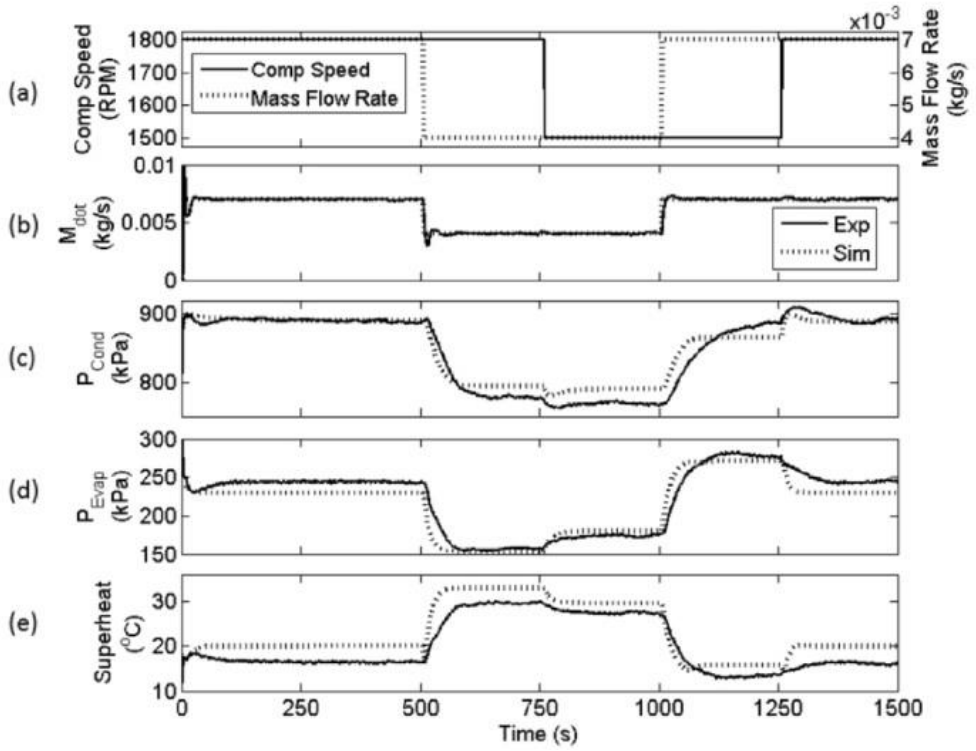


**Figure 2-33 VCM simulation: (a) input parameters; (b) mass flow rate; (c) condenser pressure; (d) evaporator pressure; (e) evaporator exit refrigerant superheat [40].**

# 3. Chapter | Methodology

## 3.1. ECS Power Consumption Model (PCM)

The integration of different blocks is proposed to obtain the power consumption of the ECS in helicopters. Each block contains different equations, variables, and generates independent results in order to reach the required power consumption for small rotorcraft in a given mission. These results give an idea of the importance of the ECS-PCM in establishing the optimal configuration for a given mission and aircraft.

The ECS-PCM consists of seven main systems each of these systems involves multiple subsystems in which are embedded the mathematical equations. The models were developed with Matlab-Simulink ®, its configuration is shown in Figure 3-1. Details of the models and their subsystems will be described in this chapter.

### 3.1.1. Executable model for a given rotorcraft mission

The executable model consists of five flight segments: ground, climb, cruise, hover, and descent. However, according to the Bell 206L-4 flight manual, the operation of the ECS is prohibited during climb, hover and descent; for that reason, the ECS-PCM calculations will apply only for two stages, ground and forward flight, during the other segments it will be considered in off mode [41]. This model requires three main factors to run the executable: Altitude, flight segment, and ISA deviation. The entire model will only require these three initial variables if the aircraft to be analysed is the Bell 206L-4, and if the flight conditions are equal to the one set in Section 4.1. Otherwise, it would be necessary to make appropriate modifications to take into account the geometry of the aircraft and flight conditions within the ECS-PCM.

The ECS-PCM has an auxiliary model that calculates physical properties of the standard atmosphere. The auxiliary model computes the air pressure, air density and the ambient temperature at a given altitude; this is essential information, for the systems operation. The executable model will therefore include two versions; the first can receive a specific point of

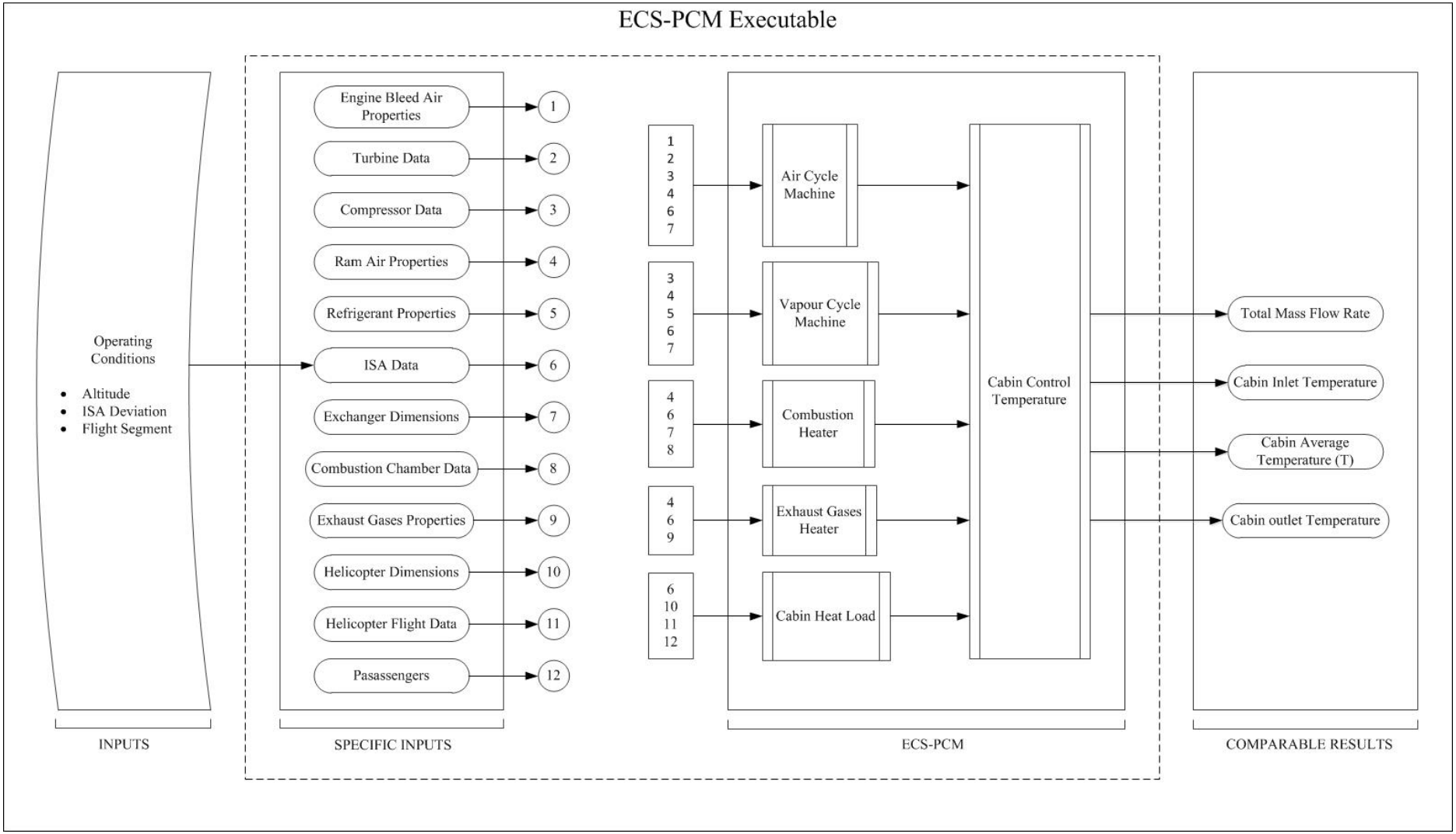


**Figure 3-1 ECS Power Consumption Model**

each flight segment. The second will be able to read a full flight path from ground to forward flight, until the aircraft touches the ground again and the engines are turned off.

The outputted data of these two models will contain the necessary information to make an assessment between the different ECS models, thus reaching a conclusion concerning the efficiency and required power consumption. Among the outputted data are: the pneumatic power consumption (required mass flow), Coefficient of Performance (COP), cabin inlet temperature, cabin outlet temperature, cabin average temperature, and the outlet temperature on each system configuration.

The inlet flight mission data is provided from a '.dat' file. Similarly, the output data will be written into a '.dat' file. The executable program will not require access to a Matlab-simulink® interface; will require only a library or Matlab Compiler Runtime (MCR), making this application accessible for users who do not have Matlab.

### 3.1.2. ECS-PCM validation and verification

Although Simulink platform provides multiple supports to identify errors in a model, it is common to make mistakes during the connection of the different mathematical blocks and symbols. Therefore, the ECS-PCM model was verified against hand calculations and compared with results from other studies in order to provide results within a reasonable range. The curve trends among others of the heat transfer and temperature changes were also verified against open literature.

Parts of the input values referred to in this study were provided by different Cranfield departments involved in the Clean Sky Project (e.g. dimensions, speeds, heights, etc.). The rest of the data was computed through iterations or assumed without exceeding reasonable ranges for the model. Similarly, this model contains aircraft design requirements for light helicopters such as the CS-27 (EASA), thus providing additional validation of the results.

### 3.1.3. Air Cycle Machine model

As described in Section 2.6.1, there are multiple configurations of ACM. For this study the Bootstrap Air Cycle Machine was chosen. This configuration consists of two heat exchangers

(Primary and Secondary), a compressor, a turbine, a reheater, a condenser, an evaporator and finally a water separator. Each of these components was modelled and integrated into the ACM model. The variables were set according to the settings of the Bell 206L-4 and the chosen flight mission. If a different aircraft geometry and flight configuration is considered, changes of variables in the exchanger model will be required. These changes are explained below.

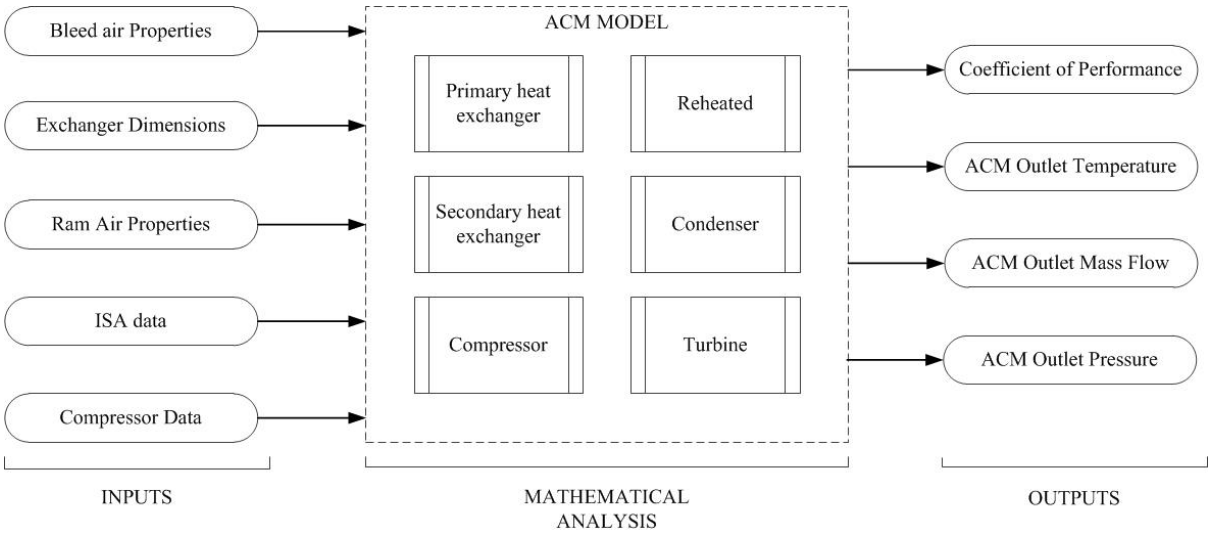


**Figure 3-2 Air Cycle Machine model**

***Exchangers***. A unique geometry of the exchanger and the corresponding equations are used to calculate the outlet temperatures, the mass flow, and pressures from the primary heat exchanger, secondary heat exchanger, superheater (reheater), evaporator, and condenser. As the operation of each of these components will be necessary to establish the geometry of the exchanger (Length, width and height), and the following input variables: the bleed air inlet temperature, pressure and mass flow, and the ram air inlet temperature, pressure and mass flow.

### 3.1.4. Vapour Cycle Machine model

The VCM is comprised of a compressor, an evaporator and a condenser. As was the case for the ACM model, exchanger geometries are set specifically for the Bell 206L-4. However, unlike the ACM, the VCM exchanger is gas-to-liquid. The liquid side is a closed circuit, so the temperatures, mass flow, and pressure depends on the refrigerant properties. The gas side

depend on the temperature and pressure provided by the atmosphere model. Thus, a change of the exchanger geometry will be necessary, if required to study the analysis of another aircraft and other mission.

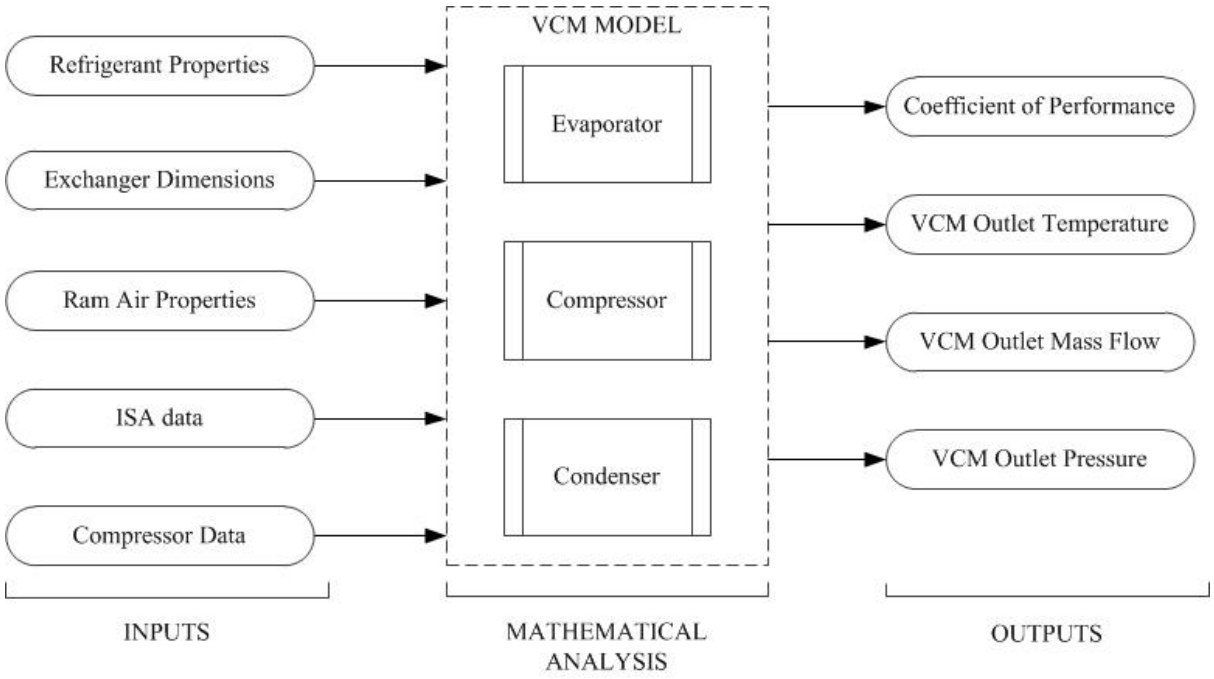


**Figure 3-3 Vapour Cycle Machine model**

### 3.1.5. Combustion Heater model

The Combustion Heater model is composed of a single heat exchanger; this system is responsible for transmitting the heat produced by the combustion chamber of the engine to the ram air. The temperature, pressure, and mass flow of ram air are inputs required by the model. The geometry of the heat exchanger should be adjusted if the configuration of the aircraft and its mission is changed. Additionally, the temperature generated inside the combustion chamber of the engine would have to be changed.

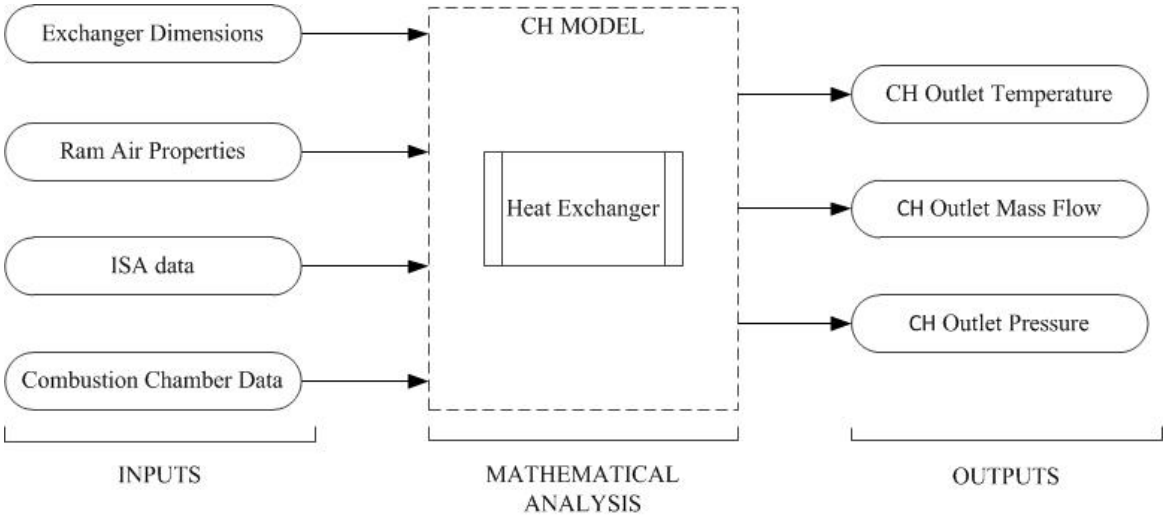


**Figure 3-4 Combustion Heater model**

### 3.1.6. Exhaust Gases Heater model

Like the CH model, the EGH model consists only of a heat exchanger. In this model the heat transfer between the exhaust gases on the engine of the helicopter and the ram air is calculated. This system requires on one side the ram temperature, pressure, and mass flow, and on the other side the exhaust gas temperature, pressure and mass flow as is shown in Figure 3-5.

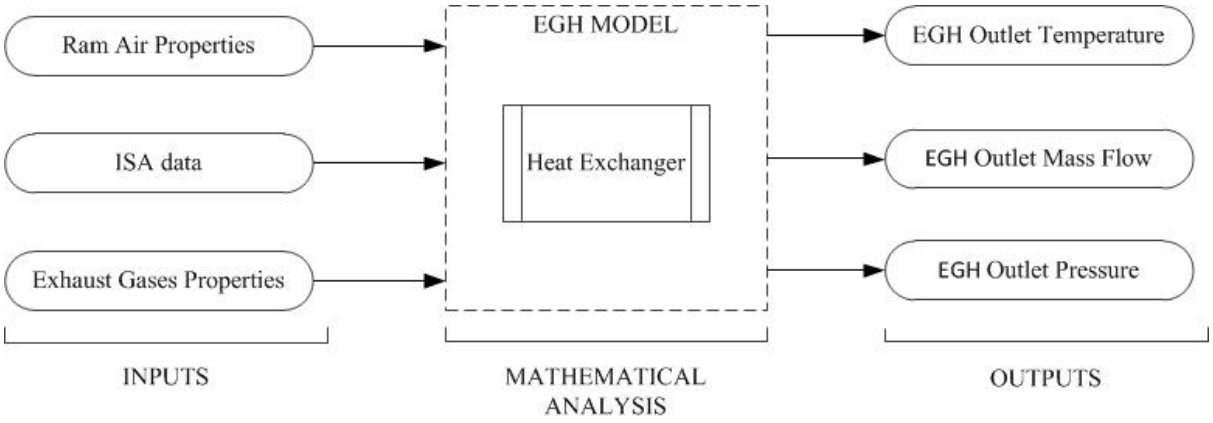


**Figure 3-5 Exhaust Gases Heater model**

### 3.1.7. Cabin heat load model

The cabin heat load model is one of the largest among all these models. Within this block are mathematical calculations to establish the heat loads generated by different sources in the

cabin. Overall this model consists of two main components, a cooling model, and a heating model. Each of these components contains separate calculations for each of the flight segments (forward flight and ground), by doing so more accurate results of the heat loads within the cabin are acquired. In addition, this model has an auxiliary model that defines the weather according to the altitude, and the flight segment in which the aircraft is located.

The cooling and heating models are divided into six parts: external surfaces (external helicopter walls), internal surfaces (internal cabin walls), solar radiation (windows, windshield, green roof), metabolic (human heat), infiltration of outside air into the cabin, electrical (lights, avionics). An extra block is added to compute the weather conditions. The general outline of cabin heat load model is shown in Figure 3-6. Within the input data are the segment flight path, the altitude of the aircraft and the International Standard Atmosphere (ISA) deviation. The segments of the flight path are defined within the model from 1 to 5, where 1 is ground, 2 is climb, 3 is cruise, 4 and 5 are hover and descent respectively.

The output of this model is the mass flow required to keep a comfortable temperature in the cabin. Like in the previous models, the cabin heat load model is configured for the Bell 206L-4 and specific to the mission established in this study. The variables within the heating and cooling model are detailed below.

***Weather condition.*** The temperature at the helicopter walls varies according to the position of the sun. The weather model is responsible for locating the position and angle of the sun by geo-positioning the rotorcraft. Thus, it is necessary to enter the time, day and month of the flight as well as its longitude and latitude.

***Helicopter flight direction and áreas.*** The heat loads on the walls will be determined by the structural areas and the rotorcraft flight direction. Therefore, the flight direction of the helicopter has to be set according to the cardinal points. For instance, if the flight path of the aircraft is from London to Cranfield and taking into consideration its global position, the helicopter would be flying from south to north. Thus if the sun is located east, the right side of the aircraft would be exposed, while the other side is not. Additionally, the area affected by the sun must be provided. For example, the area of the windows and/or the aluminium wall located on the exposed side of the helicopter.

***Occupants.*** The number of occupants (crew, and passengers) in the aircraft must be established in order to calculate the minimum required ventilation within the aircraft.

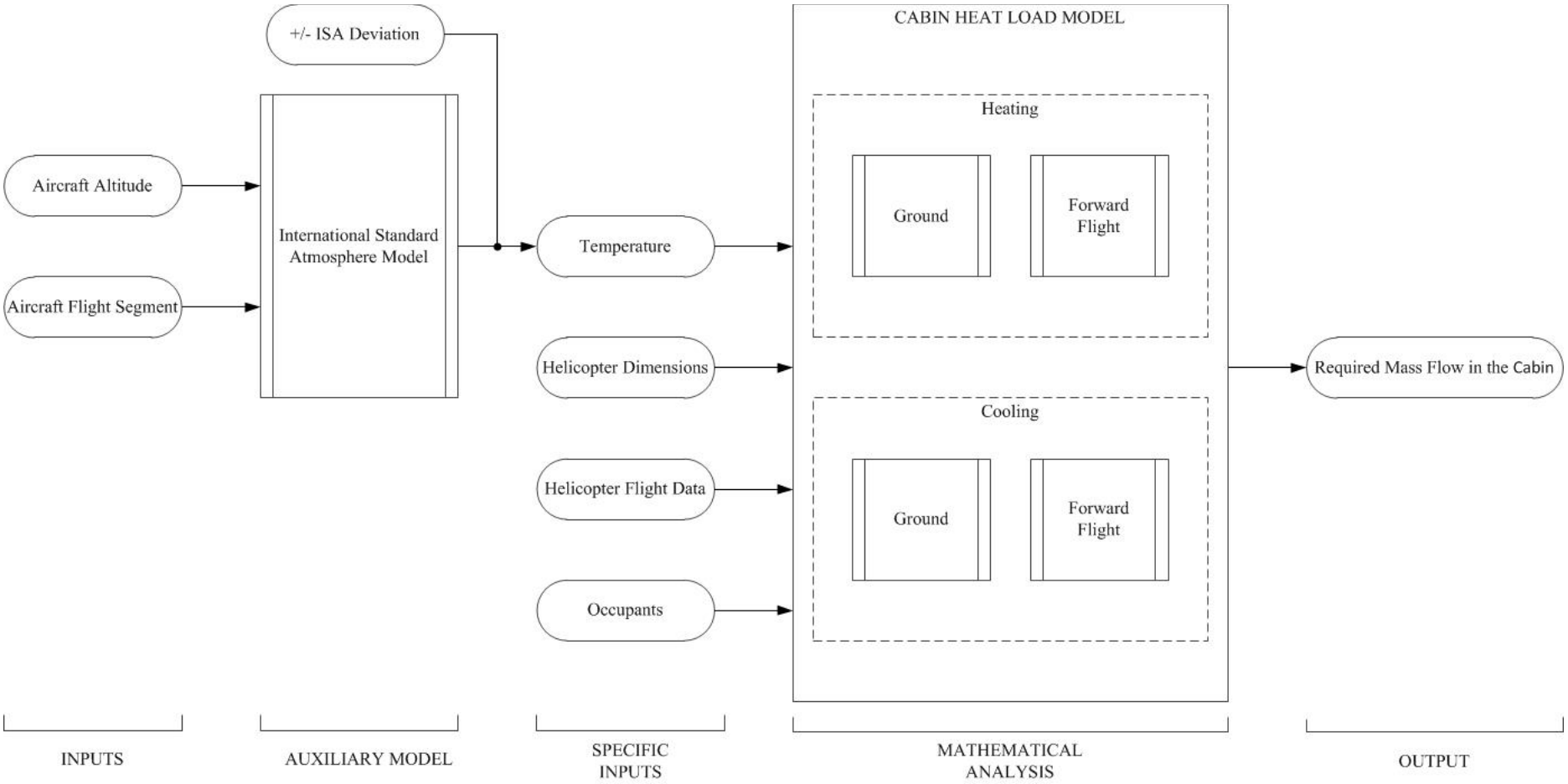


**Figure 3-6 Cabin heat load model**

### 3.1.8. Cabin model

Depending on the needs of the aircraft cabin, the cabin model would be responsible to enable or disable the subsystems and mix them if it is necessary. For instance, on a mission in a hot climate (desert), the model will enabled only the most feasible subsystem for this mission; either by mixing the cooling subsystem with the heating subsystem, or simply making use of the ACM. After enabling the subsystem that requires less mass flow, a thermal balance will be made with the results obtained by the heat loads in the cabin. Figure 3-7 shows the cabin model blocks process. The input data for this model are the temperature and mass flow supplied by the heating and cooling subsystems. The outputted data will be the average temperature within the cabin, the inlet temperature, and the outlet temperature.

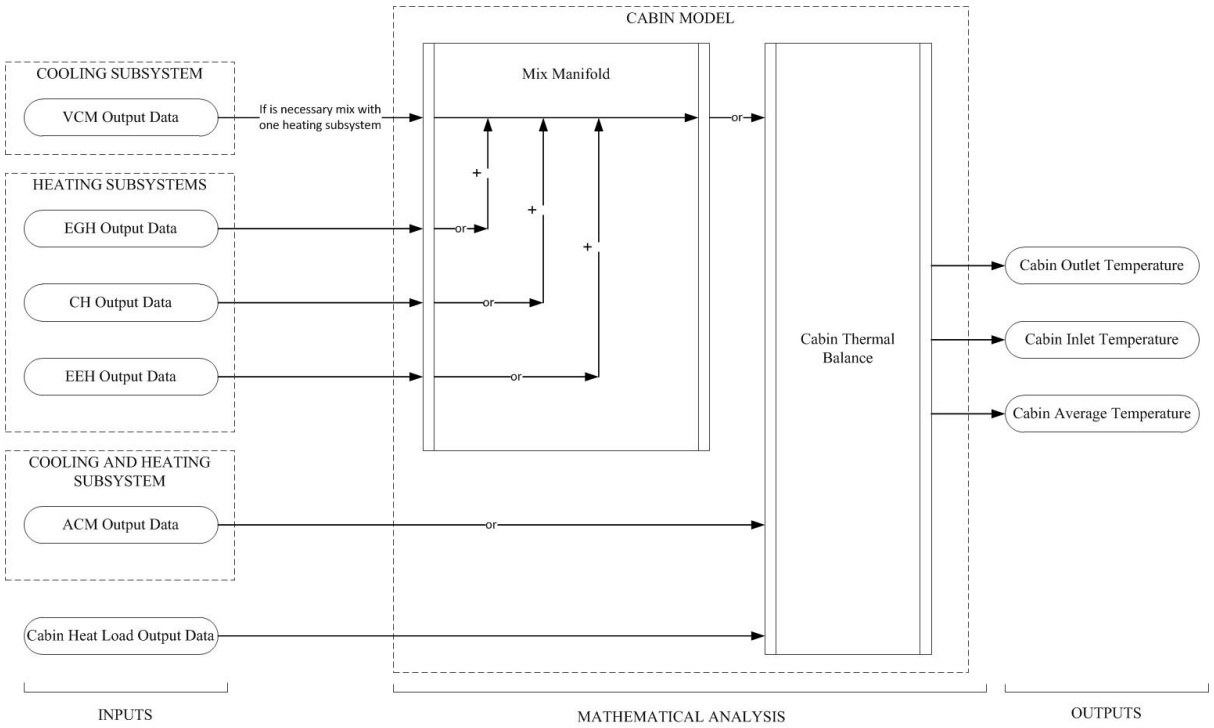


**Figure 3-7 Cabin model**

### 3.1.9. Cabin control temperature model

The temperature control model is the block responsible for mixing the heated air from the heating units with cold air from the cooling units. Initially, the model matched the variables from these two units with the variables required by the cabin (mass flow and heat load). If the desired temperature in the cabin is not reached once the variables are equaled, the model will

continue to increase the percentage of mass flow in the units until the requested temperature is achieved.

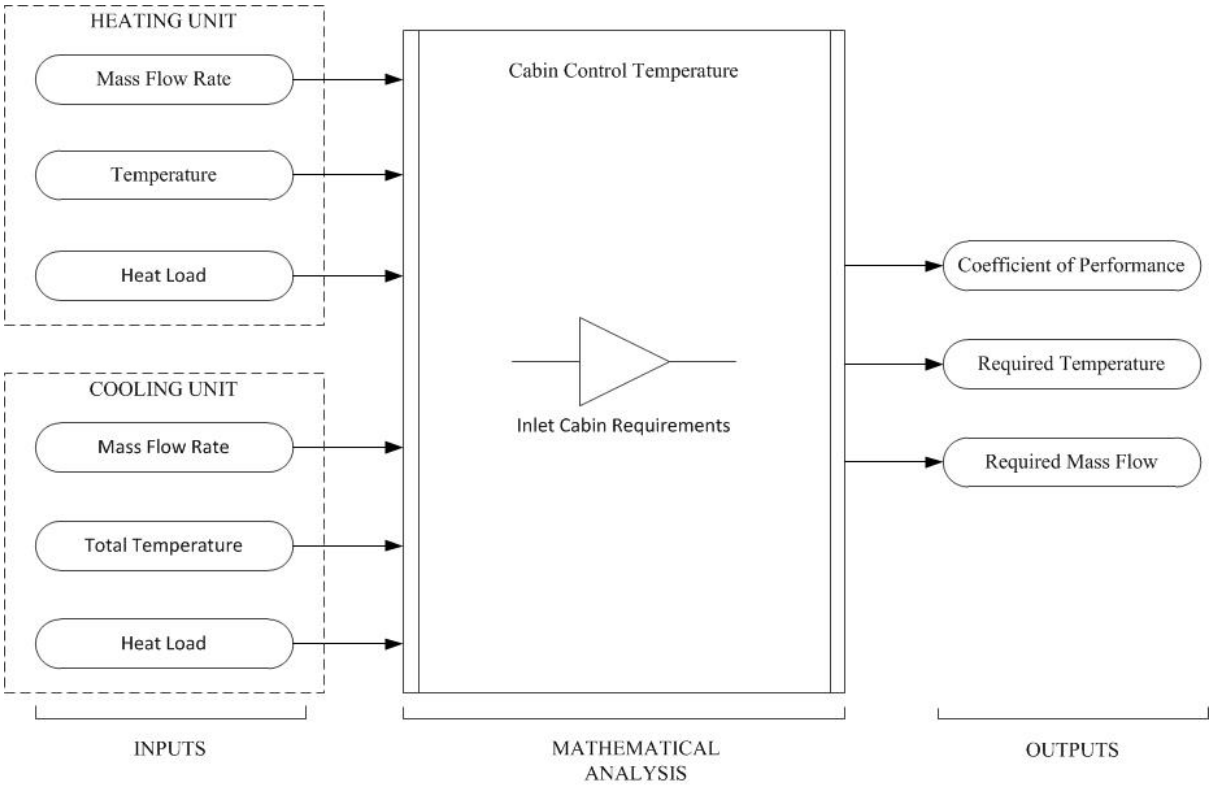


**Figure 3-8 Cabin control temperature model**

# 4. Chapter | ECS modelling development

## 4.1. Mission profile

Several mission parameters must be established for the environmental control system analysis. Among others the flight altitude, environmental conditions and the temperature inside the cabin are some of these parameters. According to the Bell 206L-4 [41] flight manual, the operation of the ECS is prohibited during climb, hover, and descent; for that reason, the ECS study will apply only for two stages, ground and forward flight. Figure 4-1 illustrates the flight path for the ECS analysis; the mission is divided into six stages: take-off, climb, cruise, descent, hover, and landing.

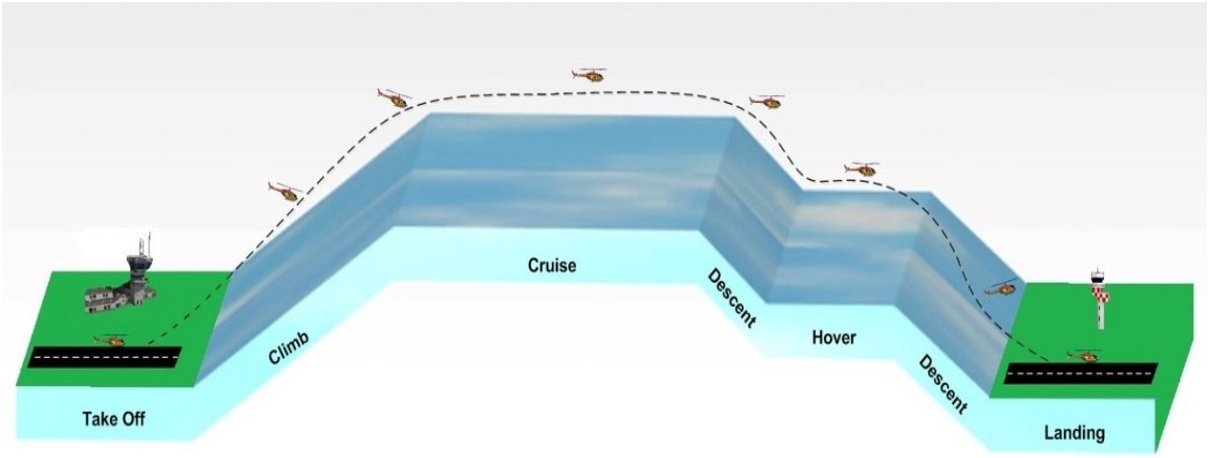


**Figure 4-1 Flight path mission**

At the end of the mission analysis after landing has been performed, the pneumatic power consumption over the entire mission of the systems is calculated. Two scenarios with different climatic conditions have been chosen; the first demonstrates the operation of the ECS to cool down the cabin during hot weather condition, while the other scenario simulates the ECS operation to warm up the cabin during cold weather.

Table 4-1 and 4-2 show the conditions for a given flight mission in the United States (warm weather) and United Kingdom (cold weather), respectively. The selected missions could not be performed in areas with extreme climates (hot or cold), due to the lack of information to generate a flight path with the data required for the simulation of the ECS. Moreover, much of the data collected were given by CleanSky, therefore it was decided to continue the

research with these data and not vary them to give a joint result at the end of the CleanSky project. Thus, the flight paths chosen for this study are the following (Figure 4-2 & 4-4):

***High temperature (303.15 K – in spring time)***

- Take off from (Departure): Miami International Airport - Florida (US)
- First waypoint: Fort Lauderdale VOR/DME - Florida (US)
- Second waypoint: Palm Beach VORTAC– Florida (US)
- Landing (Arrival): Palm Beach Gardens – Florida (US)

***Low temperature (275.15 K – in autumn time)***

- Take off from (Departure): London City Airport - England (UK)
- First waypoint: London VRP - England (UK)
- Second waypoint: Woburn Town VRP – England (UK)
- Landing (Arrival): Cranfield Airport – England (UK)

The aforementioned missions (time, flight path and positions) were automatically set by applications and software available in the public domain on the Internet: © 2014 iflightplanner online tool, and © 2014 SkyDemon Flight Planning [42, 43]. The first flight mission is waypoint located in Fort Lauderdale is a combine radio navigation point which consists of a VHF Omni Directional Radio Range (VOR) and a Distance Measuring Equipment (DME). The second waypoint located in Palm Beach is a navigation aid based on a VOR beacon and a Tactical Air Navigation System (TACAN).

The data listed in Table 4-1 corresponds to the latitude, longitude, and times that were acquired through an online tool. This tool generates a flight plan based on the aircraft and its flight. The data required about the aircraft is its manufacturer (Bell Helicopters), model (206L-4), and its performance (airspeed, rate of climb and rate of descent). This flight, as described above is from Miami International Airport to Palm Beach Garden.

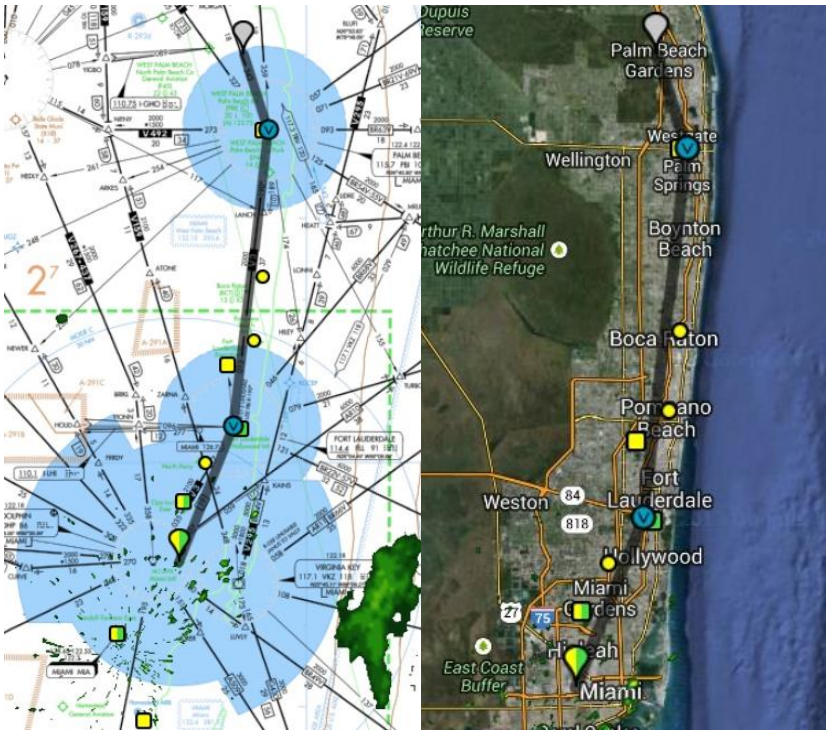


**Figure 4-2 Bell 206L-4 flight path mission 1 [42]**

**Table 4-1 Bell 206L-4 flight path mission 1 data**

| FLIGHT PATH MISSION DATA | | | | | | | |
|---|---|---|---|---|---|---|---|
| Waypoints | Segment | Latitude[B] | Longitude[B] | Altitude (m)* | Airspeed (m/s)* | Real Ambient Temperature (K)** | Time (s) |
| Miami International Airport | Ground | 25.79 | -80.28 | 2 | 0 | 303.15<br>30 °C | 300[A] |
| | Climb | | | 0-450 | 40 | 302.15<br>29 °C | 540[B] |
| Fort Lauderdale | Forward Flight | 26.07 | -80.16 | 450 | 60 | 300.15<br>27 °C | 780[B] |
| | Descent | | | 450-25 | 40 | 302.15<br>29 °C | 300[B] |
| Palm Beach | Hover | 26.67 | -80.14 | 25 | 0 | 303.15<br>30 °C | 300[B] |
| | Descent | | | 25-0 | 40 | 303.15<br>30 °C | 60[B] |
| Palm Beach Gardens | Ground | 26.83 | -80.14 | 2 | 0 | 303.15<br>30 °C | 180[A] |

[A] *Assumed data*

[B] *Data computed from © 2014 iflightplanner online tool*

**Data given by Clean Sky TE group*

***Local temperature from National Weather Service*

The total flight has a duration of 33 minutes, without taking into consideration the time on ground for engine starting and turning off. According to a consulted experienced pilot from the Colombian Army, that time on the ground depends on the operational check list. For this reason, and taking into consideration that the departure is from an International Airport, it is reasonable to assume five minutes for operational check list, engine starting, and taxi, and three minutes for taxi, and engine shutdown (Figure 4-3).

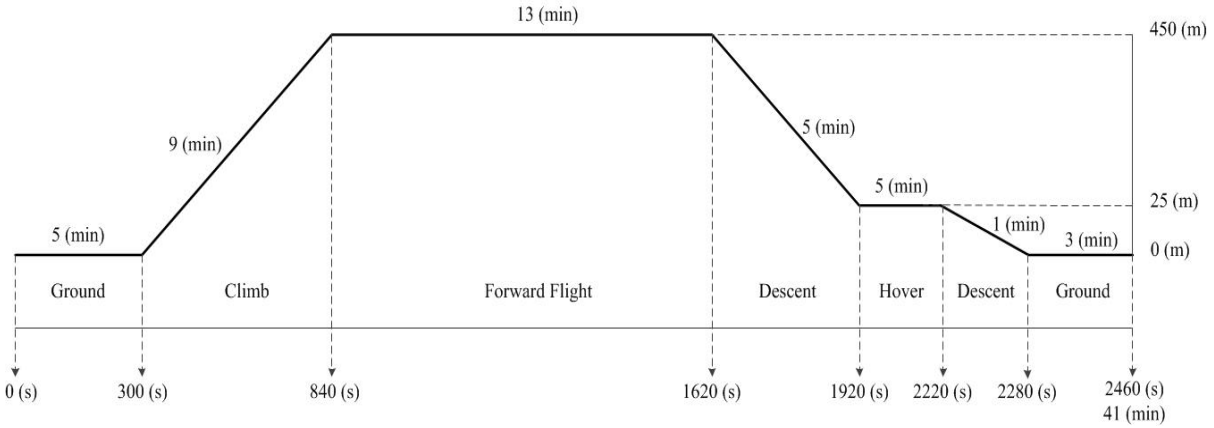


**Figure 4-3 Flight path mission 1 timing and altitude**

The Second flight mission starts in London City Airport and finalized in Cranfield Airport. As the previously flight path, this mission involves two waypoints. The first is a Visual Reference Point (VRP) located in London and the second one in Woburn Town near Cranfield. In between these two points of the mission was necessary to make a detour (white circular spots in Figure 4-4), because of the Luton Airport restricted flight area. For this mission, the hover segment is performed close to the second VRP during five minutes.

Similarly, a data list table corresponding to the second flight path was set up. The data in Table 4-2 was taken from the SkyDemon program and data supplied by Clean Sky for the Bell206L-4. As mentioned above, this flight is from London City Airport to Cranfield Airport.

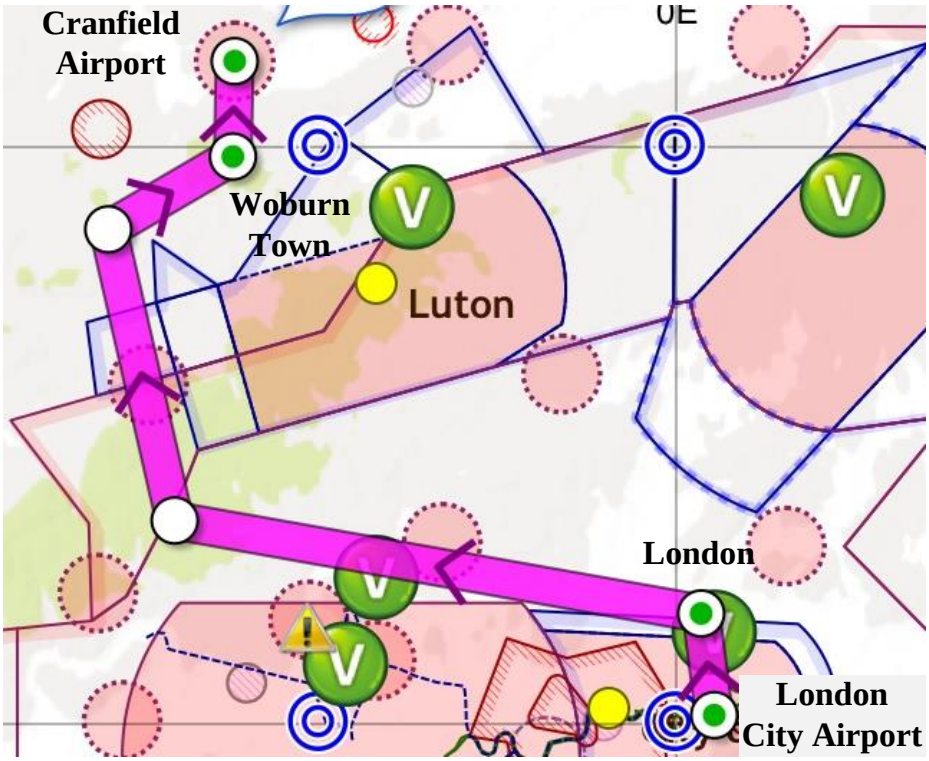


**Figure 4-4 Bell 206L-4 flight path mission 2 [43]**

**Table 4-2 Bell 206L-4 flight path mission 2 data**

| FLIGHT PATH MISSION DATA | | | | | | | |
|---|---|---|---|---|---|---|---|
| Waypoints | Segment | Latitude[B] | Longitude[B] | Altitude (m)* | Airspeed (m/s)* | Real Ambient Temperature (K)** | Time (s) |
| London City Airport | Ground | 51.47 | -0.46 | 0 | 0 | 278.15<br>5 °C | 300[A] |
| | Climb | | | 0-450 | 40 | 277.15<br>4 °C | 540[B] |
| London | Forward Flight | 51.59 | 0.03 | 450 | 60 | 275.15<br>2 °C | 300[B] |
| | Descent | | | 450-25 | 40 | 277.15<br>4 °C | 300[B] |
| Woburn Town | Hover | 51.92 | -0.79 | 134 | 0 | 277.15<br>4 °C | 300[B] |
| | Descent | | | 134-109 | 40 | 277.15<br>4 °C | 60[B] |
| Cranfield Airport | Ground | 52.07 | -0.61 | 109 | 0 | 277.15<br>4 °C | 180[A] |

[A] *Assumed data*

[B] *Data computed from © 2014 iflightplanner online tool*

**Data given by Clean Sky TE group*

***Local temperature from Met Office Service*

The total flight time is of 25 minutes, without taking into consideration the time on ground for engine starting and turning off. The assumed time on ground is of five minutes for operational check list, engine starting, and taxi, and three minutes for taxi, and engine shutdown (Figure 4-5). Altitudes were established by Clean Sky (TE), and were used for this mission in order to give continuity to existing studies performed with the current PHOENIX model. The temperatures were selected on a particular day to validate this model, and thus could be used in future simulations with different temperatures.

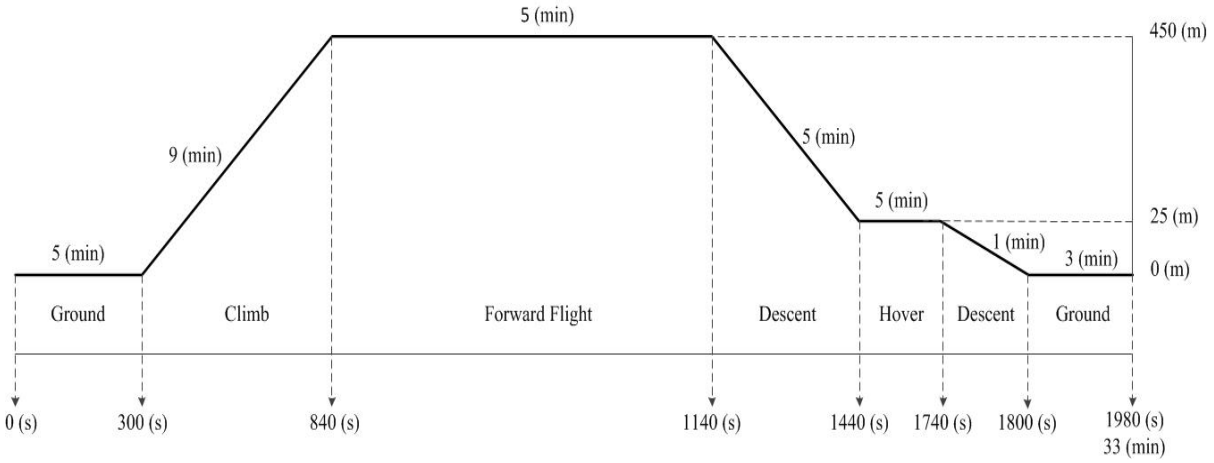


**Figure 4-5 Flight path mission 2 timing and altitude**

## 4.2. Environmental Control System load analysis

Several factors must be taken into consideration for the design of the ECS, as described in Chapter 2 and Chapter 3. The ECS load is one of these considerations; this involves the calculation of heat gained and heat lost within the aircraft. Cooling (heat lost) and heating (heat gain) loads are dependent upon cabin requirements, climatic conditions, heat flux and heat generation. In order to define the ECS load requirements, it is necessary to evaluate the various elements that comprise the total constant state ECS load. The mathematical analysis of these elements are covered in this section.

### 4.2.1. Heat transfer

In a helicopter there are six sources of heat: the kinetic heating (internal and external elements), solar heating (transparent surfaces), avionic heat load, infiltration heat load, and the occupants head load. Heat is a form of energy transferred from one object to another.

There are 3 main ways to transfer heat, by conduction (K), by convection (C), and radiation (R) [13].

Conduction occurs when two solids or fluids interact, transferring energy from the warmer side to the cooler side.

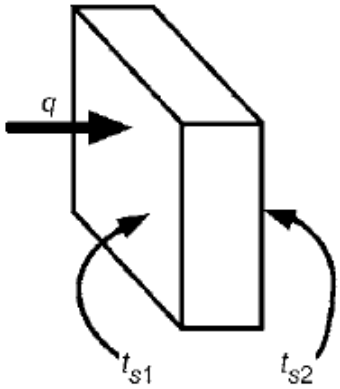


**Figure 4-6 Conduction [44]**

The general equation describing conduction is [44],

$$Qk = k\frac{(t_{s1}-t_{s2})A}{x} \qquad \textbf{(Equation 4-1)}$$

Where $k$ is the thermal conductivity of the material in W/m$^2$ K; $A$ is the surface Area, in m$^2$; $x$ is the surface is thickness, in m; and ($t_{s1}$-$t_{s2}$) represents the temperature difference, in K.

The transfer between a fluid in motion and a surface at different temperatures is called convection. When the fluid in contact is not in motion the heat transfer is performed by conduction. Fluid motion caused by an external force, such as fan flow, is forced convection.

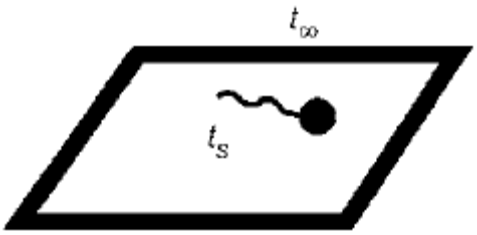


**Figure 4-7 Convection [44]**

The basic equation for the convection phenomenon is [44],

$$Q_c = hA(t_s - t_\infty) \qquad \textbf{(Equation 4-2)}$$

Where $h$ is the convective heat transfer coefficient in W/m$^2$ K; $A$ is the surface Area, in m$^2$; and ($t_s$-$t_\infty$) denotes again the temperature difference, in K.

The thermal radiation refers to energy emitted by matter when its temperature is above absolute zero. The energy is transported by electromagnetic waves and does not require the presence of a material medium as in conduction and convection heat transfer. Figure 4-8 illustrates the various modes of heat transfer.

The elementary equation for radiation transfer is [44],

$$Q_r = \varepsilon\sigma A(T_s^4) \qquad \textbf{(Equation 4-3)}$$

Where $\varepsilon$ is the surface is emissivity, $0 \leq \varepsilon \leq 1$. For a black surface, $\varepsilon$=1; $\sigma$=5.67x10$^{-8}$ in W/m$^2$ is the Stefan-Boltzmann constant; $A$ is the surface Area, in m$^2$; and $T_s^4$ is the absolute surface temperature, in K.

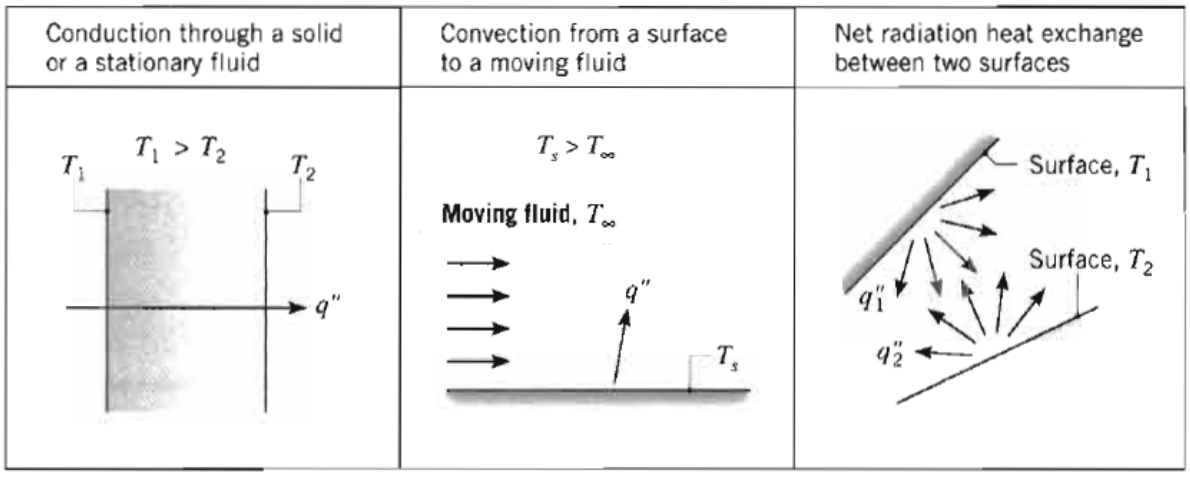


**Figure 4-8 Heat transfer modes [13]**

### 4.2.2. Kinetic heating

The kinetic heat is a result of the friction of the skin of the helicopter with the surrounding air, in other words, it is a form of forced convection between them in flight condition or ground static. This generates heat gain in the skin of the aircraft, which is transferred by convection to the cabin increasing its temperature, and the temperature of the equipment on board.

The temperature gain in the skin of the aircraft depends on its condition. In flight, for a given rotorcraft or aircraft with a speed range below Mach 2 it is satisfactory to assume that the skin temperature $T_w$ is equal to the recovery temperature $T_r$, such that:

$$T_w = T_r = T\left(1 + r\frac{\gamma-1}{2}M^2\right) \qquad \textbf{(Equation 4-4)}$$

Where $T$ is the static temperature (or ambient temperature) of the air in K; $r$=0.89 is the recovery coefficient for turbulent flow, and $r$=0.84 for laminar flow [23]; $\gamma$=1.4 is the ratio of specific heat for air; and $M$ is the aircraft's Mach number.

In static ground condition, the temperature of the skin is increased by the radiation reflected from the ground. The following equation can be used for its calculation.

$$T_{wg} = \frac{T+\alpha I_g}{h_e} \qquad \textbf{(Equation 4-5)}$$

Where $\alpha$=0.8 is the fraction of solar radiation absorbed [44]; $I_g$ is the total solar radiation at ground level in W/m$^2$; $h_e$ is the external heat transfer coefficient, in W/m$^2$.

### 4.2.3. Heating and cooling analysis

The temperature and humidity control within the aircraft is essential to maintain a safe and comfortable environment for the occupants. A comfortable level inside the cabin temperature lies around 297.15 K (24 °C), as explained in Chapter 2 under most environmental conditions. When the temperature inside the helicopter is below the comfort level, the cabin

must be heated (heating process) to reach the required temperature of 297.15 K (24 °C). When the temperature is higher, the cabin must be cooled (cooling process).

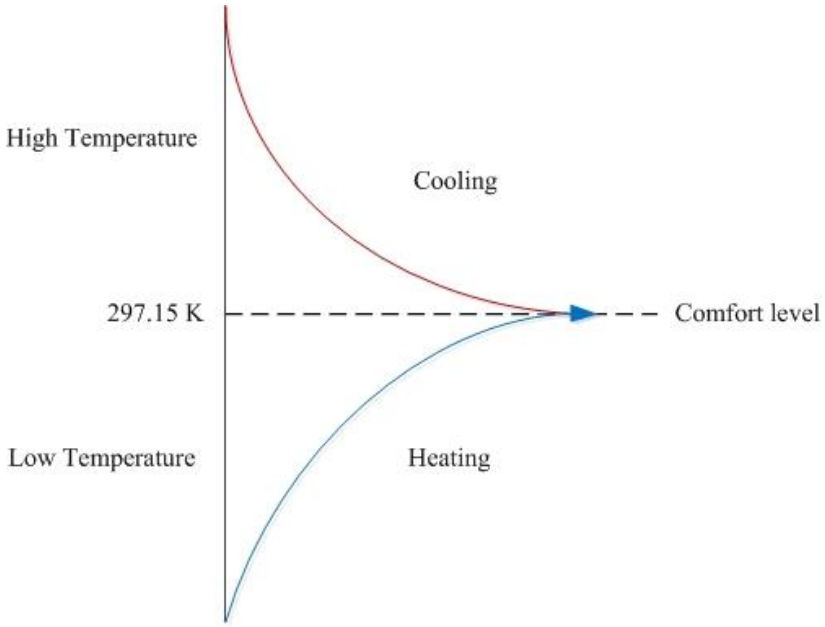


**Figure 4-9 Aircraft cooling and heating for cabin comfort**

To perform the heating and cooling analysis, it is necessary to identify losses and heat gains inside the cockpit and the passenger cabin. The total heat transfer $Q$ for heating or cooling the cabin is then.

$$Q = Q_c + Q_s + Q_o + Q_i + Q_e \qquad \textbf{(Equation 4-6)}$$

Where $Q_c$ is the convection heat load in W; $Q_s$ is the solar heat load, W; $Q_o$ is the occupant heat load, W; $Q_i$ is the infiltration heat load, W; and $Q_e$ is the electrical heat load, W.

Below 215.15 K (-60 °C), the solar radiation is negligible; the equation can be expressed as follows.

$$Q = Q_c + Q_i - (Q_o + Q_e) \qquad \textbf{(Equation 4-7)}$$

Where $Q_c$+$Q_i$ are heat losses, and $Q_o$+$Q_e$ are heat gains.

### 4.2.4. Rotorcraft surfaces heat load analysis

In order to perform the heat load calculations, it is necessary to consider the Bell 206L-4 geometry. Figure 4-10 shows the required sections from the Bell helicopter to compute the heat loads inside.

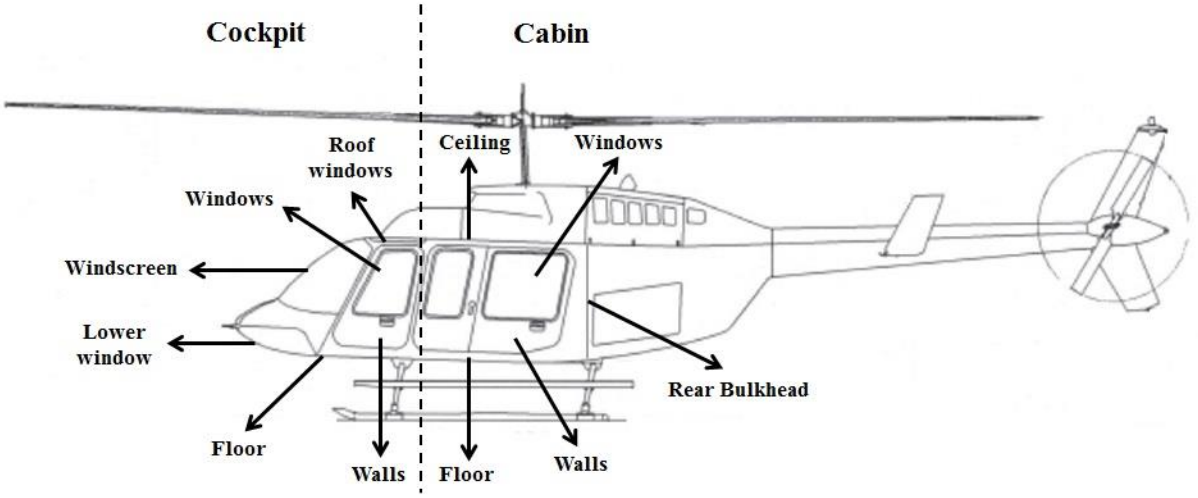


**Figure 4-10 Bell 206L-4 geometry [4]**

With the aim to perform a detailed study, the Bell 206L-4 has been divided into the cockpit and the cabin; likewise the surfaces areas have been separated. Table 4-3 shows the different surfaces area in cockpit and cabin.

**Table 4-3 Bell 206L-4 surface areas**

| **Cockpit** | |
|---|---|
| Surface | Area ($m^2$) |
| Walls | 1.24 |
| Floor | 0.65 |
| Roof windows | 0.13 |
| Windows | 0.29 |
| Windscreen | 1.4 |
| Lower windows | 0.74 |

| Cabin | |
|---|---|
| Surface | Area ($m^2$) |
| Walls | 4.27 |
| Floor | 1.93 |
| Ceiling | 2.61 |
| Windows | 1.08 |
| Rear Bulkhead | 1.4 |

Heat loads on each of the surfaces of the helicopter are calculated using the general equation for convection heat transfer. The convection heat load for the Bell 206L-4 is given by.

$$Q_c = q_1 + q_2 + q_3 + q_4 + q_5 + q_6 \quad \textbf{(Equation 4-8)}$$

Where $q_1$ is the transparency heat transfer in W; $q_2$ is the wall (un-insulated) heat transfer, W; $q_3$ is the wall (insulated) heat transfer, W; $q_4$ is the floor heat transfer, W; $q_5$ is the ceiling heat transfer, W; and $q_6$ is the rear bulkhead heat transfer, W.

Heat transfer in transparent areas (windows and windshield) of the helicopter can be obtained from the following equation [23].

$$q_1 = U_1 A_1 \Delta T \quad \textbf{(Equation 4-9)}$$

Where $U_1$ is the overall heat load coefficient of transparency area in $W/m^2$; $A_1$ is the transparency area, $m^2$; $\Delta T$ is the temperature difference.

As suggested by ASHRAE handbook fundamentals (2009), the overall heat load coefficient $U$ can be calculated based on the total resistance from outside to inside with the following equation.

$$U_1 = \frac{1}{\frac{1}{h_e} + \frac{1}{h_{kt}} + \frac{1}{h_i}} \quad \textbf{(Equation 4-10)}$$

Where $h_e$ is the external heat load coefficient in $W/m^2$; $h_{kt}$=11.6 in $W/m^2$ is the conductivity coefficient in transparency [Beenham 1969]; $h_i$ is the internal heat load coefficient, $W/m^2$.

As previously mentioned under Kinetic heating, the skin temperature in flight $T_w$ is equal to the recovery temperature $T_r$; once this assumption is taken, the external heat load coefficient $h_e$ should not be included in the above equation. For both heating and cooling, in ground static condition and flight can be used the following equation.

$$h_e = 5.678263(2.0 + 0.314V_e) \quad \textbf{(Equation 4-11)}$$

Where $V_e$ = 6.7 in m/s is the external wind velocity [23].

The internal heat load coefficient is given by

$$h_i = 5.678263(2.0 + 0.314V_i) \quad \textbf{(Equation 4-12)}$$

Where $V_i$ = 1.005 in m/s is the internal air velocity for an occupied compartment [23].

The temperatures difference varies depending on the analysis and the condition performed, as shown below.

$$\Delta T = T_c - T \ (For\ Heating\ analysis) \quad \textbf{(Equation 4-13)}$$

$$\Delta T = T_w - T_c \ (For\ cooling\ analysis\ in\ flight) \quad \textbf{(Equation 4-14)}$$

$$\Delta T = T_{wg} - T_c \ (For\ cooling\ analysis\ at\ ground) \quad \textbf{(Equation 4-15)}$$

Where $T_c$ is the cabin desired temperature in K.

The heat transfer in the helicopter walls (insulated and un-insulated) can be obtained from the following equation.

$$q_2 = U_2 A_2 \Delta T \ (For\ un - insulated\ walls) \quad \textbf{(Equation 4-16)}$$

$$q_3 = (U_3 + t) A_3 \Delta T \ (For\ insulated\ walls) \quad \textbf{(Equation 4-17)}$$

Where $U_2$ and $U_3$ is the overall heat load coefficient of the wall area in W/m$^2$; $A_2$ and $A_3$ is the wall area, m$^2$; $\Delta T$ is the temperature difference.

The overall heat load coefficient of an un-insulated wall is given by.

$$U_2 = \frac{1}{\frac{1}{h_e} + h_{kw} + \frac{1}{h_i}} \quad \textbf{(Equation 4-18)}$$

And

$$h_{kw} = \frac{x_w}{k_w} \quad \textbf{(Equation 4-19)}$$

Where $h_{kw}$ is the wall material (Aluminium alloy) heat load coefficient in W/m$^2$; $k_w$ = 170 in W/m is the thermal conductivity of the Aluminium alloy [13]; and $x_w$ = 0.001 in meters is the thickness of the Aluminium alloy [13].

For insulated surfaces, it is necessary to calculate the thermal conductivity coefficient of insulation material, in this case fiberglass. Similarly, the heat transfer increase percentage of the insulation gap area is added.

According to a research conducted by Lewis J. (1979), the increase in heat transfer is given by.

$$t = U_3 \left(\frac{t_i C}{100}\right) \quad \textbf{(Equation 4-20)}$$

Where $t$ is the total increase of thermal transmittance in percentage; $U_3$ is the overall heat load coefficient of an insulated wall, W; $t_i$ is the increase of thermal transmittance in percentage; and $C$ is the area conversion factor.

Figure 4-11 shows the heat transfer increase percentage, which can be obtained with the thickness and width of the material gap. For gap thickness is appropriate to assume a width of 0.004 m [45]. According to ASHRAE handbook fundamentals (2009), the thickness of the fuselage insulation wall is of 0.03 m and 0.02 m in floors and bulkheads.

The conversion factor of the area is obtained by interpolating data acquired by Lewis J. (1979) [45], the equation is then.

$$C = -0.358 \ln(A_3) + 1.0122 \quad \textbf{(Equation 4-21)}$$

The overall heat load coefficient of an insulated wall is given by

$$U_3 = \frac{1}{\frac{1}{h_e} + h_{kw} + h_{ki} + \frac{1}{(h_a + h_r)} + \frac{1}{h_i}} \quad \textbf{(Equation 4-22)}$$

And

$$h_{ki} = \frac{x_i}{k_i} \quad \textbf{(Equation 4-23)}$$

Where $h_{ki}$ is the insulation (glass fibre) heat load coefficient in W/m$^2$; $k_i$ = 0.048 in W/m is the thermal conductivity of the glass fibre [13]; $x_i$ = 0.03 in m is the thickness of the insulation [45]; $h_a$ is the conduction and convection heat load coefficient of the air space, W/m$^2$; and $h_r$ is the radiation heat load coefficient of the air space, W/m$^2$.

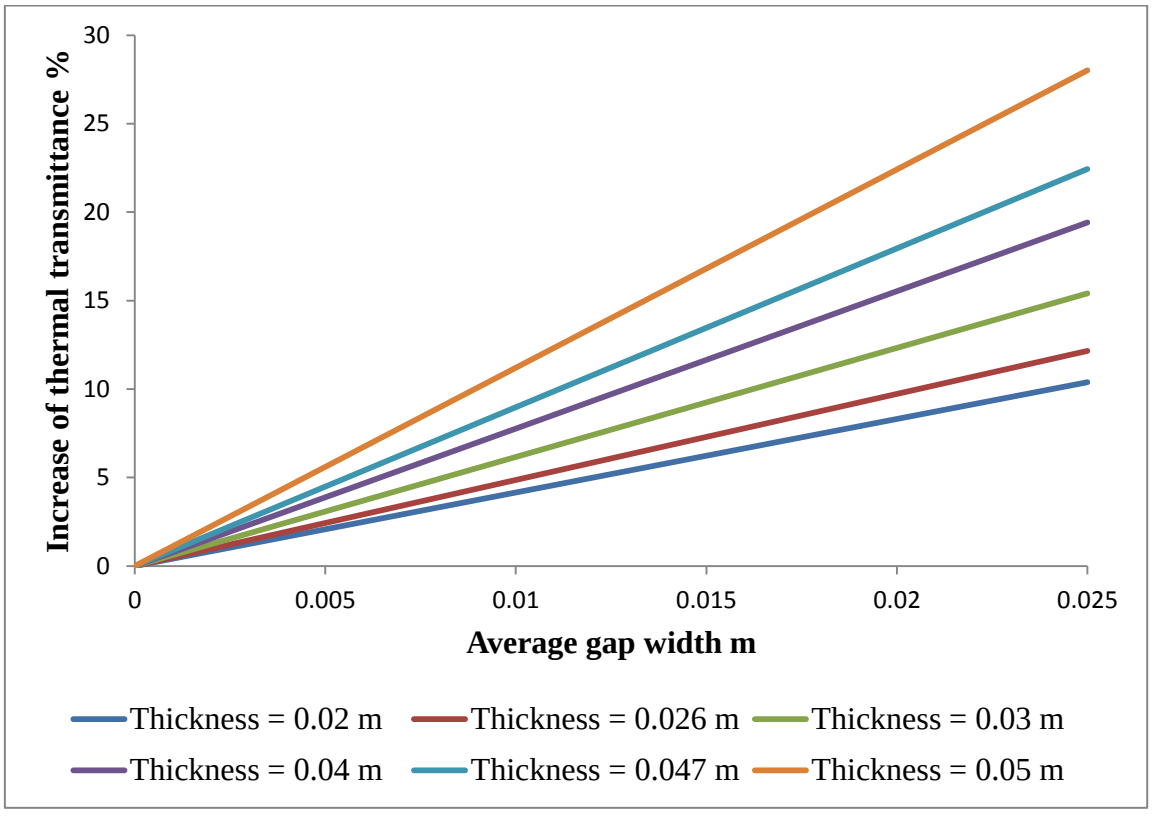


**Figure 4-11 Increase of thermal transmittance [45]**

Often, a simple wall with insulation includes an air space between the outer and inner skin, as illustrated in Figure 2-10. Heat transfer for a simple wall is given by conduction, convection and radiation $h_a$+$h_r$. An iteration process should be performed to obtain an accurate result. For a conductance by conduction and convection $h_a$ in air spaces that are vertically, can be used any of the following equations [23].

$$\frac{h_a X_a}{k_a} = N_{nu} = 1 \ (For\ N_g \leq 2000) \quad \textbf{(Equation 4-24)}$$

$$\frac{h_a X_a}{k_a} = N_{nu} = \left[\frac{0.20}{\left(\frac{L}{x_a}\right)^{\frac{1}{9}}}(N_g N_p)^{0.25}\right] \ (For\ 2x10^4 \leq N_g \leq 2.1x10^5) \quad \textbf{(Equation 4-25)}$$

$$\frac{h_a X_a}{k_a} = N_{nu} = \left[\frac{0.071}{\left(\frac{L}{X_a}\right)^{\frac{1}{9}}}(N_g N_p)^{0.333}\right] \ (For\ 2.1x10^5 \leq N_g \leq 1.1x10^9) \quad \textbf{(Equation 4-26)}$$

For air spaces which are horizontally can be used any of the following equations [23].

$$\frac{h_a X_a}{k_a} = N_{nu} = \left[0.21(N_g N_p)^{0.25}\right] \ (For\ 10^4 \leq N_g \leq 3.2x10^5) \quad \textbf{(Equation 4-27)}$$

$$\frac{h_a X_a}{k_a} = N_{nu} = \left[0.075(N_g N_p)^{0.333}\right] \ (For\ 3.2x10^5 \leq N_g \leq 10^9) \quad \textbf{(Equation 4-28)}$$

Where $k_a$ = 0.025 in W/m is the thermal conductivity of air [23]; $L$=1.19 meters is the height of air space (Bulkhead altitude), m; $X_a$ =0.177 is the width of air space, m [45]; $N_{nu}$ is the Nusselt number; $N_g$ is the Grashof number; $N_p$ = 0.72 is the Prandtl number [23].

The Grashof number $N_g$ is given by.

$$N_g = \frac{X_a^3(\rho * g)^2\left(\frac{1}{T_{av}}\right)\Delta T_a}{\mu^2} \quad \textbf{(Equation 4-29)}$$

Where $\rho$ is the density of air in kg/m$^3$; $g$ is the gravity of earth, m/s$^2$; $T_{av}$ is the air space average temperature, K; $\Delta T_a$ is the air space temperature difference, K; $\mu$ is the dynamic viscosity of air, Pa·s.

The air space average temperature $T_{av}$ and the air space temperature difference $\Delta T_a$ are given by.

$$T_{av} = \frac{T_{1i}+T_{2w}}{2} \quad \textbf{(Equation 4-30)}$$

$$\Delta T_a = T_{1i} - T_{2w} \quad \textbf{(Equation 4-31)}$$

Where $T_{1i}$ is the insulation material temperature, K; $T_{2w}$ is the internal surface wall temperature, K.

For the calculation of the temperatures $T_{1i}$ and $T_{2w}$ is necessary to assume a value for $h'_a+h'_r$, and solve the equation of the overall heat load coefficient of an insulated wall $U_3$; then one of the following equations for $T_{1i}$ is used [23].

$$T_{1i} = T + \frac{U_3}{U_{k1}}(T_c - T)(For\ Heating\ analysis) \quad \textbf{(Equation 4-32)}$$

$$T_{1i} = T_w + \frac{U_3}{U_{k1}}(T_w - T_c)(For\ cooling\ analysis\ in\ flight) \quad \textbf{(Equation 4-33)}$$

$$T_{1i} = T_{wg} + \frac{U_3}{U_{k1}}\left(T_{wg} - T_c\right)(For\ cooling\ analysis\ at\ ground) \quad \textbf{(Equation 4-34)}$$

And

$$U_{k1} = \frac{1}{\frac{1}{h_e}+h_{kw}+h_{ki}} \quad \textbf{(Equation 4-35)}$$

Where $U_{k1}$ is the overall heat load from the external surface film to air space, W/m$^2$.

The internal surface wall temperature $T_{2w}$ can be calculated with the following equation [23]

$$T_{2w} = T_c - \frac{U_3}{U_{k2}}(T_c - T)(For\ Heating\ analysis) \quad \textbf{(Equation 4-36)}$$

$$T_{2w} = T_c - \frac{U_3}{U_{k2}}(T_w - T_c)(For\ cooling\ analysis\ in\ flight) \quad \textbf{(Equation 4-37)}$$

$$T_{2w} = T_c - \frac{U_3}{U_{k2}}\left(T_{wg} - T_c\right)(For\ cooling\ analysis\ at\ ground) \quad \textbf{(Equation 4-38)}$$

And

$$U_{k2} = \frac{1}{\frac{1}{h_i}} \quad \textbf{(Equation 4-39)}$$

Where $U_{k2}$ is the overall heat load from the internal surface to air space, W/m$^2$.

Radiation coefficient is obtained from Figure 4-12 for a range of temperatures and surfaces with a configuration and emissivity factor $\frac{F_a}{F_e}$ of 0.098 [23].

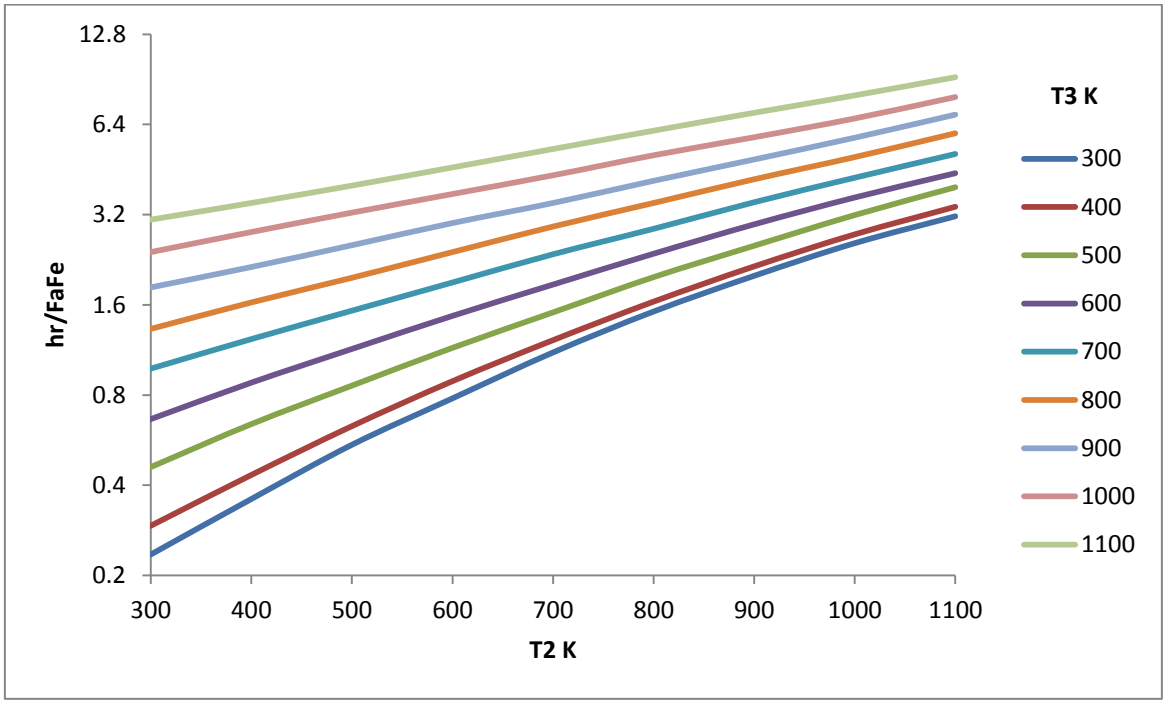


**Figure 4-12 Heat transfer coefficient for radiation [23]**

After obtaining the values of heat transfer by conduction, convection and radiation $h_a$+$h_r$, is compared to the assumed value $h'_a$+$h'_r$, if the two results are equal or close enough, iteration is completed and that value is taken.

$$h_a + h_r = h'_a + h'_r$$

The analysis of the floor heat transfer (insulated) of the helicopter is more complex, as this is composed with beams. Table 4-4 contains the dimension and temperature of the beams within the Bell 206L-4. The total heat transfer in the floor is given by the summation of the heat transfer between the wall and beams with insulation, as follows.

$$q_4 = q_{4a} + q_{4b} \quad \textbf{(Equation 4-40)}$$

And

$$q_{4a} = (U_4 + t_4)A_4\Delta T$$

$$q_{4b} = [N_b(q_{as})]$$

$$q_{as} = q_b \frac{h_S A_S T'_{as}}{U_T A_T T_c + U_B A_B \langle T, T_w, T_{wg} \rangle + h_S A_S T'_{as}} \quad \textbf{(Equation 4-41)}$$

Where $q_4$ is the total floor heat transfer in W; $q_{4a}$ is the floor wall heat transfer in W ; $q_{4b}$ is the beam heat transfer in W; $q_{as}$ is the floor air space heat load, W; $U_4 = U_3$ is the floor overall heat load coefficient in W/m$^2$; $t_4$ is the floor total increase of thermal transmittance in percentage ; $A_4$ is floor wall area, m$^2$; $N_b$ is the number of beams on the floor; $q_b$ is the beam heat transfer, W; $U_T$ is the overall heat load from internal surface to top beam, W/m$^2$; $U_B$ is the Overall heat transfer from external surface to bottom beam in W/m$^2$; $h_S$ is the heat transfer coefficient at beam sides, W/m$^2$; $A_T$ is the beam top area, m$^2$; $A_B$ is the Beam bottom area, m; $A_S$ is the beam sides area, m$^2$; $T'_{as}$ is the assumed beam sides temperature, K.

The floor total increase of thermal transmittance is calculated with the equation used in the wall calculation.

Considering that the beams are in contact with the outer wall, and hence that the initial temperature of the beam is the same as the outer wall, the following heat transfer equations can be used [23].

$$q_b = C_b u L_b \eta_b (T_{wa} - T) \ (For\ Heating\ analysis) \quad \textbf{(Equation 4-42)}$$

$$q_b = C_b u L_b \eta_b (T_w - T_{wa}) \ (For\ cooling\ analysis\ in\ flight) \quad \textbf{(Equation 4-43)}$$

$$q_b = C_b u L_b \eta_b (T_{wg} - T_{wa}) \ (For\ cooling\ analysis\ at\ ground) \quad \textbf{(Equation 4-44)}$$

Where $C_b$ = 1.18 is the perimeter of beam in m; $u$ is the unit heat load of wall surface and beam (including insulation), W/m$^2$; $L_b$ = 0.53 is the length of the beam, m; $\eta_b$ is the beam effectiveness; $T_{wa}$ is the weighted average temperature, K.

**Table 4-4 Beam areas**

| | Area (m$^2$) | Temperature (K) |
|---|---|---|
| Beam top | $A_T$ = 0.00072 | $T_c$ |
| Beam bottom | $A_B$ = 0.00072 | $T$, $T_w$, $T_{wg}$ |
| Beam sides | $A_S$ = 0.031 | $T'_{as}$ Assumed |

The unit heat load and the weighted average temperature to use in floor heat transfer equation are.

$$u = \frac{U_T A_T T_c + U_B A_B \langle T, T_w, T_{wg} \rangle + h_S A_S T'_{as}}{A_T T_c + A_B \langle T, T_w, T_{wg} \rangle + A_S T'_{as}} \quad \textbf{(Equation 4-45)}$$

$$T_{wa} = \frac{U_T A_T T_c + U_B A_B \langle T, T_w, T_{wg} \rangle + h_S A_S T'_{as}}{U_T A_T + U_B A_B + h_S A_S} \quad \textbf{(Equation 4-46)}$$

And

$$U_T = \frac{1}{h_i} \quad \textbf{(Equation 4-47)}$$

$$U_B = \frac{1}{h_e} + h_{kw} + h_{ki} \quad \textbf{(Equation 4-48)}$$

$$h_S = 5.678263(2.0 + 0.314V_b)$$

Where $V_b$ = 0 is the air velocity through floor beams.

The beam effectiveness is given by the following equation [23].

$$\eta_b = \frac{tanh m_b L_b}{m_b L_b} \quad \textbf{(Equation 4-49)}$$

And

$$m_b = \sqrt{\frac{uC_b}{k_b A_c}} \quad \textbf{(Equation 4-50)}$$

Where $m_b$ is the beam exposed area in m; $k_b$ = 17.3 in W/m is the thermal conductivity of the beam material; $A_c$ = 0.0002 is the beam cross sectional area [46], $m^2$.

To verify the assumed temperature of the beam sides $T'_{as}$ the following iteration must be computed until the required temperature at that point of the beam is acquired.

$$T_{as} = T_c - \frac{q_{as}}{U_f A_{bb}} \quad \textbf{(Equation 4-51)}$$

And

$$U_f = \frac{1}{\frac{1}{h_i} + \frac{1}{h_S}} \quad \textbf{(Equation 4-52)}$$

Where $U_f$ is the overall heat load coefficient of the floor film, $W/m^2$; $A_{bb}$ = 0.21 is the area between the beams, $m^2$.

Once the temperature at beam sides $T_{as}$ is obtained, is compared to the assumed temperature $T'_{as}$; if the two results are equal or close enough, iteration is completed and the temperature is taken.

For helicopters, the ceiling heat transfer depends on the heat generated by the engine and transferred through the wall. For the calculation of heat transfer on this surface is necessary to increase the ambient temperature $T$ for heating, or the skin temperature $T_w$ for cooling, as follows [47].

$$T_{ec} = T + 30 \quad \textbf{(Equation 4-53)}$$

$$T_{ec} = T_w + 30 \ (For\ flight\ analysis)$$

$$T_{ec} = T_{wg} + 30 \ (For\ ground\ static\ analysis)$$

Where $T_{ec}$ is the external ceiling temperature in K.

The ceiling heat transfer is then [23].

$$q_5 = (U_5 + t_5)A_5\Delta T\ (For\ insulated\ wall) \qquad \textbf{(Equation 4-54)}$$

And

$$\Delta T = T_c - T_{ec}\ (For\ Heating\ analysis)$$

$$\Delta T = T_{ec} - T_c\ (For\ cooling\ analisis)$$

Where $q_5$ is the ceiling heat transfer in W; $U_5 = U_3$ is the ceiling overall heat load coefficient in W/m$^2$; $t_5$ is the ceiling total increase of thermal transmittance in percentage; $A_5$ is the ceiling area, m$^2$.

As in the ceiling, the heat transfer on the rear bulkhead depends of the heat transmitted by helicopter mechanisms. The ambient temperature and the skin temperature should be increased by the same procedure that was performed with the helicopter roof, unlike the ceiling that is affected by the motor and must increase the temperature 30 °C, the rear bulkhead must be increased only 5 °C [47].

The rear bulkhead heat transfer is then [23].

$$q_6 = (U_6 + t_6)A_6\Delta T\ (For\ insulated\ wall) \qquad \textbf{(Equation 4-55)}$$

And

$$U_6 = \frac{1}{\frac{1}{h_e} + h_{kw} + h_{ki} + \frac{1}{h_i}} \qquad \textbf{(Equation 4-56)}$$

Where $q_6$ is the rear bulkhead heat transfer in W; $U_6$ is the rear bulkhead overall heat load coefficient in W/m$^2$; $t_6$ is the rear bulkhead total increase of thermal transmittance in percentage; and $A_6$ is the rear bulkhead area, m$^2$.

### 4.2.5. Rotorcraft heat loss analysis (Infiltration)

Helicopters are designed for low-altitude flights, for that reason does not require a pressurized cabin. Therefore, it is very common to find points of infiltration within the aircraft. These infiltrations are commonly generated in joints and edges of moving surfaces such as doors and windows. As a result, the cabin heat loss (infiltration) significantly affects the behaviour of the temperature in the interior of the aircraft. According to a studies conducted by the US Army [32], the rotorcraft infiltration rate *w* values for an small helicopter are of 0.005 kg/s and 0.01 kg/s in the cockpit and the cabin respectively. The heat loss resulting from infiltration is computed as follow:

$$Q_i = C_p w \Delta T \qquad \textbf{(Equation 4-57)}$$

Where $C_p$ = 1005 is the specific heat capacity of air at constant pressure, J/kg.

### 4.2.6. Solar radiation heat load analysis

Solar rays play a fundamental role in the heat gain inside the helicopter, since the radiation transmitted by the sun is absorbed by the surfaces of the rotorcraft affecting its temperature. The solar radiation is first absorbed by the material, and then transferred by conduction, convection or radiation to the cabin. The solar heat gain has three components: Direct solar irradiation, diffuse solar irradiation and reflected solar irradiation.

To calculate the solar radiation heat load on an aircraft, it is needed to calculate the sun incidence angle $\theta$ from the local standard time and longitude, Figure 4-13. The three solar components and thus the surface temperatures $T_{wg}$ and $T_w$ in ground and flight respectively, can then be determined. Calculations methods for these parameters are described below.

The overall equation of solar irradiation is:

$$I_g = I_D Cos\theta + I_d + I_r \ (Ground\ condition) \qquad \textbf{(Equation 4-58)}$$

$$I = I_D Cos\theta + I_d \ (Flight\ condition) \qquad \textbf{(Equation 4-59)}$$

And

$$I_r = (E_b \sin\beta + E_d)\rho_g F_g \quad \textbf{(Equation 4-60)}$$

$$I_D = E_b \cos\theta \quad \textbf{(Equation 4-61)}$$

$$I_d = E_d \mathrm{Y} \quad \textbf{(Equation 4-62)}$$

With

$$Y = \max(0.45, 0.55 + 0.437\cos\theta + 0.313cos^2\theta) \quad \textbf{(Equation 4-63)}$$

Where $I_D$ is the direct solar irradiation in W/m$^2$; $I_d$ is the diffuse solar irradiation in W/m$^2$; $I_r$ is the reflected solar irradiation W/m$^2$; $\theta$ is the incident angle between the horizontal line (ground) and the irradiated surface (helicopter) in degrees; $E_b$ is the beam normal irradiance, W/m$^2$; $E_d$ is the diffuse horizontal irradiance, W/m$^2$; $\rho_g = 0.2$ is the ground reflectance [44]; $F_g$ is the angle factor between the earth and the surface; ratio $Y$ on a vertical surface calculation.

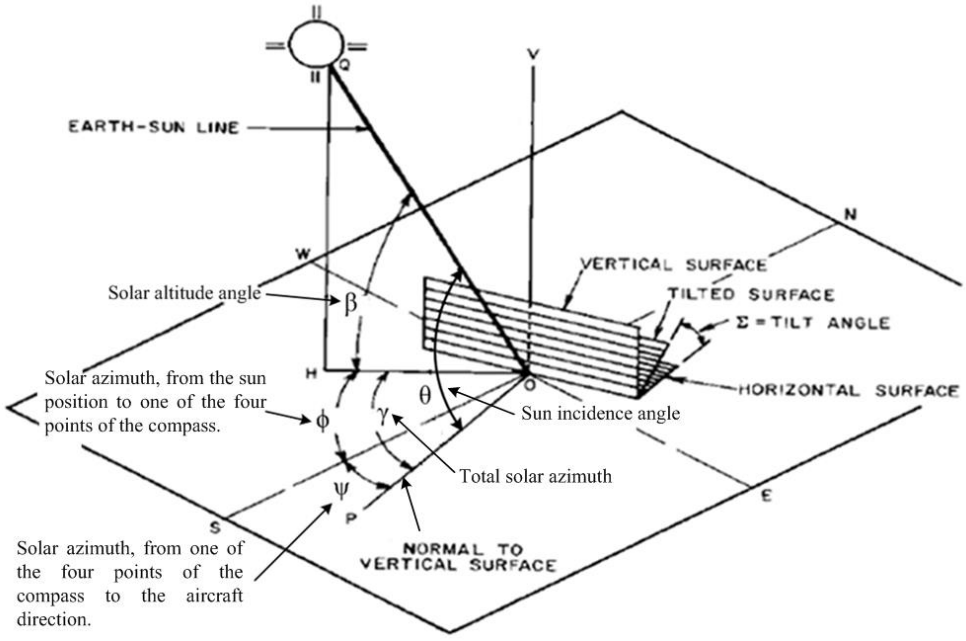


**Figure 4-13 Solar position with respect to a tilted surface [44]**

The amount of irradiation on the fuselage varies depending to the sun position or angle of incidence. The angle of incidence is the angle between the normal line to the irradiated surface (OP' in Figure 4-13) and the ground line to the sun position OQ. This angle is important because it sets the solar intensity (irradiance) on each of the sides of the helicopter. In order to set this angle in the Bell206L-4, was necessary to replace curved surfaces with plane surfaces simplifying the inclination angle analysis of irradiated surfaces. The geometry changes does not affect the results, since this are taken only as a reference point of inclination position for the mathematical analysis. Figure 4-14 shows the new geometry of the Bell206L-4 including its different faces.

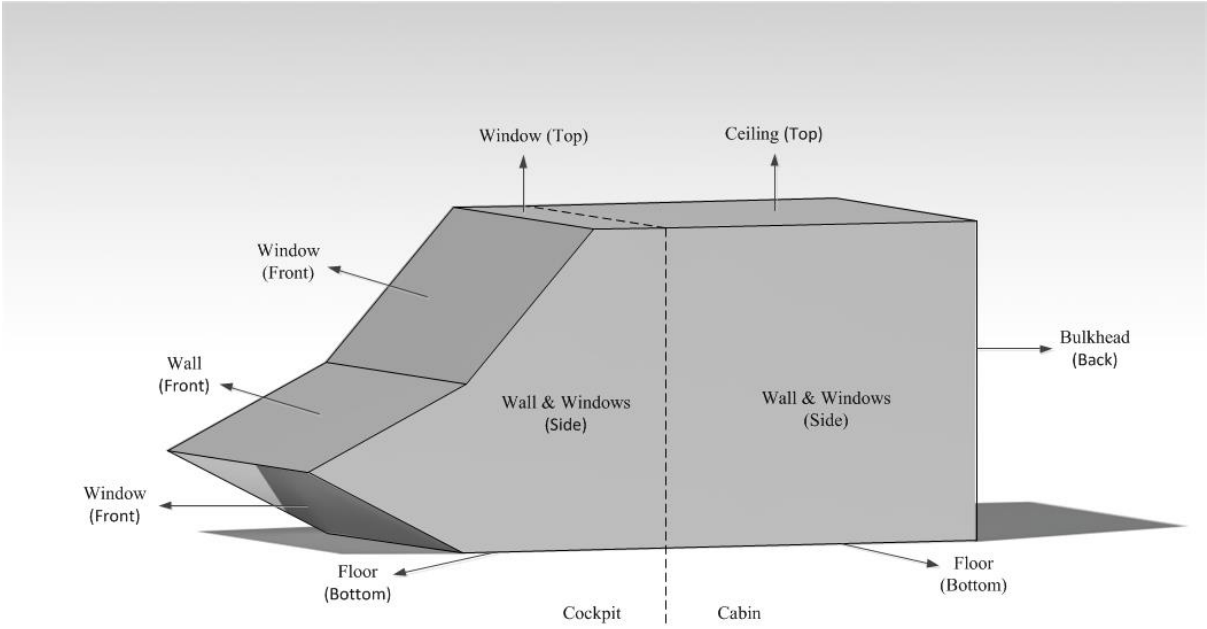


**Figure 4-14 Bell 206L-4 irradiation geometry**

The incidence angle is calculated as follows:

$$\theta = \cos^{-1}(\cos\beta\cos\gamma_s\sin\Sigma + \sin\beta\cos\Sigma)\ (For\ a\ surface\ with\ a\ tilt\ angle) \quad \textbf{(Equation 4-64)}$$

$$\theta = \cos^{-1}(\cos\beta\cos\gamma_s)\ (For\ vertical\ surfaces) \quad \textbf{(Equation 4-65)}$$

$$\theta = 90 - \beta\ (For\ horizontal\ surfaces) \quad \textbf{(Equation 4-66)}$$

Where $\beta$ is the solar altitude angle in degrees; $\gamma_s$ is the surface-solar azimuth in degrees; $\Sigma = 0^o \; to \; 180^o$ is the tilt angle in degrees of the aircraft surfaces (where 180° is a surface facing the ground).

In order to find the tilt angle of the surfaces was necessary to estimate the aerodynamic shape of the aircraft by using a 3D model designed in CATIA. First, a 3D model of the Bell 206L-4 with curve shapes was designed. Then, on this first design (curve surfaces), plane shapes were projected creating a parallel design (plane surfaces), see Figure 4-14. This new 3D model allowed approximations of the surfaces on the aircraft, thus the last step was to compute the tilt angle of the Bell 206L-4 based on the design plane surfaces.

The solar altitude angle $\beta$ (angle HOQ in Figure 4-13) varies from day to day due to the motion of the earth. Therefore, this variation depends on the flight date (day, month, and year). The solar angle can be calculated with the following equation:

$$\beta = 90^o - LAT + \delta \; (At \; noon \; time) \qquad \textbf{(Equation 4-67)}$$

$$\beta = \sin^{-1}[\cos(LAT)\cos\delta\cos H + \sin(LAT)\sin\delta] \; (Rest \; of \; day) \qquad \textbf{(Equation 4-68)}$$

And

$$\delta = 23.45 \sin\left[360\frac{284+N}{365}\right] \; (For \; northern \; hemisphere) \qquad \textbf{(Equation 4-69)}$$

$$\delta = 23.45 \sin\left[180\frac{284+N}{365}\right] \; (For \; southern \; hemisphere) \qquad \textbf{(Equation 4-70)}$$

Where *LAT* is the Aircraft latitude; $\delta$ is the solar declination (the angle between the earth-sun line and the equatorial plane), in degrees; *H* is the hour angle in degrees; *N* is the day of year.

The hour angle *H* can be determined from the following equation:

$$H = 15(AST - 12) \qquad \textbf{(Equation 4-71)}$$

And

$$AST = LST + \frac{ET}{60} + \frac{(LON-LSM)}{15} \qquad \textbf{(Equation 4-72)}$$

Where

$$ET = 2.2918(0.0075 + 0.1868\cos\Gamma - 3.2077\sin\Gamma - 1.4615\cos 2\Gamma - 4.089\sin 2\Gamma) \quad \textbf{(Equation 4-73)}$$

$$LSM = 15TZ \quad \textbf{(Equation 4-74)}$$

And

$$\Gamma = 360\frac{N-1}{365} \quad \textbf{(Equation 4-75)}$$

*AST* is the apparent solar time; *LST* is the local standard time (24-hours clock); *ET* is the equation of time in minutes; *LON* is the aircraft longitude; *LSM* is the longitude of local standard time meridian; *TZ* is the time zone.

Besides the position of the sun, it is also important to establish the position and direction of the helicopter (e.g. flight from south to north) to identified the aircraft total solar azimuth $\gamma_s$. This angle, HOP in Figure 4-13, is the angular difference between the solar azimuth (from the sun position to one of four points of the compass) $\phi$, and the solar azimuth (from one of the four points of the compass to the aircraft direction) $\psi$. The helicopter surface azimuth is the direction in which the analysed surfaces are facing the sun as illustrated in Figure 4-15.

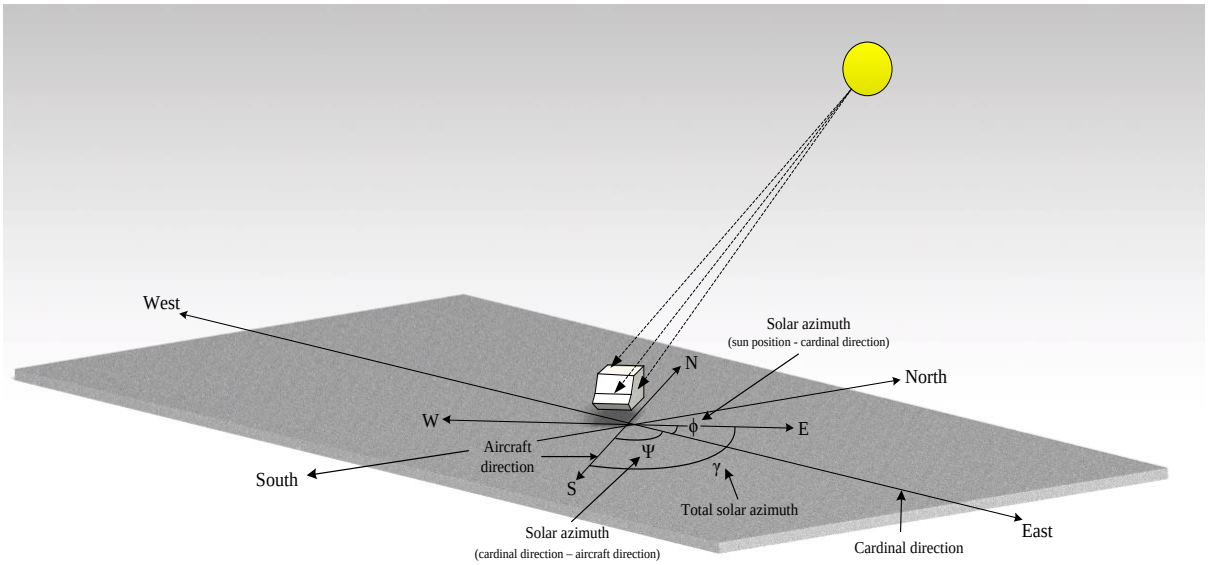


**Figure 4-15 Aircraft surface azimuth**

The $\gamma_s$ angle is given by:

$$\gamma_s = \phi \pm 180\ (For\ all\ conditions - Surfaces\ facing\ North) \quad \textbf{(Equation 4-76)}$$

$$\gamma_s = \phi - \psi\ (Morning - Surfaces\ facing\ East) \quad \textbf{(Equation 4-77)}$$

$$\gamma_s = \phi + \psi\ (Afternoon - Surfaces\ facing\ East) \quad \textbf{(Equation 4-78)}$$

$$\gamma_s = \phi + \psi\ (Morning - Surfaces\ facing\ West) \quad \textbf{(Equation 4-79)}$$

$$\gamma_s = \phi - \psi\ (Afternoon - Surfaces\ facing\ West) \quad \textbf{(Equation 4-80)}$$

$$\gamma_s = \phi\ (For\ all\ conditions - Surfaces\ facing\ South) \quad \textbf{(Equation 4-81)}$$

And

$$\phi = \sin^{-1}\left(\frac{\cos\delta \sin H}{\cos\beta}\right) \quad \textbf{(Equation 4-82)}$$

A review of the overall irradiation equations indicates that the beam $E_b$ (direct) and diffuse $E_d$ elements are needed. These two elements are calculated as [3]:

$$E_b = E_o exp^{-\tau_b m^{ab}} \quad \textbf{(Equation 4-83)}$$

$$E_d = E_o exp^{-\tau_d m^{ad}} \quad \textbf{(Equation 4-84)}$$

And

$$E_o = I_o\left[1 + 0.033\cos\left(360\frac{N-3}{365}\right)\right] \quad \textbf{(Equation 4-85)}$$

$$m = \frac{1}{\sin\beta + 0.50572(6.07995+\beta)^{-1.6364}} \quad \textbf{(Equation 4-86)}$$

$$ab = 1.219 - 0.043\tau_b - 0.151\tau_d - 0.204\tau_b\tau_d \quad \textbf{(Equation 4-87)}$$

$$ad = 0.202 + 0.852\tau_b - 0.007\tau_d - 0.357\tau_b\tau_d \quad \textbf{(Equation 4-88)}$$

Where $E_o$ is the extraterrestrial radiant flux in W/m$^2$; $I_o$ = 1355 is the solar constant, W/m$^2$; $m$ is the relative air mass; $ab$ is the beam air mas exponent; $ad$ is the diffuse air mass exponent; $\tau_b$ is the beam optical depth [44]; $\tau_d$ is the diffuse optical depth [44].

The values of $\tau_d$ and $\tau_d$ were obtained by using data from Figure 4-16 and Figure 4-17 respectively.

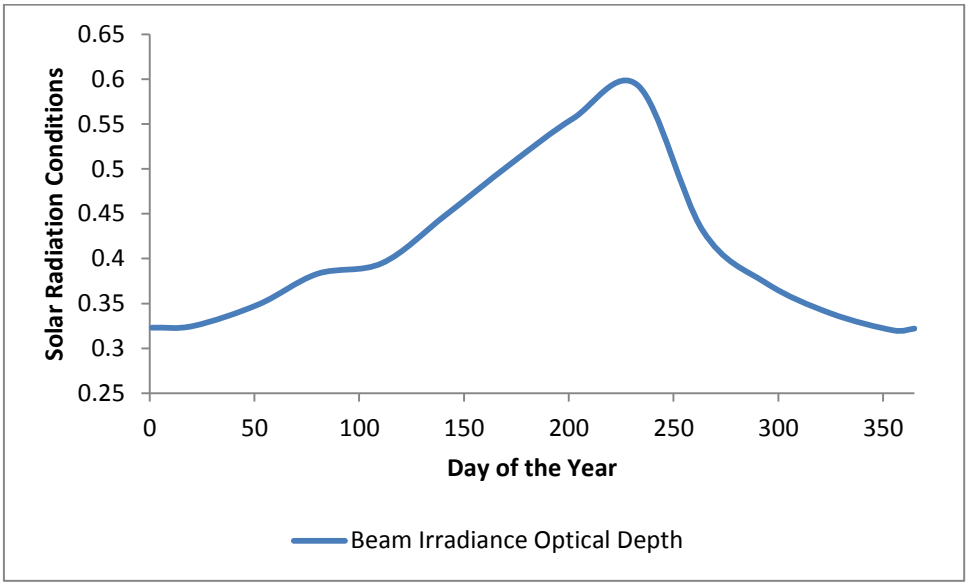


**Figure 4-16 Beam irradiance optical depth values**

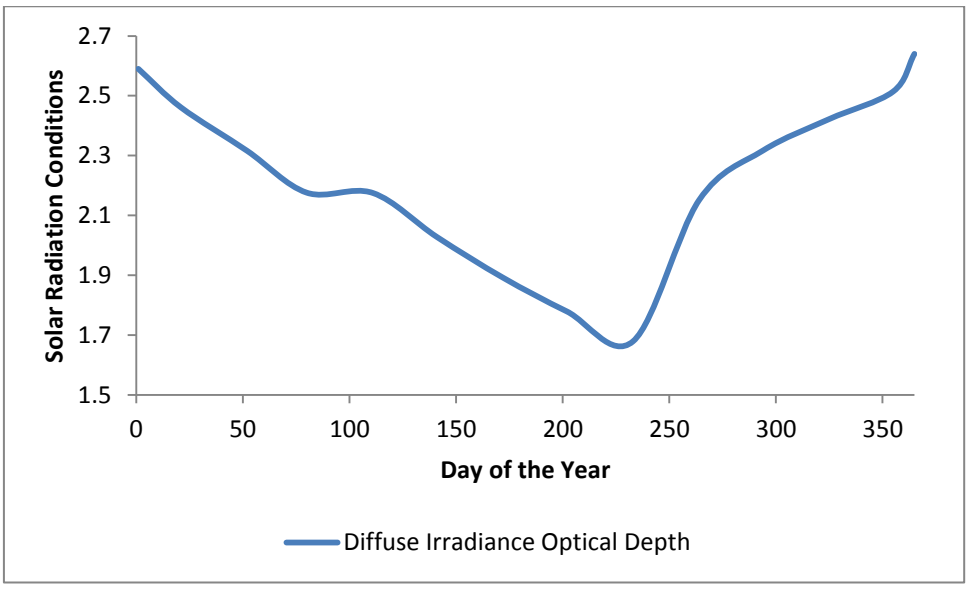


**Figure 4-17 Diffuse optical depth values**

The following equation is used to estimate the required angle factor between helicopter surface and earth for the reflected radiation $I_r$:

$$F_g = \frac{1-\cos\Sigma}{2} \quad \textbf{(Equation 4-89)}$$

### 4.2.7. Cockpit and cabin heat gain analysis

As mentioned in this chapter, the heating and cooling loads depend on weather conditions, the heat flow through the structures, and the heat generated by sources in specific areas within the helicopter. The latter refers to the heat load generated by the human body $Q_o$ (metabolic) and by electrical units $Q_e$ (Avionic and electrical equipment). These two sources are heat gains due to their constant supply of heat inside the cabin, regardless external and internal condition variations. Thus,

$$Q_{oe} = Q_o + Q_e \quad \textbf{(Equation 4-90)}$$

The heat gain from human body depends on the number of people inside the helicopter. For this analysis the maximum passenger capacity allowed within the Bell206L-4 was taken; this consists of 2 crew members and 5 occupants. The heat loss used by each crew member is of 400 W and 120 W for each occupant, distinguishing the different levels of activity [7, 14].

Heat gain resulting from human body can be expressed as:

$$Q_o = q_7 + q_8 \quad \textbf{(Equation 4-91)}$$

And

$$q_7 = M_1 N_1 \quad \textbf{(Equation 4-92)}$$

$$q_8 = M_2 N_2 \quad \textbf{(Equation 4-93)}$$

Where $q_7$ is the cockpit total metabolic heat gain, W; $q_8$ is the cabin total metabolic heat gain, W; $M_1$ = 400 is the crew metabolic rate in W; $N_1$ = 2 is the number of crew members into the

cockpit; $M_2$ = 120 is the occupants metabolic rate in W; $N_2$ = 5 is the number of occupants into the cabin.

Heat load caused by electrical units is a function of power consumed by the avionic and electrical equipment. This heat gain is expressed as:

$$Q_e = 1000(P_e P_{ef}) \quad \textbf{(Equation 4-94)}$$

Where $P_e$ = 0.225 is the electrical power for small aircraft in kVA [33]; $P_{ef}$ = 0.9 is the power factor for small aircraft [33].

## 4.3. ECS cooling and heating units analysis

Cooling and heating units are responsible for the temperature changing within the cabin by means of multiple heat exchangers and the use of turbomachines. There are different configurations of ECS, one fully equipped for cooling and heating (ACM), and one for cooling purposes only (VCM) therefore requires a complementary system to heat (EGH, CH, Bleed air). Mathematical calculations of different units for environmental control within the helicopter are described in this section. The ECS pressure losses and temperature have been neglected in this computation.

### 4.3.1. Helicopter ventilating air requirement

The European Aviation Safety Agency (EASA) has established for helicopters certification that Environmental Control Systems must provide not less than 0.005 kg/s of fresh air for each passenger and crew member, as mentioned in Chapter 2. For this reason, it is important to establish in this study the minimum requirement of air allowed for the Bell206L-4, taking into consideration its maximum passenger capacity (7 passengers). The ventilating minimum air requirement is expressed by the equation:

$$\dot{m}_t = \dot{m}_1 + \dot{m}_2 \quad \textbf{(Equation 4-95)}$$

And

$$\dot{m}_1 = \dot{m}_r N_1 \ (For\ cockpit) \quad \textbf{(Equation 4-96)}$$

$$\dot{m}_2 = \dot{m}_r N_2 \ (For\ cabin) \quad \textbf{(Equation 4-97)}$$

Where $\dot{m}_t$ is the total required mass flow rate (ventilating air) in kg/s; $\dot{m}_1$ is the cockpit required mass flow rate, kg/s; $\dot{m}_2$ is the cabin required mass flow rate, kg/s; $\dot{m}_r = 0.005$ is the required mass flow rate per passenger. The above equation is valid for the following ranges: $\Delta T_3 \leq \Delta T_2$ (For cockpit), $\Delta T_4 \leq \Delta T_2$ (For cabin).

The maximum allowable temperature differences are given by:

$$\Delta T_2 = T_M - T_c \quad \textbf{(Equation 4-98)}$$

$$\Delta T_3 = \frac{Q_c + Q_i}{C_p \dot{m}_1} \ (For\ cockpit) \quad \textbf{(Equation 4-99)}$$

$$\Delta T_4 = \frac{Q_c + Q_i}{C_p \dot{m}_2} \ (For\ cabin) \quad \textbf{(Equation 4-100)}$$

Where $\Delta T_2$ is the rotorcraft maximum allowable temperature difference in K; $\Delta T_3$ is the cockpit maximum allowable temperature difference, K; $\Delta T_4$ is the cabin maximum allowable temperature difference, K; $T_M$ = 355.37 is the maximum ducts surface temperature, K [32].

The ventilating minimum air requirement for $\Delta T_3 > \Delta T_2$ (For cockpit) and $\Delta T_4 > \Delta T_2$ (For cabin) is given by:

$$\dot{m}_t = \dot{m}_3 + \dot{m}_4$$

And

$$\dot{m}_3 = \frac{Q_c + Q_i}{C_p \Delta T_2} \ (For\ cockpit) \quad \textbf{(Equation 4-101)}$$

$$\dot{m}_4 = \frac{Q_c + Q_i}{C_p \Delta T_2} \ (For\ cabin) \quad \textbf{(Equation 4-102)}$$

### 4.3.2. Air Cycle unit analysis

The ACM is a unit that meets all ECS functions, heating, cooling and ventilation. Multiple configurations have been developed based on this unit in order to reach the required temperature and performance for certain aircraft. Commonly, helicopters Air Cycle Machine system use an air-to-air heat exchanger with ambient air as a source to reduce the temperature of the turbine bleed air. Additionally, a small expansion turbine is used to reduce the air cooling below ambient conditions. The condensed moisture in the cooling air is extracted by mechanical means, generally using a water separator. At the end of the system is placed a control valve; this valve modulates cold air with warm air to reach the required temperature inside the helicopter. Figure 4-18 illustrates the ACM variables and components to analyse in this section.

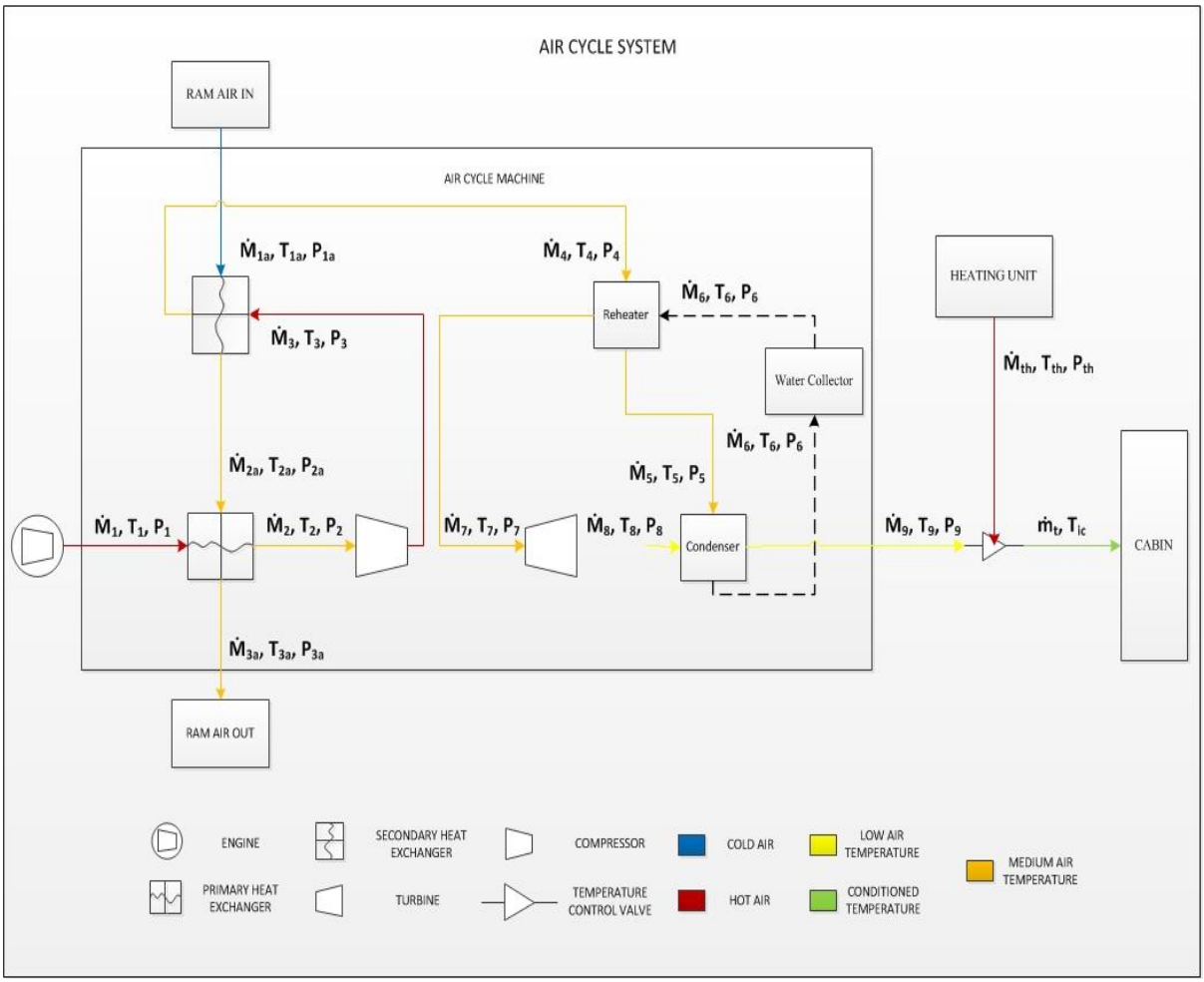


**Figure 4-18 ACM unit variables and components**

***Primary Heat Exchanger (PHX), Secondary Heat Exchanger (SHX), Reheater, Condenser***. To begin this analysis is necessary to calculate the performance of a heat exchanger and determine the heat transfer and mass flow required by the fluids involved, Figure 2-17. Outlet temperatures in a heat exchanger are given by the following equations:

$$T_{ho} = T_{hi} - \frac{Q_{hx}}{C_h} \ (For\ cooled\ air\ side) \qquad \textbf{(Equation 4-103)}$$

$$T_{co} = T_{ci} + \frac{Q_{hx}}{C_c} \ (For\ heated\ air\ side)$$

And

$$dQ_{hx} = U_{hx}(T_{hi} - T_{ci})dA \qquad \textbf{(Equation 4-104)}$$

$$Q_{hx} = \varepsilon_{hx}(T_{hi} - T_{ci})C_{min} \qquad \textbf{(Equation 4-105)}$$

Where $T_{ho}$ is the outlet temperature from the exchanger hot side in K; $T_{hi}$ is the inlet temperature from the exchanger hot side, K; $T_{co}$ is the outlet temperature from the exchanger cold side in K; $T_{ci}$ is the inlet temperature from the exchanger cold side, K; $C_h$ is the hot side fluid capacity rate in W/K; $C_c$ is the cold side fluid capacity rate in W/K; $Q_{hx}$ is the heat transfer rate in W; $U_{hx}$ is the heat exchanger overall heat transfer coefficient in W/m2 $\varepsilon_{hx}$ is the exchanger effectiveness; $C_{min}$ is the minimum value between $C_c$ and $C_h$.

Initial temperatures $T_{hi}$ y $T_{ci}$ in SHX, corresponds to the temperature of the turbine bleed air and ambient temperature respectively. According to the engine maintenance manual, the Bell206L-4 turbine (RR Allison 250- C30P) bleed air temperature is of 473.15 K, with a constant pressure of 275790 Pa. The properties of air are obtained from any source of thermophysical properties (see, Appendix A)

To determine $T_{ho}$ and $T_{co}$ it is necessary to calculate $C_c$ and $C_h$ first:

$$C_h = \dot{m}_h C_{ph} \qquad \textbf{(Equation 4-106)}$$

$$C_c = \dot{m}_c C_{pc}$$

Where $\dot{m}_h$ is the hot fluid mass flow rate in kg/s; $\dot{m}_c$ is the cold fluid mass flow rate in kg/s; $C_{ph}$ is the hot fluid specific heat capacity in J/kg; $C_{pc}$ is the cold fluid specific heat capacity in J/kg.

The effectiveness for an unmixed crossflow exchanger is given by:

$$\varepsilon_{hx} = 1 - exp\left[(exp(-NTU^{0.78}C^*) - 1)\frac{NTU^{0.22}}{C^*}\right] \quad \textbf{(Equation 4-107)}$$

And

$$NTU = \frac{(UA)_{hx}}{C_{min}} = \frac{1}{C_{min}}\int_0^A UdA \quad \textbf{(Equation 4-108)}$$

$$C^* = \frac{C_{min}}{C_{max}} \quad \textbf{(Equation 4-109)}$$

Where NTU is the Number of Transfer Units; $C^*$ is the heat capacity rate ratio; $C_{max}$ is the maximum value between $C_c$ and $C_h$.

Heat transfer inside heat exchangers behaves in the same way that heat loads throughout the helicopter structure. At constant state, the heat is transferred from the hot fluid to the cold fluid through convection and conduction. As heat loads within the cabin were computed, heat exchanger needs to calculate the differential thermal resistance *U* present in a given area *A*. Furthermore, oxide formation (fouling film) existing in most heat exchangers should be considered. The overall differential thermal resistance *UA* consists of component resistances in series as follows:

$$\frac{1}{(UdA)_{hx}} = dR_h + dR_1 + dR_w + dR_2 + dR_c \quad \textbf{(Equation 4-110)}$$

$$\frac{1}{(UA)_{hx}} = R_h + R_1 + R_w + R_2 + R_c$$

Or

$$\frac{1}{(UdA)_{hx}} = \frac{1}{\eta_{oh}h_h dA_t} + \frac{R_{fh}}{\eta_{oh}h_h dA_t} + \frac{\delta_w}{dA_w k_w} + \frac{1}{\eta_{oc}h_c dA_t} + \frac{R_{fc}}{\eta_{oc}h_c dA_t}$$

$$\frac{1}{(UA)_{hx}} = \frac{1}{\eta_{oh} h_h A_t} + \frac{R_{fh}}{\eta_{oh} h_h A_t} + \frac{\delta_w}{A_w k_w} + \frac{1}{\eta_{oc} h_c A_t} + \frac{R_{fc}}{\eta_{oc} h_c A_t} \quad \textbf{(Equation 4-111)}$$

Where $R_h$ is the hot side film convection resistance in W; $R_1$ is the hot side fouling resistance, W; $R_w$ is the wall thermal resistance, W; $R_2$ is the cold side fouling resistance, W; $R_c$ is the cold side film convection resistance, W; $R_{fh}$ = 0.000176 is the hot side fouling resistance (for compressed air) in $m^2K/W$ [48]; $R_{fc} = R_{fh}$ is the cold side fouling resistance in $m^2K/W$; $\eta_{oh}$ is the overall surface effectiveness for the hot side; $\eta_{oc}$ is the overall surface effectiveness for the cold side; $h_h$ is the hot side heat transfer coefficient in $W/m^2$; $h_c$ is the cold side heat transfer coefficient, $W/m^2$; $k_w$ = 60 is the wall material (nickel alloy) thermal conductivity in W/m [44]; $A_t$ is the total surface area $m^2$; $A_w$ is the total wall area for heat conduction, $m^2$; $\delta_w$= 0.0001 is the wall thickness (Fin thickness) in m [49].

The overall surface effectiveness for the chosen heat exchanger characteristics (section 2.8.1) is expressed as:

$$\eta_{oh} = 1 - \frac{A_s}{A_t}\left(1 - \eta_{fh}\right) \ (For\ hot\ side) \quad \textbf{(Equation 4-112)}$$

$$\eta_{oc} = 1 - \frac{A_s}{A_t}\left(1 - \eta_{fc}\right) \ (For\ cold\ side)$$

Where $A_s$ is the secondary surface area, m; $\eta_{fh}$ is the hot side fin efficiency; $\eta_{fc}$ is the cold side fin efficiency.

The exchanger fin efficiency is given by:

$$\eta_{fh} = \frac{\tanh\left(m_h L_{fh}\right)}{m_h L_{fh}} \quad \textbf{(Equation 4-113)}$$

$$\eta_{fc} = \frac{\tanh\left(m_c L_{fc}\right)}{m_c L_{fc}}$$

And

$$m_h = \sqrt{\frac{h_h c_h}{k_h A_s}} \qquad \textbf{(Equation 4-114)}$$

$$m_c = \sqrt{\frac{h_c c_c}{k_c A_s}}$$

Where $m_h$ is the hot side edge exposed area in m; mc is the cold side edge exposed area, m; $L_{fh}$ is the hot side fin length, m; $L_{fc}$ is the cold side tube length, m; $c_h$ is the hot side wetted perimeter, m; $c_c$ is the cold side wetted perimeter; $k_h$ = 60 is the fin material (nickel alloy) thermal conductivity in W/m [44]; $k_c = k_h$ is the tube material thermal conductivity W/m.

The total surface areas within the heat exchanger vary according to its outer dimensions. To define these dimensions, it is required to iterate the surfaces on each side of the fluid (hot and cold) until the ECS necessities are achieve with the dimensions, Figure 4-19. The selected dimensions were assumed and varied within allowed ranges for the exchanger material and configuration, until a satisfactory result for the system was obtained. Table 4-5 contains geometric characteristics of the heat exchanger.

**Table 4-5 Heat exchanger initial geometrical characteristics**

| Primary Measurement | Assumed Value | Abbreviation | *Parameters | Unit |
|---|---|---|---|---|
| Core Width | 0.3 | $W_c$ | | m |
| Air-side plate spacing | 0.01142 | b | $0.0028 \leq b \leq 0.02$ | m |
| Number of fin passages | 22 | $N_{fp}$ | | ------- |
| Fin flow length | 0.3 | $L_f$ | | m |
| Fin thickness | 0.0001 | $X_f$ | $2.54X10^{-5} \leq P_f \leq 0.00016$ | m |
| Fin pitch | 0.001 | $P_f$ | $0.00051 \leq P_f \leq 0.0033$ | m |
| Tube pitch | 0.01645 | $P_t$ | $0.00751 \leq P_t \leq 0.025$ | m |
| Tube width | 0.12 | $W_t$ | | m |
| Tube height | 0.002 | $H_t$ | | m |
| Louver angle | 30 | $\theta_l$ | $8.4 \leq \theta \leq 35^\circ$ | deg |
| Louver pitch | 0.00175 | $P_l$ | $0.0005 \leq P_l \leq 0.003$ | m |
| Louver cut length | 0.0048 | $L_{lc}$ | $0.0021 \leq L_{lc} \leq 0.0185$ | m |

* Ranges of allowed parameters for the chosen heat exchanger equations

Having established the initial values, other geometries required for the exchanger analysis can be calculated. The following are the geometrical characteristics of a unit cell:

Primary surface area (tube)

$$A_{pcell} = 2W_t(P_f - X_f) + 2P_f H_t \quad \textbf{(Equation 4-115)}$$

Louver fin length

$$L_{lf} = \left[\left(b^2 + P_f^2\right)^{\frac{1}{2}} - X_f\right] \quad \textbf{(Equation 4-116)}$$

Secondary surface area (fin)

$$A_{scell} = 2L_f L_{lf} \quad \textbf{(Equation 4-117)}$$

Total heat transfer surface area

$$A_{tcell} = A_{pcell} + A_{scell} \quad \textbf{(Equation 4-118)}$$

Free flow area

$$A_{ocell} = P_f b - X_f L_{lf} \quad \textbf{(Equation 4-119)}$$

Frontal area

$$A_{fcell} = P_f(b + H_t) \quad \textbf{(Equation 4-120)}$$

Wall conduction area per unit cell

$$A_{wcell} = W_t W_c \quad \textbf{(Equation 4-121)}$$

Total number of fins

$$N_f = N_{fp}\frac{W_c}{P_f} \quad \textbf{(Equation 4-122)}$$

The total geometrical characteristics are calculated with the following equations:

$$A_p = N_f A_{pcell} \quad \textbf{(Equation 4-123)}$$

$$A_s = N_f A_{scell} \quad \textbf{(Equation 4-124)}$$

$$A_t = N_f A_{tcell} \quad \textbf{(Equation 4-125)}$$

$$A_o = N_f A_{ocell} \quad \textbf{(Equation 4-126)}$$

$$A_f = N_f A_{fcell} \quad \textbf{(Equation 4-127)} \qquad A_w = (N_p - 1)A_{wcell} \quad \textbf{(Equation 4-128)}$$

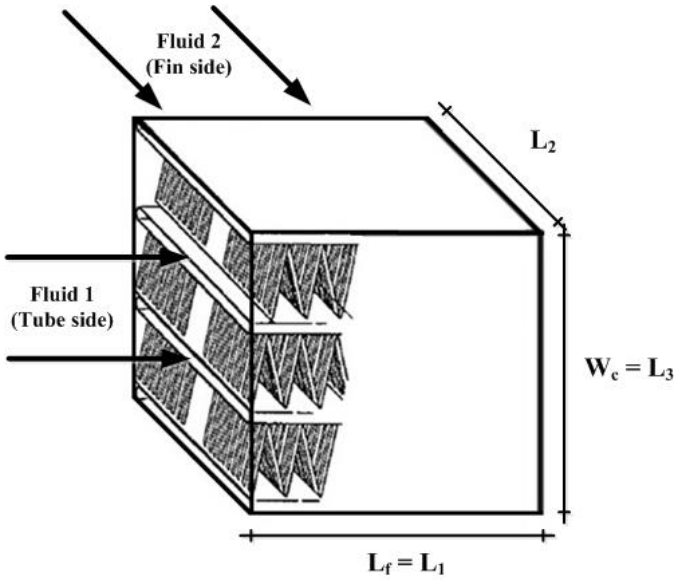


**Figure 4-19 Corrugated louver fin exchanger geometry**

Distance $L_2$ is computed from the following equation:

$$L_2 = \frac{P_f(b+H_t)}{N_f} \quad \textbf{(Equation 4-129)}$$

In addition to mathematical calculations provided above, the overall differential thermal resistance *UA* includes among its equation the heat transfer coefficients as follows:

$$h_h = \frac{N_{uh} G_h c_{ph}}{(P_r)^{\frac{2}{3}}} \quad \textbf{(Equation 4-130)}$$

$$h_c = \frac{N_{uc} G_c c_{pc}}{(P_r)^{\frac{2}{3}}}$$

And

$$G_h = \frac{\dot{m}_h}{A_o} \quad \textbf{(Equation 4-131)}$$

$$G_c = \frac{\dot{m}_c}{A_o}$$

Where $N_{uh}$ is the Nusselt number of the hot fluid; $N_{uc}$ is the Nusselt number of the cold fluid; $G_h$ is the hot side mass flux in kg/m$^2$; $G_c$ is the cold side mass flux, kg/m$^2$; $P_r$ = 0.72 is the Prandtl number of the fluid [23].

For engineering applications it is very common to use experimental data or analytical solutions with constant properties; then is used a correction factor into the result value that takes into consideration variations in the properties. Among others, a widely used method in heat exchangers is the ratio method. This correction factor evaluated over the surface temperature, the ratio of some pertinent property. Therefore, this correction factor is a function of temperature. The ratio method for gases can be calculated by the following equations for Nusselt numbers ($N_{uh}$, $N_{uc}$) and friction factor ($f_c$, $f_h$):

$$N_{uh} = N_{uh}{}' \left(\frac{T_{wh}}{T_{mh}}\right)^n \quad \textbf{(Equation 4-132)} \qquad N_{uc} = N_{uc}{}' \left(\frac{T_{wc}}{T_{mc}}\right)^n$$

$$f_h = f_h{}' \left(\frac{T_{wh}}{T_{mh}}\right)^o \quad \textbf{(Equation 4-133)} \qquad f_c = f_c{}' \left(\frac{T_{wc}}{T_{mc}}\right)^o$$

Where $N_{uh}{}'$ is the hot side Nusselt number for constant fluid properties; $N_{uc}{}'$ is the cold side Nusselt number for constant fluid properties; $f_h{}'$ is the hot side friction factor for constant fluid properties; $f_c{}'$ is the cold side friction factor for constant fluid properties; $T_{wh}$ is the absolute wall temperature from the hot side in K; $T_{wc}$ is the absolute wall temperature from the cold side, K; $T_{mh}$ is the absolute mean temperature from the hot side, K; $T_{mc}$ is the absolute mean temperature from the cold side, K; *n* and *o* are the ratio method correlations.

The values of the exponents' *n* and *m* for turbulent and laminar flows are summarized in Table 4-6 for heating and cooling situations. The dimensionless Reynolds number ($R_{eh}$ and $R_{ec}$) needed to determine whether the fluid is turbulent or laminar is expressed as:

$$R_{eh} = \frac{G_h P_l}{\mu_h} \quad \textbf{(Equation 4-134)}$$

$$R_{ec} = \frac{G_c P_l}{\mu_c}$$

Where $\mu_h$ is the hot fluid viscosity in kg/m.s (Pa.s); $\mu_c$ is the cold fluid viscosity, Pa.s.

**Table 4-6 Property ratio correlations [34]**

| Fluid Flow | Exponent | Heating | Cooling |
|---|---|---|---|
| Laminar | n | 0.0 | 0.0 |
| | o | 1.0 for $1 < \frac{T_{wh}}{T_{mh}} < 3$ | 0.81 for $0.5 < \frac{T_{wh}}{T_{mh}} < 1$ |
| Turbulent | n* | $-\left[\log_{10}\left(\frac{T_{wh}}{T_{mh}}\right)\right]^{\frac{1}{4}} + 0.3$ for $1 < \frac{T_{wh}}{T_{mh}} < 5$, $0.6 < P_r < 0.9$, $10^4 < R_{eh} < 10^6$, $\frac{P_l}{D_h} > 40$ | 0.0 |
| | o | $-0.1$ for $1 < \frac{T_{wh}}{T_{mh}} < 2.4$ | -0.1 |

* $N_{uh} = 5 + 0.012{R_{eh}}^{0.83}(P_r + 0.29)\left(\frac{T_{wh}}{T_{mh}}\right)^n$

The Nusselt number for constant fluid properties on the corrugated louver fins is obtained by Chang and Wang (1997) and Wang (2000) as follows:

$$N_{uh}{}' = R_{eh}^{-0.49}\left(\frac{\theta_l}{90}\right)^{0.27}\left(\frac{P_f}{P_l}\right)^{-0.14}\left(\frac{b}{P_l}\right)^{-0.29}\left(\frac{W_t}{P_l}\right)^{-0.23}\left(\frac{L_{lc}}{P_l}\right)^{0.68}\left(\frac{P_t}{P_l}\right)^{-0.28}\left(\frac{X_f}{P_l}\right)^{-0.05} \quad \textbf{(Equation 4-135)}$$

$$N_{uc}{}' = R_{eh}^{-0.49}\left(\frac{\theta_l}{90}\right)^{0.27}\left(\frac{P_f}{P_l}\right)^{-0.14}\left(\frac{b}{P_l}\right)^{-0.29}\left(\frac{W_t}{P_l}\right)^{-0.23}\left(\frac{L_{lc}}{P_l}\right)^{0.68}\left(\frac{P_t}{P_l}\right)^{-0.28}\left(\frac{X_f}{P_l}\right)^{-0.05}$$

The Fanning friction factor based on the same calculations by Chang et al. (2000) is:

$$f_h{}' = f_1 f_2 f_3 \quad \textbf{(Equation 4-136)}$$

$$f_c{}' = f_3 f_4 f_5$$

Where

$$f_1 = 14.39 R_{eh}^{\left(-0.805\frac{P_f}{b}\right)}\left\{\ln\left[1.0 + \left(\frac{P_f}{P_l}\right)\right]\right\}^{3.04} \quad \textbf{(Equation 4-137)}$$

$$f_2 = \left\{\ln\left[0.9 + \left(\frac{X_f}{P_f}\right)^{0.48}\right]\right\}^{-1.435}\left(\frac{D_h}{P_l}\right)^{-3.01}[\ln(0.5R_{eh})]^{-3.01} \quad \textbf{(Equation 4-138)}$$

$$f_3 = \left(\frac{P_f}{L_{lc}}\right)^{-0.308}\left(\frac{L_f}{L_{lc}}\right)^{-0.308}\left(e^{-0.1167\frac{P_t}{H_t}}\right)\theta_l^{0.35} \quad \textbf{(Equation 4-139)}$$

$$f_4 = 14.39R_{ec}^{\left(-0.805\frac{P_f}{b}\right)}\left\{\ln\left[1.0+\left(\frac{P_f}{P_l}\right)\right]\right\}^{3.04} \quad \textbf{(Equation 4-140)}$$

$$f_5 = \left\{\ln\left[0.9+\left(\frac{X_f}{P_f}\right)^{0.48}\right]\right\}^{-1.435}\left(\frac{D_h}{P_l}\right)^{-3.01}[\ln(0.5R_{ec})]^{-3.01} \quad \textbf{(Equation 4-141)}$$

$D_h$ is the hydraulic diameter of the fin geometry in m; the above equations are valid for $R_{ec} < 150$.

Additional equations valid for $150 < R_{eh} < 5000$ are given below:

$$f_1 = 4.97R_{eh}^{\left(0.6049-\frac{1.064}{\theta_l^{0.2}}\right)}\left\{\ln\left[0.9+\left(\frac{X_f}{P_f}\right)^{0.5}\right]\right\}^{-0.527} \quad \textbf{(Equation 4-142)}$$

$$f_2 = \left[\left(\frac{D_h}{P_l}\right)\ln(0.3R_{eh})\right]^{-2.966}\left(\frac{P_f}{L_{lc}}\right)^{-0.7931\left(\frac{P_t}{b}\right)} \quad \textbf{(Equation 4-143)}$$

$$f_3 = \left(\frac{P_t}{H_t}\right)^{-0.0446}\left\{\ln\left[1.2+\left(\frac{P_l}{P_f}\right)^{1.4}\right]\right\}^{-3.553}\theta_l^{-0.477} \quad \textbf{(Equation 4-144)}$$

$$f_4 = 4.97R_{ec}^{\left(0.6049-\frac{1.064}{\theta_l^{0.2}}\right)}\left\{\ln\left[0.9+\left(\frac{X_f}{P_f}\right)^{0.5}\right]\right\}^{-0.527} \quad \textbf{(Equation 4-145)}$$

$$f_5 = \left[\left(\frac{D_h}{P_l}\right)\ln(0.3R_{ec})\right]^{-2.966}\left(\frac{P_f}{L_{lc}}\right)^{-0.7931\left(\frac{P_t}{b}\right)} \quad \textbf{(Equation 4-146)}$$

The hydraulic diameter is given by:

$$D_h = \frac{4A_oL_f}{A_t} \quad \textbf{(Equation 4-147)}$$

A review of the ratio method equations indicates that the wall temperature and the mean temperature are needed. Thus, the wall temperature is computed from:

$$T_{wh} = T_{mh} - (R_h + R_1)Q_{hx} \quad \textbf{(Equation 4-148)}$$

$$T_{wc} = T_{mc} + (R_c + R_2)Q_{hx}$$

The mean temperature is obtained as follows:

$$T_{mh} = \frac{T_{hi}+T_{ho}}{2} \ (For\ C^* \geq 0.5) \quad \textbf{(Equation 4-149)}$$

$$T_{mc} = \frac{T_{ci} + T_{co}}{2} \ (For\ C^* \geq 0.5)$$

If $C^* < 0.5$ then

$$T_{mh} = T'_{mh} + \Delta T_{lm} \quad \textbf{(Equation 4-150)}$$

$$T_{mc} = T'_{mc} - \Delta T_{lm}$$

And

$$T'_{mh} = \frac{T_{hi}+T_{ho}}{2} \quad \textbf{(Equation 4-151)}$$

$$T'_{mc} = \frac{T_{ci} + T_{co}}{2}$$

$$\Delta T_{lm} = \frac{\Delta T_{t1} - \Delta T_{t2}}{\ln\left(\frac{\Delta T_{t1}}{\Delta T_{t2}}\right)} \quad \textbf{(Equation 4-152)}$$

And

$$\Delta T_{t1} = T_{hi} - T_{co} \quad \textbf{(Equation 4-153)}$$

$$\Delta T_{t2} = T_{ho} - T_{ci} \quad \textbf{(Equation 4-154)}$$

Where $T'_{mh}$is the mean temperature on the hot side in K; $T'_{mc}$ is the mean temperature on the cold side, K; $\Delta T_{lm}$ is the log-mean temperature difference, K; $\Delta T_{t1} and\ \Delta T_{t2}$ are terminal temperature differences.

Since the outlet temperatures are not known, they are estimated initially. According to Ramesh K. and Dusan P. (2003), an acceptable value $\varepsilon'_{hx}$ for the chosen heat exchanger configuration, Section 2.8.1, is among 65% to 75%. Once this value is assumed, an iteration of $T'_{ho}$, $T'_{co}$ and $\varepsilon'_{hx}$ should be computed until the values converge:

$$T'_{ho} = T_{ho} \qquad \textbf{(Equation 4-155)}$$

$$T'_{co} = T_{co}$$

$$\varepsilon'_{hx} = \varepsilon_{hx} \qquad \textbf{(Equation 4-156)}$$

The outlet temperature is estimated with the following equation:

$$T'_{ho} = T_{hi} - \varepsilon'_{hx}\left[\frac{C_{min}}{C_h}\right](T_{hi} - T_{ci}) \qquad \textbf{(Equation 4-157)}$$

$$T'_{co} = T_{ci} - \varepsilon'_{hx}\left[\frac{C_{min}}{C_c}\right](T_{hi} - T_{ci})$$

The path of a fluid through the heat exchanged involves a uniform flow and a static pressure distribution flow. First, the fluid contracts at the exchanger inlet; subsequently, the fluid experiences friction (e.g. skin, leading edge and perforated fin) through the exchanger core. At the exit of the core, the fluid expands and the total pressure drops. Figure 4-20 illustrates the pressure behaviour in one of the passages of the exchanger.

$$\Delta p = \Delta p_{1-2} + \Delta p_{2-3} - \Delta p_{3-4} \qquad \textbf{(Equation 4-158)}$$

Where $\Delta p$ is the total pressure drop in Pa; $\Delta p_{1-2}$ is the pressure drop at the core entrance due to contraction, Pa; $\Delta p_{2-3}$ is the pressure drop within the core, Pa; $\Delta p_{3-4}$ is the pressure rise at the core exit, Pa.

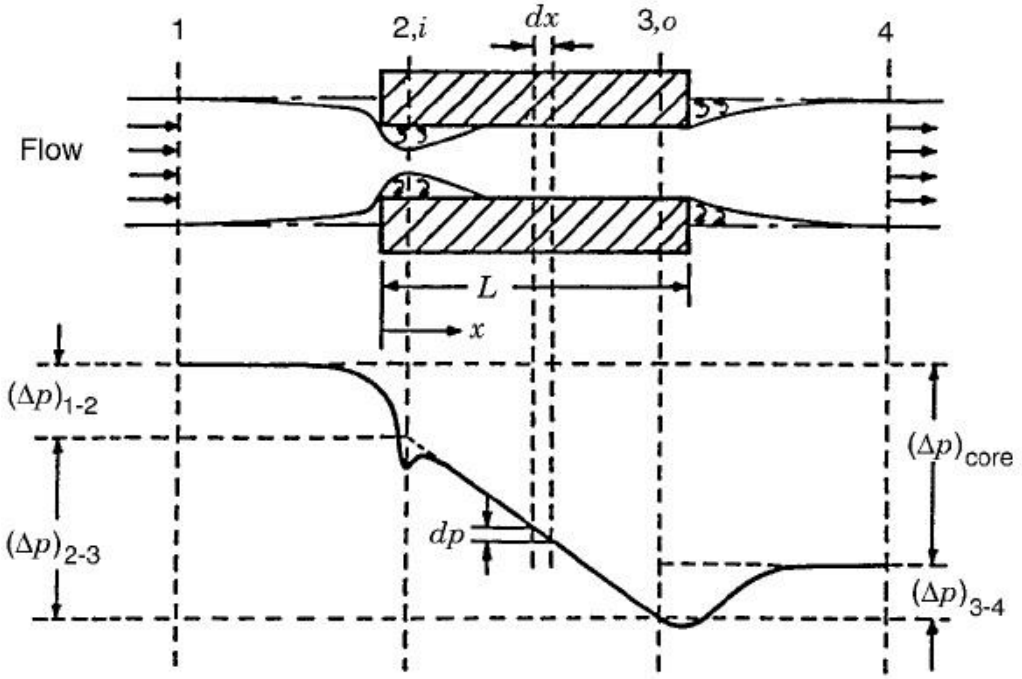


**Figure 4-20 Pressure drop within one passage of a heat exchanger [49]**

Differential pressures are given by the following equations:

$$\Delta p_{1-2} = 1 - \sigma^2 + k_{co} \; (For\ hot\ and\ cold\ side) \qquad \textbf{(Equation 4-159)}$$

$$\Delta p_{h2-3} = -\frac{dp}{dx} = \frac{G_{hx}^2}{2g_c}\left[\frac{2}{\rho_{hx}^2}\frac{dp}{dx} + f_{hx}\frac{W_c}{\rho_{hx} r_h}\right]$$

$$\Delta p_{h2-3} = \frac{G_h^2}{2g_c\rho_{hi}}\left[2\left(\frac{\rho_{hi}}{\rho_{ho}} - 1\right) + f_h\frac{W_c}{r_h}\rho_{hi}\left(\frac{1}{\rho}\right)_{hm}\right] \; (For\ hot\ side) \qquad \textbf{(Equation 4-160)}$$

$$\Delta p_{c2-3} = \frac{G_c^2}{2g_c\rho_{ci}}\left[2\left(\frac{\rho_{ci}}{\rho_{co}} - 1\right) + f_c\frac{W_c}{r_h}\rho_{ci}\left(\frac{1}{\rho}\right)_{cm}\right] \; (For\ cold\ side)$$

$$\Delta p_{h3-4} = (1 - \sigma^2 + k_e)\frac{\rho_{hi}}{\rho_{ho}} \; (For\ hot\ side) \qquad \textbf{(Equation 4-161)}$$

$$\Delta p_{c3-4} = (1 - \sigma^2 + k_e)\frac{\rho_{ci}}{\rho_{co}} \; (For\ cold\ side)$$

Thus

$$\Delta p_h = \frac{G_h^2}{2g_c\rho_{hi}}\left[(1-\sigma^2+k_{co})+2\left(\frac{\rho_{hi}}{\rho_{ho}}-1\right)+f_h\frac{W_c}{r_h}\rho_{hi}\left(\frac{1}{\rho}\right)_{hm}-(1-\sigma^2+k_e)\frac{\rho_{hi}}{\rho_{ho}}\right] \quad \textbf{(Equation 4-162)}$$

$$\Delta p_c = \frac{G_c^2}{2g_c\rho_{ci}}\left[(1-\sigma^2+k_{co})+2\left(\frac{\rho_{ci}}{\rho_{co}}-1\right)+f_c\frac{W_c}{r_h}\rho_{ci}\left(\frac{1}{\rho}\right)_{cm}-(1-\sigma^2+k_e)\frac{\rho_{ci}}{\rho_{co}}\right]$$

And

$$\sigma = \frac{A_o}{A_f} \quad \textbf{(Equation 4-163)} \qquad r_h = \frac{D_h}{4} \quad \textbf{(Equation 4-164)}$$

$$\rho_{hi} = \frac{P_{hi}}{RT_{hi}} \quad \textbf{(Equation 4-165)} \qquad \rho_{ci} = \frac{P_{ci}}{RT_{ci}} \quad \textbf{(Equation 4-166)}$$

$$\rho_{ho} = \frac{P_{ho}}{RT_{ho}} \quad \textbf{(Equation 4-167)} \qquad \rho_{co} = \frac{P_{co}}{RT_{co}} \quad \textbf{(Equation 4-168)}$$

$$\left(\frac{1}{\rho}\right)_{hx} = \frac{1}{W_c}\int_0^{W_c}\frac{dx}{\rho_{hx}}$$

$$\left(\frac{1}{\rho}\right)_{hm} = \frac{1}{2}\left(\frac{1}{\rho_{hi}}+\frac{1}{\rho_{ho}}\right) \quad \textbf{(Equation 4-169)} \qquad \left(\frac{1}{\rho}\right)_{cm} = \frac{1}{2}\left(\frac{1}{\rho_{ci}}+\frac{1}{\rho_{co}}\right)$$

Where $\Delta p_h$ is the pressure drop in the hot side, Pa; $\Delta p_c$ is the pressure drop in the cold side, Pa; $\sigma$ is the free flow area ratio; $k_{co}$ is the contraction pressure loss coefficient; $k_e$ is the exit pressure loss coefficient; $G_{hx}$ is the mass flux from the hot or cold side in kg/m$^2$; $f_{hx}$ is the Fanning friction factor from the hot or cold side; $\rho_{hx}$ is the fluid density from the hot or cold side in kg/m$^3$; $\rho_{hi}$ is the inlet fluid density from the hot side, kg/m$^3$; $\rho_{ci}$ is the inlet fluid density from the cold side, kg/m$^3$; $\rho_{ho}$ is the outlet fluid density from the hot side, kg/m$^3$; $\rho_{co}$ is the outlet fluid density from the cold side, kg/m$^3$; $r_h$ is the hydraulic radius in m; $\left(\frac{1}{\rho}\right)_{hx}$ is

the hot or cold side mean density; $\left(\frac{1}{\rho}\right)_{hm}$ is the hot side mean density, kg/m$^3$; $\left(\frac{1}{\rho}\right)_{cm}$ is the cold side mean density, kg/m$^3$.

Values of the contraction loss coefficient $k_{co}$ and the exit loss coefficient $k_e$ for a crossflow plate-louver fin heat exchanger are presented in Figure 4-21.

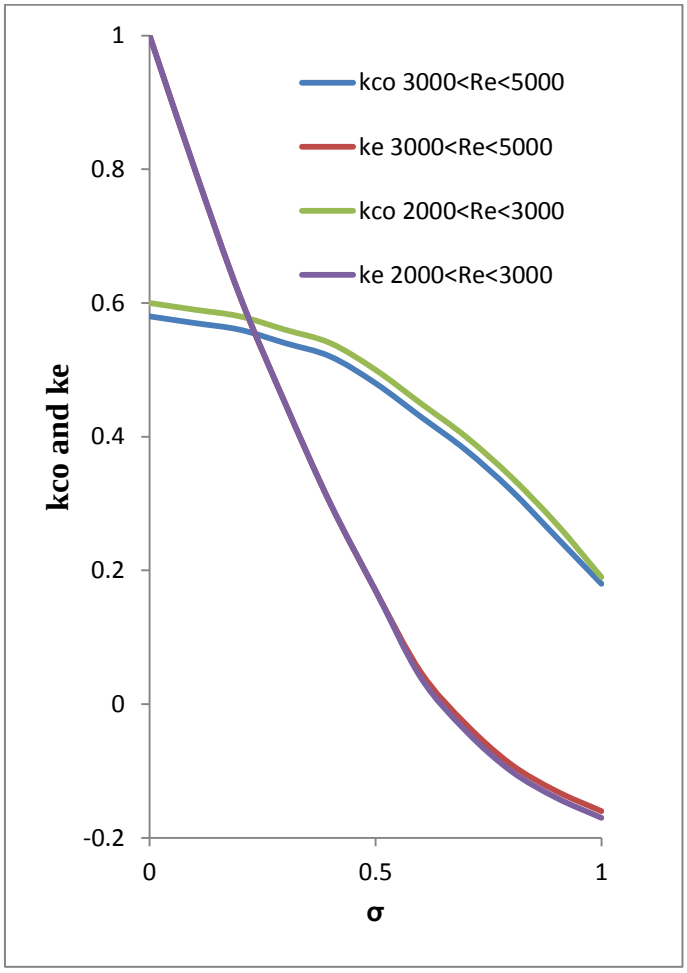


**Figure 4-21 Entrance and exit pressure loss coefficients [49]**

***Compressor.*** The Cold Air Unit analysis starts with the compressor due to the fact that the compressor performance defines the required values for the reheater, the condenser and the turbine. In this section of the ACM, the bleed air temperature provided to the compressor has been reduced by the PHX and SHX. By means of an adiabatic process (isentropic) within the compressor, the temperature and pressure increased. According to the Instituto Tecnológico de Aeronáutica (ITA) [53], the maximum downstream temperature allowed in the compressor is of 523.15 K in order to protect the distribution pipelines.

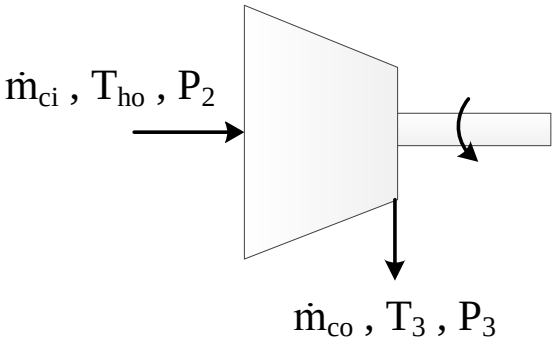


**Figure 4-22 CAU compressor**

The compressor discharge temperature and pressure are calculated using the compressor work equation as follows:

$$\dot{m}_{ci}C_p(T_3 - T_{ho}) = \dot{m}_{co}C_p\frac{T_{ho}}{\eta_c}\left[\left(P_{rc}^{\frac{\gamma-1}{\gamma}}\right) - 1\right]$$

$$T_3 = T_{ho} + \frac{T_{ho}}{\eta_c}\left[\left(P_{rc}^{\frac{\gamma-1}{\gamma}}\right) - 1\right] \quad \textbf{(Equation 4-170)}$$

$$P_3 = P_2P_{rc} \quad \textbf{(Equation 4-171)}$$

And

$$P_2 = P_1 - \Delta p \quad \textbf{(Equation 4-172)}$$

Where $T_3$ compressor outlet temperature; $\dot{m}_{ci} = \dot{M}_2$ is the PHX outlet mass flow rate, is the compressor inlet mass flow rate in kg/s; $\dot{m}_{co} = \dot{m}_{ci}$ is the compressor outlet mass flow rate, kg/s; $\eta_c = 0.8$ is the assumed compressor efficiency [54]; $P_{rc}$ = 1.5 is the assumed compressor pressure ratio [54]; $P_3$ is the compressor outlet pressure; $P_2$ is the PHX outlet pressure in Pa; $P_1$ = Engine bleed air pressure, is the PHX inlet pressure Pa.

***Turbine.*** Once the bleed air leaves the compressor, it goes through the SHX and then passes through the high pressure water separator (reheater, condenser, and water separator). Subsequently, the warm air from the reheater is expanded in the turbine isentropically,

generating a drop in the temperature and pressure. Air temperature at this stage reaches below-zero temperatures. Simultaneously, the expansion of air creates a mechanical power to drive the shaft connected to the compressor. The turbine outlet pressure can be assumed to be the ambient temperature.

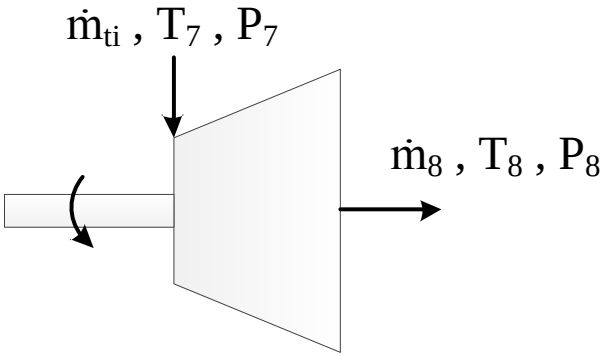


**Figure 4-23 CAU turbine**

From the compressor-turbine power balance equation, the turbine discharge temperature and pressure are expressed as:

$$\dot{m}_{co} C_p \frac{T_{ho}}{\eta_c} \left[ \left( P_{rc}^{\frac{\gamma-1}{\gamma}} \right) - 1 \right] = \dot{m}_{ti} C_p (T_7 - T_8)$$

As the compressor and turbine flow rates are the same and is modelled as a perfect gas, it reduce to.

$$\frac{T_{ho}}{\eta_c} \left[ \left( P_{rc}^{\frac{\gamma-1}{\gamma}} \right) - 1 \right] = (T_7 - T_8)$$

Thus

$$T_8 = T_7 - \frac{T_{ho}}{\eta_c} \left[ \left( P_{rc}^{\frac{\gamma-1}{\gamma}} \right) - 1 \right] \qquad \textbf{(Equation 4-173)}$$

$$P_8 = P_{c1} \qquad \textbf{(Equation 4-174)}$$

Where $T_8$ is the turbine outlet temperature in K; $T_7$ is the turbine inlet temperature, K; $\dot{m}_{ti} = \dot{m}_{co} = \dot{M}_7$ is the turbine inlet mass flow rate in kg/s; $P_8$ is the turbine outlet temperature in Pa; $P_{c1}$ is the atmospheric pressure, Pa.

### 4.3.3. Vapour Cycle unit analysis

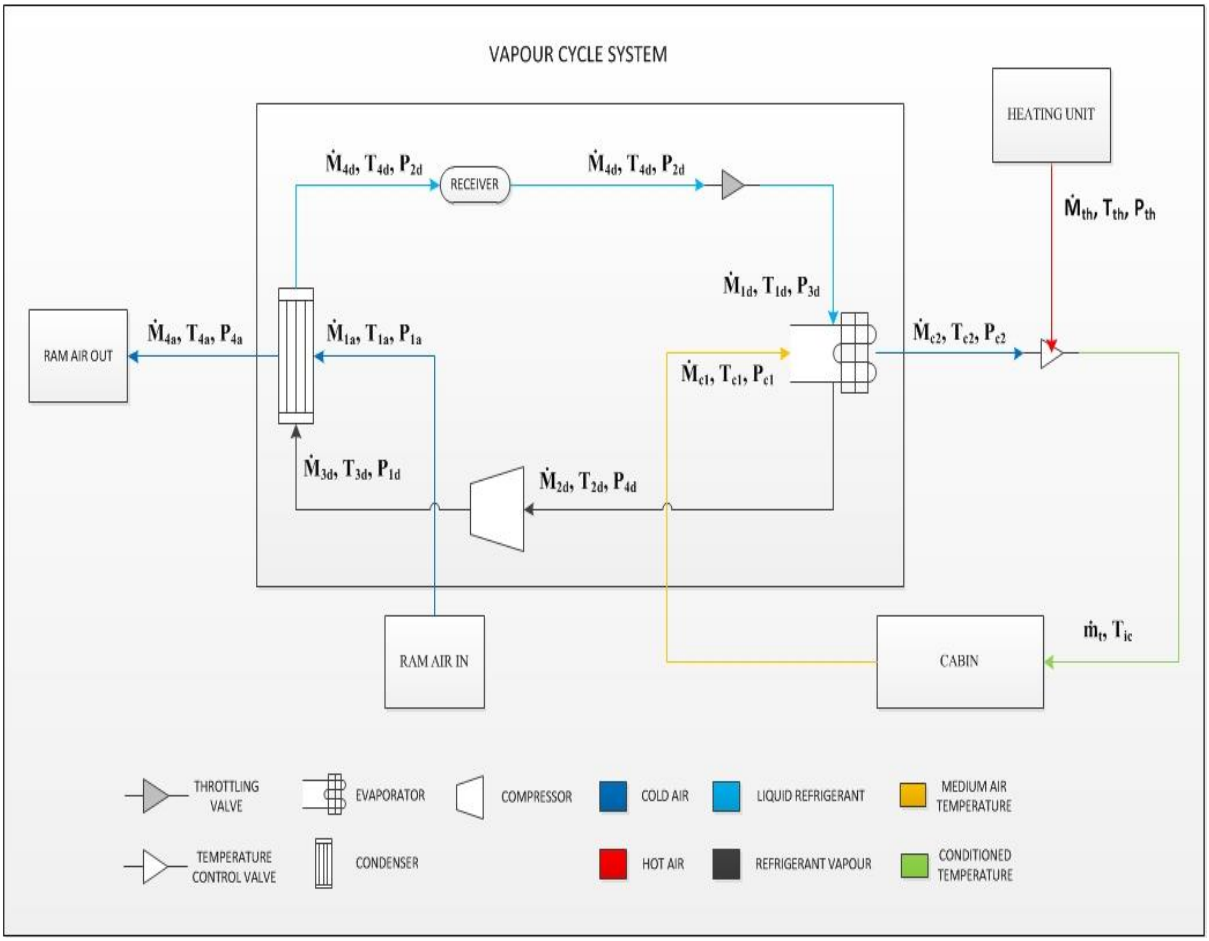


**Figure 4-24 VCM unit variables and components**

Vapour cycle system reduces the cabin heat by means of an evaporative heat exchanger. Evaporation of the liquid refrigerant in the evaporator absorbs heat from the heat source fluid. The refrigerant is then compressed to a higher pressure and temperature. The motor-driven compressor is responsible for the circulation of the fluid (refrigerant) in the system. Subsequently, the refrigerant acquired heat is rejected within a condenser and cooled. In the condenser, ram air (ambient air) is used to reduce the refrigerant temperature. The refrigerant liquid leaving the condenser is expanded to a lower pressure and temperature through a throttling valve, and then flows to the evaporator. Figure 2-13 shows schematically the VCM closed circuit system.

The mathematical analysis for the vapour cycle unit is similar to that for the ACM. The evaporator and the condenser are calculated as gas-to-liquid heat exchangers, where the liquid must be a refrigerant and the gas is the ambient air or recirculated air from the cabin. A research conducted by the Northern Research and Engineering Corporation [55], concluded that Freon 11 (R11) is the optimum refrigerant for a VCM because of its low levels of toxicity and high coefficient of performance within an evaporator and a condenser. The properties of Freon 11 are shown in Appendix A. Figure 4-24 illustrates the VCM variables and components to analyse in this section.

***Evaporator, condenser***. The evaporator (vaporizer) is a heat exchanger with liquid-to-steam phase change. Similarly, in a condenser the steam is condensed to a liquid by means of a heat exchanger. The evaporator and condenser analysis (heat exchanger) into the VCM varies according to its geometrical dimensions and classification. As in the previous section, a cross flow louver-fin heat exchanger was selected for the analysis of the evaporator and condenser. Its dimensions are established by using the dimensions calculation in section 4.3.2. The thermal analysis is determined by following the steps outlined in section 4.3.2 (PHX, SHX, Reheater, Condenser). In the VCM close circuit side (liquid refrigerant), the temperature and the pressure are constants within the vaporizer and the condenser. In order to maintain an appropriated temperature in the cycle, the constant pressure established through the evaporator is of 34473 Pa [56]. When the temperature remains constant the heat capacity rate ratio $C^* = 0$, thus the exchanger efficiency may be obtained from the following equation:

$$\varepsilon_{vc} = 1 - \exp(-NTU) \qquad \textbf{(Equation 4-175)}$$

And

$$NTU = \ln\frac{T_{hi}-T_{ci}}{T_{hi}-T_{co}} \ (For\ T_{hi} = constant) \qquad \textbf{(Equation 4-176)}$$

$$NTU = \ln\frac{T_{hi}-T_{ci}}{T_{ho}-T_{ci}} \ (For\ T_{ci} = constant)$$

Where $\varepsilon_{vc}$ is the condenser and vaporizer effectiveness of the refrigerant side.

The condenser mean temperature difference must be calculated as:

$$T_{mh} = \Delta T_{lm} * F \quad \textbf{(Equation 4-177)}$$

$$T_{mc} = \frac{T_{hi} + T_{ho}}{2}$$

The evaporator mean temperature is given by:

$$T_{mc} = \Delta T_{lm} * F \quad \textbf{(Equation 4-178)}$$

$$T_{mh} = \frac{T_{ci} + T_{co}}{2}$$

And

$$\Delta T_{lm} = \frac{\Delta T_{t1} - \Delta T_{t2}}{\ln\left(\frac{\Delta T_{t1}}{\Delta T_{t2}}\right)} \quad \textbf{(Equation 4-179)}$$

Where

$\Delta T_{t1} = T_H - T_{ci}\ (Condenser)$**(Equation 4-180)** $\Delta T_{t2} = T_H - T_{co}\ (Condenser)$**(Equation 4-181)**

$\Delta T_{t1} = T_H - T_{hi}\ (Evaporator)$**(Equation 4-182)** $\Delta T_{t2} = T_H - T_{ho}\ (Evaporator)$**(Equation 4-183)**

$F$ = 1 is a constant given for a condenser and evaporator heat exchanger [48]. $T_H$ = 296.15is the assumed refrigerant (R11) saturation temperature.

***Compressor***. In the compressor stage, the temperature of the vaporised refrigerant increases and a constant circulation of the steam is generated into the VCM circuit. The compressor is electric-motor driven. The general equations used in the ACM compressor analysis are used to compute the VCM compressor. A value of $\eta_c = 0.8$ is assumed for the compressor efficiency, with a compressor ratio of $P_{rc}$ = 1.5.

***Expansion valve***. An expansion valve is located at the end of the closed loop side. This valve is responsible for expanding and cooling the refrigerant to reach its initial temperature. Friction-losses (pressure drop) of the valve have been neglected. The final temperature of the valve must be equal to the initial temperature of the evaporator.

$$T_{4d} = T_{1d} \qquad \textbf{(Equation 4-184)}$$

Where $T_{4d}$ is the valve outlet temperature in K; $T_{1d}$ is the evaporator inlet temperature, K.

### 4.3.4. Heating units analysis

Different heating methods are currently found in helicopters. The selection of the heater depends upon the specific application and lightest configuration. This section analysed four types of heaters in order to obtain a satisfactory heating within the rotorcraft: Bleed air, Combustion Heater, and Exhaust Heater.

***Bleed air***. Heating may be supplied to the occupied areas of an aircraft by bleeding the compressor engine and mixing the bleed air with cold air from the ACM or the VCM. This method is the simplest and lightest for heating. Because of possible contamination of the bleed air, this heating method has been used primarily for military applications. The amount of bleed air depends entirely on the required cabin temperature as shown in Figure 4-25. The hot fluid mass flow and temperature varies according to the cold unit and cabin required ventilation:

$$\dot{m}_{ba} = \dot{m}_t - \dot{M}_{tc} \qquad \textbf{(Equation 4-185)}$$

Where $\dot{m}_{ba}$ is the bleed air mass flow rate in kg/s; $\dot{M}_{tc}$ is the cooling unit (ACM or VCM) mass flow rate, kg/s.

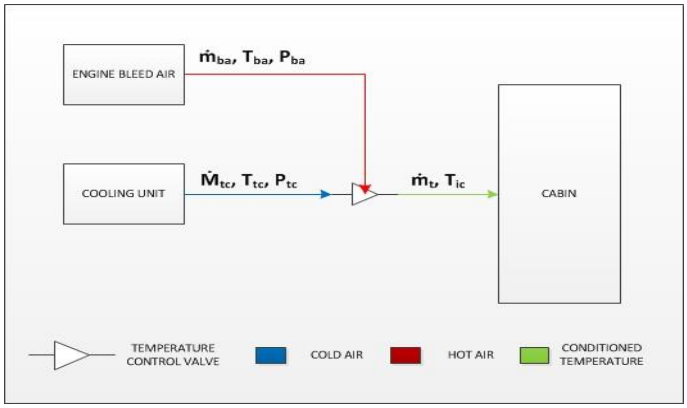


**Figure 4-25 ECS bleed air supply**

***Combustion Heater (CH)***. The combustion heater comprises an internal burner operating within a combustion chamber around which the cabin air supply air is directed. The temperature of the cabin air is increased by the transfer of heat from the wall of the combustion chamber. The hot air then passes to the cabin to maintain the required cabin temperature. Combustion heaters are large and heavy and for ground operation, a combustion air blower is required. The CH variables and components analysed in this section are illustrated in Figure 4-26.

The thermal analysis of the combustion heater considered the raised equations in sections 4.3.2 and 4.3.3. As shown in Figure 4-25, the combustion chamber temperature is constant, varying (increasing) the cabin air temperature. This same behaviour is performed by the evaporator and the condenser of the ACM and the VCM. Therefore, the study of the CH is based entirely on the procedure and calculations developed above.

The combustion chamber temperature can reach up to 1800 K [57]. However, for this analysis a temperature of 1000 K was set due to the fact that this is the maximum temperature allowed by the chosen heat exchanger configuration and its materials [34].

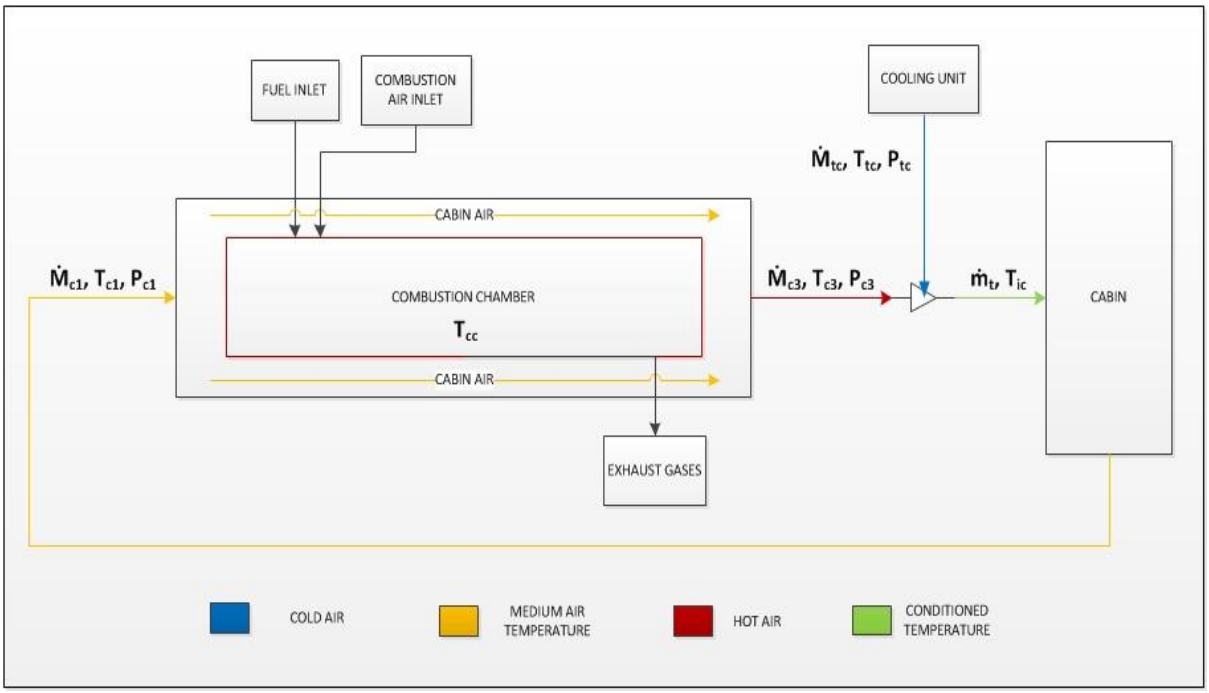


**Figure 4-26 CH unit variables and components**

***Exhaust Heater (EGH)***.

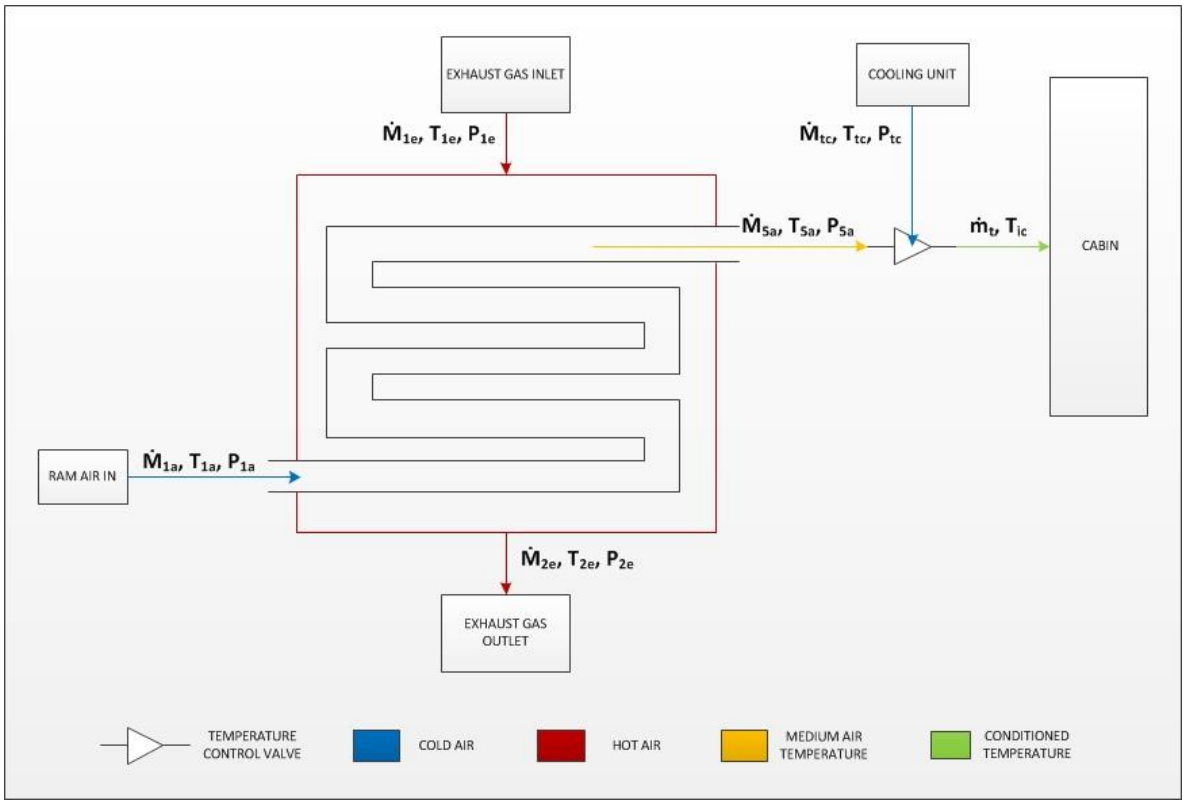


**Figure 4-27 EGH unit variables and components**

A portion of the exhaust gases are transmitted to a heat exchanger in order to heat ram air or recirculated air from the cabin, then is directed to the areas requiring heating. Figure 4-27 shows schematically the EGH variables and components. The thermal analysis of the exhaust heating unit is performed under heat exchanger equations used in section 4.3.2. According to the National Advisory Committee for Aeronautics (NACA), the exhaust gases temperature is of 1000 K, with a constant pressure of 546000 Pa [57].

### 4.3.5. Power consumption analysis

***Pneumatic power consumption.*** An adequate supply of air (bleed air or ram air) is required through the cold unit to maintain the flow and thus generate the amount of cooling or heating required by the cabin. For instance, the ACM requires enough mass flow within the system to reduce the initial bleed air temperature, and then a direct mass flow from the engine is added to the resulting ACM air to provide a suitable temperature in the cabin. The sum of these two temperatures and the mass flow are equal to the values required by the cabin. Unfortunately, the use of pneumatic air significantly affects engine performance by increasing fuel consumption. Therefore, it is important to determine the pneumatic power consumption over the ECS either single or as a combined system of heating and cooling unit.

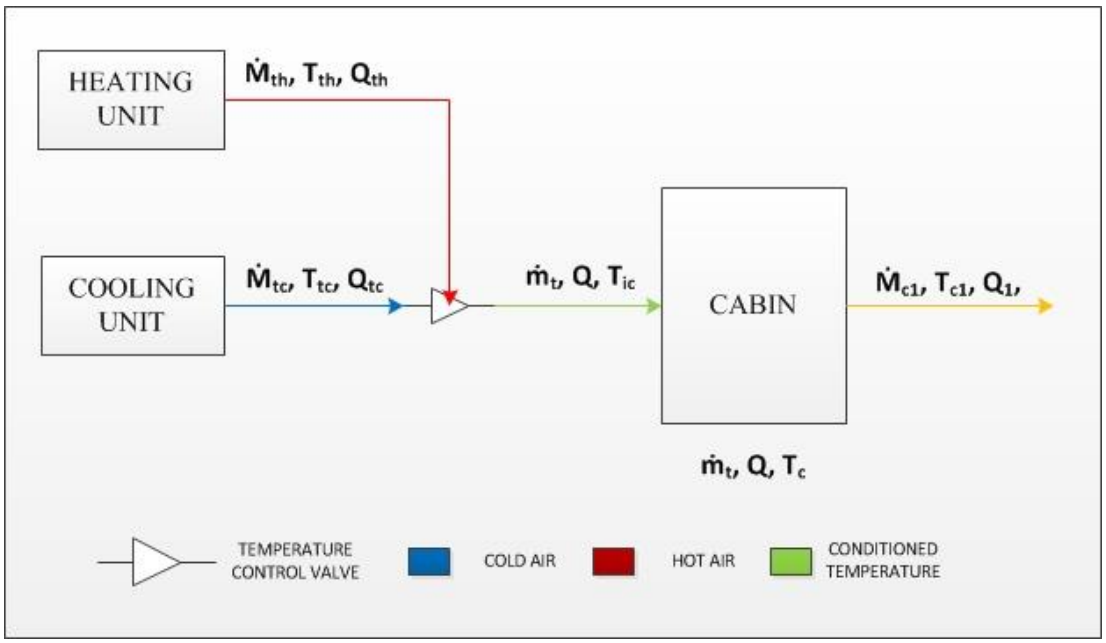


**Figure 4-28 Mass flow, temperature and heat load distribution**

To set the pneumatic power consumption($\dot{M}_{th}\ or\ \dot{M}_{tc}$), it is necessary to iterate the system computations with an assumed mass flow ($\dot{M'}_{th}\ or\ \dot{M'}_{tc}$) and obtain the following values: the heat load in each of the environmental control units ($Q_{th}$ or $Q_{tc}$), and unit temperatures ($T_{th}\ or\ T_{tc}$). In addition, the total heat load ($Q$), the mass flow or ventilation ($\dot{m}_t$), and temperature ($T_c$) of the cabin are required, see Sections 4.2 and 4.3.1. Once these values are acquired, the inlet and outlet temperatures of the cabin are computed as:

$T_{ic} = T_c - \frac{Q}{\dot{m}_t C_p}\ (Cooling)$ **(Equation 4-186)**

$T_{c1} = T_c + \frac{Q}{\dot{m}_t C_p}\ (Cooling)$ **(Equation 4-187)**

$$T_{ic} = T_c + \frac{Q}{\dot{m}_t C_p}\ (Heating)$$

$$T_{c1} = T_c - \frac{Q}{\dot{m}_t C_p}\ (Heating)$$

As mentioned above, the input variables in the cabin are computed by adding the variables generated by the cooling unit to the variables from the heating unit. Therefore, the required mass flow in the ACM is determined as follows:

$$\dot{M}_{tc} = \frac{Q_{tc}}{C_p(T_{ic} - T_{tc})} \quad \textbf{(Equation 4-188)}$$

The above result is iterated until the assumed mass flow equals to the mass flow acquired.

$$\dot{M'}_{tc} = \dot{M}_{tc}$$

Therefore, the mass flow, temperature, and the heat load in the heating unit are given as:

$$\dot{M}_{th} = \dot{m}_t - \dot{M}_{tc} \quad \textbf{(Equation 4-189)}$$

$$T_{th} = T_{ic} - T_{tc} \quad \textbf{(Equation 4-190)}$$

$$Q_{th} = Q - Q_{tc} \quad \textbf{(Equation 4-191)}$$

It should be noted that this result is the minimum required ventilation in the cabin. Therefore, percentage increase of the ventilation may be required in the cooling unit (to cool down), or in the heating unit (to heat up), if the resulting temperature is not high enough to cool or heat the cabin.

The VCM closed circuit does not need pneumatic power; however it is necessary the use of a heating unit to control the cabin inlet temperature. The heating unit on the other hand, requires a pneumatic power from the engine. The variables of the circulating air in the VCM (air cooled in the evaporator) are equal to the output variables of the cabin; neglecting losses within the cabin. As in the ACM, the required ventilation in the heat unit increased depending on the obtained temperature in the VCM. Thus, the variables ($\dot{M}_{th}, T_{th}, Q_{th}$) are given by the equations used above.

***Coefficient of performance.*** The coefficient of performance is used to quantify the performance of refrigeration cycles. The COP is the ratio of the required output to the set input. Many factors can vary the COP value, such as the efficiencies, temperatures and losses from the condenser, evaporator, and compressor; also the refrigeration fluid characteristics. The coefficient of performance measures the efficiency advantage between the systems, a low COP means greater loss of power and fuel consumption. The coefficient of performance of the ACM (Bootstrap system) is calculated as follows:

$$COP_{ACM} = \frac{5}{M^2}\left(1 - \frac{T_9}{T_1}\right) \qquad \textbf{(Equation 4-192)}$$

Where $COP_{ACM}$ is the Air Cycle Machine coefficient of performance; $M$ is the helicopter Mach number.

The following equation is used to calculate the COP of the VCM:

$$COP_{VCM} = \frac{h_{2d} - h_{1d}}{h_{3d} - h_{2d}} \qquad \textbf{(Equation 4-193)}$$

Where $h_{2d} - h_{1d}$ is the heat absorbed in the evaporator in J/kg; $h_{3d} - h_{2d}$ is the VCM isentropic compression, J/kg. These values are obtained from a pressure-enthalpy diagram at a defined saturation temperature of the compressor and evaporator, Appendix A.

# 5. Chapter | Analysis and discussion of results

## 5.1. ECS-PCM simulation

The results of this simulation confirm that the executable model ECS-PCM is Medium-fidelity. However, based on engineering experience developed in this area during this year of MSc studies, its results meet the requirements to carry out this study. The simulations are validated by comparing the dynamic model with the results and curves trends of public data. In addition, two case studies were carried out in chapter four to show ECS behaviour in different environments. For this purpose, a mission was selected in a warm environment to reduce the temperature within the cabin by means of the cooling system. Another mission is performed in a cold environment, where the heating system is activated; increasing the heat in the helicopter cabin. The conditions are given in Section 4.1, and the model analysis is described in Appendix B. The results of the simulation are discussed in this chapter.

### 5.1.1. Cabin heat loads

The temperature in the cabin depends on the total heat load generated by different sources; which are determined with calculations discussed above for the model. A larger amount of air flow (mass flow rate) circulating in the cabin is required in order to counteract high heat load. As shown in Table 5-1, if the cabin temperature is not significantly affected by the internal environment (heat loads), the required mass flow is of 0.035 kg/s. According to EASA, this value is the minimum required ventilation for 7 people in a light helicopter category. However, the cabin temperature increase or decrease if the heat loads rises, causing an equivalent increase in the minimum ventilation required. Results obtained through the simulation of the cabin are discussed in this Section.

The temperature into the cabin is set to 297.15 K, below this temperature the cabin ambient is considered cold, so the mass flow must increase to balance the heat loss. On the other hand, if the temperature is above this value the cabin is considered hot, thus the mass flow increases until a desired value for the cabin is reached. Case studies set in Section 4.1 were simulated and its results compared with public available data. Results of the mass flow and cabin heat load from the simulated case studies are shown in Figure 5-1.

**Table 5-1 Cabin heat load case study results**

| Mass flow rate (kg/s) | Cabin Heat load (W) | Outside Temperature (K) | Transparency heat load (W) | Wall heat load (W) | Floor heat load (W) | Ceiling heat load (W) | Bulkhead heat load (W) | Solar radiation heat load (W) | Infiltration Heat load (W) |
|---|---|---|---|---|---|---|---|---|---|
| 0.035 | -176.9 | 300.15 | -67.88 | -51.03 | -8.07 | -1.86 | -1.73 | N/A | -46.36 |
| 0.035 | -120.3 | 299.15 | -45.81 | -34.44 | -5.44 | -1.8 | -1.5 | N/A | -31.28 |
| 0.035 | -63.64 | 298.15 | -23.73 | -17.84 | -2.82 | -1.74 | -1.3 | N/A | -16.21 |
| 0.035 | -6.997 | 297.15 | -1.65 | -1.2 | -0.19 | -1.68 | -1.08 | N/A | -1.131 |
| 0.035 | -10.62 | 296.15 | 20.42 | 17.92 | 4.459 | -62.78 | -4.58 | N/A | 13.94 |
| 0.035 | 47.46 | 295.15 | 42.5 | 38.08 | 9.814 | -68.08 | -3.8 | N/A | 29.02 |
| 0.035 | 110.1 | 294.15 | 64.57 | 58.57 | 15.38 | -69.78 | -2.7 | N/A | 44.09 |
| 0.035 | 174.7 | 293.15 | 86.65 | 79.28 | 21.08 | -70 | -1.5 | N/A | 59.17 |
| 0.035 | 240.5 | 292.15 | 108.7 | 100.1 | 26.87 | -69.39 | -0.1 | N/A | 74.24 |
| 0.035 | 307.1 | 291.15 | 130.8 | 121.1 | 32.74 | -68.23 | 1.36 | N/A | 89.32 |
| 0.035 | 374.4 | 290.15 | 152.9 | 142.2 | 38.67 | -66.7 | 2.9 | N/A | 104.4 |
| 0.035 | 442.1 | 289.15 | 175 | 163.4 | 44.66 | -64.88 | 4.48 | N/A | 119.5 |
| 0.035 | 510.2 | 288.15 | 197 | 184.7 | 50.7 | -62.84 | 6.112 | N/A | 134.5 |
| 0.035 | 578.6 | 287.15 | 219.1 | 206 | 56.77 | -60.63 | 7.773 | N/A | 149.6 |
| 0.035 | 647.3 | 286.15 | 241.2 | 227.4 | 62.89 | -58.27 | 9.465 | N/A | 164.7 |
| 0.035 | 716.3 | 285.15 | 263.3 | 248.8 | 69.03 | -55.78 | 11.18 | N/A | 179.8 |
| 0.035 | 785.5 | 284.15 | 285.3 | 270.3 | 75.21 | -53.18 | 12.93 | N/A | 194.8 |
| 0.035 | 854.8 | 283.15 | 307.4 | 291.9 | 81.42 | -50.5 | 14.69 | N/A | 209.9 |
| 0.035 | 924.4 | 282.15 | 329.5 | 313.5 | 87.66 | -47.73 | 16.48 | N/A | 225 |
| 0.0354 | 994.1 | 281.15 | 351.6 | 335.1 | 93.92 | -44.89 | 18.28 | N/A | 240.1 |
| 0.036 | 1064 | 280.15 | 373.6 | 356.8 | 100.2 | -41.99 | 20.1 | N/A | 255.1 |
| 0.0367 | 1134 | 279.15 | 395.7 | 378.5 | 106.5 | -39.02 | 21.94 | N/A | 270.2 |
| 0.0373 | 1204 | 278.15 | 417.8 | 400.3 | 112.8 | -36.01 | 23.79 | N/A | 285.3 |
| 0.038 | 1274 | 277.15 | 439.9 | 422.1 | 120.2 | -35.94 | 25.65 | N/A | 300.4 |
| 0.0386 | 1345 | 276.15 | 461.9 | 443.9 | 125.5 | -29.83 | 27.53 | N/A | 315.4 |
| 0.0393 | 1415 | 275.15 | 484 | 465.8 | 131.9 | -26.68 | 29.42 | N/A | 330.5 |

This study takes into consideration five heat loads; convection $Q_c$, solar $Q_s$, occupant $Q_o$, infiltration $Q_i$, and electrical $Q_e$. The occupants and electrical heat load are constant during the chosen missions. The other three loads vary according to the mission conditions; this variation affects the required mass flow value within the cabin. The missions were taken on a completely cloudy environment, thus the heat loads due to solar radiation are negligible (N/A in Table 5-1).

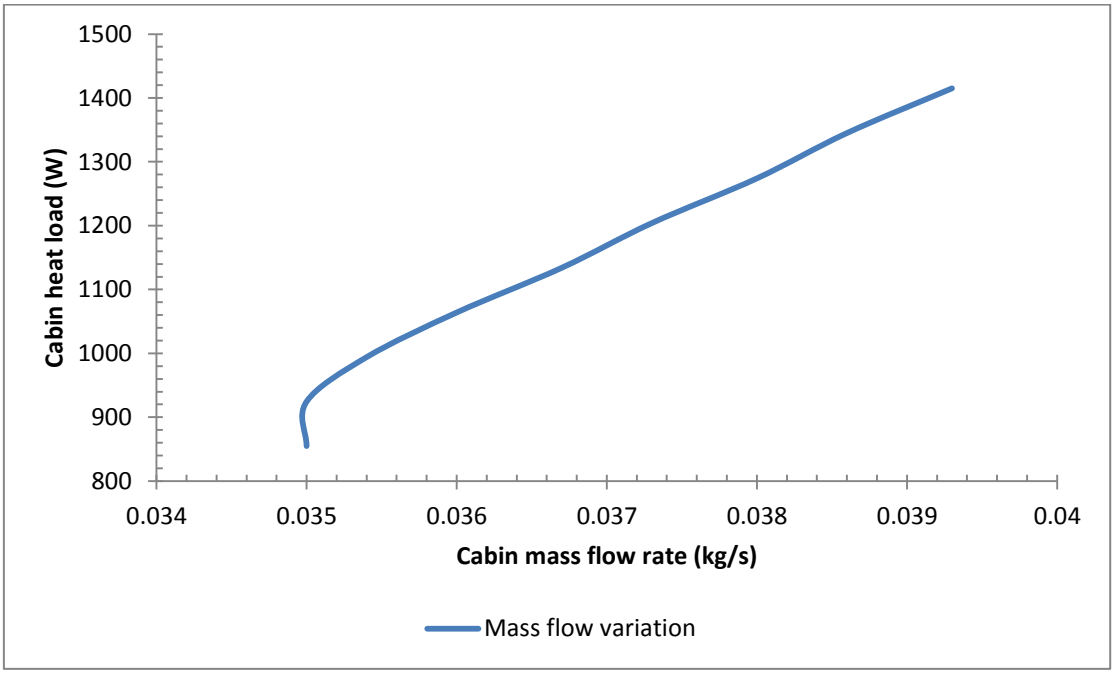


**Figure 5-1 Mass flow rate variation due to cabin heat load**

As is shown in Figure 5-1, the mass flow rate varies due to the cabin heat load increment. The mass flow remains constant to the minimum value due to the fact that its temperature has not change enough to affect the desired temperature inside the cabin. The mass flow starts to increment is value when the heat loads reach 994 W.

Figure 5-2 shows the mass flow behaviour due to temperature variation; at lower temperature additional mass flow is required. From a certain temperature (approximately 280 K) the mass flow becomes constant at 0.035 kg /s.

Results in Table 5-1 shows the effect of heat loads from different sources into the cabin temperature. Results initiated with a cabin temperature between 275.15K and 297.15K where the desired temperature is achieved; subsequently, the temperature was increased until the established temperature of the Miami case study, 300.15K. Throughout this change, each heat

source affected the cabin temperature, thus increasing the mass flow rate. Figure 5-3 shows the heat sources behaviour regarding the temperature in the cabin. In heating stage, an increase is generated in heat loads. However, the ceiling load contributes negative values, it means that the heat source does not subtract energy, but rather is supplying energy for heating the cabin.

Once the desired temperature is reached in the cabin, the values are inverted (positive values become negative and negative to positive) due to the change of energy required. This phase requires that the heat loads heating the aircraft is established, and then be counteracted with a proper mass flow value. Therefore, the heat load generated by the ceiling is used in this stage to increases the temperature of the cabin, increasing the required mass flow to reduce the added temperature provided by the ceiling.

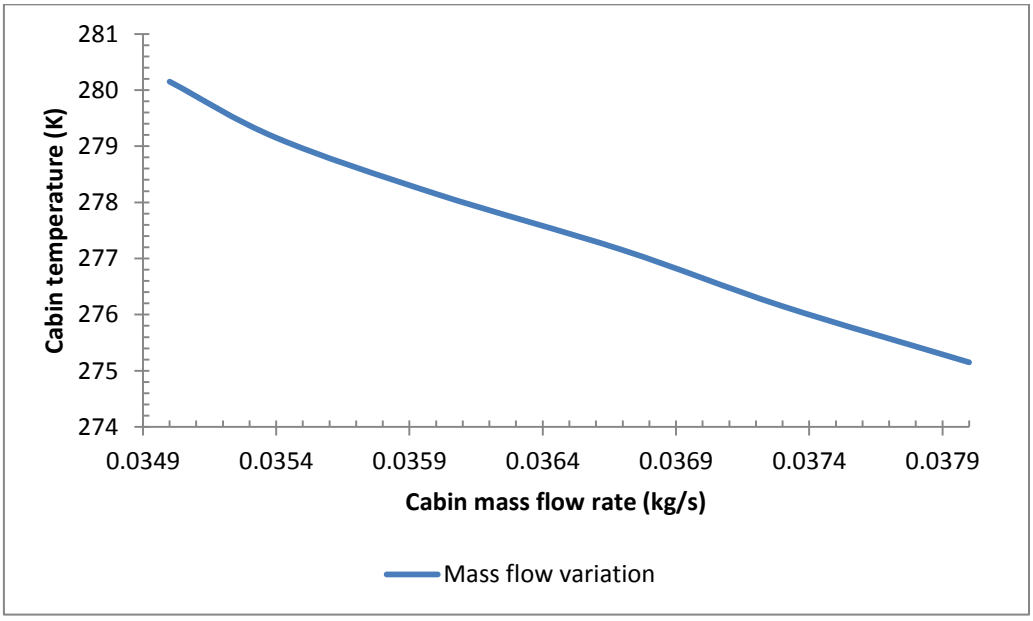


**Figure 5-2 Mass flow variation due to cabin temperature**

Figure 5-4 shows the heat load variation due to the cabin temperature. This load is the sum of all heat sources affecting the temperature and hence the mass flow required by the aircraft. The overall cabin heat load decreases as the temperature increases. Above 297.15K the temperature is increasing (cooling process), and the heat load contributes negative values, this is due to the fact that the heat source does not subtract energy from the cabin in this stage; while below this value the temperature is dropping (heating process), therefore the load

increases. However, the ceiling load contributes negative values, it means that the heat source does not subtract energy, but rather is supplying energy for heating the cabin.

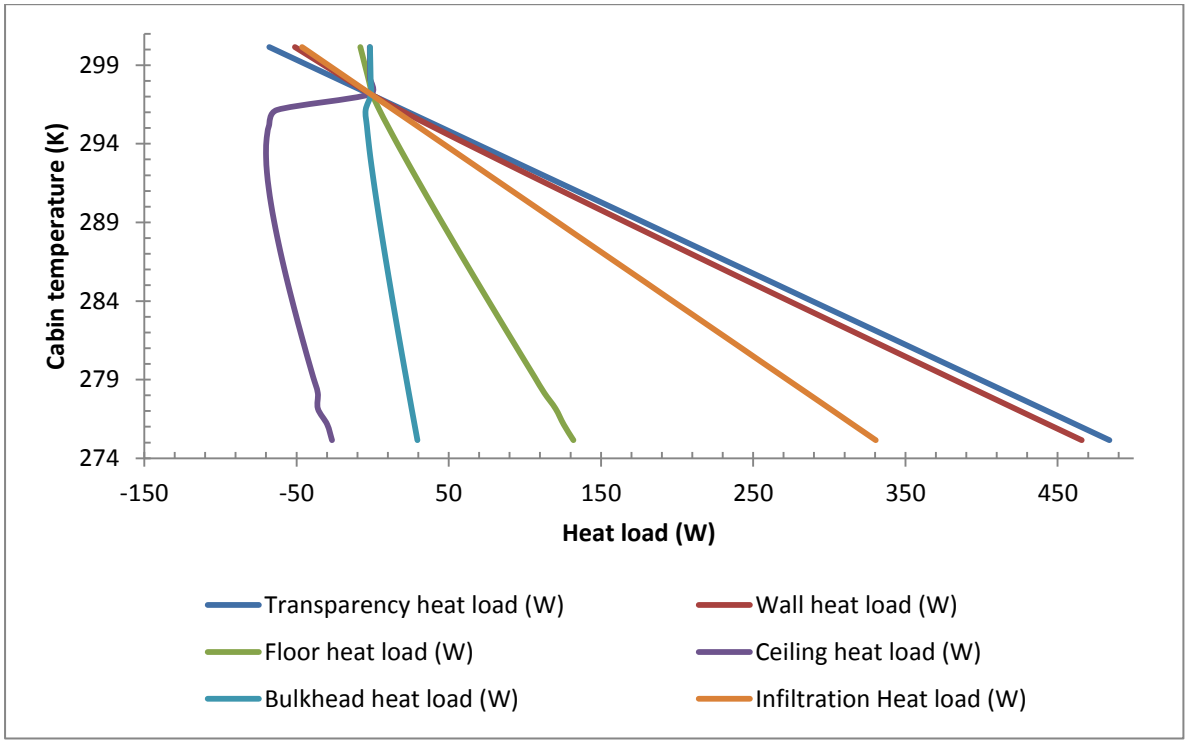


**Figure 5-3 Heat load components**

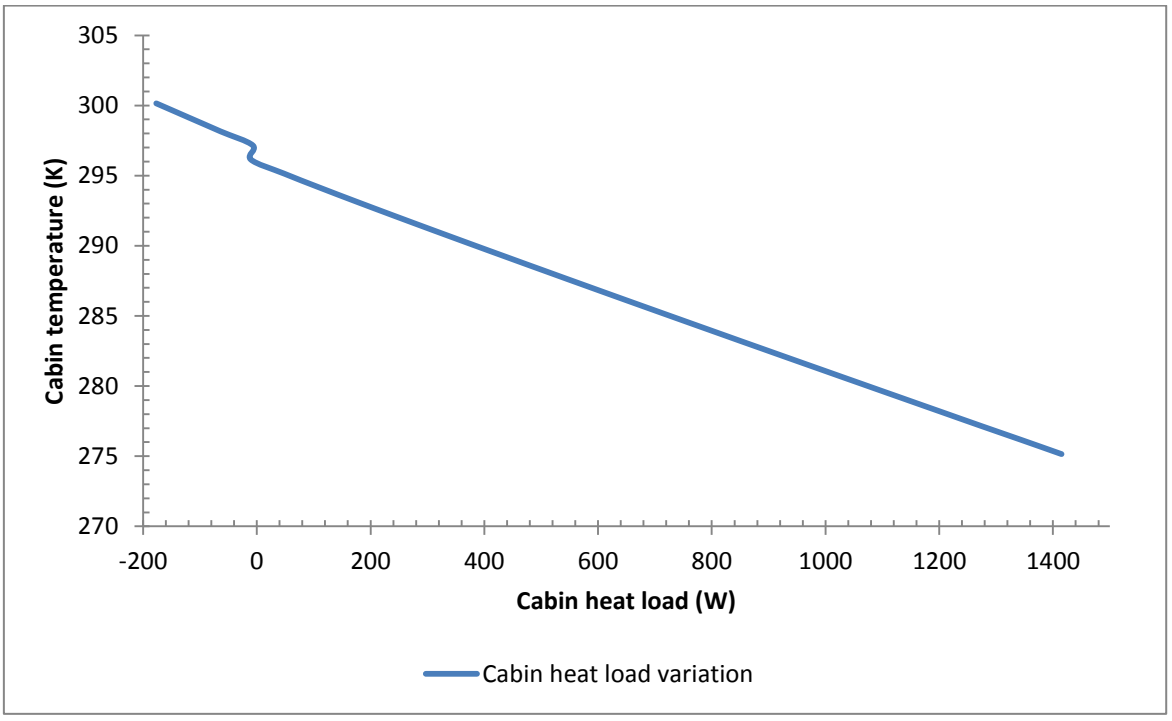


**Figure 5-4 Cabin heat load variation due to cabin temperature**

The resultant variables of the cabin analysis, behaves according to public trendlines and results from other studies. A new mission (new aircraft and flight conditions) was set into the ECS-PCM model In order to validate this study. Results from simulation were compared with the results given by the Engineering Design Handbook (1976) [32], an analysis of a helicopter ventilation. Table 5-2 shows the results obtained and its margin of error (deviation).

**Table 5-2 Comparison of simulation results**

| Parameter | ECS-PCM simulation | Public data | Deviation |
|---|---|---|---|
| Transparency heat load (W) | 4815 | 4745 | 1.48 |
| Insulated wall heat load (W) | 682 | 665 | 2.56 |
| Uninsulated Wall heat load (W) | 15660 | 15578 | 0.53 |
| Floor heat load (W) | 7094 | 7032 | 0.88 |
| Infiltration heat load (W) | 21088 | 21087 | ------ |
| Rear ramp insulated (W) | 4088 | 4071 | 0.42 |
| Insulated ceiling (W) | 594 | 577 | 2.95 |
| Uninsulated ceiling (W) | 7173 | 7111 | 0.87 |
| Cabin heat load (W) | 61194 | 60883 | 0.51 |
| Cabin mass flow rate (kg/s) | 0.56 | 0.56 | ------ |

### 5.1.2. Air Cycle Machine

As mentioned throughout this study, the ACM is a complex thermodynamic system composed of several components. Each component is responsible for varying the temperature of the hot stream to reach a desirable temperature for the cabin. The ACM depends on three variables: the temperature of the fluids, pressure, and mass flow rate. The efficiency of the complete system is determined by the coefficient of performance, and this varies according to the efficiency provided by each of the components. This Section contemplates the results obtained in the simulation of the ACM unit. The results shown below are from the UK case study only. The Miami mission simulation is not included due to constants results obtained from its low heat gain into the cabin.

The ACM includes two heat exchangers, one reheater, a condenser, and a unit of compression and expansion. As mentioned in Section 4.3.2, the heat transfer within the reheater and the

condenser is the same as in a heat exchanger, therefore the analysis of these two components are based on exchanger calculations. Table 5-3 shows the temperature and pressure obtained from the ACM components at the lowest mission (case study) temperature.

**Table 5-3 ACM components inlet values**

| | Inlet Temperature (K) | | Inlet Pressure (Pa) | | Inlet mass flow rate (kg/s) | |
|---|---|---|---|---|---|---|
| | Cold side | Hot side | Cold side | Hot side | Cold side | Hot side |
| Primary heat exchanger | 281.7 | 473.15 | $9.559x10^{04}$ | $2.757x10^{05}$ | 0.303 | 0.056 |
| Compressor | N/A | 281.7 | N/A | $2.758x10^{05}$ | 0.303 | 0.056 |
| Secondary heat exchanger | 275.2 | 324.9 | $9.603x10^{04}$ | $4.137x10^{05}$ | 0.303 | 0.056 |
| | High pressure | Low pressure | High pressure | Low pressure | High pressure | Low pressure |
| Reheater | 275.2 | 274.5 | $4.137x10^{05}$ | $4.137x10^{05}$ | 0.056 | 0.056 |
| Turbine | N/A | 275.2 | N/A | $4.136x10^{05}$ | 0.056 | 0.056 |
| Condenser | 275.2 | 232 | $4.137x10^{05}$ | $9.603x10^{04}$ | 0.056 | 0.056 |

The heat exchanger requires cold and a hot fluid with their respective temperatures and pressures. Section 4.3.2 shows that the cold fluid (ram air) first passes through the SHX; its temperature and pressure are given by atmospheric condition. The hot fluid goes first within the PHX; its inlet values are given by the Bell206L-4 engine bleed air. These data are provided in Section 4.3.2. The initial temperature of the PHX (on the cold side) is obtained from iterations performed in Matlab-Simulink ®; similarly for the SHX initial temperature (hot side). Table 5-3 shows the initial values of each component.

The temperature variation across the ACM is shown in Figure 5-5. In the PHX and SHX, the inlet temperature is reduced by ram air and delivered to the compressor and reheater respectively. In the compressor the air is compressed and its temperature increases, this variation depends on the selected compression ratio and adiabatic efficiency. Furthermore, the reheater is the first stage of the water separator unit; where the temperature variation is not high. Similarly, the condenser (high pressure side) will remain with a minor change in temperature; in the low pressure side, the fluid outlet temperature of the turbine is increases.

The temperature will remain constant within the water separator, its main purpose involves separating water droplets formed in the fluid due to condensation. The temperature drop in the turbine, as well as the compressor, depends on the expansion ratio and the adiabatic efficiency selected.

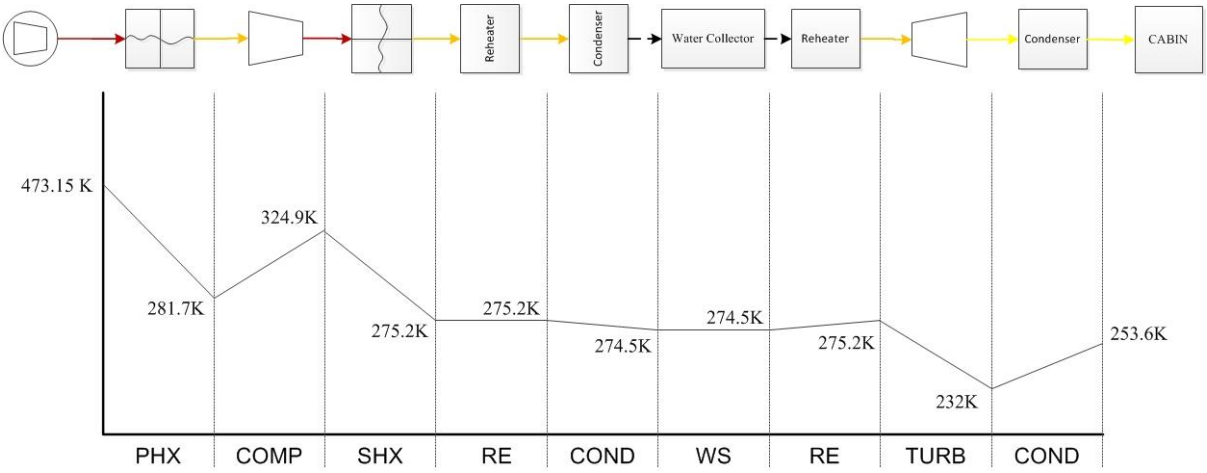


**Figure 5-5 Temperature variation through the ACM**

The temperature behaviour of the ACM unit was compared with the parameters found in Airbus-320 training manual. The variables presented in both cases represent changes of temperature of the ACM components. These changes have the same trend as the one presented by Airbus, thus the behaviour of the components are according to what is expected to be in a bootstrap ACM.

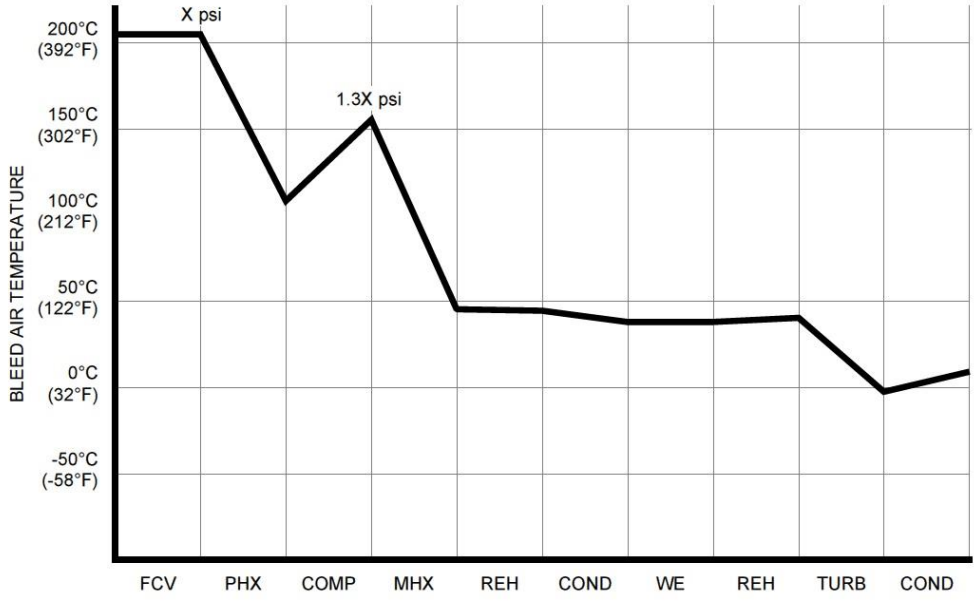


**Figure 5-6 Airbus 320 air conditioning parameters [2]**

### 5.1.3. Heat exchanger

The heat exchanger is a fundamental component in both ACM and VCM, as for the heating units. This element transfers temperature between two fluids by means of a corrugate louver fin and a tube. Before being integrated into different units, a validation of the exchanger was performed. To this end, the results from the developed exchanger were compared with data supplied by public sources. The input data for the simulation was set with same values provided from Fundamentals of Heat Exchanger Design (2003). Table 5-7 contains the compared parameters and deviation against public data.

**Table 5-4**

| Parameter | Exchanger simulation | | Public data | | Deviation | |
|---|---|---|---|---|---|---|
| | Gas[A] | Air[B] | Gas | Air | Gas | Air |
| Heat transfer coefficient ($W/m^2$) | 361.1 | 336.99 | 360.83 | 336.81 | 0.075 | 0.053 |
| Effectiveness | 0.83 | | 0.83 | | ----- | |
| Heat transfer rate (W) | 1083824 | | 1083800 | | 0.0022 | |
| Outlet temperature (K) | 591.9 | 978.6 | 591.5 | 978.2 | 0.068 | 0.041 |
| Pressure drop (Pa) | 8415 | | 8394 | | 0.250 | |

*A= Hot fluid side*
*B= Cold fluid side*

Results in Table 5-7 were used only for validating purpose of the exchanger model, therefore, the case studies given in this document were not taken into account. The results show that the model developed is of high-fidelity for the proposed configuration of heat exchanger. The inlet temperatures of gas and air are 1173.15K and 473.15K respectively. The mass flow rate is of 1.66 kg / s for the gas, and 2.00 kg / s for air. As required within the analysed units, the heat exchanger increasing the cold fluid temperature, while reducing the temperature of the hot fluid. Its effectiveness is within the acceptable range for a gas-to-air or air-to-air heat exchanger. Once the model is validated, it is integrated into the heating and cooling units.

### 5.1.4. Vapour Cycle Machine.

The Vapour Cycle Machine is a closed cycle unit and consists of three variables (temperature, pressure and mass flow) independent for each fluid. Heat transfer occurs between a refrigerant (Freon 11 or R 11) and the ram air from atmosphere or recirculated air from the cabin. The efficiency of the complete system is determined by the coefficient of performance, and this varies according to the enthalpy and entropy of the R11 through the components, see Appendix A. This Section contemplates the results obtained in the simulation of the VCM unit. The results shown below are from the case study maximum cold value and from an increased value of the hot environment case. In order to obtain valid results, the hot value of the Miami case was increased to 313.15 K due to constants results obtained from its low heat gain into the cabin.

The VCM includes an evaporator, a condenser, a compressor, and an expansion valve. The analysis of the evaporator and the condenser are based on exchanger calculations. Table 5-5 shows the temperature and pressure variation through the closed cycle.

**Table 5-5 VCM components inlet values: (a) cooling condition; (b) heating condition.**

| | Inlet Temperature (K) | | Inlet Pressure (Pa) | | Inlet mass flow rate kg/s | |
|---|---|---|---|---|---|---|
| | Refrigerant | Air | Refrigerant | Air | Refrigerant | Air |
| Evaporator | 268.15 | 332.9 | $2.447x10^{04}$ | $2.757x10^{05}$ | 0.303 | 0.039 |
| Compressor | 268.15 | N/A | $2.447x10^{04}$ | N/A | 0.303 | 0.039 |
| Condenser | 309.3 | 313.2 | $5.171x10^{04}$ | $9.603x10^{04}$ | 0.303 | 0.039 |
| Expansion valve | 309.3 | N/A | $5.171x10^{04}$ | N/A | 0.303 | 0.039 |

(a)

| | Inlet Temperature (K) | | Inlet Pressure (Pa) | | Inlet mass flow rate kg/s | |
|---|---|---|---|---|---|---|
| | Refrigerant | Air | Refrigerant | Air | Refrigerant | Air |
| Evaporator | 268.15 | 261.4 | $2.447x10^{04}$ | $2.757x10^{05}$ | 0.303 | 0.039 |
| Compressor | 268.15 | N/A | $2.447x10^{04}$ | N/A | 0.303 | 0.039 |
| Condenser | 309.3 | 275.2 | $5.171x10^{04}$ | $9.603x10^{04}$ | 0.303 | 0.039 |
| Expansion valve | 309.3 | N/A | $5.171x10^{04}$ | N/A | 0.303 | 0.039 |

(b)

VCM cycle temperature and pressure are constant within the evaporator and the condenser. The initial temperature of the refrigerant in the cycle (inlet temperature in the evaporator), was selected with the Pressure-enthalpy diagram of the R11, see Appendix A. At this pressure, the saturation temperature of the refrigerant is of 268.15 K.

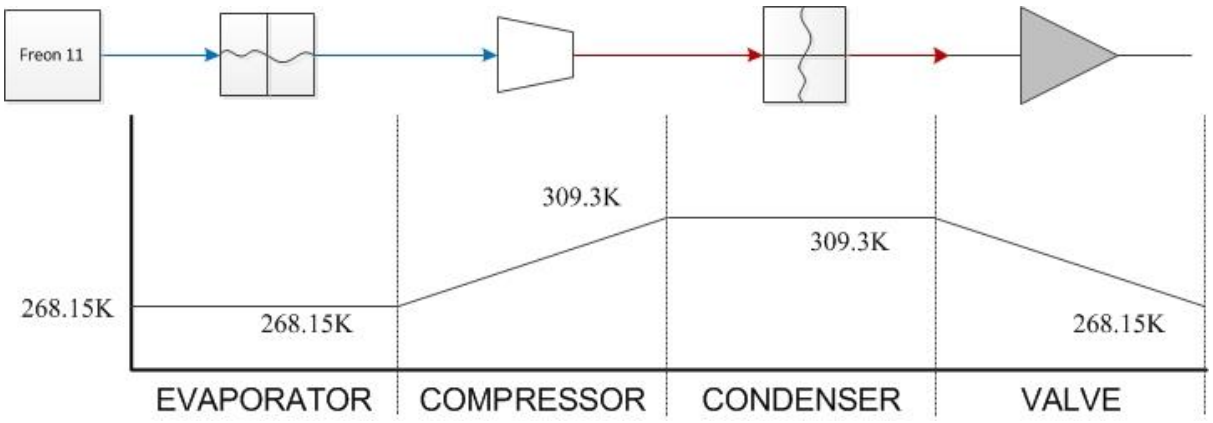


**Figure 5-7 Closed cycle VCM temperature variation**

The temperature behaviour of the VCM unit was compared with a reversed Carnot cycle. The variables presented in both cases represent changes of temperature in the close cycle of the VCM components. These changes have the same trend as the one presented by a reversed Carnot cycle, thus the behaviour of the components are according to what is expected to be in a VCM.

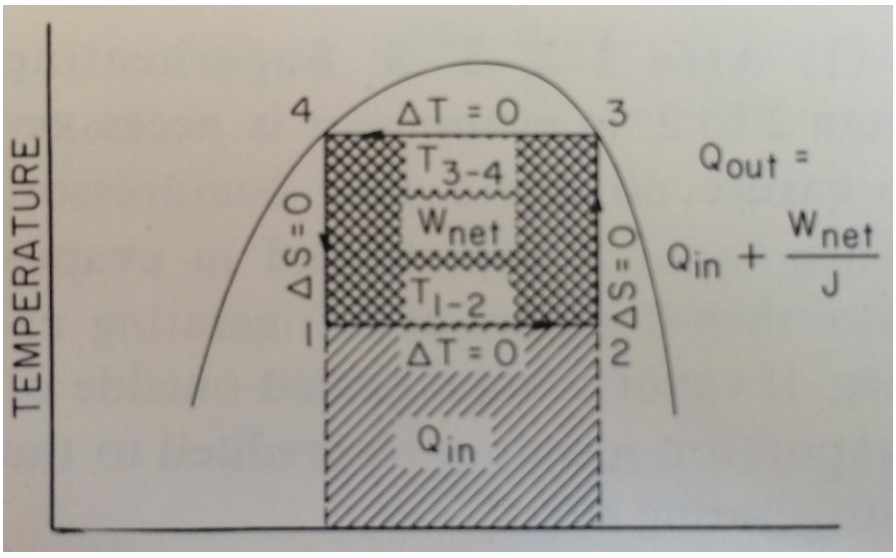


**Figure 5-8 Ideal refrigeration cycle [23]**

Recirculated cabin air temperature pass through the evaporator and it is levelled to 267.4K, then is distributed in the cabin. Figure 5-9 shows the evaporator temperature variation for both cooling and heating conditions in the cabin; also, condenser rams air temperature variation.

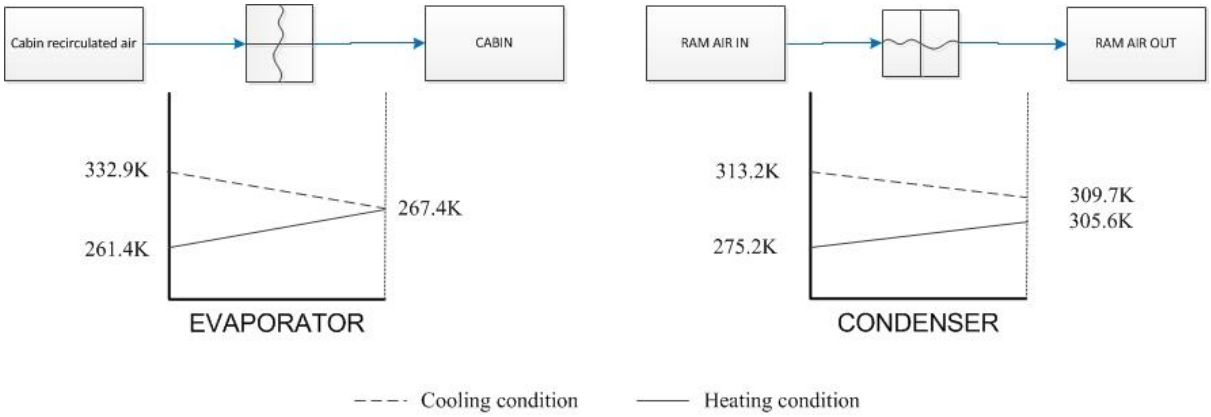


**Figure 5-9 Cabin conditioned air temperature**

### 5.1.5. Pneumatic power and COP

This study considers variations in temperature inside the cabin. From these temperatures, it is possible to make an estimate of the variables used in each of the unit's models. This section contemplated the results of the proposed missions. As in section 5.1.4, the case study in Florida was increased to 313.15 K in order to avoid constant values. Table 5-6 shows the results obtained from this study at both the cabin heating and cooling units.

**Table 5-6 ECS simulation results**

| Parameter | Result heating | Result cooling |
|---|---|---|
| Cabin inlet temperature (K) | 332.9 | 238.9 |
| Cabin outlet temperature (K) | 261.1 | 355.4 |
| Cabin required mass flow rate (kg/s) | 0.039 | 0.051 |
| ACM required mass flow rate (kg/s) | 0.043 | 0.056 |
| VCM required mass flow rate (kg/s) | 0.0 | 0.0 |
| CH required mass flow rate (kg/s) | 0.031 | N/A |
| EGH required mass flow rate (kg/s) | 0.033 | N/A |
| Bleed air required mass flow rate (kg/s) | 0.035 | N/A |
| ACM-CH configuration mass flow (kg/s) | 0.074 | 0.097 |
| ACM-EGH configuration mass flow (kg/s) | 0.076 | 0.099 |

| Parameter | Result heating | Result cooling |
|---|---|---|
| ACM-Bleed air mass flow (kg/s) | 0.078 | 0.102 |
| VCM-CH configuration mass flow (kg/s) | 0.031 | 0 |
| VCM-EGH configuration mass flow (kg/s) | 0.033 | 0 |
| VCM-Bleed air mass flow (kg/s) | 0.035 | 0 |

These results show that it is necessary to have an inlet temperature of 332.9K (heating) and 238.9K (cooling) to achieve a desire temperature of 297.15K inside the helicopter cabin. The minimum ventilation in the cabin is set to 0.39 kg/s (heating) and 0.051 kg/s (cooling), thus the required ventilation values from the ECS configurations should not be below this. As mentioned in previous chapters, it is necessary to have a mixed configuration between units for warming. Therefore, the results of the cooling units (ACM and VCM) were mixed with the results of the heating units (CH, EGH, Bleed air).

As shown in Table 5-6, for heating condition the VCM-CH configuration requires less pneumatic power than the others; however this setting could add extra weight and required the use of an additional combustion chamber, increasing the fuel consumption of the rotorcraft. Similar conditions are presented with the VCM-EGH; this configuration could add unwanted weight in the helicopter. The VCM-Bleed air does not requires of a heavy configuration for its functionality, nonetheless this configuration could present contaminants in the air.

On the other hand, the required mass flow for cooling conditions, shown in Table 5-6, re-affirms that a VCM unit does not required of any additional unit or pneumatic power, thus avoiding the fuel consumption increase. However, as mentioned before this unit only works in warm and hot environments and is weightier than the ACM unit. In both case studies, the ACM has higher pneumatic power consumption in any configuration than the presented by the VCM.

The performance of the input temperature, the output temperature and average temperature in the cabin, are shown in Figure 5-10. The ECS-PCM takes 440 seconds to achieve the required temperature, after this time it remains constant until the ECS is turned off.

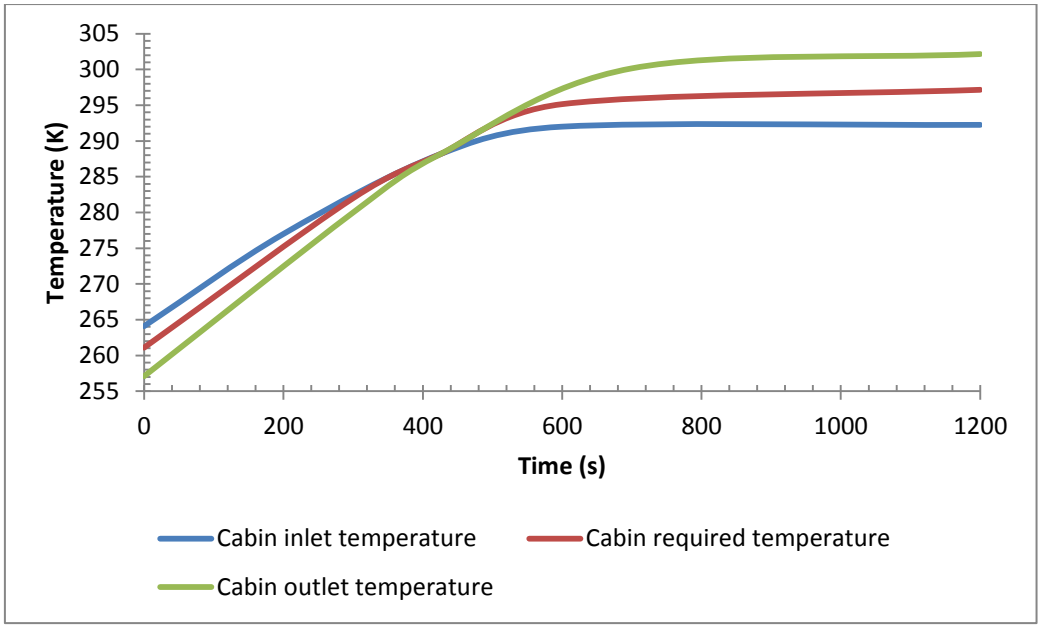


**Figure 5-10 Temperatures variation for a mass flow rate of 0.39 kg/s**

Additionally, the Coefficient of Performance factor is considered in this study in order to compare the efficiency between the analysed unit's configurations. The Coefficient of Performance was computed by using equations 4-192 and 4-193. Results in Table 5-7 shown that the VCM presents a higher coefficient of performance than the ACM, therefore, generates less fuel consumption in the helicopter.

**Table 5-7 Cycles Coefficient of Performance**

| Parameter | Result |
|---|---|
| ACM COP | 0.18 |
| VCM COP | 2.3 |

# 6. Chapter I Conclusion & recommendations for future work

## 6.1. Conclusion

The power consumption is a major problem presented in helicopters with an Environmental Control System configuration. The power consumption leads to increased fuel consumption, restricting the flight time, and making the rotorcraft less efficient. A suitable temperature inside the cabin is essential for the comfort and welfare of crew and passengers, without proper ventilation, occupants may suffer discomfort or even loss of consciousness. The temperature inside the cabin can reach extreme levels, from below freezing point to elevated temperatures at 318.15 K.

According to the European Aviation Safety Agency (EASA), the minimum ventilation required for a light rotorcraft is of 0.005 kg/s per occupant. On the other hand, the Society of Automotive Engineers (SAE) determines that the temperature inside the cabin should be 297.15 K in order to maintain the comfort of the occupants. Considering the above requirements and the research question, a numerical model was developed to estimate the power consumption produced by the ECS under different configurations (VCM, ACM, CH, etc.). Similarly, a numerical model was developed to simulate and assess the conditions in the cockpit and cabin, based on the behaviour of the heat load, ventilation, and temperatures. For this study were not included the entire factors that can affect the metabolic heat load. For instance, the heat transfer of the cloth (for passengers and crew) is not taken into consideration on this model.

The research question was answered, a simulation model was created to numerically predict the power requirements of different cooling and heating ECSs found on different modern aircraft. However, the model is functional under the following specifications: the data specification of the aircraft is introduced into the model manually each time the aircraft is changed, also the aircraft aerodynamic shape have to be similar to the one created for the Bell 206L-4; with a roof, floor, side walls, bulkhead, windscreen (no canopy), and similar front shape (no cone shape), as it is shown in Figure 4-14.

In order to demonstrate the simulation model, two case studies analysis has been carried out at 313.15 K and 275K for a cruise flight condition at 450 m. This study shows that significant

amounts of mass flow are required approximately 0.035 kg /s (cooling) and 0.051 kg /s (Heating), to preserve the temperature in the cabin. The required inlet in the cabin varies between 332.9K (Heating) and 261.1K (Cooling).

The obtained results of the model variables shows, without considering the weights of the units and air quality, that the VCM-CH is the best configuration for the case studies developed in this work. The VCM is the best choice if the ambient conditions for the helicopter are always in hot environments. If the helicopter mission condition is always in a cold environment, the paramount option is again the VCM-CH. The validation process of the model shows that this model is Media-fidelity. However, based on engineering experience developed during this research in this area, its results meet the requirements required in this project.

## 6.2. Recommendations for future work

For future research involving the study of power consumption of the Environmental Control System a deeper study of the following factor is recommended:

The Combustion Heater analysis does not contain a deep study of the internal combustion chamber. A further study would allow an accurate analysis of the conditions (temperature) inside the chamber and thus optimize the results of heat transfer.

This study considered a plate-fin heat exchanger due to its widely used in aviation industry and its high efficiency in heat transfer. However, this author recommends performing an analysis taking into consideration different exchanger configurations for the ECS.

The Electric Heater Element (EEH) is not included in this study. This author recommends the study of the heating unit and thus a more thorough comparison of all units involved.

The distribution in the cabin, humidity and air circulation were not taken into consideration in this research. It is recommended to optimize the cabin model with a detailed study of these factors, and thus increase the fidelity of the model developed.

A calculation of the specific fuel consumption and the weight of the components were not considered in this research. A deeper comparison is recommended for these factors.

# References


[1]. Endres, G., (2006), *helicopter markets and systems*, 15th ed, Jane's Information Group, Coulsdon.

[2]. Airbus, (2005), *Aircraft Characteristics Airport and Maintenance Planning*, 27th ed., Airbus S.A.S., France.

[3]. ASHRAE, (1966), *Thermal comfort conditions*, 55.66th ed., ASHRAE standard, New York.

[4]. Bell Helicopter (2010), Dimensions and Areas, in *Maintenance Manual*, , pp. 6-3-6-4; 6-5.

[5]. Bertolini, E., Eury, S., Hecker, P., Huguet, M. and Sanna-randaccio, F. (2012), *CLEAN SKY 2 Impact Assessment*, Final Report, Clean Sky.

[6]. Boelter, L. M., Elswick, W. R., Sanders, V. D., Rubesin, M. W., (1954), *Prelimirary Investigation of a Combustion-Type Aircraft Heater*, 2428, National Advisory Committee for Aeronautics, Washington.

[7]. Dr.Lawson, C.P., (2012), *AVD Lecture notes-Environmental Control Systems Requirements and Analysis*, Cranfield University.

[8]. Edwards, M. and Edwards, E. (1990), *The Aircraft cabin: managing the human factors*, Gower, Aldershot.

[9]. European Aviation Safety Agency (2012), *Certification Specifications and Acceptable Means of Compliance for Large Aeroplanes*, CS-25, European Aviation Safety Agency.

[10]. European Aviation Safety Agency (2012), *Certification Specifications for Small Rotorcraft*, CS-27, European Aviation Safety Agency.

[11]. Federal Aviation Regulation, (March 6, 2013), *Part 25-Airworthiness Standards: Transport Category Airplanes Subpart D-Design and construction; 25.841-Pressurized cabins* , available at: http://www.ecfr.gov/cgi-bin/text-

idx?c=ecfr&SID=1d5ec5a3a2fcee886a5fb20c2649d9f8&rgn=div8&view=text&node=14:1.0.1.3.11.4.180.71&idno=14 (accessed 2013, March/08).

[12]. Hegbom, T., (1997), *Integrating Electrical Heating Elements in Product Design*, first ed, Marcel Dekker, Inc., New York.

[13]. Incropera, F. P. and DeWitt, D. P. (2002), *Fundamentals of heat and mass transfer*, 5th ed, Wiley, New York.

[14]. ISO, (1989), *Hot environments-Estimation of the heat stress on working man, based on the WBGT-index (wet bulb globe temperature)*, Second ed., International Organization for Standardization, Switzerland.

[15]. Jackson, P. A., Munson, K., Peacock, L. T., Bushell, S. and Willis, D. (2011), *All the Worlds Aircraft*, Jane's Information Group, Coulsdon.

[16]. Kroes, M. J., Watkins, W. A., and Delp, F., (2007), *Aircraft Maintenance & Repair*, sixth ed, McGraw-Hill, Glencoe.

[17]. Lind, A. R., and Leithead, C. S., (1964), *Heat stress and heat disorders*, F.A. Davis, London.

[18]. Moir, I. and Seabridge, A. G. (2008), *Aircraft systems: mechanical, electrical, and avionics subsystems integration*, 3rd ed, Wiley, Chichester, West Sussex, England; Hoboken, NJ.

[19]. Nagda, N. L. (2000), *Air quality and comfort in airliner cabins: [papers presented at the symposium of the same name]*, Astm, West Conshohocken, PA.

[20]. Parsons, K. C. (2003), *Human thermal environments: The effects of hot, moderate and cold environments on human health, comfort and performance*, 2nd ed.

[21]. Rebbechi, B., (1980), *A Review of Aircraft Cabin Conditioning for Operations in Australia*, 159, Department of Defence, Melbourne, Victoria.

[22]. Rivolier, J. (1988), *Man in the Antarctic*, Taylor & Francis, London.

[23]. SAE Aerospace (1992), *Applied Thermodynamics Manual*, Third ed, Society of Automotive Engineers, INC., New York.

[24]. Sonntag, R. E., Borgnakke, C. and Van Wylen, G. J. (2003), *Fundamentals of thermodynamics*, 6th ed, Wiley, New York.

[25]. Vega Diaz, R., Lawson, C. P. and Cranfield University. School of Engineering (2011), *Analysis of an electric environmental control system to reduce the energy consumption of fixed-wing and rotary-wing aircraft [electronic resource]*.

[26]. Wang, S. K., and Lavan, Z., (1999), *Air-Conditioning and Refrigeration*, CRC Press LLC, Boca Raton.

[27]. Clean Sky, (May 19, 2014), Activities, available at: http://www.cleansky.eu/content/homepage/activities, (accessed 2014, May/19).

[28]. ACARE (2012), *WG1 contribution to the strategic research and innovation agenda*, Advisory Council for Aviation Research and Innovation in Europe.

[29]. Linares Bejarano, C., Smith, H. and Cranfield University. School of Engineering (2011), *Environmental impact assessment of the operation of conventional helicopters at misión level*.

[30]. Zhang, T., Yin, S., and Wang, S. (2009), *An under-aisle air distribution system facilitating humidification of commercial aircraft cabins*, Elsevier Ltd., China.

[31]. SAE Aerospace (2008), *Aerospace recommended practice 292 (ARP292): Environmental Control System for Helicopters*, Third ed, Society of Automotive Engineers, INC., New York.

[32]. National Technical Information Service (1974), *Engineering design handbook. Helicopter engineering part two*, Army materiel command, Alexandria, Virginia.

[33]. National Technical Information Service (1974), *Engineering design handbook. Helicopter engineering part one*, Army materiel command, Alexandria, Virginia.

[34]. Rohsenow, W., Hartnett, J., Cho, Y. (1998), *Handbook of heat transfer*, Third ed, McGraw Hill, New York, NY.

[35]. Ebeling, A., (1968), *Fundamentals of aircraft environmental control*, Hayden book Co., Wisconsin, Madison.

[36]. Liu et al. (2012), *State of the art methods for studying air distributions in commercial airliner cabins,* Tianjin University, China.

[37]. Biu, D., Hamdaoui, M., and Vuyst, F., (May 17, 2014), *POD-ISAT: A new and efficient reduced order modelling method for the representation of parameterized finite element solutions. Application to aircraft air control systems*, International journal for numerical methods in engineering, available at: http://www.interscience.wiley.com (accessed 2014, May/26).

[38]. Kok et al. (2006), *Enhancement of aircraft cabin comfort studies by coupling of models for human thermoregulation, internal radiation, and turbulent flows*, European conference on computational fluid dynamics, TU Delft, The Netherlands.

[39]. Tu, Y., Lin, G., and Beijing University (2011), *Dynamic simulation of aircraft environmental control system based on Flowmaster*, Journal of aircraft, Vol 48, No. 6, Beijing, China.

[40]. Kania et al. (2012), *A dynamic modelling toolbox for air vehicle vapour cycle systems,* Society of Automotive Engineers, INC., New York.

[41]. Air Comm Corporation (1988), *Bell 206L series cabin heater system installation instructions*, Report 206H-203M, Boulder municipal airport, Boulder.

[42]. Online flight planning resource, (May 30, 2014), Planning, available at: http://www.iflightplanner.com/ (accessed 2014, May/30)

[43]. Online flight planning resource, (May 30, 2014), Flight planning, available at: http://www.skydemon.aero/ (accessed 2014, May/30)

[44]. ASHRAE handbook (2009), *Fundamentals*, American Society of Heating, Refrigerating and Air-Conditioning Engineers Inc., Atlanta, Georgia.

[45]. Lewis, J., (1993), *Thermal evaluation of the effects of gaps between adjacent roof insulation panels*, Research and development division Owens-Corning fiberglas corporation, Granville, Ohio.

[46]. Bell model 206A/B series (1998), *Maintenance Manual*, Bell helicopter, Fort Worth, Texas.

[47]. Shetty, J., Lawson, C. P. and Cranfield University. School of Engineering (2012), *Cabin heat loads modelling and dynamic simulation of ECS for a single seater fighter aircraft*.

[48]. Sadik K., Hongtan L., (2002), *Heat exchanger selection, rating, and thermal design,* Second ed, CRC press LLC, Boca raton, Florida.

[49]. Shah, R., Sekulic, D., (2003), *Fundamentals of heat exchanger design,* John Wiley & Sons Inc., Lexington, Kentucky.

[50]. Chang, Y., and Wang, C., (1997), *A generalized heat transfer correlation for louver fin geometry*.

[51]. Chang, Y., Hsu, Y., and Wang C., (2000), *A generalized friction correlation for louver fin geometry.*

[52]. Hesselgreaves, J., (2001), *Compact heat exchangers, selection, design and operation*, Elsevier science Ltd., Kidlington, Oxford.

[53]. Conceicao, S., Zaparoli, E., and Leal, W., (2007), *Thermodynamic study of aircraft air conditioning air cycle machines. 3-wheel x 4-wheel,* Society of Automotive Engineers, Technical paper, Sao Paulo, Brazil.

[54]. Lemieux et al. (2013), *Air-cycle environmental control system and methods for automotive applications,* Patent application publication, Pub. No.: US 2013/0180270 A1, United States.

[55]. Ginwala, K., (1961), *Engineering study of vapour cycle cooling equipment for zero-gravity environment,* Command United States Air Force, Wright-Patterson Air Force base, Ohio.

[56]. Rebbechi, B., (1981), *A vapour cycle cabin cooling system for the Sea King MK. 50 helicopter,* Department of Defence, Defence science and technology organisation, Aeronautical research laboratories, Melbourne, Victoria.

[57]. Bolter at al. (1949), *An investigation of aircraft heaters. XXXI summary of laboratory testing of several exhaust-gas and air heat exchangers,* National Advisory Committee for Aeronautics, Technical note No. 1455, Washington.

[58]. Military Specification (1983), *Environmental control system. Aircraft. General requirements for*, Naval air sytems command.

[59]. Military Specification (1997), *Global climatic data for developing military products*, Department of Defense, United States.

# A. Appendix – Thermophysical properties of matter

*Insulating Materials and Systems*

| Description/Composition | Typical Properties at 300 K: Density, $\rho$ (kg/m$^3$) | Thermal Conductivity, $k$ (W/m · K) | Specific Heat, $c_p$ (J/kg · K) |
|---|---|---|---|
| Blanket and Batt | | | |
| Glass fiber, paper faced | 16 | 0.046 | — |
| | 28 | 0.038 | — |
| | 40 | 0.035 | — |
| Glass fiber, coated; duct liner | 32 | 0.038 | 835 |
| Board and Slab | | | |
| Cellular glass | 145 | 0.058 | 1000 |
| Glass fiber, organic bonded | 105 | 0.036 | 795 |
| Polystyrene, expanded | | | |
| Extruded (R-12) | 55 | 0.027 | 1210 |
| Molded beads | 16 | 0.040 | 1210 |
| Mineral fiberboard; roofing material | 265 | 0.049 | — |
| Wood, shredded/cemented | 350 | 0.087 | 1590 |
| Cork | 120 | 0.039 | 1800 |
| Loose Fill | | | |
| Cork, granulated | 160 | 0.045 | — |
| Diatomaceous silica, coarse | 350 | 0.069 | — |
| Powder | 400 | 0.091 | — |
| Diatomaceous silica, fine powder | 200 | 0.052 | — |
| | 275 | 0.061 | — |
| Glass fiber, poured or blown | 16 | 0.043 | 835 |
| Vermiculite, flakes | 80 | 0.068 | 835 |
| | 160 | 0.063 | 1000 |
| Formed/Foamed-in-Place | | | |
| Mineral wool granules with asbestos/inorganic binders, sprayed | 190 | 0.046 | — |
| Polyvinyl acetate cork mastic; sprayed or troweled | — | 0.100 | — |
| Urethane, two-part mixture; rigid foam | 70 | 0.026 | 1045 |
| Reflective | | | |
| Aluminum foil separating fluffy glass mats; 10–12 layers, evacuated; for cryogenic applications (150 K) | 40 | 0.00016 | — |
| Aluminum foil and glass paper laminate; 75–150 layers; evacuated; for cryogenic application (150 K) | 120 | 0.000017 | — |
| Typical silica powder, evacuated | 160 | 0.0017 | — |

**Figure A-1 Properties of insulating materials [13]**

| Description/ Composition | Maximum Service Temperature (K) | Typical Density ($kg/m^3$) | Typical Thermal Conductivity, $k$ (W/m · K), at Various Temperatures (K) | | | | | | | | | | | | | |
|---|---|---|---|---|---|---|---|---|---|---|---|---|---|---|---|---|
| | | | 200 | 215 | 230 | 240 | 255 | 270 | 285 | 300 | 310 | 365 | 420 | 530 | 645 | 750 |
| Blankets | | | | | | | | | | | | | | | | |
| Blanket, mineral fiber, | 920 | 96–192 | | | | | | | | | 0.038 | 0.046 | 0.056 | 0.078 | | |
| metal reinforced | 815 | 40–96 | | | | | | | | | 0.035 | 0.045 | 0.058 | 0.088 | | |
| Blanket, mineral fiber, glass; fine fiber, | 450 | 10 | | | | 0.036 | 0.038 | 0.040 | 0.043 | 0.048 | 0.052 | 0.076 | | | | |
| organic bonded | | 12 | | | | 0.035 | 0.036 | 0.039 | 0.042 | 0.046 | 0.049 | 0.069 | | | | |
| | | 16 | | | | 0.033 | 0.035 | 0.036 | 0.039 | 0.042 | 0.046 | 0.062 | | | | |
| | | 24 | | | | 0.030 | 0.032 | 0.033 | 0.036 | 0.039 | 0.040 | 0.053 | | | | |
| | | 32 | | | | 0.029 | 0.030 | 0.032 | 0.033 | 0.036 | 0.038 | 0.048 | | | | |
| | | 48 | | | | 0.027 | 0.029 | 0.030 | 0.032 | 0.033 | 0.035 | 0.045 | | | | |
| Blanket, alumina–silica fiber | 1530 | 48 | | | | | | | | | | | | 0.071 | 0.105 | 0.150 |
| | | 64 | | | | | | | | | | | | 0.059 | 0.087 | 0.125 |
| | | 96 | | | | | | | | | | | | 0.052 | 0.076 | 0.100 |
| | | 128 | | | | | | | | | | | | 0.049 | 0.068 | 0.091 |
| Felt, semirigid; | 480 | 50–125 | | | | | | 0.035 | 0.036 | 0.038 | 0.039 | 0.051 | 0.063 | | | |
| organic bonded | 730 | 50 | 0.023 | 0.025 | 0.026 | 0.027 | 0.029 | 0.030 | 0.032 | 0.033 | 0.035 | 0.051 | 0.079 | | | |
| Felt, laminated; no binder | 920 | 120 | | | | | | | | | | | 0.051 | 0.065 | 0.087 | |
| Blocks, Boards, and Pipe Insulations | | | | | | | | | | | | | | | | |
| Asbestos paper, laminated and corrugated | | | | | | | | | | | | | | | | |
| 4-ply | 420 | 190 | | | | | | | | 0.078 | 0.082 | 0.098 | | | | |
| 6-ply | 420 | 255 | | | | | | | | 0.071 | 0.074 | 0.085 | | | | |
| 8-ply | 420 | 300 | | | | | | | | 0.068 | 0.071 | 0.082 | | | | |
| Magnesia, 85% | 590 | 185 | | | | | | | | | 0.051 | 0.055 | 0.061 | | | |
| Calcium silicate | 920 | 190 | | | | | | | | | 0.055 | 0.059 | 0.063 | 0.075 | 0.089 | 0.104 |

**Figure A-2 Continued [13]**

*Other Materials*

| Description/ Composition | Temperature (K) | Density, $\rho$ (kg/m$^3$) | Thermal Conductivity, $k$ (W/m · K) | Specific Heat, $c_p$ (J/kg · K) |
|---|---|---|---|---|
| Asphalt | 300 | 2115 | 0.062 | 920 |
| Bakelite | 300 | 1300 | 1.4 | 1465 |
| Brick, refractory | | | | |
| Carborundum | 872 | — | 18.5 | — |
| | 1672 | — | 11.0 | — |
| Chrome brick | 473 | 3010 | 2.3 | 835 |
| | 823 | | 2.5 | |
| | 1173 | | 2.0 | |
| Diatomaceous | 478 | — | 0.25 | — |
| silica, fired | 1145 | — | 0.30 | |
| Fireclay, burnt 1600 K | 773 | 2050 | 1.0 | 960 |
| | 1073 | — | 1.1 | |
| | 1373 | — | 1.1 | |
| Fireclay, burnt 1725 K | 773 | 2325 | 1.3 | 960 |
| | 1073 | | 1.4 | |
| | 1373 | | 1.4 | |
| Fireclay brick | 478 | 2645 | 1.0 | 960 |
| | 922 | | 1.5 | |
| | 1478 | | 1.8 | |
| Magnesite | 478 | — | 3.8 | 1130 |
| | 922 | — | 2.8 | |
| | 1478 | | 1.9 | |
| Clay | 300 | 1460 | 1.3 | 880 |
| Coal, anthracite | 300 | 1350 | 0.26 | 1260 |
| Concrete (stone mix) | 300 | 2300 | 1.4 | 880 |
| Cotton | 300 | 80 | 0.06 | 1300 |
| Foodstuffs | | | | |
| Banana (75.7% water content) | 300 | 980 | 0.481 | 3350 |
| Apple, red (75% water content) | 300 | 840 | 0.513 | 3600 |
| Cake, batter | 300 | 720 | 0.223 | — |
| Cake, fully baked | 300 | 280 | 0.121 | — |
| Chicken meat, white | 198 | — | 1.60 | — |
| (74.4% water content) | 233 | — | 1.49 | |
| | 253 | | 1.35 | |
| | 263 | | 1.20 | |
| | 273 | | 0.476 | |
| | 283 | | 0.480 | |
| | 293 | | 0.489 | |
| Glass | | | | |
| Plate (soda lime) | 300 | 2500 | 1.4 | 750 |
| Pyrex | 300 | 2225 | 1.4 | 835 |

**Figure A-3 Continued [13]**

| $T$ (K) | $\rho$ (kg/m$^3$) | $c_p$ (kJ/kg · K) | $\mu \cdot 10^7$ (N · s/m$^2$) | $\nu \cdot 10^6$ (m$^2$/s) | $k \cdot 10^3$ (W/m · K) | $\alpha \cdot 10^6$ (m$^2$/s) | $Pr$ |
|---|---|---|---|---|---|---|---|
| **Air** | | | | | | | |
| 100 | 3.5562 | 1.032 | 71.1 | 2.00 | 9.34 | 2.54 | 0.786 |
| 150 | 2.3364 | 1.012 | 103.4 | 4.426 | 13.8 | 5.84 | 0.758 |
| 200 | 1.7458 | 1.007 | 132.5 | 7.590 | 18.1 | 10.3 | 0.737 |
| 250 | 1.3947 | 1.006 | 159.6 | 11.44 | 22.3 | 15.9 | 0.720 |
| 300 | 1.1614 | 1.007 | 184.6 | 15.89 | 26.3 | 22.5 | 0.707 |
| 350 | 0.9950 | 1.009 | 208.2 | 20.92 | 30.0 | 29.9 | 0.700 |
| 400 | 0.8711 | 1.014 | 230.1 | 26.41 | 33.8 | 38.3 | 0.690 |
| 450 | 0.7740 | 1.021 | 250.7 | 32.39 | 37.3 | 47.2 | 0.686 |
| 500 | 0.6964 | 1.030 | 270.1 | 38.79 | 40.7 | 56.7 | 0.684 |
| 550 | 0.6329 | 1.040 | 288.4 | 45.57 | 43.9 | 66.7 | 0.683 |
| 600 | 0.5804 | 1.051 | 305.8 | 52.69 | 46.9 | 76.9 | 0.685 |
| 650 | 0.5356 | 1.063 | 322.5 | 60.21 | 49.7 | 87.3 | 0.690 |
| 700 | 0.4975 | 1.075 | 338.8 | 68.10 | 52.4 | 98.0 | 0.695 |
| 750 | 0.4643 | 1.087 | 354.6 | 76.37 | 54.9 | 109 | 0.702 |
| 800 | 0.4354 | 1.099 | 369.8 | 84.93 | 57.3 | 120 | 0.709 |
| 850 | 0.4097 | 1.110 | 384.3 | 93.80 | 59.6 | 131 | 0.716 |
| 900 | 0.3868 | 1.121 | 398.1 | 102.9 | 62.0 | 143 | 0.720 |
| 950 | 0.3666 | 1.131 | 411.3 | 112.2 | 64.3 | 155 | 0.723 |
| 1000 | 0.3482 | 1.141 | 424.4 | 121.9 | 66.7 | 168 | 0.726 |
| 1100 | 0.3166 | 1.159 | 449.0 | 141.8 | 71.5 | 195 | 0.728 |
| 1200 | 0.2902 | 1.175 | 473.0 | 162.9 | 76.3 | 224 | 0.728 |
| 1300 | 0.2679 | 1.189 | 496.0 | 185.1 | 82 | 238 | 0.719 |
| 1400 | 0.2488 | 1.207 | 530 | 213 | 91 | 303 | 0.703 |
| 1500 | 0.2322 | 1.230 | 557 | 240 | 100 | 350 | 0.685 |
| 1600 | 0.2177 | 1.248 | 584 | 268 | 106 | 390 | 0.688 |
| 1700 | 0.2049 | 1.267 | 611 | 298 | 113 | 435 | 0.685 |
| 1800 | 0.1935 | 1.286 | 637 | 329 | 120 | 482 | 0.683 |
| 1900 | 0.1833 | 1.307 | 663 | 362 | 128 | 534 | 0.677 |
| 2000 | 0.1741 | 1.337 | 689 | 396 | 137 | 589 | 0.672 |
| 2100 | 0.1658 | 1.372 | 715 | 431 | 147 | 646 | 0.667 |
| 2200 | 0.1582 | 1.417 | 740 | 468 | 160 | 714 | 0.655 |
| 2300 | 0.1513 | 1.478 | 766 | 506 | 175 | 783 | 0.647 |
| 2400 | 0.1448 | 1.558 | 792 | 547 | 196 | 869 | 0.630 |
| 2500 | 0.1389 | 1.665 | 818 | 589 | 222 | 960 | 0.613 |
| 3000 | 0.1135 | 2.726 | 955 | 841 | 486 | 1570 | 0.536 |

**Figure A-4 Properties of air [13]**

| Description/Composition | $\alpha_S$ | $\varepsilon^b$ | $\alpha_S/\varepsilon$ | $\tau_S$ |
|---|---|---|---|---|
| Aluminum | | | | |
| Polished | 0.09 | 0.03 | 3.0 | |
| Anodized | 0.14 | 0.84 | 0.17 | |
| Quartz overcoated | 0.11 | 0.37 | 0.30 | |
| Foil | 0.15 | 0.05 | 3.0 | |
| Brick, red (Purdue) | 0.63 | 0.93 | 0.68 | |
| Concrete | 0.60 | 0.88 | 0.68 | |
| Galvanized sheet metal | | | | |
| Clean, new | 0.65 | 0.13 | 5.0 | |
| Oxidized, weathered | 0.80 | 0.28 | 2.9 | |
| Glass, 3.2-mm thickness | | | | |
| Float or tempered | | | | 0.79 |
| Low iron oxide type | | | | 0.88 |
| Metal, plated | | | | |
| Black sulfide | 0.92 | 0.10 | 9.2 | |
| Black cobalt oxide | 0.93 | 0.30 | 3.1 | |
| Black nickel oxide | 0.92 | 0.08 | 11 | |
| Black chrome | 0.87 | 0.09 | 9.7 | |
| Mylar, 0.13-mm thickness | | | | 0.87 |
| Paints | | | | |
| Black (Parsons) | 0.98 | 0.98 | 1.0 | |
| White, acrylic | 0.26 | 0.90 | 0.29 | |
| White, zinc oxide | 0.16 | 0.93 | 0.17 | |
| Plexiglas, 3.2-mm thickness | | | | 0.90 |
| Snow | | | | |
| Fine particles, fresh | 0.13 | 0.82 | 0.16 | |
| Ice granules | 0.33 | 0.89 | 0.37 | |
| Tedlar, 0.10-mm thickness | | | | 0.92 |
| Teflon, 0.13-mm thickness | | | | 0.92 |

**Figure A-5 Solar radiative properties [13]**

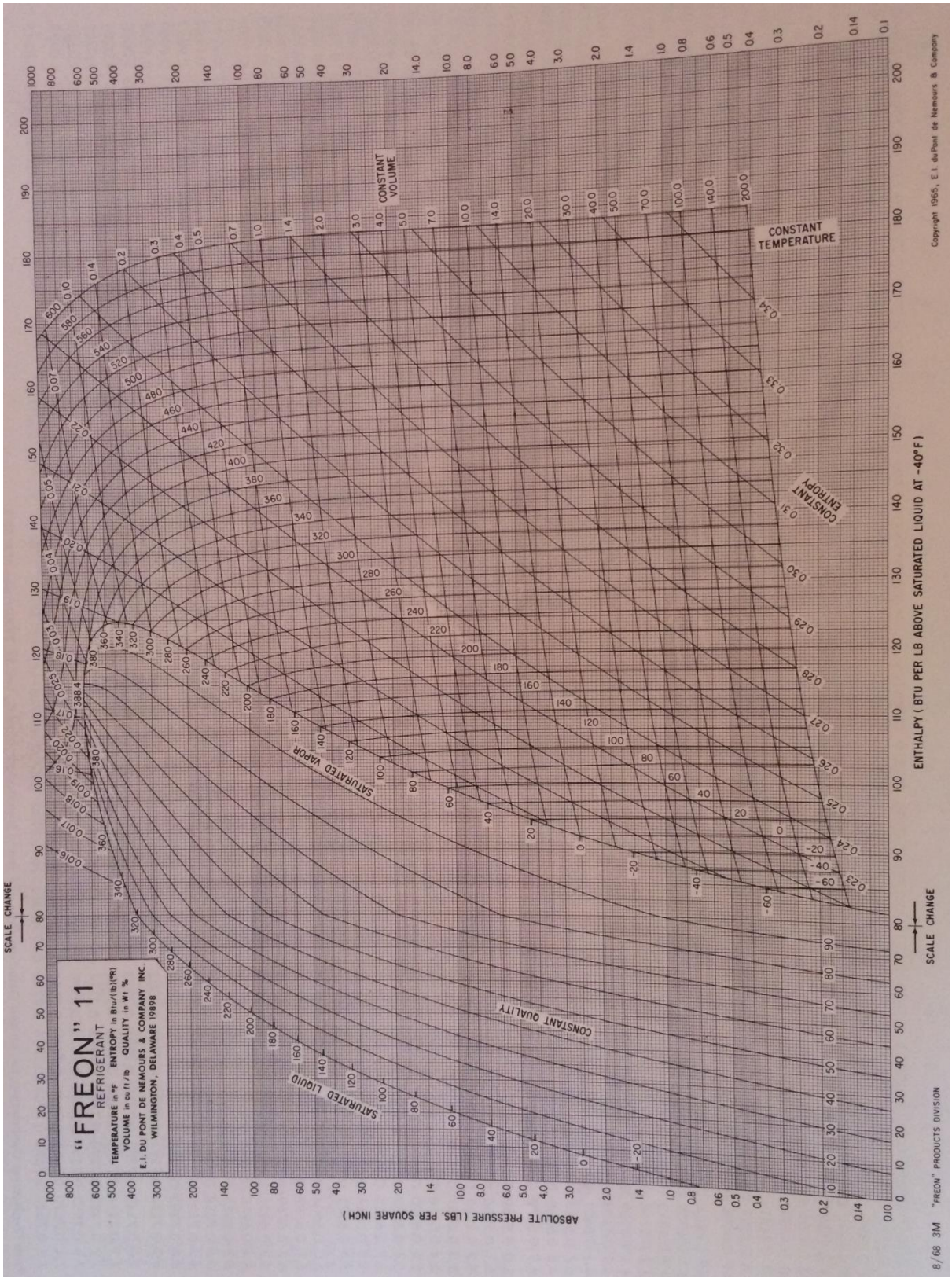


**Figure A-6 Pressure-enthalpy diagram [23]**

# B. Appendix – Cabin heat load calculation

The mathematical analysis of heat loads in the cabin begins by considering the geometry of the Bell 206L-4 (Figure 4-10). These geometries were calculated from a 3D model designed in CATIA; see Figure B-1, B-2. The helicopter dimensions used in the ECS-PCM model were taken from the maintenance manuals of the Bell206L-4. The resulting areas are shown in Table 4-3. This chapter shows the necessary calculations to understand the dynamics of the equations; including the flight path analysis conducted in UK. The flight path calculations corresponding to Miami-Florida were performed using the same design process performed in this chapter. Flight path data used in this study are shown in Table 4.2.

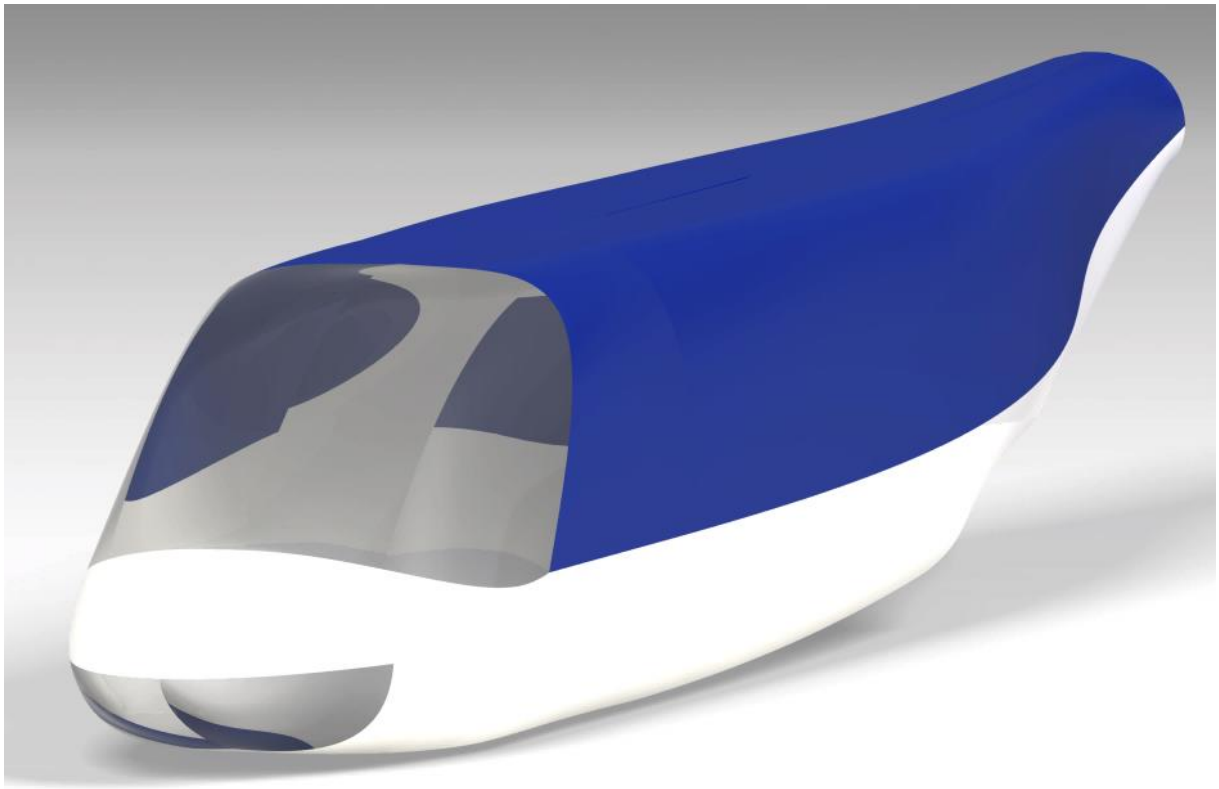

**Figure B-1 Bell206L-4 3D design areas**

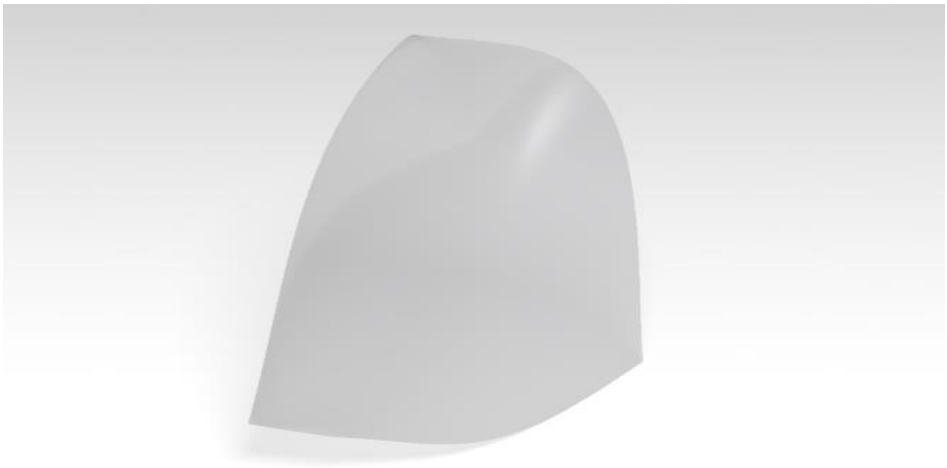

**Figure B-2 Bell206L-4 windshield design**

This study begins by setting the ambient temperature in flight with its corresponding ISA deviation. This temperature was obtained by means of a predetermined block on Matlab-Simulink ® (Atmospheric block). The ground temperature at London City Airport, at an Elevation of 24 m is of 278.15 K. In flight, the temperature varies to 277.15 at an altitude of 450 m above sea level. The necessary helicopter heat load can be calculated once these temperatures are established. The following calculations use equations specified in Section 4.2.

$$h_e = 5.678263\big(2.0 + 0.314(6.7m/s)\big) = 50.58\, W/m^2$$

$$h_i = 5.678263\big(2.0 + 0.314(1.005m/s)\big) = 17.24\, W/m^2$$

Thus the heat load of the transparency area is

$$U_1 = \frac{1}{\frac{1}{50.58W/m^2} + \frac{1}{11.6W/m^2} + \frac{1}{17.24W/m^2}} = 6\, W/m^2$$

$$q_{1a} = 6W/m^2 * 2.54m^2(297.15K - 275.2K) \; = 339.6W\; (Cockpit)$$

$$q_{1b} = 6W/m^2 * 1.08m^2(297.15K - 275.2K) \; = 144.4W\; (Cabin)$$

The wall (un-insulated) heat load is given by:

$$U_{2a} = \frac{1}{\frac{1}{50.58W/m^2} + 8.824x10^{-06}W/m^2 + \frac{1}{17.24W/m^2}} = 12.86W/m^2$$

$$q_{2a} = 12.86W/m^2 * 1.24m^2(297.15K - 275.2K) \ = 349.5W \ (Cockpit)$$

For the cabin wall (insulated) heat load, is necessary to calculate the air space coefficient between the outer and inner skin. Iteration must be performed; assumed values have to be compared with the resulting values of the computation. The iteration process is as follows:

$$h'_a + h'_r = 3.14W/m^2 \ (Assumed \ value)$$

$$U'_{2b} = \frac{1}{\frac{1}{50.58W/m^2} + 8.824x10^{-06}W/m^2 + 0.41W/m^2 + \frac{1}{3.14W/m^2} + \frac{1}{17.24W/m^2}}$$

$$U'_{2b} = 1.23W/m^2$$

$$U_{k1} = \frac{1}{\frac{1}{50.58W/m^2} + 8.824x10^{-06}W/m^2 + 0.41W/m^2} = 2.291W/m^2$$

$$U_{k2} = \frac{1}{\frac{1}{17.24W/m^2}} = 17.24W/m^2$$

Now

$$T_{1i} = \ 275.2K + \frac{3.14W/m^2}{2.291W/m^2}(297.15K - 275.2K) = 287K$$

$$T_{2w} = \ 297.15K - \frac{3.14W/m^2}{17.24W/m^2}(297.15K - 275.2K) = 295.6K$$

$$\Delta T_a = 295.6K - 287K = 8.58K$$

$$T_{av} = \frac{295.6K + 287K}{2} = 291.3K$$

$$N_g = \frac{0.177^3 m(1.173kg/m^3 * 9.8m/s^2)^2 \left(\frac{1}{291.3K}\right) 8.58K}{(3.102x10^{-10})^2} = 6.98x10^{07}$$

The air space coefficient for a vertical wall with $2.1x10^5 \leq N_g \leq 1.1x10^9$ is defined as:

$$\frac{h_a X_a}{k_a} = \left[\frac{0.071}{\left(\frac{1.19m}{0.177m}\right)^{\frac{1}{9}}}(6.98x10^{07} * 0.72)^{0.333}\right] = 22.08$$

$$h_a = \frac{22.08(0.025W/m)}{0.177m} = 3.11W/m^2$$

The radiation heat load coefficient $h_r$ is obtained from Figure 4-12, then:

$$h_r = 0.021$$

Thus

$$h_a + h_r = 3.14W/m^2 = h'_a + h'_r$$

The cabin wall heat load coefficient is computed once the iteration is complete and the result is equal to the assumed value.

$$U_{2b} = U'_{2b} = 1.23W/m^2$$

The increase of thermal transmittance $t_i$ is taken from Figure 4-11 for a gap width of 0.0045m. The following calculations are used to find the heat transfer from the cabin insulated walls.

$$C = -0.358 \ln(4.27m) + 1.0122 = 0.49$$

$$t = 1.23W/m^2\left(\frac{1.87 * 0.49}{100}\right) = 0.011$$

Thus

$$q_{2b} = 4.27m(1.23W/m^2 + 0.011)(297.15K - 275.2K) = 116.2W\ (Cabin)$$

The floor heat load transfer includes the computation of heat through both the beams and the cabin liner (vertical insulated wall). Each factor is analysed separately and then its results are added. Cabin and cockpit cabin liner are calculated by using the same equations used for an insulated wall. However, the conduction and convection heat load $h_a$ in the floor uses a horizontal wall analysis. Therefore, bearing in mind the properties of the floor (material and areas) and using its results for an insulated wall, the heat load $h_a$ is given as:

$$h'_a + h'_r = 3.76W/m^2\ (Assumed\ value)$$

And

$$N_g = 6.22x10^{07}$$

The air space coefficient for a horizontal wall with $3.2x10^5 \leq N_g \leq 10^9$ is defined as

$$\frac{h_a k_a}{x_a} = [0.075(6.22x10^{07} * 0.72)^{0.333}] = 26.48$$

$$h_a = 3.74$$

$$h_r = 0.021$$

Thus

$$h_a + h_r = 3.76W/m^2 = h'_a + h'_r$$

The helicopter heat load coefficient of the cabin liner is computed as:

$$U_3 = \frac{1}{\frac{1}{50.58W/m^2} + 0.41W/m^2 + \frac{1}{3.76W/m^2} + \frac{1}{17.24W/m^2}} = 1.31W/m^2$$

The heat transfer results from insulated walls for a cockpit floor area of 0.65m and a cabin floor area of 1.93m are:

$$t_{3a} = 0.028\ (Cockpit)$$

$$t_{3b} = 0.019\ (Cabin)$$

Thus, the heat loads for these areas are given as:

$$q_{3c} = 0.65m(1.31W/m^2 + 0.028)(297.15K - 275.2K) = 19.15W\ (Cockpit)$$

$$q_{3d} = 1.93m(1.31W/m^2 + 0.019)(297.15K - 275.2K) = 56.47W\ (Cabin)$$

As mentioned above, the heat load through the beams are considered in this analysis and added to the results of the cabin liner. Beams areas and temperatures are given in Table 4-4; the beam side temperature has been assumed $T'_{as}$=294.4K and iterated through the model until the result is equal or close enough to the assumed value $T'_{as}=T_{as}$. The heat load produced by the beam is computed as follows:

$$U_T = \frac{1}{17.24W/m^2} = 0.058W/m^2$$

$$U_B = \frac{1}{50.58W/m^2} + 8.824x10^{-06}W/m^2 + 0.41W/m^2 = 0.43W/m^2$$

The air velocity through floor beams $V_b$ is taken as zero, considering that the beams are isolated and without any contact with the outside environment.

$$U_S = h_S = 5.678263(2.0 + 0.314(0m/s)) = 11.35W/m^2$$

Table B-1 shows the beams values for temperatures and heat transfer coefficient. The unit heat load and the weighted average temperature needed for the floor heat transfer equation are computed as:

**Table B-1 Beam values**

| | Area ($m^2$) | U ($W/m^2$) | Temperature (K) | UAT (W.K) | UA (W) | AT ($m^2$.K) |
|---|---|---|---|---|---|---|
| Beam top | 0.00072 | 0.058 | 297.15 | 0.012 | 0.00041 | 0.21 |
| Beam bottom | 0.00072 | 0.43 | 275.2 | 0.086 | 0.0003 | 0.19 |
| Beam sides | 0.031 | 11.35 | 294.4 | 103.6 | 0.35 | 9.12 |
| Total | | | | 103.7 | 0.35 | 9.53 |

Using Table B-1

$$u = \frac{0.012\text{W.K} + 0.085\text{W.K} + 103.6\text{W.K}}{0.21\text{m}^2\text{.K} + 0.19\text{m}^2\text{.K} + 9.12\text{m}^2\text{.K}} = 10.87 W/m^2$$

And

$$T_{wa} = \frac{0.012\text{W.K} + 0.085\text{W.K} + 103.6\text{W.K}}{0.00041W + 0.0003W + 0.35W} = 294.3K$$

The beam effectiveness is given by the following equation:

$$m_b = \sqrt{\frac{10.87 W/m^2 (1.18m)}{17.3 W/m (0.0002 m^2)}} = 60.89m$$

$$\eta_b = \frac{\tanh(60.89m * 0.53m)}{60.89m(0.53m)} = 0.03$$

Thus

$$q_b = 1.18m * 10.87 W/m^2 * 0.53m * 0.03(294.3K - 275.2K) = 4.06W$$

$$q_{as} = 4.06W \left(\frac{103.6W.K}{0.012\text{W.K} + 0.085\text{W.K} + 103.6\text{W.K}}\right) = 0.99W$$

The assumed temperature of the beam sides $T'_{as}$ is compare with the next result.

$$U_f = \frac{1}{\frac{1}{17.24 W/m^2} + \frac{1}{11.35 W/m^2}} = 6.84 W/m^2$$

$$T_{as} = 297.15K - \frac{0.99W}{6.84W/m^2(0.21m^2)} = 294.4K = T'_{as}$$

The beams air space heat load can be taken once the iteration is finished and the beam side temperature is acquired. The beams heat load can be computed for a cockpit with 5 beams in the floor, and a cabin with 9 beams as follows:

$$q_{3e} = [5(0.99W)] = 20.11W(Cockpit)$$

$$q_{3f} = [9(0.99W)] = 36.2W(Cabin)$$

The total heat load in the floor is:

$$q_{3a} = 19.15W + 20.11W = 39.26W\ (Cockpit)$$

$$q_{3b} = 56.47W + 36.2W = 92.67W\ (Cabin)$$

As mentioned in Section 4.2.4, the ceiling heat transfer depends on the heat transmitted by the engine to the ceiling wall. On the other hand, the ceiling wall (insulated) is calculated using the same method used for the horizontal insulated wall. Therefore, the computation is as follows:

$$T_{ec} = 275.2K + 30 = 305.2K$$

$$h_a + h_r = 3.76W/m^2 = h'_a + h'_r$$

The ceiling heat load coefficient is computed as:

$$U_5 = \frac{1}{\frac{1}{50.58W/m^2} + 8.824x10^{-06}W/m^2 + 0.41W/m^2 + \frac{1}{3.76W/m^2} + \frac{1}{17.24W/m^2}}$$

$$U_5 = 1.31W/m^2$$

The heat transfer results from insulated walls for a ceiling area of 2.48m is:

$$t_5 = 0.016$$

Thus, the heat load for this area is given as:

$$q_5 = 2.48m(1.31W/m^2 + 0.016) * (297.15K - 305.2K) = -26.68W$$

This negative result shown that the cabin is not losing heat; is gaining heat from the ceiling.

The same procedure of the ceiling is performed for the bulkhead (vertical insulated wall) heat load calculation. The heat transfer in the bulkhead wall depends on the heat transmitted by the helicopter mechanisms.

$$T_{ec} = 275.2K + 5 = 280.2K$$

$$h_a + h_r = 3.14W/m^2 = h'_a + h'_r$$

The ceiling heat load coefficient is computed as:

$$U_6 = \frac{1}{\frac{1}{50.58W/m^2} + 8.824x10^{-06}W/m^2 + 0.41W/m^2 + \frac{1}{3.14W/m^2} + \frac{1}{17.24W/m^2}}$$

$$U_6 = 1.23W/m^2$$

The heat transfer results from insulated walls for a bulkhead area of 1.39m is:

$$t_6 = 0.020$$

Thus, the heat load for this area is given as:

$$q_6 = 1.39m(1.23W/m^2 + 0.020) * (297.15K - 280.2K) = 29.42W$$

The heat loss resulting from infiltration is computed using the equation and data provided in Section 4.2.5 as follow:

$$Q_{ia} = 1005J/kg * 0.005 \text{ kg/s}(297.15K - 275.2K) = 110.2\text{W (Cockpit)}$$

$$Q_{ib} = 1005J/kg(0.01\ \text{kg/s}) = 220.3\text{W (Cabin)}$$

$$Q_{ib} = 110.2\text{W} + 220.3\text{W} = 330.5\ \text{(Cabin)}$$

The heat loads generated by the human body and by electrical units are computed with the data and equations given in Section 4.2.7 as follows:

$$q_7 = 400W * 2 = 800W\ (Crew\ members)$$

$$q_8 = 200W * 5 = 1000W\ (Passengers)$$

$$Q_o = 800W + 1000W = 1800W$$

$$Q_e = 1000(0.225 * 0.9) = 202.5W$$

The total heat load in the Bell 206L-4 helicopter is:

$$Q_1 = 339.6W + 349.5W + 39.26W = 728.4W$$

$$Q_2 = 144.4W + 116.2W + 92.67 + (-26.68) + 29.42 = 356W$$

$$Q_c = 728.4W + 356W = 1084.4W$$

$$Q = 1084W + 330.5W + 1800W + 202.5 = 3417W$$

The cabin required ventilation is given as:

$$\dot{m}_1 = 0.005\text{kg/s}(2) = \ 0.01kg/s\ (For\ cockpit)$$

$$\dot{m}_2 = 0.005\text{kg/s}(5) = \ 0.025kg/s\ (For\ cockpit)$$

$$\Delta T_2 = 355.37\text{K} - 297.15K = 58.22K$$

$$\Delta T_3 = \frac{728.4W + 110.2\text{W}}{1005J/kg(0.01kg/s)} = 83.44K(For\ cockpit)$$

$$\Delta T_4 = \frac{356W + 220.3W}{1005J/kg(0.025kg/s)} = 22.94K(For\ cabin)$$

As $\Delta T_3 > \Delta T_2$ and $\Delta T_4 \leq \Delta T_2$, therefore

$$\dot{m}_1 = \frac{728.4W + 110.2\text{W}}{1005J/kg(58.22K)} = 0.014kg/s\ (for\ \Delta T_3 > \Delta T_2)$$

$$\dot{m}_2 = 0.005\text{kg/s}(5) = 0.025kg/s\ (for\ \Delta T_4 \leq \Delta T_2)$$

$$\dot{m}_t = 0.014kg/s + 0.025kg/s = 0.039\ kg/s$$

# C. Appendix – Matlab/Simulink model

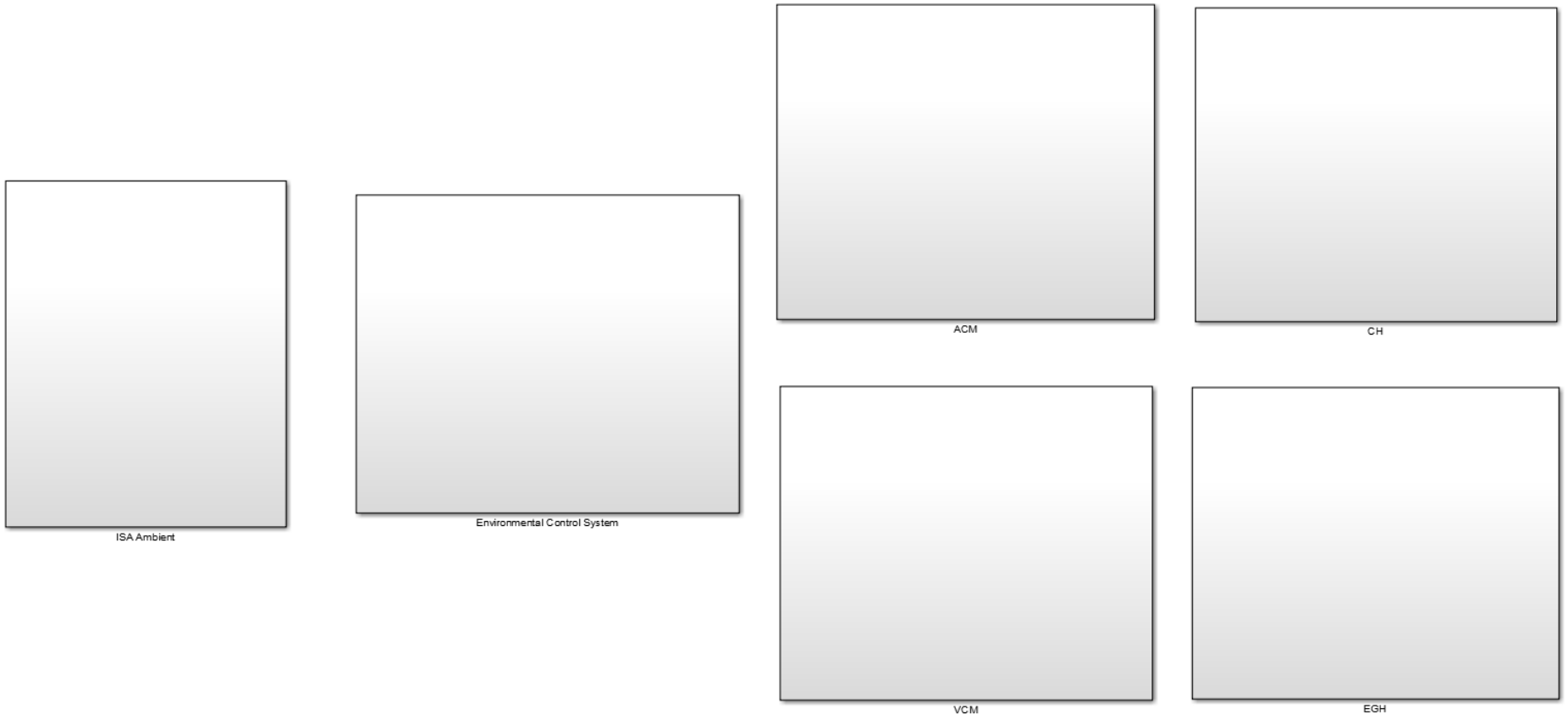


**Figure C-1 ECS-PCM simulation model**

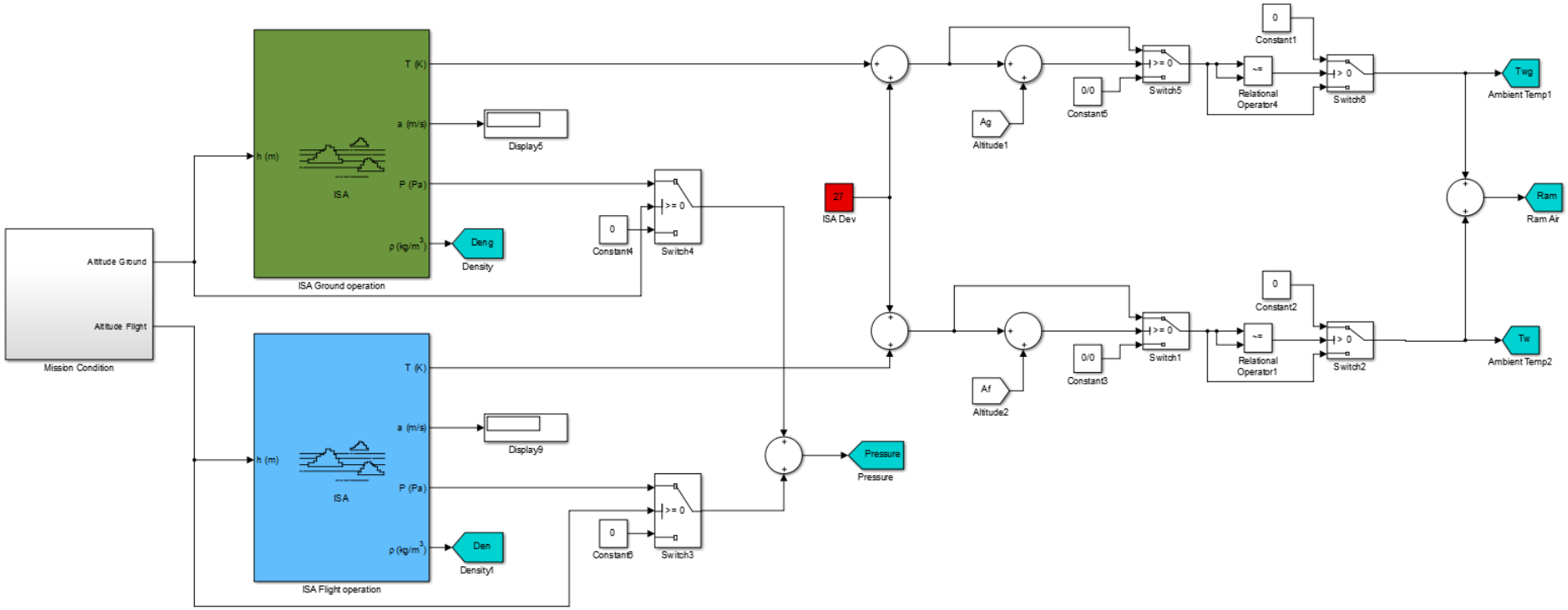


**Figure C-2 Isa Ambient block**

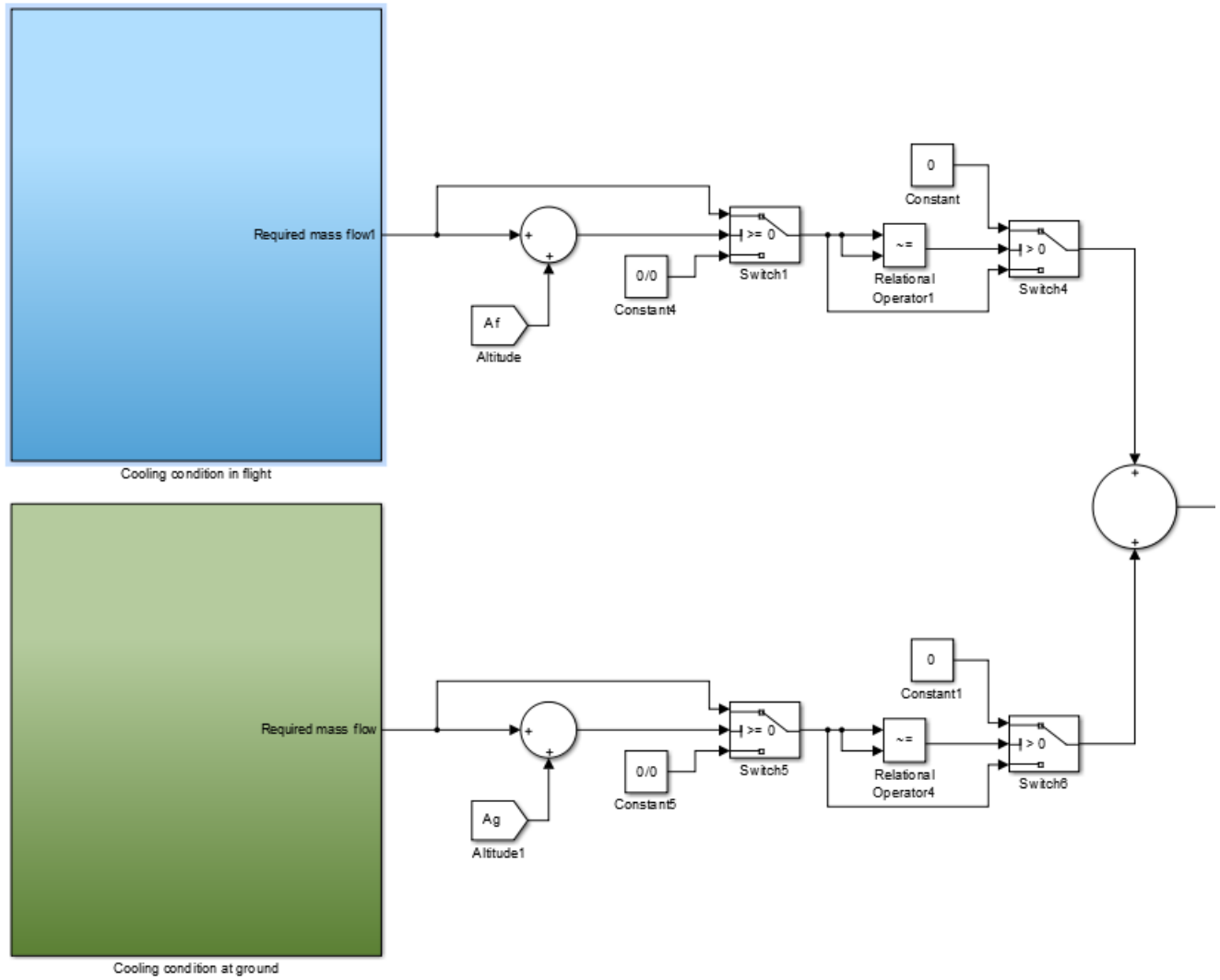


**Figure C-3 Environmental Control System block-A**

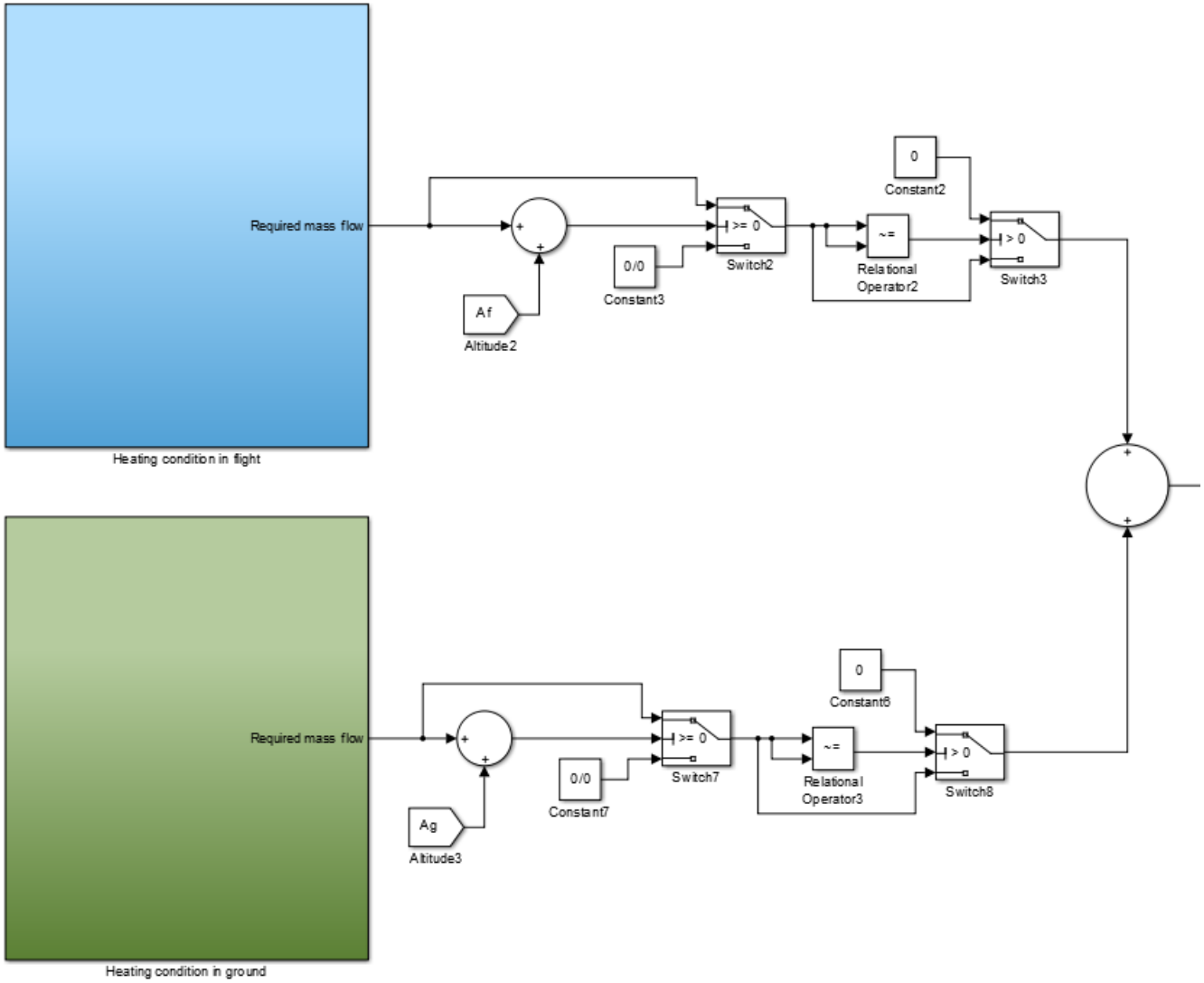


**Figure C-4 Environmental Control System block-B**

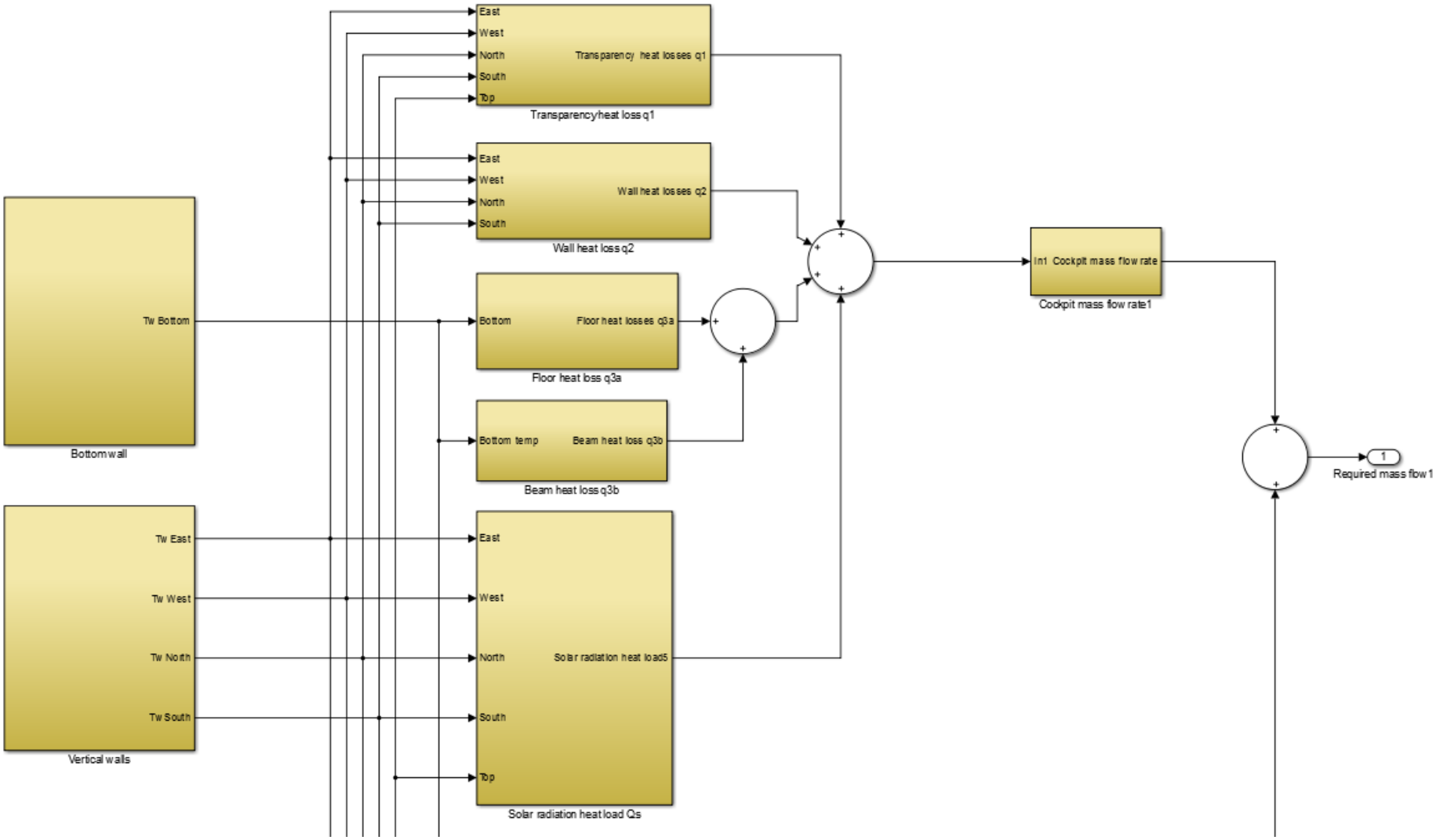


**Figure C-5 Environmental Control System block-Cockpit heat loads**

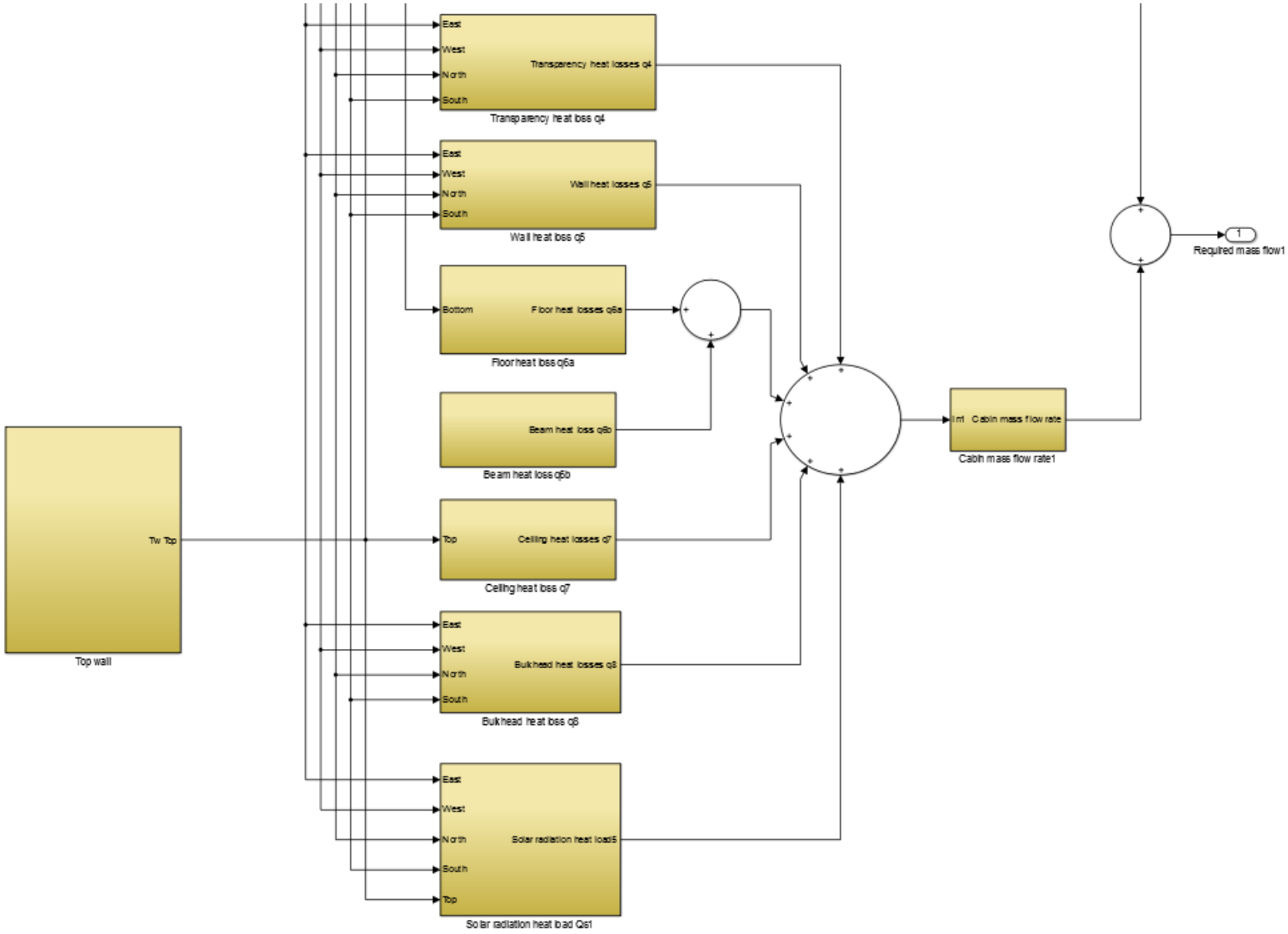


**Figure C-6 Environmental Control System block-Cabin heat loads**

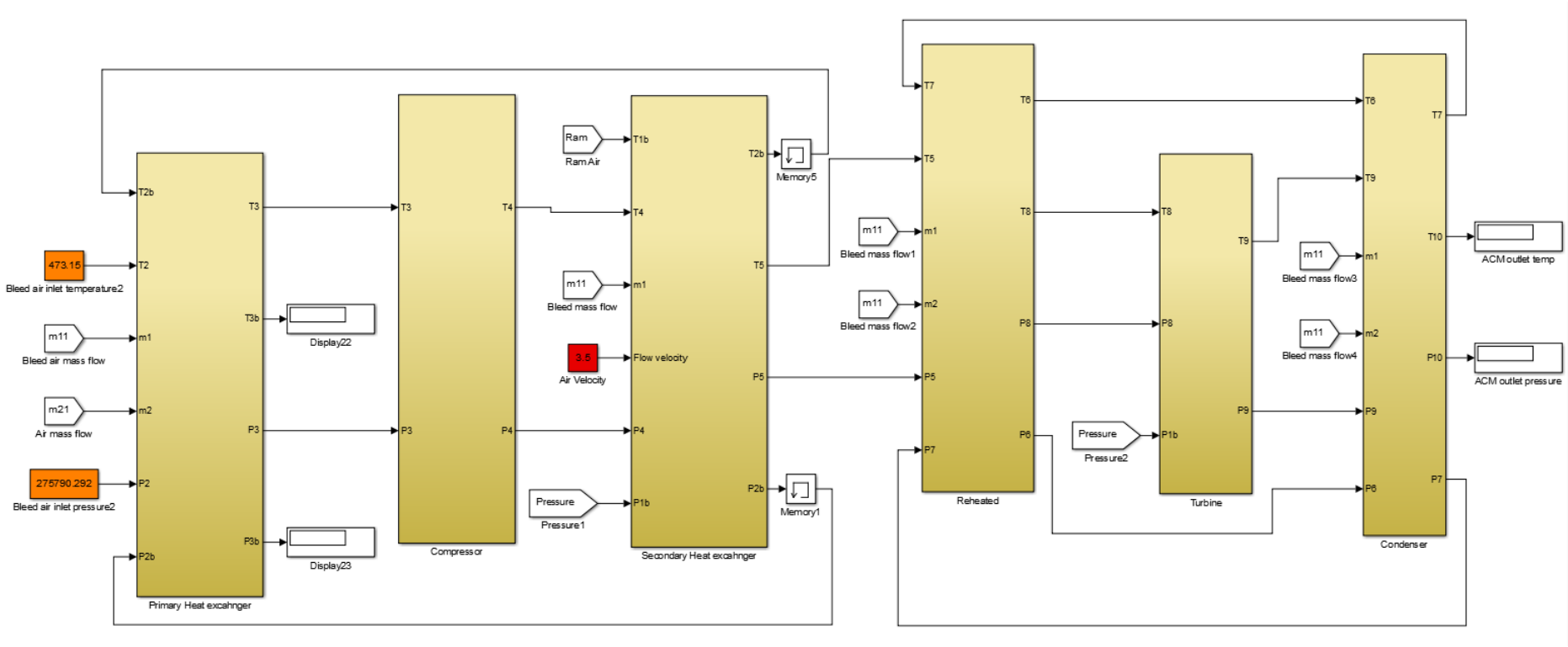


**Figure C-7 Air Cycle Machine block model**

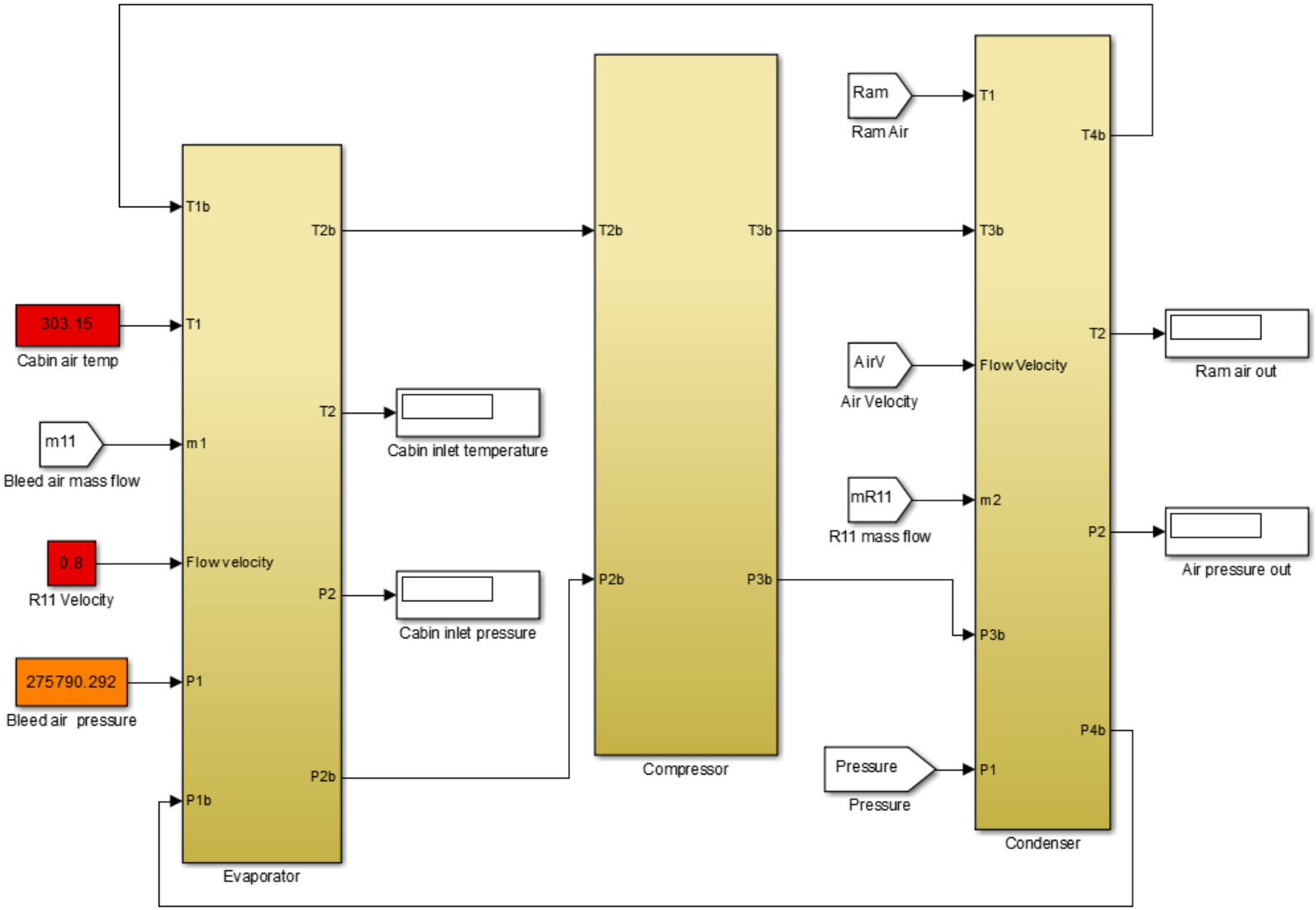


**Figure C-8 Vapour Cycle Machine block model**

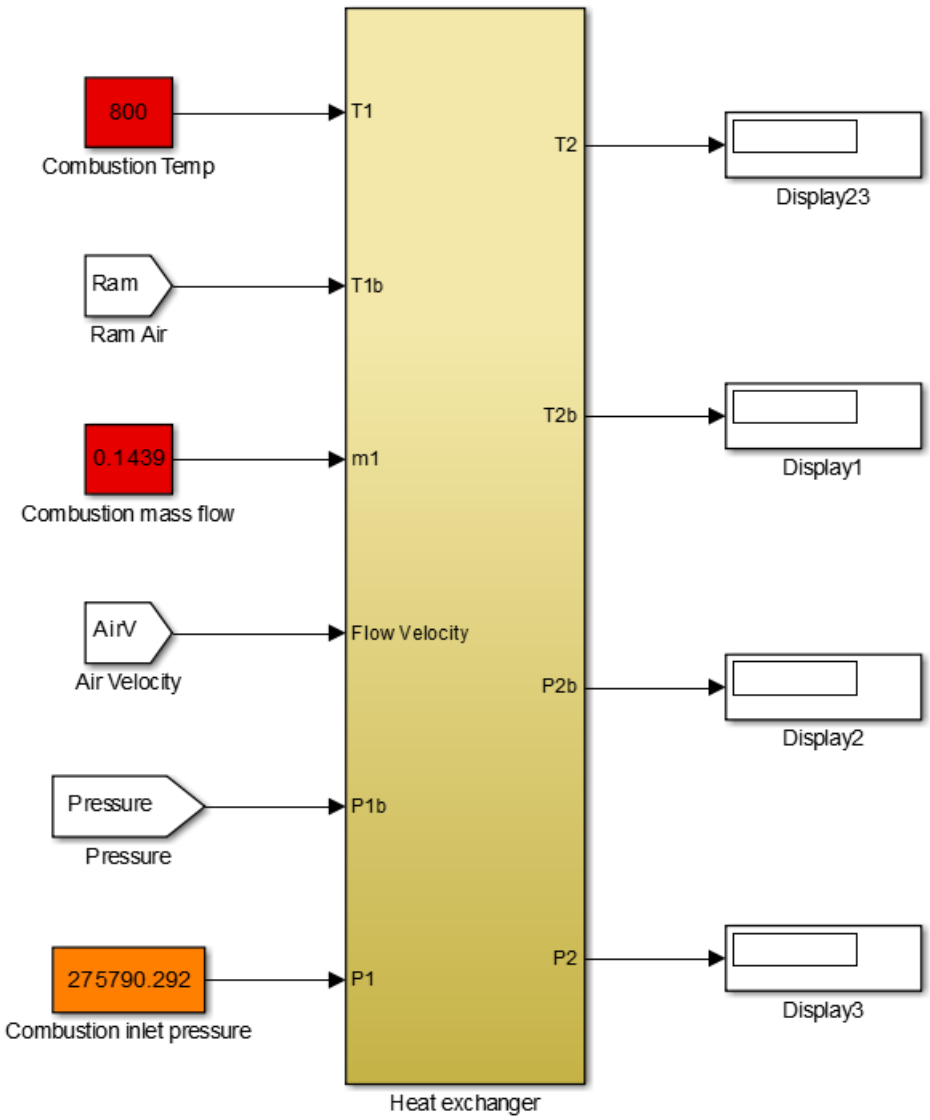


**Figure C-9 Combustion Heater block model**

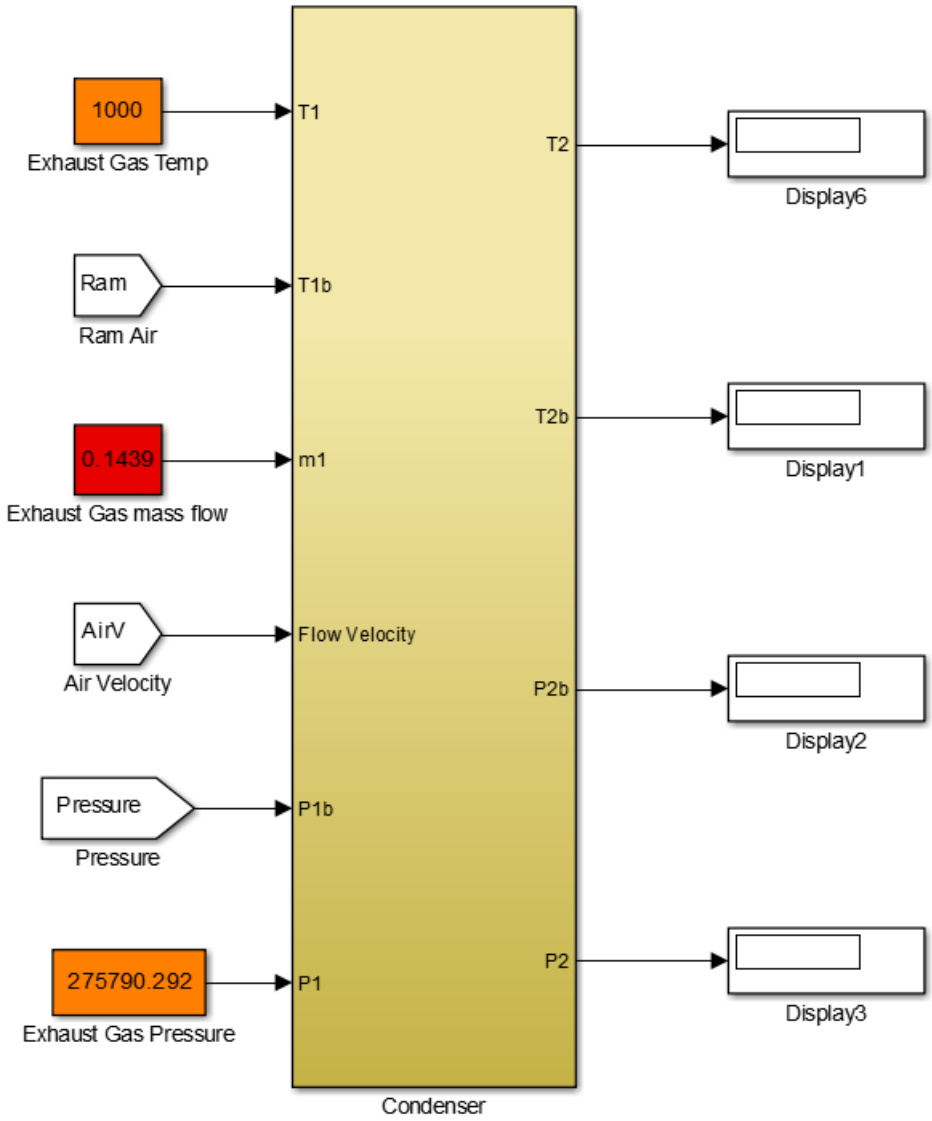


**Figure C-10 Exhaust Gases Heater block model**